INVESTIGATING THE ANTIBACTERIAL POTENCY AND SPECTRUM OF ACTIVITY OF THE ANTIBIOTIC THIOMARINOL

by

YUIKO TAKEBAYASHI

A thesis submitted to The University of Birmingham for the degree of DOCTOR OF PHILOSOPHY

Institute of Microbiology and Infection
School of Biosciences
College of Life and Environmental Sciences
The University of Birmingham
June 2014

ABSTRACT

Thiomarinol is a novel hybrid antibiotic produced by *Pseudoalteromonas rava* sp. nov. SANK 73390. It is structurally similar to a clinically significant antibiotic mupirocin, but includes an additional pyrrothine moiety joined to the mupirocin-like marinolic acid via an amide bond. Thiomarinol has been shown to be more potent against a wider range of microorganisms. This potency was hypothesised to be due to either an increase in inhibition of its target enzyme, isoleucyl-tRNA synthetase (IleS) or an increase in antibiotic uptake and/or inefficient efflux by bacterial cells or a combination of both.

Computer modelling identified eight residues on the IleS active site that may be responsible for increased binding of thiomarinol. A hydrophobic “patch” was also identified near the KMSKS loop that may allow pyrrothine to increase the overall binding affinity. Antibacterial susceptibility tests with *Salmonella enterica* serovar Typhimurium deleted for various efflux transporters identified the TolC-AcrAB complex as being more important in removing mupirocin from cells than thiomarinol. This suggests that thiomarinol is more able to avoid efflux from at least Gram-negative bacteria, allowing its intracellular concentration to rise rapidly. These findings lead to the hypothesis that thiomarinol potency is conferred by a dual mechanism of hindering efflux and increased binding affinity to IleS.

ACKNOWLEDGEMENTS

I would firstly like to thank my supervisor Prof. Christopher M Thomas for his invaluable knowledge, patience and support for the last four years. Thank you to my co-supervisor Dr. Peter J Winn for supervising my time spent at CSB. Thank you to the Darwin Trust of Edinburgh for funding my research, to our collaborators at the University of Bristol and all others in the IMI and School of Biosciences for helping me along the way.

A massive thank you to everyone in S101. In particular, Rachel for taking me under her wings and helping me settle into my PhD life; Yousra for being a great friend; Rohit for helping me through my computational queries; Tony for helping me navigate my thoughts; Jo for her infinite knowledge of mupirocin biosynthesis; Elton for his many years of lab wisdom; Daisuke for guiding me through the joys of thiomarinol extraction and beyond.

Thank you to all past and present lunchtime friends, those hilarious memories will stick with me forever. A special thank you to Dave for supporting me through the writing up stage – I hope those packed lunches made up for what you had to put up with.

Finally, I would like to express my utmost gratitude to my parents for their unwavering support and for believing in me. I could not have gotten this far without you and I hope I have made you both proud.

TABLE OF CONTENTS

LIST OF FIGURES

LIST OF TABLES

LIST OF ABBREVIATIONS

aaAMP	Aminoacyl-adenosine-monophosphate
ABC	ATP-binding cassette
ACP	Acyl carrier protein
AI	Auto induction
Ala	Alanine
APS	Ammonium persulphate
Arg	Arginine
Asn	Asparagine
Asp	Aspartic acid
AT	Acyltransferase
ATP	Adenosine triphosphate
BLAST	Basic Local Alignment Search Tool
Bq	Becquerel
BSA	Bovine serum albumin
BSAC	British Society for Antimicrobial Chemotherapy
Ci	Curie
CoA	Coenzyme A
CPM	Counts per minute
Cys	Cysteine
DH	Dehydratase
dH_2O	Sterile distilled water
DMSO	Dimethyl sulfoxide
DNA	Deoxyribonucleic acid
dNTP	Deoxyribonucleotide triphosphate
DPM	Disintegrations per minute

DTT	Dithiotheitol
EDTA	Ethylenediaminetetraacetic acid
ER	Enoyl reductase
Gly	Glycine
GST	Glutathione-S-transferase
His	Histidine
HPLC	High performance liquid chromatography
Ile	Isoleucine
Ile-AMP	Isoleucyl-adenylate
IleS	Isoleucyl-tRNA synthetase
IM	Inner membrane
IPTG	Isopropyl-β-D-thiogalactoside
KR	Ketoreductase
KS	Ketosynthase
K_i	Inhibitory constant
K_m	Michaelis constant
L-agar	Luria-Bertani agar
L-broth	Luria-Bertani broth
Leu	Leucine
Lys	Lysine
Macp	Mupirocin acyl carrier protein
MATE	Multidrug and toxic compound extrusion
MFS	Major facilitator superfamily
MIC	Minimal inhibitory concentration
Mmp	Mupirocin multifunctional protein
MRSA	Methicillin-resistant *Staphyloccocus aureus*
MSSA	Methicillin-sensitive *Staphylococcus aureus*

NCIMB	The National Collection of Industrial, Food and Marine Bacteria
Ni-NTA	Nickel-nitriloacetic acid
NMR	Nuclear magnetic resonance
NRPS	Non-ribosomal peptide synthase
OD	Optical density
OM	Outer membrane
PBP2	Penicillin-binding protein 2
PCR	Polymerase chain reaction
PDB	Protein Data Bank
Phe	Phenylalanine
PKS	Polyketide synthase
PP_i	Pyrophosphate
Pro	Proline
RNA	Ribonucleic acid
RND	Resistance-nodulation division
SAM	S-adenosyl methionine
SDS	Sodium dodecyl sulfate
SDS-PAGE	SDS polyacrylamide gel electrophoresis
SMR	Small multidrug resistance
SSM	Secondary stage media
STE	Sodium Tris EDTA
TE	Thioesterase
TEMED	N, N, N', N'-tetramethylethylene diamine
Thr	Threonine
T_m	Melting temperature
Tmp	Thiomarinol multifunctional protein
Tris	Tris(hydroxymethyl)aminomethane

Tyr	Tyrosine
TyrS	Tyrosyl-tRNA synthetase
UV	Ultraviolet
Val	Valine
V_{max}	Maximum velocity
WT	Wild-type

CHAPTER 1

1 INTRODUCTION

1.1 An overview of antibiotic resistance

In the past few years, antibiotic resistance in healthcare institutions has become a topic frequently featured by the media, instigating concern amongst the public regarding the future and/or limit of effective antibiotic treatments. Bacterial resistance often results in treatment failure, which can be fatal. This is especially so for critically immunocompromised patients but also for immunocompetent individuals. Numerous antibiotic resistant pathogens have been so far described, ranging from methicillin-resistant *Staphylococcus aureus* (MRSA) to multi-drug resistant Gram-negative bacilli (Spellberg *et al*., 2008). As widely publicised in research journals and media reports, antibiotic resistance has indisputably become a global health concern, affecting both the developed and developing world (Davies, 2013).

With hindsight, it is perhaps unsurprising that we are now faced with the reality of antimicrobial resistance. Following the accidental discovery of penicillin in August 1928 by Sir Alexander Fleming and the subsequent successes of early antibiotic therapies, the general sentiment of the medical community was that the "war against microbes was won" (Spellberg *et al*., 2008). However, this was clearly not the case, as Fleming went on to select and characterise mutants resistant to penicillin soon after he had discovered the antibiotic (Alekshun and Levy, 2007). Various studies and surveillances have since been performed to illustrate the prevalence of antibiotic resistance in hospitals and farm animals, where antimicrobials are heavily utilised (Aarestrup, 2004; Garcia-Migura *et al*., 2014).

Importantly, antimicrobial resistance has also been detected in natural habitats, where microbes are not intensively exposed to high and concentrated levels of antibiotics compared to the clinical environment. One particular study showed a collection of soil-dwelling *Streptomyces* (responsible for producing many clinical antibiotics) to be multi-resistant to a range of natural, synthetic derivatives and completely synthetic antimicrobials (D'Costa *et al*., 2006). Antibiotic producers are known to carry resistance elements in clusters to protect themselves against their own antimicrobial agents, as well as those produced by near-by competitors. Thus, many theorise that antimicrobial resistance mechanisms originated from antibiotic-producing organisms, as a means to protect themselves against auto-toxicity. Orthologous mobile genes of these resistance elements have been identified in clinically resistant pathogens, consistent with this evolutionary theory (D'Costa *et al*., 2006).

Studies have illustrated the capability of microorganisms to adapt, exhibit resistance and survive under various environmental selection pressures. It has become clear that antibiotic resistance is not a new phenomenon. On the contrary, it is a natural and evolutionary process that microbes have undergone for approximately 3.5 billion years (Spellberg *et al*., 2008). Nosocomial and agricultural antibiotic resistance has become a threat to public healthcare because of our increases in antibiotic usage before our complete understanding of microbial survival mechanisms. It is clear that we need to stay vigilant with the epidemiology and rate of antibiotic resistance, continue with our efforts in understanding resistance and advance our developments in newer therapeutic agents. Such efforts are important for preventing increased morbidity, mortality and the costs of treating infectious diseases (Hawkey and Jones, 2009).

1.2 Antibiotic resistance mechanisms

With the increase in bacteria against which antibiotic treatment is ineffective due to resistance, there is urgency in understanding how resistance can arise and how this can be prevented or interfered with. There are various mechanisms by which antimicrobials function that are summarised in Table 1.1.

Table 1.1. Summary of antimicrobial mode of action (reproduced from Tenover, 2006).

Principal mode of action of antimicrobials	Examples
Interference with cell wall synthesis	β-lactams: penicillins, cephalosporins, carbapenems, monobactams
	Glycopeptides: vancomycin
Protein synthesis inhibition	Bind to 50S ribosomal subunit: macrolides, chloramphenicol
	Bind to 30S ribosomal subunit: aminoglycosides, tetracyclines
	Bind to bacterial isoleucyl-tRNA synthetase: mupirocin
Interference with nucleic acid synthesis	Inhibit DNA synthesis: fluoroquinolones
	Inhibit RNA synthesis: rifampin
Inhibition of metabolic pathway	Sulfonamides, folic acid analogues
Disruption of bacterial membrane structure	Polymyxins, daptomycin

Bacteria that are innately susceptible to these antibiotics can become resistant by acquiring any of the following mechanisms by vertical or horizontal evolution. (Some bacteria are innately more resistant to certain classes of drugs, such as Gram-negative microorganisms to penicillins as these drugs cannot penetrate the outer membrane easily.) Vertical evolution involves the bacteria acquiring resistance from chromosomal mutation while horizontal evolution relies on the bacteria acquiring resistance genetic elements from other resistant microorganisms (Tenover, 2006). Firstly, bacteria may acquire genes that code for enzymes that can inactivate antimicrobials, such as β-lactamases. Secondly, they may acquire or upregulate efflux transporters that can transport antimicrobials out of the

cell before they reach their intracellular targets and cause damage. Similarly, they may downregulate or alter their porin expression to prevent antimicrobials from entering the cell. Thirdly, bacteria may acquire mutations that alter bacterial drug targets, preventing the antimicrobials from binding. Finally, bacteria may bypass the targets compromised by the antimicrobials, by producing them using alternative pathways or by producing altered versions that are less susceptible to the antimicrobials.

1.3 Methicillin-resistant Staphylococcus aureus (MRSA)

Methicillin-resistant *Staphylococcus aureus* or MRSA is one of the few so called "superbugs" that have caught the media limelight in recent years. Its parent strain or methicillin-sensitive *S. aureus* has been prevalent in the nosocomial environment, with transmissions occurring between immunocompromised patients, and causing secondary skin infections, to invasive bacteraemia and septic arthritis (Morell and Balkin, 2010). MRSA was firstly detected in Europe in 1961, two years after methicillin was introduced as a solution to treating Gram-positive bacteria that had acquired resistance to penicillin through β-lactamase production. By the 1980s, MRSA was widespread at a global level, both in hospitals and eventually in communities (Morell and Balkin, 2010; Walsh, 2003).

The most common resistance mechanism of MRSA was found to be through the acquisition of the chromosomal *mecA* gene, which expresses an altered form of penicillin-binding protein 2 (PBP2) called PBP2A. The native protein, PBP2 is part of a family of PBPs that are involved in peptidoglycan biosynthesis. PBP2 in particular is involved in cross-linking adjacent peptidoglycan chains (transpeptidation) and most β-lactams function by inhibiting these transpeptidase PBPs, which weaken the peptidoglycan wall and eventually cause cell

lysis. This new PBP2A protein has a lower binding affinity to methicillin and also higher rates of methicillin release, allowing it to continue cell wall assembly in the presence of the antibiotic (Stapleton and Taylor, 2002).

In response to these problems with MRSA, mupirocin was first introduced in 1983 as a potential antibiotic for skin infections and nasal carriage of MRSA (Dacre *et al*., 1983; Wuite *et al*., 1983). At that time, it was sold commercially by GlaxoSmithKline as Bactroban, and later by generic drug sales by Medimetriks and Teva Pharmaceuticals (Thomas *et al*., 2010). At present, it is used globally as a topical treatment for various bacterial infections and is considered an important antibiotic for reducing the risk of MRSA transmission in hospitals (Gilpin *et al*., 2010).

1.4 Mupirocin

Mupirocin is a polyketide antibiotic produced by the soil bacterium *Pseudomonas fluorescens.* It is composed of a mixture of pseudomonic acids. First described in 1971, mupirocin has a range of activity against aerobic Gram-positive and selected Gram-negative bacteria (Nicolaou *et al*., 2009). Mupirocin is mainly made up of pseudomonic acid A (90%), pseudomonic acid B (8%), pseudomonic acid C (< 2%) and pseudomonic acid D (< 2 %) (El-Sayed *et al*., 2003) (Figure 1.1). It is clinically used as a topical treatment against impetigo and secondary wound infections caused by *S. aureus* and *Streptococcus pyogenes* (Patel *et al*., 2009). It is also used as a nosocomial control measure against the spread of MRSA infection, through eradication of MRSA nasal carriage in patients and medical staff (Patel *et al*., 2009).

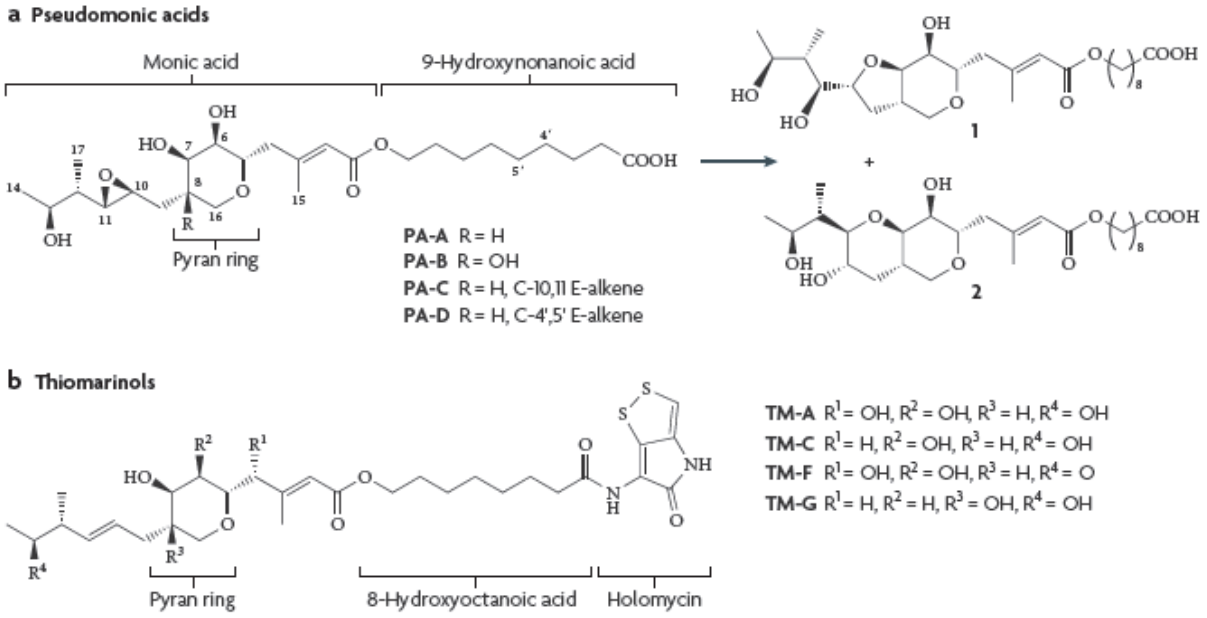

Figure 1.1. Structures of mupirocin and selected thiomarinol compounds (reproduced from Thomas *et al*., 2010). (a) Pseudomonic acid A is made up of a C_{17} monic acid esterified to a C_9 saturated fatty acid, 9-hydroxynonanoic acid. The two cyclic ethers (products 1 and 2) are formed when the 7-hydroxyl group on the 10, 11-epoxide is attacked under either acidic or basic conditions (outside the range of pH 4-9). (b) Thiomarinols are structurally similar to pseudomonic acids but have a pseudomonic acid analogue (marinolic acid) and pyrrothine moiety (such as holomycin) at the end.

1.5 Biosynthesis of mupirocin

Mupirocin biosynthesis requires a 74 kb region in the chromosome called the *mup* cluster (El-Sayed *et al*., 2003). This cluster encodes 35 open reading frames (ORFs), of which six are mupirocin multifunctional polypeptides (*mmpA* to *mmpF*); of these five encode polyketide synthases (El-Sayed *et al*., 2003; Hothersall *et al*., 2007). Expression of this cluster is regulated by the quorum-sensing genes *N*-acylhomoserine lactone (AHL) synthase *mupI* and transcriptional regulator *mupR* (El-Sayed *et al*., 2001). The functions encoded by the *mup* cluster are summarized in Table 1.2.

Table 1.2. Summary of functions encoded by the mupirocin biosynthesis cluster (reproduced from Thomas *et al*., 2010)*.

ORF	Deduced functions of the encoded protein
mupA	Reduced flavin mononucleotide ($FMNH_2$) oxygenase
mmpA	Polyketide synthase (ketosynthase, acyl carrier protein and ketoreductase)
mupB	3-Oxo-acyl carrier protein synthase
mmpB	Polyketide synthase (ketosynthase, dehydratase, ketoreductase, acyl carrier protein and thioesterase)
mmpC	Acyltransferase and enoyl reductase
mmpD	Polyketide synthase (ketosynthase, dehydratase, ketoreductase, methyltransferase and acyl carrier protein)
mupC	Dienoyl CoA reductase
macpA	Acyl carrier protein
mupD	3-Oxo-acyl carrier protein reductase
mupE	Enoyl reductase
macpB	Acyl carrier protein
mupF	Ketoreductase
macpC	Acyl carrier protein
mupG	3-Oxo-acyl carrier protein synthase
mupH	β-hydroxyl-β-methyl glutarate CoA synthase
mupJ	Enoyl CoA hydratase
mupK	Enoyl CoA hydratase
mmpE	Polyketide synthase (ketosynthase and hydroxylase)
mupL	Hydrolase
mupM	Isoleucyl-tRNA synthetase
mupN	Phosphopantetheinyl transferase
mupO	Cytochrome P450
mupP	Unknown
mupQ	Acyl CoA synthase
mupS	3-Oxo-acyl carrier protein reductase
macpD	Acyl carrier protein
mmpF	Polyketide synthase (ketosynthase)
macpE	Acyl carrier protein
mupT	Ferrodoxin dioxygenase
mupU	Acyl CoA synthase
mupV	Oxidoreductase
mupW	Dioxygenase
mupR	Transcriptional activator
mupX	Amidase
mupI	*N* -Acyl homoserine lactone synthase

**macp*, mupirocin acyl carrier protein gene; *mmp*, mupirocin multifunctional polypeptide gene.

Mupirocin is synthesised by a Type I polyketide synthase (PKS) system, which is comprised of large multifunctional enzymes organised in non-iterative modules. The starting unit for polyketide synthesis is an acyl-CoA precursor (such as acetyl-CoA in the case of mupirocin synthesis). In some systems there is a very clear loading function, whereas in the mupirocin system such a function is not obvious and it may be that acetate is loaded directly to the first ketosynthase (KS) or indirectly via the first acyl carrier protein (ACP) by an acyltransferase (AT) before transfer to the first KS to start biosynthesis. Once the KS is occupied the ACP is loaded with the appropriate acyl-CoA (malonyl-CoA in the mupirocin system) before the KS catalyses a Claisen condensation, in which the acetate's carboxylic acid forms a β-carbonyl group as part of the ACP-bound polyketide chain. The β-carbonyl group is then either left unreduced or modified by a combination of reactions by ketoreductases (KR), dehydratases (DH) and enoyl reductases (ER). This process is repeated along the modules until the polyketide is complete, and the chain remains on the ACP as a thiolester until it is released by a terminal thioesterase (TE) via hydrolysis. The released polyketide backbone may then undergo further modification to reach its final form, such as a variety of reductions and the addition of functional moieties. These post-PKS processes yield the wide selection of polyketides with different structures and functions.

The proposed mupirocin synthesis pathway is summarised in a review by Thomas and colleagues (Figure 1.2) (Thomas *et al*., 2010).

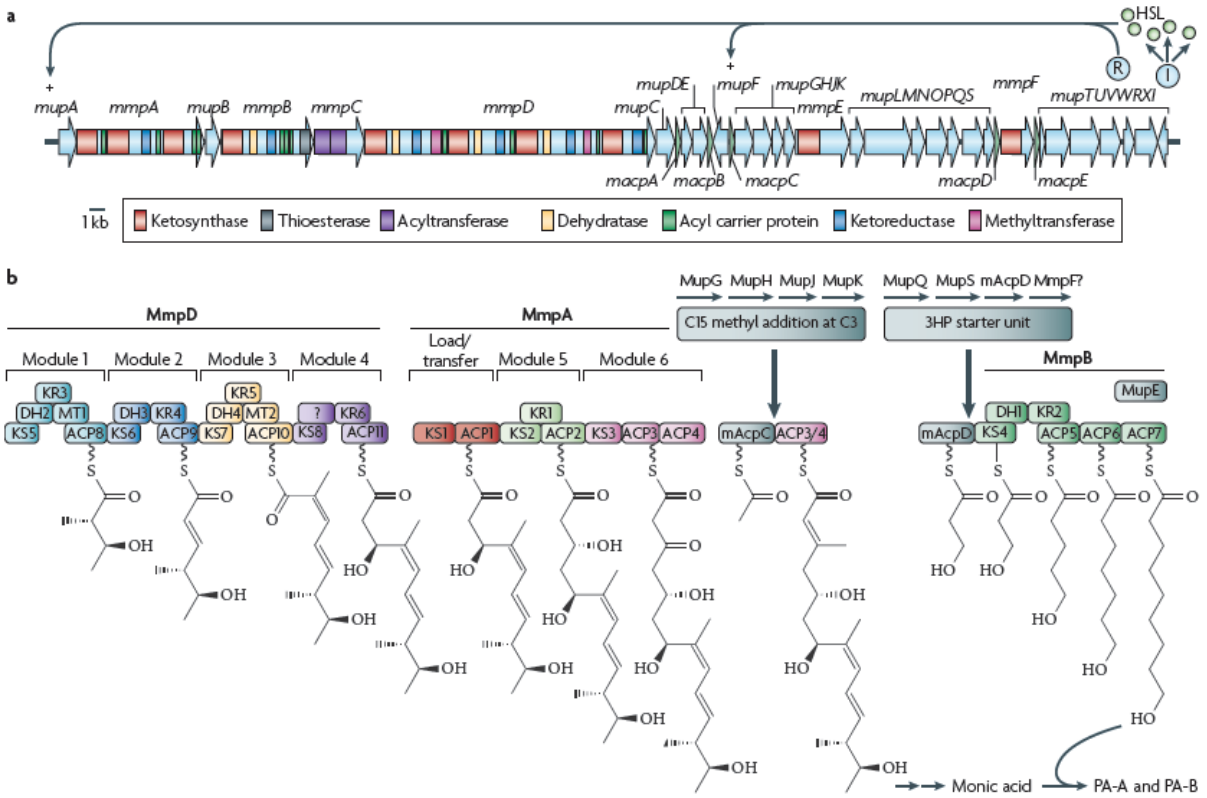

Figure 1.2. The currently proposed mupirocin biosynthesis pathway (reproduced from Thomas *et al*., 2010). (a) The mupirocin biosynthesis (mup) cluster and (b) the proposed biosynthesis pathway of the polyketide backbone. DH, dehyratase; HSL, homoserine lactone; I, MupI; KR, ketoreductase; KS, ketosynthases; Mmp, mupirocin multifunctional polypeptide; MT, methyltransferase; PA, pseudomonic acid.

MmpD and MmpA are hypothesised to produce the monic acid component of mupirocin. MmpB is thought to be involved in the synthesis of 9-hydroxynonanoic acid. mAcpD, MupS and MupQ are suggested to collectively produce the starter compound of 9-hydroxynonanoic acid, 3-hydroxypropionate, although further work is required to support this. It is also unclear as to whether monic acid is joined to 3-hydroxypropionate before being transferred to MmpB for further elongation, or whether 9-hydroxynonanoic acid is made before joining monic acid, although preliminary data indicate the former to be more plausible (Thomas *et al*., Unpublished).

1.6 Aminoacyl-tRNA synthetases

Mupirocin and all pseudomonic acids act by competitively inhibiting bacterial isoleucyl-tRNA synthetases (IleSs) (Figure 1.3). IleS belongs to a group of 20 aminoacyl-tRNA synthetases, which are responsible for charging tRNA with the cognate amino acid to generate aminoacyl-tRNA (Figure 1.4).

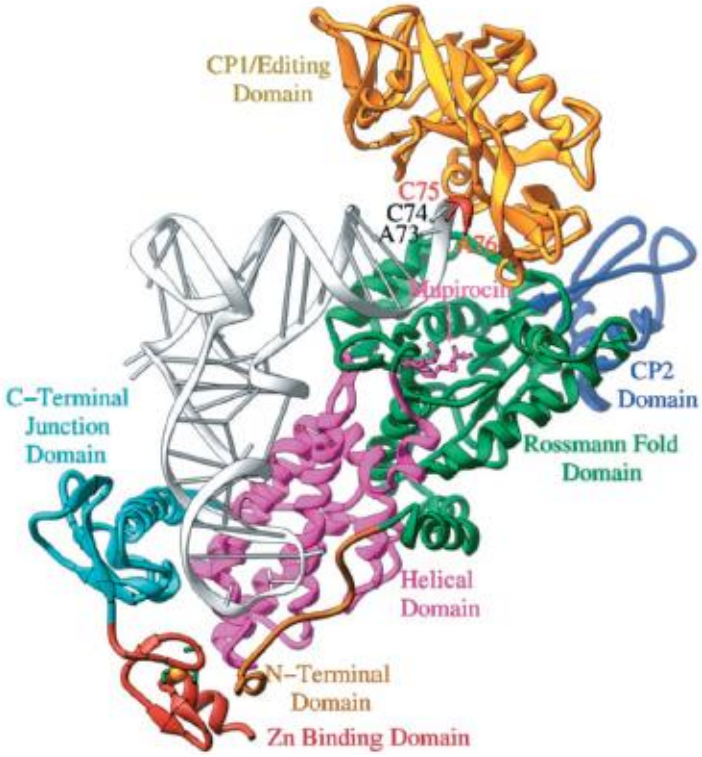

Figure 1.3. Crystal structure of IleS complexed with mupirocin and tRNA^{Ile} (PDB: 1QU2) (reproduced from Silvian *et al*., 1999).

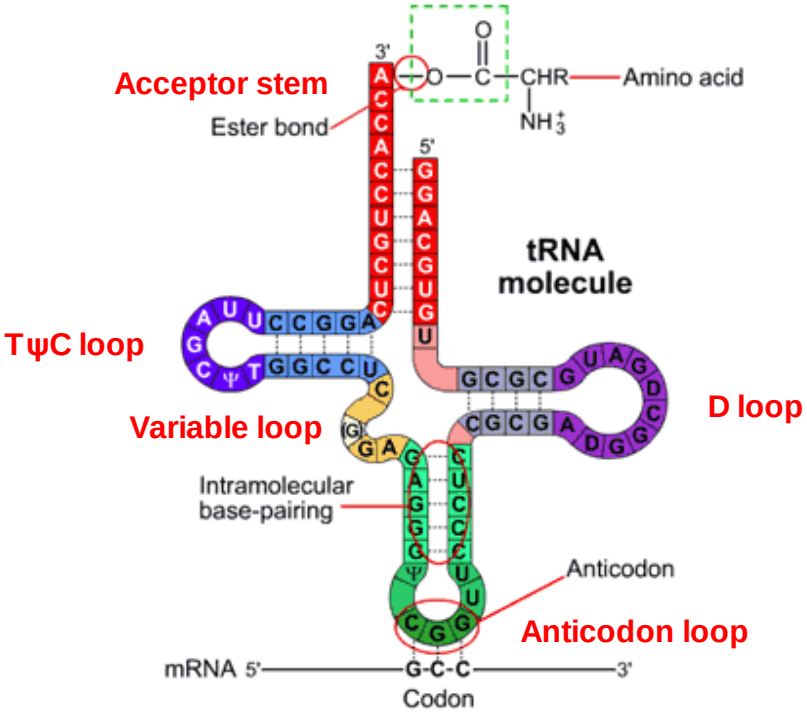

Figure 1.4. Cloverleaf secondary structure of aminoacyl-tRNA (adapted from http://www.wiley.com/college/boyer/0470003790/structure/tRNA/trna_intro.htm). All tRNAs end in –CCA and therefore, the activated amino acid always attaches to an adenylate residue.

Each amino acid has its specific tRNA to which it must be correctly bound and hence, each aminoacyl-tRNA synthetase ensures this process by recognising the two substrates. The enzymes are divided into two classes (Table 1.3) based on their signature sequence motifs in the active site for amino acid activation and aminoacyl-tRNA synthesis (collectively known as aminoacylation) (Eriani *et al*., 1990). The catalytic site of class I aminoacyl-tRNA synthetases are comprised of three or more β-strands linked by two α-helices. They have two dinucleotide-binding Rossman folds which contain the two amino acid motifs "HIGH" and "KMSKS". On the other hand, the active site of class II enzymes is a barrel-like structure of anti-parallel β sheet with loops and α-helices around it (Ochsner *et al*., 2007). Both Class I and Class II catalytic sites are important for the binding of amino acid and adenosine triphosphate (ATP) (Vondenhoff and Van Aerschot, 2011).

Table 1.3. Class I and II aminoacyl-tRNA synthetases*.

Class I aminoacyl-tRNA synthetases			Class II aminoacyl-tRNA synthetases		
a	b	c	a	b	c
Methionyl (MetS) Isoleucyl (IleS) Valyl (ValS) Leucyl (LeuS) Cystinyl (CysS)	Tyrosyl (TyrS) Tryptophanyl (TrpS) Lysyl (LysSI)	Arginyl (ArgS) Glutaminyl (GlnS) Glutamyl (GluS)	Seryl (SerS) Threonyl (ThrS) Prolyl (ProS) Histidyl (HisS) Alanyl (AlaS) Glycyl (GlyS)	Asparginyl (AsnS) Aspartyl (AspS) Lysyl (LysSII)	Phenylalanyl (PheS)

*Both classes are further subdivided based on their sequence homology and domain structure (Ochsner *et al*., 2007). Lysyl-tRNA synthetase is classified in both classes because while most organisms contain the class II structural enzyme, some bacteria and archaea only have the class I enzyme (Vondenhoff and Van Aerschot, 2011).

1.6.1 Function

Class I and II aminoacyl-tRNA synthetases have three binding sites used for charging a tRNA with an amino acid: the ATP site, the amino acid site and the tRNA site. They charge tRNA by a two-step aminoacylation reaction (Figure 1.5) in which the amino acid first reacts

with ATP to form an aminoacyl-adenylate. ATP is cleaved to provide this step with energy. Secondly, the activated amino acid is covalently attached to the tRNA, releasing AMP.

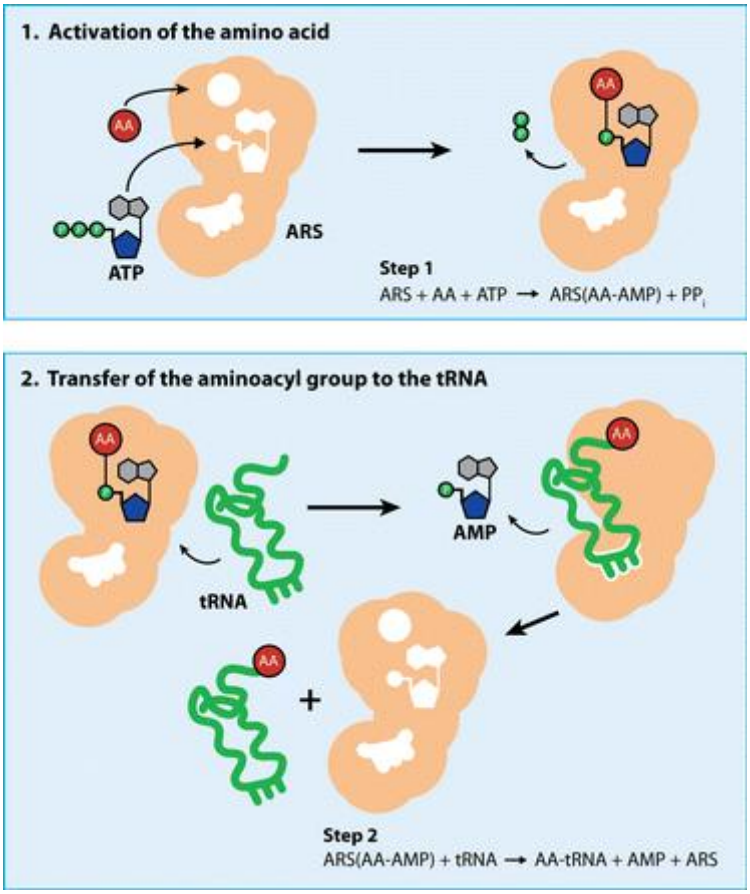

Figure 1.5. Two-step mechanism of (1) amino acid activation and (2) aminoacyl-adenylate transfer to the cognate tRNA (reproduced from Antonellis & Green, 2008). Abbreviations: ARS, aminoacyl-tRNA synthetase; AA, amino acid.

This process can be further discussed at a biochemical level. During amino acid activation, the nucleophilic carboxylate group of amino acid attacks the α-phosphate of ATP, giving aminoacyl-adenosine-monophosphate (aaAMP) and pyrophosphate (PP_i). The reactive aaAMP remains tightly but noncovalently bound to the aminoacyl-tRNA synthetase (Moran *et al*., 2011). Following activation, the carboxyl group of the aaAMP is esterified by a nucleophilic attack onto the 2'- or 3' ribose hydroxyl group at the 3'-end of the tRNA,

resulting in an aminoacyl-tRNA (Figure 1.6). The position of esterification (2'- or 3' hydroxyl group) is dependent on the aminoacyl-tRNA synthetase catalysing the reaction. However, an amino acid which is initially attached to the 2'-hydroxyl group is shifted to the 3'-hydroxyl group in an additional reaction (Moran *et al*., 2011). Once correctly aminoacylated, the aminoacyl-tRNA interacts with the bacterial elongation factor EF-Tu to translate mRNA in the ribosome.

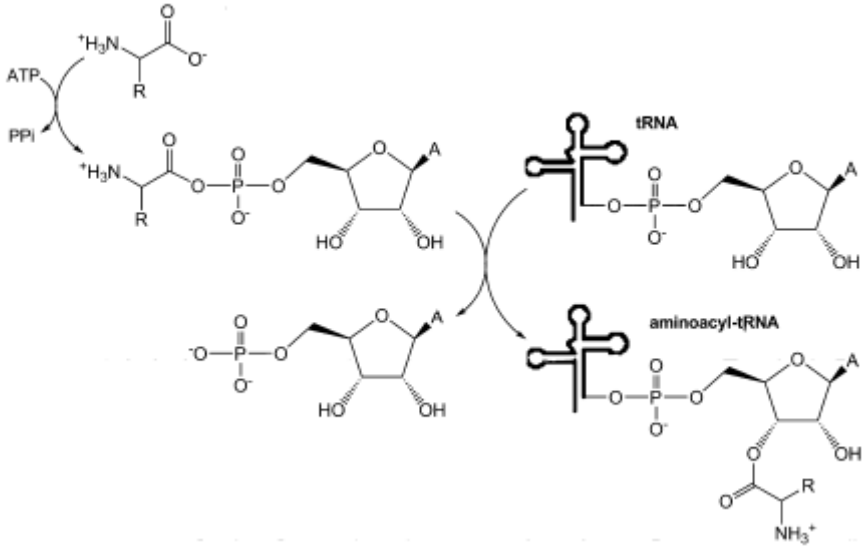

Figure 1.6. Two step mechanism of aminoacylation in Class II aminoacyl-tRNA synthetases (reproduced from Vondenhoff & Van Aerschot, 2011). Class I aminoacyl-tRNA synthetases esterify the amino acid at the 2'-hydroxyl group of the ribose moiety of the 3'-adenosine tRNA. Class II enzymes esterify at the 3'-hydroxyl group (as shown above).

In some cases, incorrectly aminoacylated tRNAs are formed. The consequence of misaminoacylation leads to mistranslation, and the consequences may range from toxicity to cell death (Guo and Schimmel, 2012). To prevent such errors, two editing mechanisms - a pre- and post-transfer editing exist, in which the amino acid is hydrolysed from ATP and tRNA respectively (Fukunaga and Yokoyama, 2006; Martinis and Boniecki, 2010).

Collectively known as the double-sieve model, pre-transfer editing takes place in the synthetic site and the post-transfer editing in the editing site of the aminoacyl-tRNA synthetase. The synthetic site acts as the first filter to eliminate amino acids that are too large or do not establish the correct interactions with the active site. However, some smaller amino acids, such as valine instead of isoleucine in IleS, may slip through unnoticed because they are able to establish enough interaction with the active site. The editing site follows this up by hydrolysing misactivated amino acids from the tRNA. Correctly activated amino acids are unable to fit in the editing site and therefore remain unhydrolysed.

1.6.2 HIGH and KMSKS catalytic domains

The above mentioned two step mechanism of aminoacylation takes place in the catalytic domain. In Class I aminoacyl-tRNA synthetases, this catalytic domain is distinguished by the conserved HIGH and KMSKS motifs. Both motifs have been extensively studied by site-directed mutagenesis and structural studies and observed to interact directly with each other and also with ATP (Perona *et al*., 1993).

In the conserved HIGH motif, the first histidine was observed to play a key role in stabilising the transition state in *Bacillus stearothermophilus* (*B. stearothermophilus*) TyrS via interaction with the γ-phosphoryl group of ATP (Soll *et al*., 1995). On the other hand, the second histidine was shown to play a minor role in stabilising the transition state complex and also the tyrosyl-adenylate through interaction with the ribose group.

In the bacterial KMSKS domain, the second lysine is highly conserved among the Class I aminoacyl-tRNA synthetases (Landès *et al*., 1995) and shown to interact with the α-phosphate of the ATP in the transition state (Yaremchuk *et al*., 2002). However most

eukaryotic and some of archaeal TyrS lack this second lysine: for example, human TyrS has a KMSSS motif. Kinetic studies indicated that potassium functionally compensates for the lack of the second lysine in human TyrS and that the potassium stabilises the transition state for tyrosine activation via interaction with the pyrophosphate moiety of ATP (Austin and First, 2002a). This particular study highlights an interesting point that the KMSKS motifs in the human and *B. stearothermophilus* TyrS play similar roles but the extent to which human KMSSS catalyses tyrosine activation is significantly less than in *B. stearothermophilus* TyrS.

The first lysine in the crystal structures of *Escherichia coli* TyrS was found to bind to the tRNA backbone and stabilise the tRNA conformation to produce an open active site (Kobayashi *et al*., 2005). A detailed suggestion on ATP binding and tyrosine activation by the KMSKS loop can be found in the above mentioned paper. The main chain carbonyl group of the methionine residue was observed to hydrogen bond with the main chain amino group of the glycine of the HIGH motif (Perona *et al*., 1993). Finally, the two serines have also been observed to stabilise the transition state for tyrosine activation by interacting with the pyrophosphate moiety of ATP in human TyrS (Austin and First, 2002b).

1.7 Mupirocin mode of action

As mentioned previously, mupirocin and other pseudomonic acids act by competitively inhibiting bacterial IleS. In order to inhibit IleS, this particular class of antibiotics mimics the key elements involved in the aminoacylation of tRNA. According to the crystal structure of *S. aureus* IleS complexed with mupirocin, this antibiotic prevents normal aminoacylation by imitating isoleucine and ATP (with its C14 monic acid end and pyran ring respectively), blocking their binding sites (Silvian *et al.*, 1999).

The 9-hydroxynonanoic acid was observed to stabilize the entire complex by the carboxylate tail binding to the second lysine residue of the KMSKS motif (Lys598) (Silvian *et al.*, 1999). In the crystal structure of *Thermus thermophilus* IleS, stabilisation was observed to differ slightly – with the 9-hydroxynonanoic acid lying along the KMSKS loop and interacting with the side and main chain of the conserved methionine residue (Nakama *et al*., 2001). The difference in binding is thought to be due to the difference in conformation of the two IleS from *S. aureus* and *T. thermophilus*. The crystal structure of the former is in closed conformation while the latter is opened (Nakama *et al*., 2001).

Once mupirocin blocks the active site of IleS and prevents the charging of isoleucyl-tRNA with isoleucine, it leads to a depletion of aminoacylated isoleucyl-tRNA and an accumulation of uncharged isoleucyl-tRNAs (Reiss *et al*., 2012). An increase in uncharged tRNAs signals the cell of amino acid starvation and triggers the stringent response. The uncharged tRNAs enter the ribosomal A site and block the ribosome, leading to inhibition of protein synthesis.

When the ribosome is blocked from functioning properly, the ribosome-associated RelA protein responds by catalysing the production of GTP 3’-diphosphate (pppGpp) and GDP 3’-diphosphate (ppGpp) from ATP and GTP/GDP. In *E. coli*, ppGpp then binds to RNA polymerase (RNAP) which blocks rRNA and tRNA gene transcription. Cell division and DNA synthesis initiation are also halted. In *Bacillus subtilis*, ppGpp does not directly affect RNAP activity; it is the decrease in intracellular GTP concentration (due to pppGpp synthesis) that affects rRNA gene transcription (Krásný and Gourse, 2004). In *S. aureus*, several genes are

thought to play a role in instigating the stringent response. A comprehensive study on the global response of *S. aureus* to mupirocin has recently been published (Reiss *et al*., 2012).

1.8 Mupirocin resistance

Mupirocin encompasses many desirable traits of an effective clinical drug. For example, mupirocin is approximately 10,000 times more potent on the bacterial IleS than on the corresponding eukaryotic enzyme, as it can only bind weakly to the latter (Hughes and Mellows, 1980; Marion *et al*., 2009; Nicolaou *et al*., 2009). This is essential in any pharmaceutical drug, because weak affinity to the eukaryotic equivalents of any drug target minimises eukaryotic toxicity and ensures its selectivity. Thus mupirocin and the pseudomonic acids have ideal structures and biological activity as pharmaceutical compounds. However, like many of the other antibiotics administered clinically, there are also potential issues to be addressed, such as mupirocin resistance.

In *S. aureus*, mupirocin susceptibility and resistance has been described in three common categories (Patel *et al*., 2009). First, there is susceptibility, in which wild type bacteria succumb to a minimal inhibitory concentration (MIC) of mupirocin at ≤ 4 μg/ml. Second, there is low-level resistance, conferred by mutations in the native tRNA synthetase at a MIC range of 8-64 μg/ml. Lastly there is high-level resistance at a MIC of ≥ 512 μg/ml, in which resistance is mediated by the plasmid-encoded *mupA*, a secondary tRNA synthetase.

Low-level resistance in clinical isolates of *S. aureus*, as well as other species such as *E. coli* has been shown to be acquired by one single amino acid change in the Rossman fold region of IleS (Antonio *et al*., 2002; Yanagisawa *et al*., 1994). The Rossman fold is normally the site of ATP binding and also where the 9-hydroxynonanoic acid of mupirocin binds. In *S.*

aureus (PDB: 1FFY), a Val-to-Phe change at either residue 588 or 631 was observed to confer low-level mupirocin resistance (Antonio *et al*., 2002). The change of residue to a much bulkier phenylalanine is suggested to disrupt the hydrophobic pocket of the Rossman fold, creating a van der Waals clash between the aromatic ring and the 9-hydroxynonanoic acid of mupirocin. It is also speculated that the bulky Phe588 can only be accommodated in the pocket of IleS by torsional rotation, leading to some solvent exposure of the benzene ring. This may trigger conformational changes and result in a loss of Val588 hydrogen bonding with mupirocin.

On the other hand, high-level resistance to mupirocin is usually conferred by the presence of IleSs that have similarity to the eukaryotic enzymes, likely acquired by horizontal gene transfer. For example, mupirocin-producing strain of *P. fluorescens* expresses two different chromosomal IleSs, one of which is similar to eukaryotic IleSs called *mupM* (Yanagisawa and Kawakami, 2003). With this extra eukaryotic-type enzyme on hand, the strain is able to continue its protein biosynthesis, even when challenged with high concentrations of pseudomonic acids. Alternatively, clinical strains of *S. aureus* confer high-level resistance to mupirocin by expressing a eukaryote-like IleS from the plasmid-mediated *mupA* (Hodgson *et al*., 1994). Collectively, these mupirocin-resistant eukaryote-like IleSs are called IleS2 and the mupirocin-sensitive proteins called IleS1. A summary of organisms with or without IleS2 and the relationship between IleS2 and mupirocin sensitivity is shown below (Table 1.4). While several studies have indicated high-level mupirocin resistance in *S. aureus* to be associated with mupirocin-treatment failure, the actual clinical significance of both high and low-level mupirocin resistance is yet to be elucidated by further epidemiological studies (Patel *et al*., 2009).

Furthermore, a new high-level mupirocin resistance gene called *mupB* was recently identified from Canadian clinical MRSA strains (Seah *et al*., 2012). This new gene has 65.5% DNA sequence identity with *mupA* but only 45.5% identity with *ileS*. The protein shares 58.1% amino acid identity with MupA and 25.4% identity with IleS. Although limited in homology, the Class I conserved HIGH and KMSKS motifs were also identified in MupB. So far, there has been no other report of *mupB* detection.

Table 1.4. Summary of organisms with or without IleS2 enzyme and the relativity to mupirocin sensitivity (Brown *et al*., 2003; Ferreira *et al*., 2002; Sassanfar *et al*., 1996; Serafini *et al*., 2011; Yanagisawa and Kawakami, 2003).

Organism	ileS1-like	ileS2-like (plasmid/ chromosomal)	Mupirocin Sensitivity	Mupirocin MIC (µg/ml)
Mycobacterium tuberculosis	-	+	Resistant	>100
Bifidobacteria spp.*	-	+	Resistant	>1,800, >2,000
Oceanobacillus iheyensis	-	+	Not Tested	-
Staphylococcus aureus	+	-	Sensitive	0.12
Staphyloccocus aureus	+	+	Resistant	>512
Staphylococcus epidermidis	+	-	Sensitive	12, 16
Staphylococcus epidermidis	+	+	Resistant	>1024
Bacillus cereus	+	+	Not Tested	-
Bacillus anthracis	+	+	Resistant	64
Pseudomonas fluorescens	+	+	Resistant	>1,000

1.9 IleS1 versus IleS2

Intrinsic mupirocin resistance has also been observed in some bacterial species. A recent study on Bifidobacteria species investigated the reason behind this inherent resistance, in which the majority of the species tested exhibited high mupirocin resistance of over 2,000 µg/ml and a few were considered susceptible (relative to the former high concentrations) when affected at concentrations higher than 1,800 µg/ml (Serafini *et al*., 2011). Unlike mupirocin-resistant *S. aureus* carrying a secondary eukaryote-like IleS2, Bifidobacteria species were found to express only one chromosomal IleS. When these

Bifidobacteria IleS sequences were compared to IleS1 and IleS2 sequences of mupirocin-resistant *P. fluorescens* and *S. aureus*, as well as other mupirocin-sensitive organisms such as *E. coli*, it was noted that all organisms possessing high level resistance to mupirocin contained a tyrosine or alanine residue in the first region (HIGH or RG1) of the ligand binding site (or the Rossman fold) (Serafini *et al*., 2011). All Bifidobacteria species contained a tyrosine in RG1. Therefore, a tyrosine or alanine residue in the ligand binding site of the target enzyme may be responsible for conferring intrinsic resistance to mupirocin.

An evolutionary study by Brown and colleagues also highlighted the occurrence of horizontal gene transfer of these IleS2 proteins (Brown *et al*., 2003) (Figure 1.7). IleS2 in *P. fluorescens*, *B. cereus*, *B. anthracis* and *S. aureus* were found to phylogenetically cluster amongst themselves and other intrinsically mupirocin-resistant organisms such as *O. iheyensis*. Phylogenetically, this cluster is more closely related to eukaryotic IleSs than the IleS1 of the above listed organisms. Additionally, this cluster of bacterial genes sits between the archael and eukaryotic IleSs, suggesting that it did not evolve as part of the organisms' genome but rather was acquired horizontally. The BLAST results of TmlM also indicated its closer homology to eukaryotic IleS, with 50% identity to mouse/rat and 48% to human IleS (Chapter 3, Figure 3.4B).

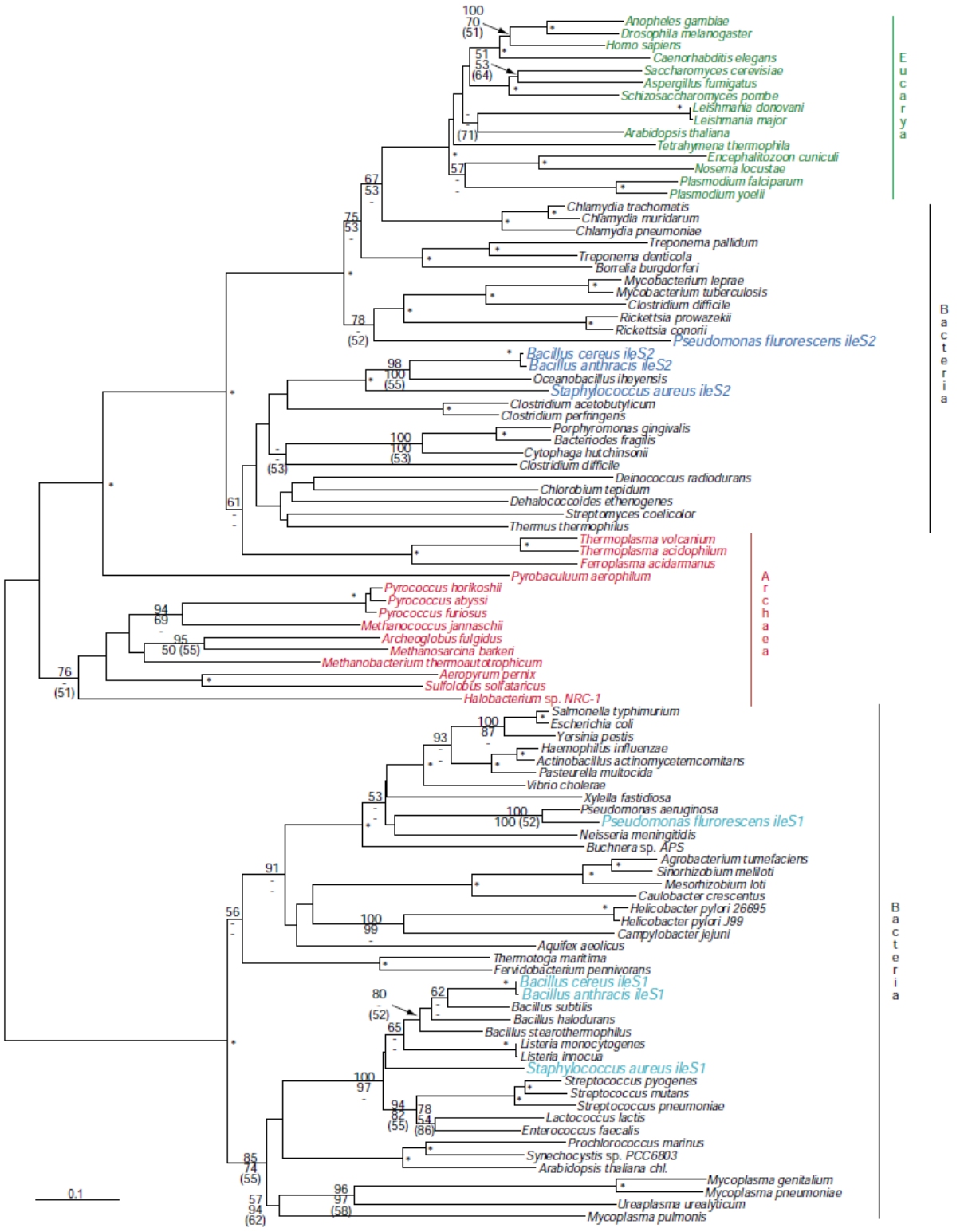

Figure 1.7. Phylogeny of isoleucyl-transfer-RNA synthetase protein sequences (reproduced from Brown *et al.*, 2003).

1.10 Thiomarinol

In addition to the potential risk of high-level mupirocin resistance spreading through horizontal gene transfer of IleS2 enzymes, mupirocin has other limitations as a systemic drug, despite the many attributes highlighted above as a topical treatment. Firstly it cannot be administered orally, as it is readily inactivated in body fluids, in which the ester bond between the monic acid and 9-hydroxynonanoic acid is hydrolysed (Sutherland *et al*., 1985). Secondly it binds strongly to serum, reducing its bioavailability (Sutherland *et al*., 1985). To address the concerns on rising mupirocin resistance in particular, efforts have been directed at deriving improved analogues of mupirocin. As such, potential analogues called thiomarinols (Figure 1.1) were found to be naturally produced by a marine bacterium *Pseudoaltermonas rava* sp. nov. SANK 73390.

Thiomarinol A and H were the first of these potential compounds to be discovered in 1993 and 1992 respectively, followed by the other minor components; thiomarinol B and C in 1995 and thiomarinol D, E, F and G in 1997 (Shiozawa *et al*., 1993, 1995, 1997; Stierle and Stierle, 1992). Thiomarinols display structural similarities to pseudomonic acids, and appear as a hybrid of two types of antibiotics; pseudomonic acids and pyrrothines such as holomycin and holothin, the precursor of the former compound (Shiozawa *et al*., 1993). For example, thiomarinol A and H both consist of a pseudomonic acid analogue called marinolic acid (an 8-hydroxyoctanoic acid instead of a 9-hydroxynonanoic acid) and holomycin and anhydroornithine respectively (Shiozawa *et al*., 1993, 1995; Stierle and Stierle, 1992) (Figure 1.1). Compared to pseudomonic acid A, thiomarinol A shows a broader spectrum activity against both Gram-positive and Gram-negative bacteria (Shiozawa *et al*., 1993) (Table 1.5).

Thiomarinol H also has shown equal activity to that of tetracycline and streptomycin against *S. aureus* (Stierle and Stierle, 1992). The increased potency of these thiomarinol compounds indicates potential as new pharmaceutical analogues. Furthermore, thiomarinol H has recently been chemically synthesized (Marion *et al*., 2009), as well as thiomarinol analogues engineered by mutagenesis and mutasynthesis (Murphy *et al*., 2011). These advances indicate the possibilities of further hybrid production of mupirocin and thiomarinol derivatives.

Table 1.5. Summary of mupirocin, thiomarinol and holomycin MIC against various organisms (Shiozawa *et al*., 1993; Sutherland *et al*., 1985; Oliva *et al*., 2001).

	MIC (µg/ml)		
Test organism	**Mupirocin**	**Thiomarinol**	**Holomycin**
Gram positive			
Staphylococcus aureus	0.12-0.25	<0.01	4
Enterococcus faecalis	<0.05 - >100	<0.01	4
Gram negative			
Klebsiella pneumoniae	50	0.78	8
Escherichia coli	>100, 128	3.13	<2
Pseudomonas aeruginosa	>100, 6400	0.39	64
Salmonella enteritidis	100	3.13	-
Enterobacter cloacae	>100	6.25	-
Serratia marcescens	>100	25	-
Morganella morganii	>100	12.5	64
Proteus vulgaris	100	0.39	-
Proteus mirabilis	-	-	4
Haemophilus influenza	-	-	<0.3

1.11 Thiomarinol mode of action

The exact mode of action of thiomarinol is yet to be elucidated. However, hypotheses can be drawn from its structural similarity to mupirocin, for which the mode of action is better understood. Experiments comparing these two antibiotics have established the wider spectrum of activity of thiomarinol (Shiozawa *et al*., 1993). However, the activity of marinolic

acid, the pseudomonic acid analogue of thiomarinol, has been shown to be less potent than mupirocin, and inhibits *S. aureus* at a MIC of 1 µg/ml and 0.125 µg/ml respectively (Fukuda *et al*., 2011). This strongly suggests that the pyrrothine moiety is responsible for the increased potency of thiomarinol, although holomycin on its own has weaker activity against *S. aureus* than thiomarinol (MIC values of 4 and <0.01 µg/ml respectively) (Qin *et al*., 2013a). On the contrary, holomycin has greater activity against *E. coli* than thiomarinol as shown in Table 1.5.

Due to the hybrid nature of thiomarinol, it can be speculated that the antibiotic targets more than one cellular function. The mupirocin-like marinolic acid may have a similar function to mupirocin and competitively inhibit IleS and consequently inhibit protein synthesis. The holomycin moiety, on the other hand, is part of the dithiolopyrrolone group of antibiotics and is produced by the likes of *Streptomyces* species, *Photobacterium halotolerans* (Wietz *et al*., 2010) and *Yersinia ruckeri* (Qin *et al*., 2013b) as an independent antibiotic. The exact mechanism is not yet understood but dithiolopyrrolones have been shown to inhibit RNA polymerase at the stage of RNA elongation (Khachatourians and Tipper, 1974; Oliva *et al*., 2001). Holomycin may therefore be contributing to the potency of thiomarinol by the additional targeting of RNA synthesis.

However, preliminary data indicate that thiomarinol functions by solely inhibiting IleS (Fukuda *et al*., 2011). A single thiomarinol resistance gene, *tmlM* was identified on the plasmid pTML1 carrying the biosynthetic genes of the antibiotic. When this resistance gene was expressed in thiomarinol-susceptible *E. coli*, a high resistance phenotype was conferred (MIC ≥ 16 µg/ml), suggesting that the target of thiomarinol is only IleS. When the mupirocin

resistant IleS *mupM* was expressed in the same manner as *tmlM* and challenged with thiomarinol, it only conferred weak resistance of MIC= 1μg/ml. The baseline MIC of *E. coli* carrying the empty expression vector was 0.5 μg/ml. Therefore, thiomarinol may simply have a more potent effect on the same IleS target. To date, there are no reports on detection or analysis of thiomarinol resistance other than the native *tmlM* gene.

Based on the above understanding of thiomarinol so far, the observed potency of this hybrid antibiotic is hypothesised to be conferred by the following possibilities of (1) increased binding to IleS, (2) efficient uptake by susceptible cells, (3) prevention of efflux by susceptible cells or (4) a combination of all the above mentioned.

1.12 Biosynthesis of thiomarinol

Work carried out by Fukuda and colleagues identified the biosynthesis genes of thiomarinol to be encoded in an approximately 97 kb plasmid named pTML1 (Fukuda *et al*., 2011). Similarly to mupirocin, thiomarinol is also synthesised by type I polyketide synthase (PKS) genes. 27 ORFs out of the total 45 are hypothesised to encode products responsible for producing the marinolic acid component and 7 ORFs were found to be similar to several putative non-ribosomal peptide synthetase (NRPS) gene clusters and thus hypothesised to be responsible for producing the pyrrothine moiety. Mutational studies of *tmlU* have shown individual production of marinolic acid and pyrrothine but no intact thiomarinol products; hence it is hypothesised that TmlU is involved in joining the marinolic acid and pyrrothine moiety together (Fukuda *et al*., 2011). The gene order from *tmpA* to *tmpD* are organised similarly to the mupirocin biosynthesis cluster (El-Sayed *et al*., 2003) but with the thiomarinol biosynthesis cluster carrying an extra ACP in module 3 of TmpD and in module 6

of TmpA, and 2 extra ACPs in TmpB (one in a group of four and one after the KS domain). The cluster also lacks an mAcpE at the end of pseudomonic acid production and instead carries an extra KS and ACP in TmpB, indicating tailoring steps may occur at this site. A schematic summary of the thiomarinol biosynthesis cluster is shown below (Figure 1.8)

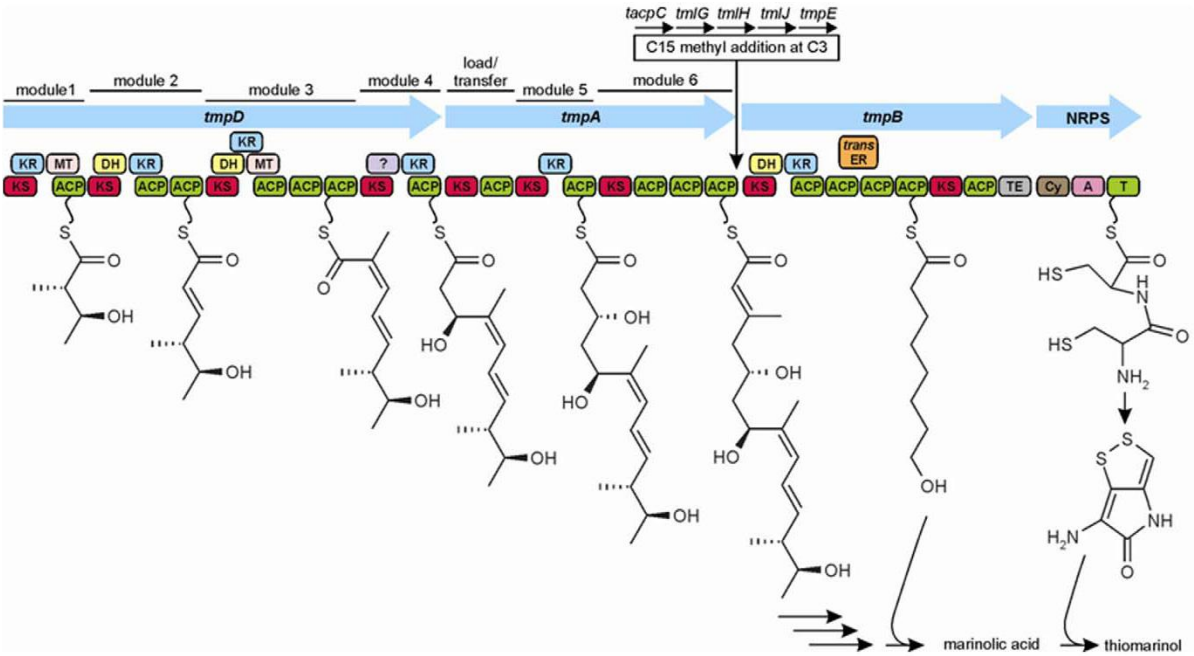

Figure 1.8. Proposed thiomarinol biosynthesis pathway (reproduced from Fukuda *et al*., 2011). KS, Ketosynthase; ACP, Acyl Carrier Protein, KR, Ketoreductase; DH, Dehydratase; ER, Enoyl Reductase; MT, Methyl Transferase; TE, Thioesterase, C, Condensation; A, Aminoacyl Adenylation Domain; T, Thiolation Domain or Peptidyl Carrier Protein.

1.13 Statement of objectives

This study will investigate the mode of action of thiomarinol and the two main hypotheses as to why it is more potent and broader spectrum antibiotic than mupirocin. The known target enzyme of mupirocin (IleS) will be the focal enzyme of study. The first hypothesis to be examined is that the pyrrothine moiety potentiates thiomarinol activity by increasing the binding affinity of thiomarinol and its target enzyme. The second is that the susceptible bacterial cell uptakes and accumulates thiomarinol better than mupirocin.

This study was designed to utilise both experimental and computational methods to address the above hypotheses. The plan was to attempt to identify key amino acid residues in the IleS enzyme that may be involved in increasing the binding affinity to thiomarinol, as well as conferring individual resistance phenotypes. Aminoacylation assays would be used in an attempt to characterise and compare the binding affinities (K_i) of thiomarinol and mupirocin. The study would also attempt to produce ^{14}C labelled thiomarinol and mupirocin, which would hopefully allow us to track the transport of these antibiotics in and out of bacterial cells and deduce whether uptake and/or efflux are key mechanisms of the former for its increased potency.

CHAPTER 2

2 GENERATING THIOMARINOL-RESISTANT MUPM MUTANTS USING SPONTANEOUS AND UV MUTAGENESIS

2.1 Introduction

Isoleucyl-tRNA synthetase (IleS) is the known target enzyme of mupirocin. As discussed in Chapter 1, high-level resistance to mupirocin has been linked to either the presence of a second, plasmid- or chromosomally-encoded, eukaryotic-like IleS (called generically as IleS2) or the presence of just this eukaryotic-like enzyme as the sole IleS (Chapter 1, Table 1.4). MupM and MupA are both eukaryotic-like chromosomal IleS2 enzymes carried by *Pseudomonas fluorescens* and methicillin resistant or sensitive *Staphylococcus aureus* (MRSA/MSSA) respectively that confer high-level resistance against mupirocin. The only known resistance mechanism against thiomarinol is also a eukaryotic-like plasmid-encoded IleS2 called TmlM carried by the producer *Pseudoalteromonas rava* sp. nov. SANK73390. Based on the structural similarity between mupirocin and thiomarinol and the only mechanism of resistance against thiomarinol being an IleS2, IleS was chosen as the focal enzyme of this study.

The aims of this section were firstly to identify the MIC values of thiomarinol against wild-type *Escherichia coli* DH5α (expressing no IleS2 by carrying an empty pJH10 vector) and also those expressing MupA, MupM and TmlM. Following MIC determination, these *E. coli* strains were challenged with thiomarinol concentrations ≥ MICs directly or after UV irradiation respectively, in order to select for spontaneous and UV-induced thiomarinol-resistant mutants. It was hoped that these mutants would reveal the amino acid residues in

the enzyme responsible for the resistance phenotype, as well as the site of pyrrothine binding without changing the MIC for mupirocin.

2.2 Materials and Methods

2.2.1 Bacterial strains, growth conditions and plasmids

All bacterial strains and plasmids used in this study are listed in Table 2.1 and Table 2.2.

All bacterial strains were grown overnight at 37°C in L-broth (Oxoid, United Kingdom) before being sub-cultured for future experiments. Tetracycline (15 µg/ml) was added in the cultures for selection of plasmid pJH10, and 1 mM IPTG was added to induce expression of *mupA*, *mupM* and *tmlM*. Ampicillin (100 µg/ml) was used for selection of plasmid pUC18.

Table 2.1. Bacterial strains used in this study.

Bacterial Strain	Genotype	Phenotype	Source/Reference
E. coli DH5α	*endA1 recA hsdR17 lacZΔM15 supE44 gyrA96 thi-I relA1* F^-	High transformation efficiency strain.	Gibco BRL
E. coli GM2163	F^- *dam-13:Tn9 dcm-6 ara-14 hisG4 leuB6 thi-1 lacY1 galK2 galT22 glnV44 hsdR2 xlyA5 mtl-1 rpsL 136 rtbD1 tonA31 tsx78 mcrA mcrB1*	For producing non-methylated DNA to cut with Dam or Dcm sensitive restriction enzymes. Also useful for mutagenesis, where non-dam methylated DNA is more prone to mutation that cannot be corrected by mismatch repair.	Woodcock *et al.*, 1989
P. rava sp. SANK73390	-	Thiomarinol producer.	Daiichi-Sankyo

Table 2.2. Plasmids used in this study.

Plasmid	Size (kb)	Properties	Source/Reference
pUC18	2.7	pMB1 replicon, Apr, *lacZ* , polylinker	Yanisch-Perron *et al.,* 1985
pJH10	14.5	IncQ replicon, pOLE1 IncC1 deleted, with EcoRI-SacI polycloning site, Tcr from pDM1.2	El-Sayed *et al.,* 2003
pJH10mupA	17.7	pJH10 derivative with cloned 3233 bp *mup A* fragment (EcoRI-XbaI)	Fukuda *et al.,* 2010
pJH10mupM	17.5	pJH10 derivative with cloned 3092 bp *mupM* fragment (EcoRI-XbaI)	El-Sayed *et al.,* 2003
pJH10tmlM	17.6	pJH10 derivative with cloned 3146 bp *tmlM* fragment (EcoRI-XbaI)	Fukuda *et al.,* 2010
pUC18mupM	5.7	pUC17 derivative with cloned 3092 bp mupM fragment (EcoRI-XbaI)	E. Stephens; This study
pJH10mupMO1	17.5	pJH10mupM with putative thiomarinol resistance phenotype	C. Riemer
pJH10mupMN1	17.5	pJH10mupM with putative thiomarinol resistance phenotype	C. Riemer

2.2.2 Thiomarinol production, extraction and quantification

A single colony of *P. rava* sp. nov. SANK 73390 was inoculated into 25 ml Marine Broth (BD, United Kingdom) and the culture grown at 23°C at 200 rpm before 5 ml was sub-cultured into 500 ml fresh Marine Broth and grown for another 2 days in the same conditions. To stabilise the thiomarinol compounds, the pH of the culture was then adjusted to approximately 6.0 by adding 5 ml of 1M HCl. A volume of acetone equal to that of the culture (500 ml) was added and mixed, and the culture left in the refrigerator for at least 1 hr to allow complete decomposition of the bacterial cell walls. The acetone was then evaporated using a rotary evaporator before an equal volume of ethyl acetate (500 ml) was added and mixed well to extract the thiomarinols. The mixture was decanted into a separating funnel, where the thiomarinols separated from the remaining cell debris to form a clear yellow upper layer. The bottom cloudy layer was discarded while the ethyl acetate in the yellow layer was completely evaporated using the rotary evaporator. The dried

thiomarinol extract was dissolved in 2 ml absolute methanol and stored in the refrigerator until further use. Further dilutions of the thiomarinol extract were prepared using methanol only. The concentration of extracted thiomarinol was quantified using the HPLC and thiomarinol A powder stock provided by Daiichi Sankyo (Tokyo, Japan) as a standard. HPLC was performed using the Unipoint LC system software and a reverse phase C18 column (15 cm x 4.6 mm) at a UV detection of 385 nm. A mobile phase water/acetonitrile ratio of 65% and 35% respectively was used with 0.01% acetonitrile trifluoroacetic acid. The programme was run for 24 minutes at 1 ml/min flow rate and thiomarinol A detected at around 8 minutes.

2.2.3 Determination of Minimal Inhibitory Concentration

Two final inoculum sizes were used in determining the MICs: 5 x 10^5 cfu/ml and 5 x 10^4 cfu/ml. The former inoculum follows the guideline provided by the British Society for Antimicrobial Chemotherapy (BSAC) and the latter was used previously by the group. Overnight cultures were diluted to the appropriate cell density using L-broth. Thiomarinol serial dilutions were prepared with L-broth containing 15 µg/ml tetracycline and 1 mM IPTG and made at one step higher concentrations than the final dilution range required, i.e. for final dilution range of 1, 2, 4, 8, 16, 32, 64, 128 µg/ml, master mixes of 2, 4, 8, 16, 32, 64, 128, 256 µg/ml were prepared to compensate for the addition of an equal volume of inoculum. Likewise, tetracycline and IPTG concentrations were also doubled in the mixture. 75 µl of each thiomarinol dilution was distributed into 64-well flat bottom cell culture plates and inoculated with 75 µl of the diluted overnight cultures. The final methanol concentration in

each well was ≤ 5%. (v/v) The plates were incubated overnight at 37°C at 200 rpm and the optical density read at 620 nm using a plate reader.

2.2.4 Generating and validating spontaneous mutants

Overnight cultures of DH5α carrying pJH10, pJH10tmlM and pJH10mupM were sub-cultured to a cell density of 5 x 10^5 cells/ml in 5 ml L-broth containing 15 µg/ml tetracycline and 32, 64 or 128 µg/ml thiomarinol. These cultures were incubated for 2 days, at which point they were re-inoculated into fresh medium with the same tetracycline and thiomarinol concentrations and grown overnight in the same conditions. The overnight cultures were then streaked onto L-agar with 15 µg/ml tetracycline to yield single colonies. These single colonies (along with single colonies of the same strains untreated with thiomarinol as negative control) were then streaked with a toothpick from the centre of the L-agar plate to the edge in a repeated order of potential mutant followed by its wild-type parent strain. 8, 64 or 128 µg of thiomarinol were impregnated onto 9 mm paper discs (Whatman, United Kingdom) and dried for at least 30 min before being carefully placed in the centre of the streaked L-agar plates. The plates were incubated overnight at 37°C and the mutants validated as "true mutants" if they grew closer to the thiomarinol disc than their wild-type strains.

2.2.5 Generating UV-induced mutants

Overnight cultures of GM2163 carrying pJH10mupM were sub-cultured in 5 ml L-broth containing 15 µg/ml tetracycline and grown to an OD_{600nm} of 0.4-0.6. The GM2163 strain was chosen for this study because of its *dam*$^-$ and *dcm*$^-$ genotype, in which it is unable to methylate DNA and is consequently more prone to induced mutations. An aliquot of the

culture (2 ml) was then transferred into a glass petri dish and subjected to irradiation for up to 14 minutes in an UV light box. At 60 sec intervals, 100 µl of culture was collected, spread on L-agar containing 15 µg/ml tetracycline and wrapped in foil to prevent photoreactivation. The covered plates were incubated overnight at 37°C. Single colonies were then tested in the same thiomarinol streak test method outlined above.

2.2.6 Preparation of competent bacteria

DH5α bacteria were made competent by following the protocol of Cohen *et al*. (1972). Volumes of L-broth (5 ml) were inoculated with a single colony and incubated overnight at 37°C at 200 rpm, following which the culture was diluted 1:50 with fresh L-broth and grown again in the same conditions until an OD_{600nm} 0.4-0.6. The bacteria were harvested at 5,000 x*g* for 7 min at 4°C and the supernatant discarded. The cell pellet was re-suspended in 2 ml of 100 mM pre-chilled calcium chloride ($CaCl_2$) per 5 ml of culture, vortexed and left on ice for 20 min before centrifugation at 5,000 x*g* for 7 min at 4 °C. The supernatant was again discarded and the cell pellet re-suspended gently in 0.5 ml of 100 mM pre-chilled $CaCl_2$ per 5 ml culture. The competent cells were then stored at 4°C until future use.

2.2.7 Plasmid DNA isolation and transformation

Mutant plasmids pJH10mupA and pJH10mupM were prepared using Bioneer Accuprep® Plasmid Extraction Kit and transformed into competent cells by adding 5 µl of the plasmid extraction into 100 µl of competent cells. The mixture was gently mixed by tapping and left on ice for 30 min before heatshocking at 42°C for 2 min. 1 ml L-broth was then introduced and the suspension incubated at 37°C at 200 rpm for at least 1 hr. 50 µl of the

incubated suspension was spread on L-agar plates with 15 µg/ml tetracycline and incubated overnight at 37°C.

2.2.8 Cloning mutant genes into new vectors

Mutant plasmids prepared as outlined above were digested using EcoRI and XbaI to excise the *mupM* gene. The recipient vector pJH10 or pUC18 was also cut using the same restriction enzymes. For cloning *mupM* into pJH10, the vector (and insert) was isolated from the GM2163 strain, to ensure no dam methylation of the XbaI site. The DNA fragment was then ligated into new pJH10 or pUC18 vectors using the Quick Ligation™ Kit (New England Labs) and introduced by transformation into DH5α as outlined above.

2.2.9 DNA Sequencing

All thiomarinol-resistant spontaneous and UV *mupM* mutants were sequenced in the high copy number pUC18 vector using the primers listed in Table 2.3.

Table 2.3 Oligonucleotide primers used for checking the sequence of spontaneous and UV *mupM* mutants.

Gene/Vector	Sequence Checking Primer	Source/Reference
mupM	5'-gaattcatgagtacggaagaagtgg-3' 5'-gtcgacatcgccgtgctc-3' 5'-acaaagccacgccagtcatc-3' 5'-tgcatgacaaggggcatgtc-3' 5'-cttcgtacagatgggcgatg-3' 5'-aggtgatgggcagcatcgc-3' 5'-caagttcagtgaagagtcggt-3' 5'-cgccagtacctgtcgtacg-3' 5'-aagctttctagatcaggccagtacgctacg-3'	Claire Riemer
pUC18	5'-gttttcccagtcacgac-3' 5'-caggaaacagctatgac-3'	Promega, UK

2.3 Results

2.3.1 MIC values are dependent on inoculum size

The first part of the study was to determine the thiomarinol MIC values of wild-type DH5α and DH5α expressing thiomarinol resistant *tmlM* and mupirocin resistant *mupM* and *mupA*. Two final inoculum sizes were used as outlined in the methods. The larger inoculum (5×10^5 cfu/ml) was recommended by BSAC (http://www.bsac.org.uk) and the MIC against this cell density was at least two-fold higher than that against the lower inoculum of 5×10^4 cfu/ml (Table 2.4).

Table 2.4. Summary of thiomarinol MIC values*.

	Thiomarinol MIC (µg/ml)	
Strain	5×10^4 cfu/ml	5×10^5 cfu/ml
DH5α pJH10	4-8	8-16
DH5α pJH10mupA	16-32	> 128
DH5α pJH10mupM	16-32	32-64
DH5α pJH10tmlM	> 128	> 128

*Two inoculum sizes were used, the larger recommended by BSAC. The smaller was also used in previous MIC studies by other lab colleagues and used in this study for comparative purposes. The MIC tests were repeated at least three individual times in duplicate. A variability of 2-fold was observed in some MIC values during repetition and was noted as such (e.g. 4-8) instead of an average value. Values > 128 indicate that the MIC exceeds the tested concentration in this study.

In addition to the slight discrepancies between MIC values, it was also observed that at the higher thiomarinol concentrations of 64 and 128 µg/ml (and this being before inoculation and incubation), the basal OD_{620nm} values of the culture broth were more than double that of plain L-broth i.e. the cultures looked cloudy and less transparent. Therefore, un-inoculated L-broth containing various concentrations of thiomarinol was also included in the cell culture plates and the basal optical density deducted from all values after growth. At

zero thiomarinol concentration, the basal OD_{620nm} was approximately 0.05. At a thiomarinol concentration of 128 µg/ml, OD_{620nm} was approximately 0.4.

2.3.2 *mupM* spontaneous mutants

The overall strategy devised in this study to generate thiomarinol-resistant spontaneous and UV mutants is summarised in Figure 2.1.

In the initial stages of generating spontaneous mutants, 5 ml L-broth cultures of DH5α (pJH10) and strains carrying *mupA*, *mupM* and *tmlM* were grown up to 3 days in 32 or 64 µg/ml thiomarinol. The required days of incubation until detectable growth of the cultures ranged from overnight to 3 days (Table 2.5).

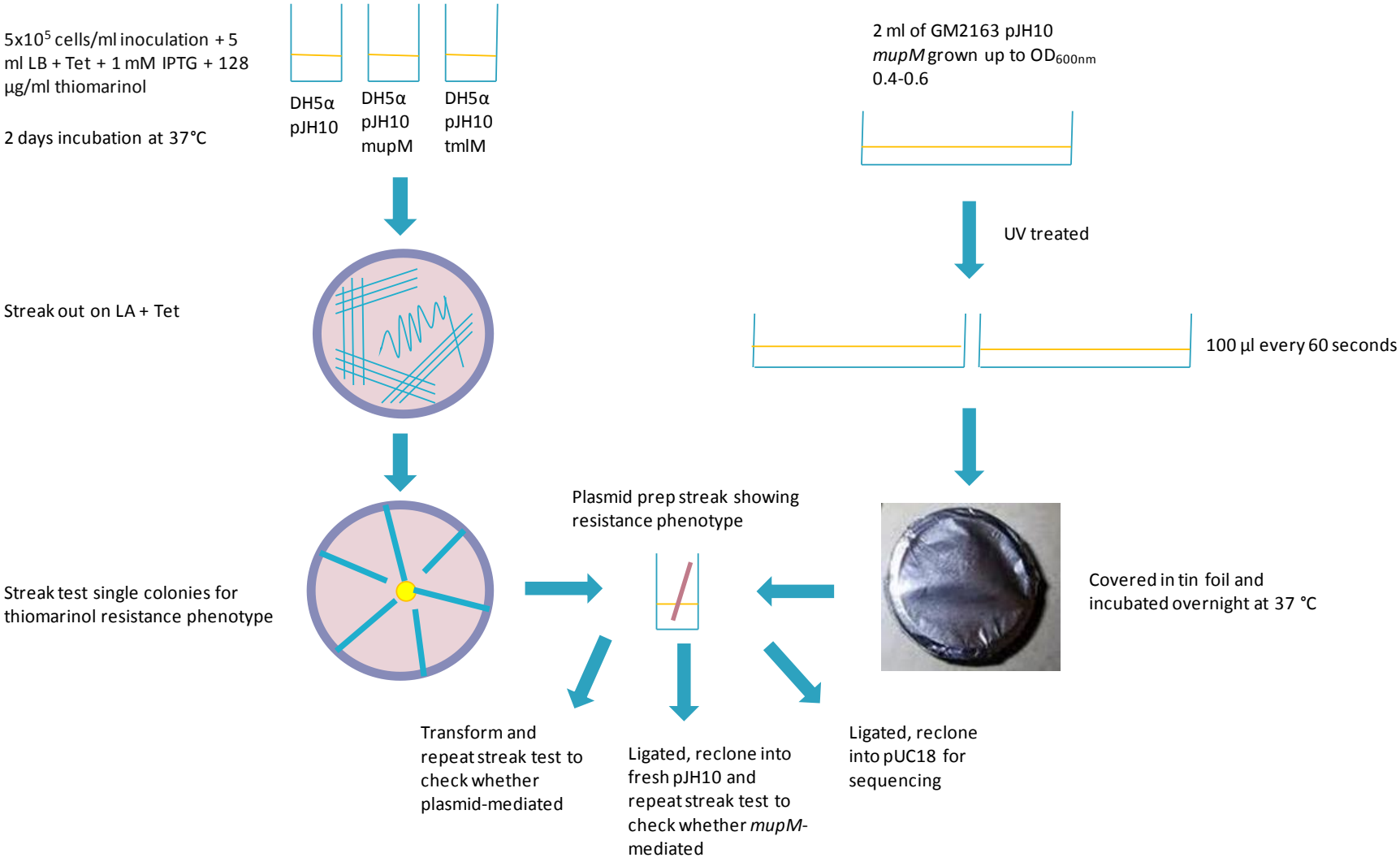

Figure 2.1. Flow diagram of methodology used to generate thiomarinol-resistant spontaneous and UV mutants.

Table 2.5. Initial incubation period for generating spontaneous mutants in 32 and 64 µg/ml thiomarinol*.

	Strain	Day 1	Day 2	Day3
32 µg/ml	DH5α pJH10	-	+	+
	DH5α pJH10mupA	+		
	DH5α pJH10mupM	-	+	
	DH5α pJH10tmlM	+		
64 µg/ml	DH5α pJH10	-	-	-
	DH5α pJH10mupA	-	+	
	DH5α pJH10mupM	-	-	+
	DH5α pJH10tmlM	+		

*+ indicates visible culture growth and – indicates no growth.

As expected, DH5α (pJH10) failed to grow in 64 µg/ml thiomarinol, even after 3 days of incubation, while DH5α (pJH10tmlM) grew well after overnight incubation at both thiomarinol concentrations. DH5α (pJH10mupM), on the other hand, grew after 3 days of incubation but failed to grow overnight when re-inoculated into fresh L-broth with thiomarinol and tetracycline. This indicates that no "true mutants" have been obtained and suggests that the thiomarinol activity in the culture may significantly decrease by day 3 of incubation. Therefore, only cultures that grew after a maximum of 2 days incubation were progressed to the next stage of streaking to isolate potential thiomarinol-resistant mutants.

mupA mutants grew overnight in 32 and 64 µg/ml of thiomarinol while *mupM* mutants only grew in 32 µg/ml thiomarinol. *mupA* and *mupM* cultures that initially grew in 32 µg/ml thiomarinol were re-inoculated in the higher 64 µg/ml concentration to determine whether they could also grow at the higher concentration. Only *mupA* mutants were confirmed as growing well in the latter concentration. *mupM* mutants did not show signs of

visible growth. At this stage, *mupM* was selected to use for further optimisation of the methods and *mupA* left to follow up on once an effective protocol was determined.

After several attempts to grow DH5α (pJH10mupM) cultures at thiomarinol concentrations of 32 and 64 µg/ml but with varying degrees of success, 128 µg/ml was tested to see if it could yield visible growth. Growth was observed after 2 days incubation for all tested cultures and this higher thiomarinol concentration was chosen for yielding all future mutants. Cultures that grew were streaked against discs impregnated with 64 µg thiomarinol as detailed in the Methods. A selection of representative streak test plates is shown in Figure 2.2 and Figure 2.3. The streak test indicated that some of the putative mutants were able to grow up to the thiomarinol impregnated discs while others failed to grow as close (Figure 2.2; Figure 2.3). The streaks that grew closest to the disc were taken for further experimentation to determine whether this thiomarinol resistance phenotype was firstly plasmid-mediated and secondly conferred by the mutated *mupM* gene and not other changes in the expression vector.

The plasmids from the mutants of interest were isolated by standard procedure and transformed into new DH5α cells and found to still exhibit the same thiomarinol resistance phenotype on the streak test (Figure 2.4). The plasmid preparations from spontaneous *mupM* mutants obtained in a previous study performed by Claire Riemer (pJH10mupMO1 (O1) and pJH10mupMN1 (N1)) were also transformed and streaked (Figure 2.5).

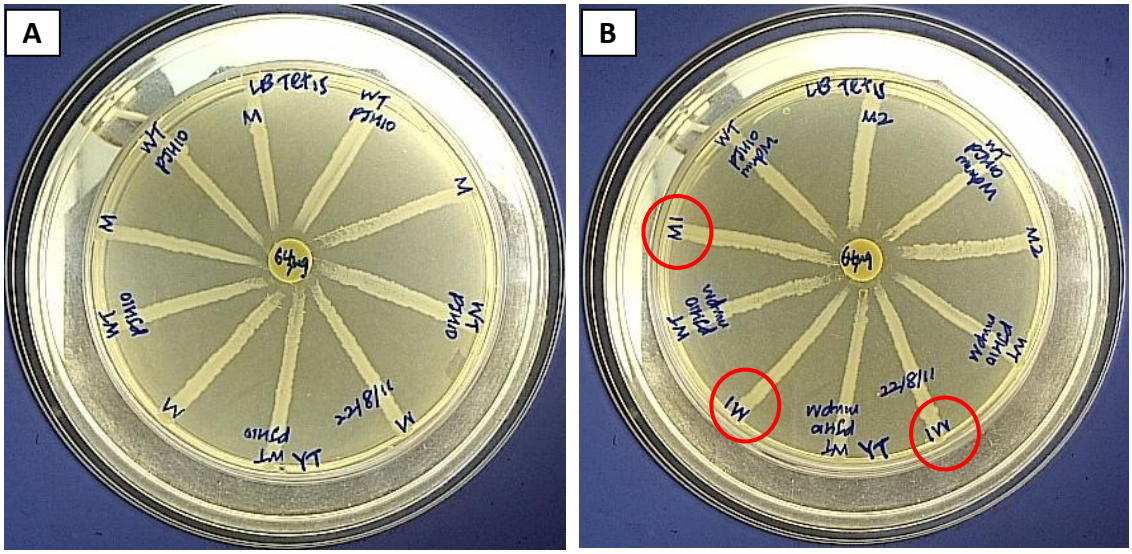

Figure 2.2. Spontaneous *mupM* mutants identified on L-agar streak tests (circled in red). *mupM* mutant streaks are labelled "M1" and "M2". DH5α (pJH10) streaks that were treated with thiomarinol are labelled "M". Wild-type DH5α (pJH10) that were not treated are labelled "WT pJH10". (A) DH5α (pJH10) cultures (M) were grown for 2 days in 128 µg/ml thiomarinol as a control before streaking, to ensure no alternative resistance phenotype arose from the empty vector. As expected, all M streaks grew to the same distance as the wild-type streaks. (B) M1 (circled in red) was streaked in triplicate and all streaks grew closer to the thiomarinol disk compared to wild-type, implying their putative thiomarinol resistance phenotype.

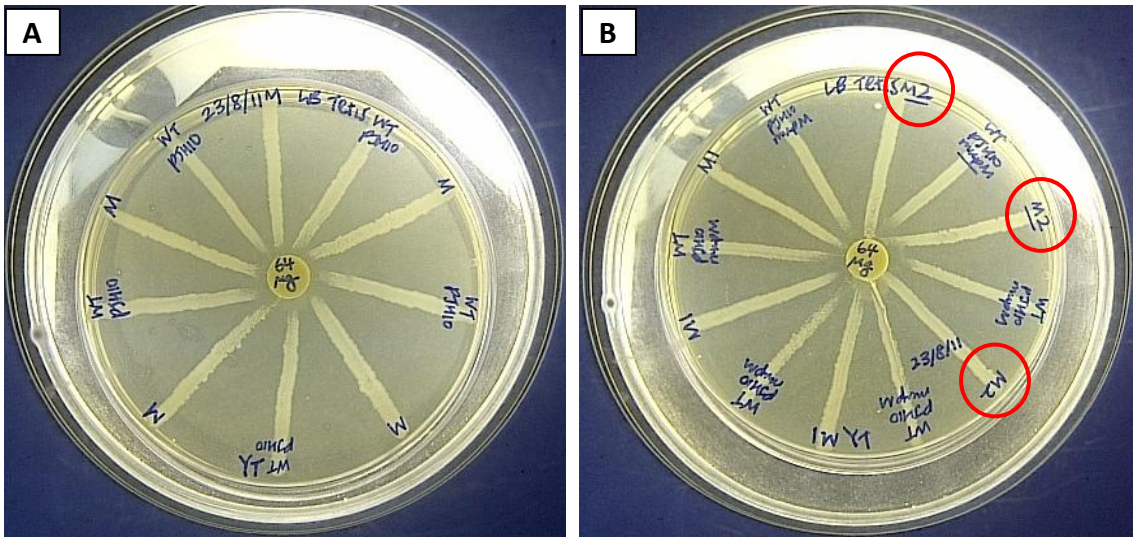

Figure 2.3. Spontaneous *mupM* mutants identified on L-agar streak tests (circled in red). (A) Control M streaks as mentioned above. (B) M2 streaks (circled in red) grew closest to the thiomarinol disk.

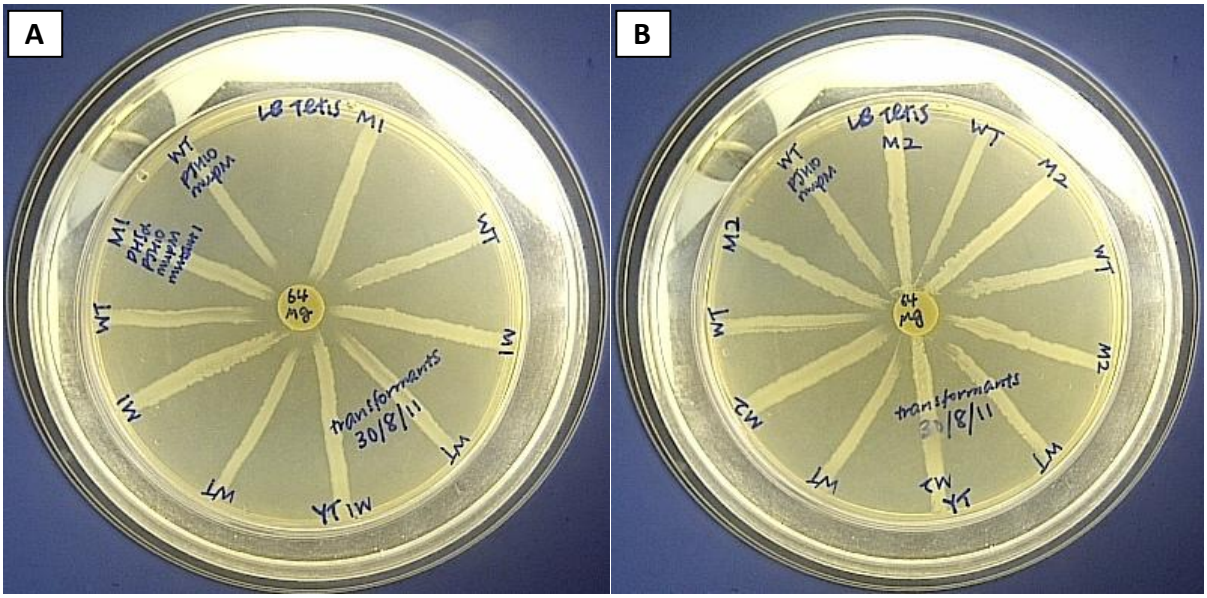

Figure 2.4. Streak tests of transformed spontaneous *mupM* mutants (A) M1 and (B) M2. M1 results were replicated 5 times and M2 results replicated 6 times.

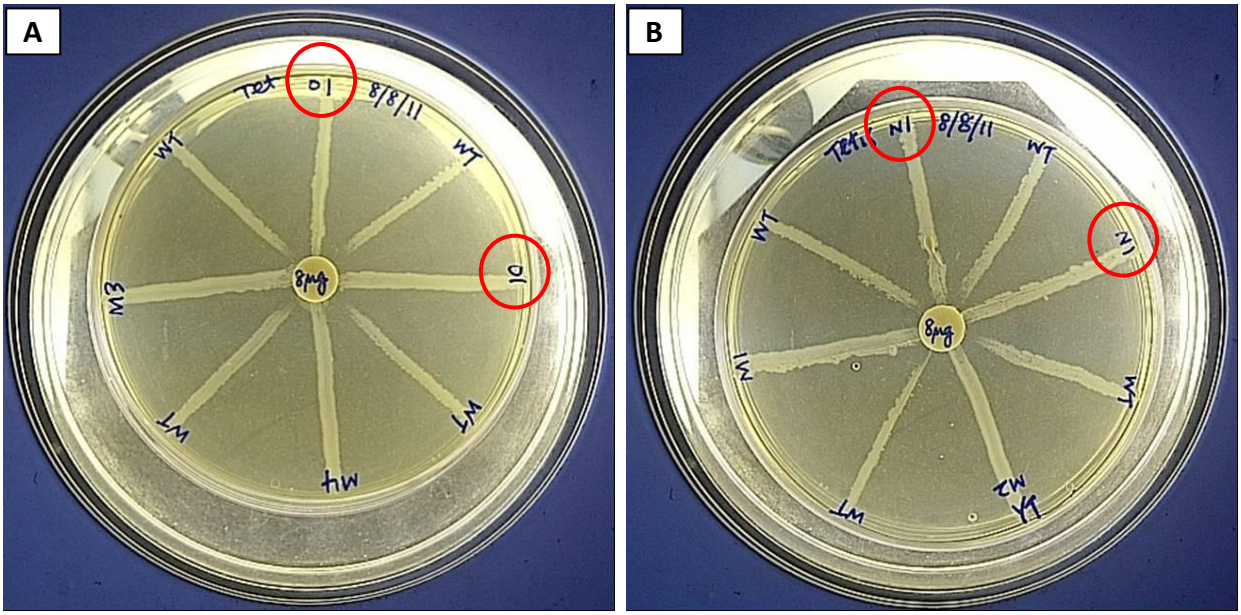

Figure 2.5. Streak tests of transformed spontaneous *mupM* mutants yielded in this study (M1-4) and from a previous study by Claire Riemer (O1 and N1). (A and B) The streak test was repeated twice for each mutant. M1, 2 and 4 showed visible thiomarinol resistance phenotype in both tests.

The newly transformed DH5α bacteria were able to grow up to the thiomarinol disks in the simple plate tests, confirming that the resistance phenotype is plasmid-mediated. The *mupM* genes from these mutant plasmids were re-cloned into new pJH10 vector to determine whether the resistance phenotype is solely due to changes in the *mupM* gene. The genes were also inserted into pUC18, a high-copy number vector for sequencing to determine what changes, if any, had occurred in *mupM*.

Streak tests were performed to determine whether the increased thiomarinol resistance conferred by the mutant plasmids is associated with the *mupM* gene. The results of these tests were disappointing; instead of the clear resistance indicated by the streaks growing close to the disc, as observed for the original *mupM* expression plasmids, none of the plasmids containing the re-cloned *mupM* gene showed any difference in growth to the wild-type thiomarinol-sensitive controls (Figure 2.6). A selection of original and cloned mutants was re-streaked against each other towards a larger 128 μg thiomarinol impregnated disc for better visual comparison but no differences were detectable (Figure 2.7).

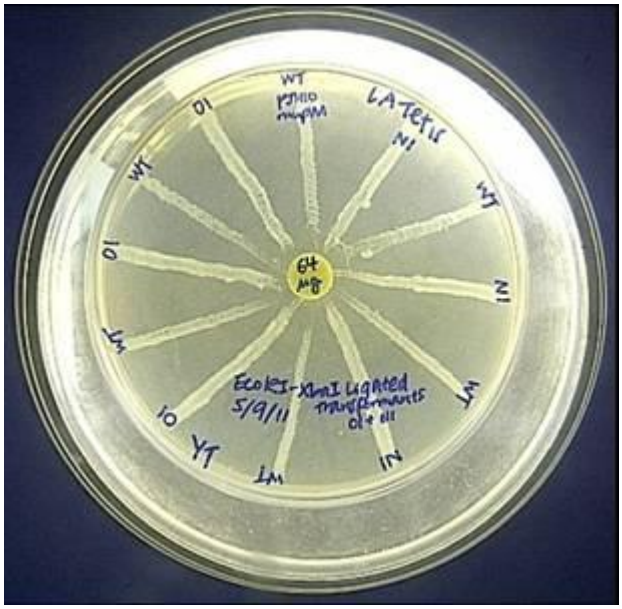

Figure 2.6. Thiomarinol resistance streak test for strains carrying pJH10 with re-cloned *mupM* fragments from mutants O1 and N1. Clones derived from O1 and N1 were replicated 3 times and wild-type streaks were all replicated 6 times.

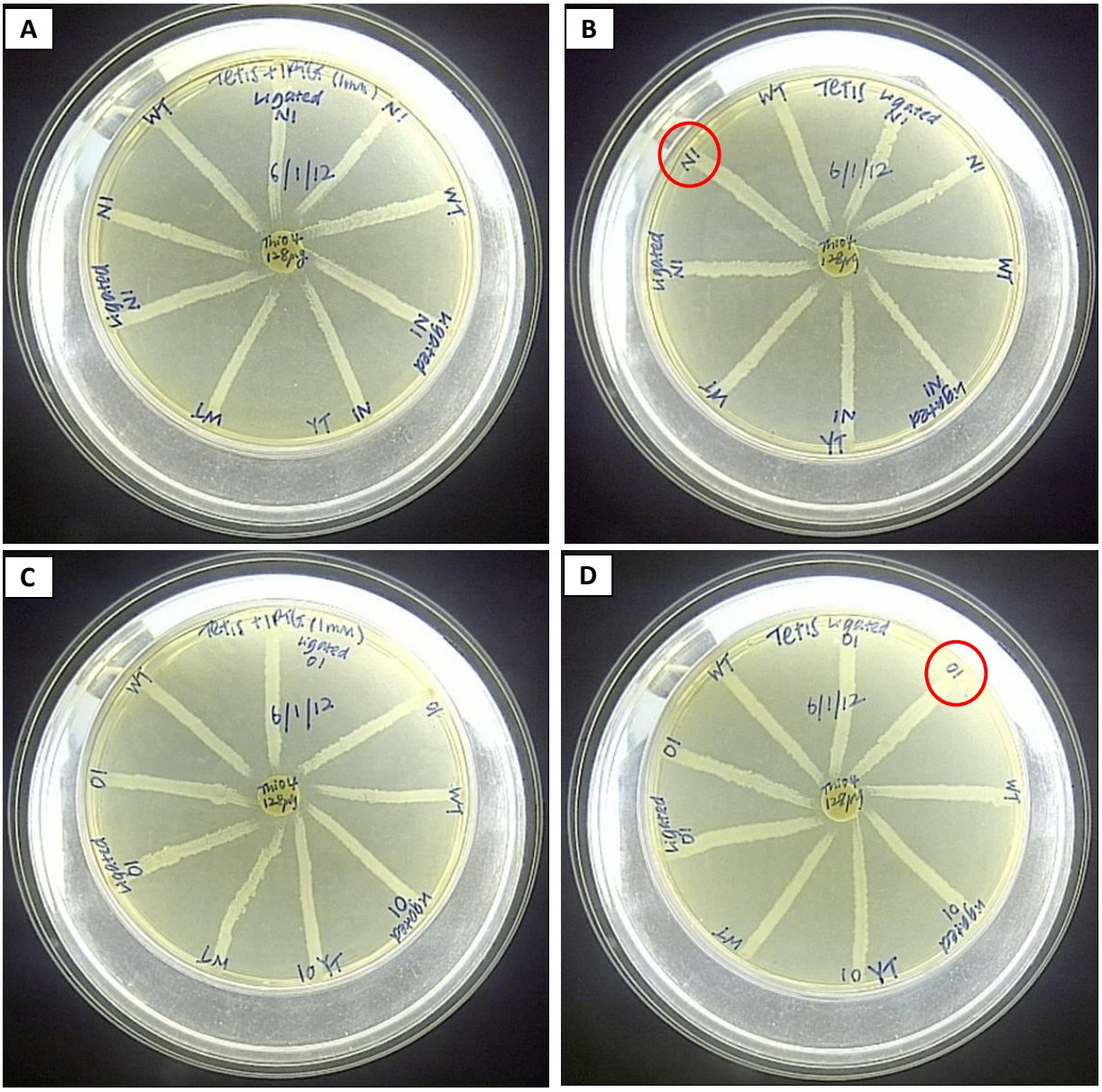

Figure 2.7. Repeat of streak tests comparing the original and re-cloned mutants *mupM* fragments against wild-type. (A and B) Repeat streak tests of N1 mutants. (C and D) Repeat streak tests of O1 mutants. Two original mutant streaks appear to display thiomarinol resistance (circled in red) but were deemed unreliable because the results are not reproduced by the other streaks on the same plates.

A selection of the mutants was sequenced using the primers designed by Claire Riemer (Table 2.3). Sequencing results initially showed two amino acid changes in the MupM mutants, where Thr400 and Val886 were both changed to alanines. However, the same two changes were identified across all potential mutants, raising suspicion that these were not true mutations but perhaps represented errors in the original sequencing. The wild-type *mupM* cloned into pUC18 in this study, as well as a stock previously prepared by Elton Stephens were both sequenced and were found to have the same sequences as the putative mutants. This therefore confirmed that these "changes" were almost certain to be due to errors in the original sequencing or deposit process and Tony Haines has included these in the list of corrections that have been made to the reference sequence file. No further possible mutations were identified in the *mupM* sequence results. (A detailed discussion on these sequencing errors can be found in Chapter 4.)

To ensure that there was no mistake concerning the resistance conferred by the mutant plasmids, an MIC test of thiomarinol was performed on the same selection of original and cloned mutants. The results indicated that bacteria carrying the original mutant plasmids had reduced susceptibility to thiomarinol than bacteria carrying the plasmids produced by re-cloning the *mupM* gene from the mutant plasmids (Figure 2.8). However, the difference in MIC is at or below the 2-fold change and therefore not considered significant.

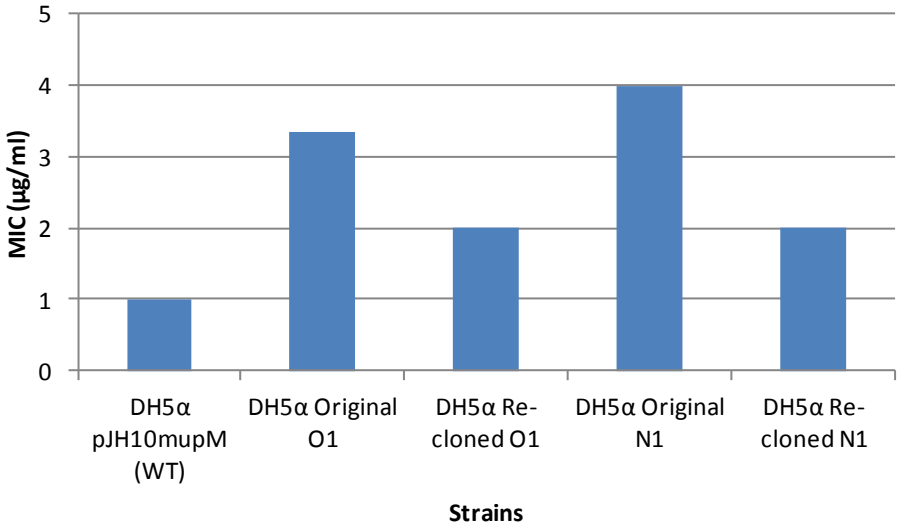

Figure 2.8. Thiomarinol MIC for DH5α (pJH10mupM) (Wild-Type) with original O1 and N1 mutants and ligated O1 and N1 clones. No IPTG induction. The MIC values are an average of samples in triplicates. The MIC of wild-type was unexpected compared to previously obtained values and repeated later in this study. The original O1 and N1 mutants are two-fold more tolerant to thiomarinol compared to the re-cloned genes.

Following observation that the level of thiomarinol resistance differed between original and cloned *mupM* mutants, it was hypothesised that this increased resistance in the original mutants was conferred by the overexpression of *mupM*, caused by the changes in the vector instead of the *mupM* gene. If increase in resistance could be achieved by simple overexpression, then it would be possible for mutation to occur in the *lac* repressor which would result in misfolding and consequent de-repression. This would be more likely than site-specific mutation(s) occurring in the *tac* promoter, with associated increase in promoter strength and *mupM* expression, because the *tac* promoter already possesses almost perfect -10 and -35 regions. When the *lac* repressor activity was screened in a preliminary study by Claire Riemer using GFP, results suggested that the *lac* repressor was not functioning properly. A wild-type and mutant pJH10mupM were individually expressed in DH5α with another high copy number plasmid based on the vector *pBR322* and carrying a *gfp* gene

under the control of a *lac* promoter. If the *lac* repressor on pJH10mupM was functioning correctly, it would also repress the *lac* promoter on *pBR322* and prevent *gfp* expression. It was observed that both wild-type and mutant pJH10mupM cells produced GFP, indicating the vector to have leaky expression, with or without IPTG induction.

To investigate this observation further, an MIC test with and without IPTG was performed using the original and cloned mutants. It was expected that the original mutants would have the same MIC values with or without IPTG because if the repressor was truly mutated, it would be unable to repress *mupM* expression in the presence or absence of IPTG. However, it was expected that in the presence of IPTG, the MIC results of the re-cloned mutants would shift up to the value of the original mutants' because IPTG would de-repress LacI and allow an increase in *mupM* expression. Results were inconclusive, with one out of the two mutants demonstrating the hypothesised shift in MIC values and the other not showing any difference (Figure 2.9).

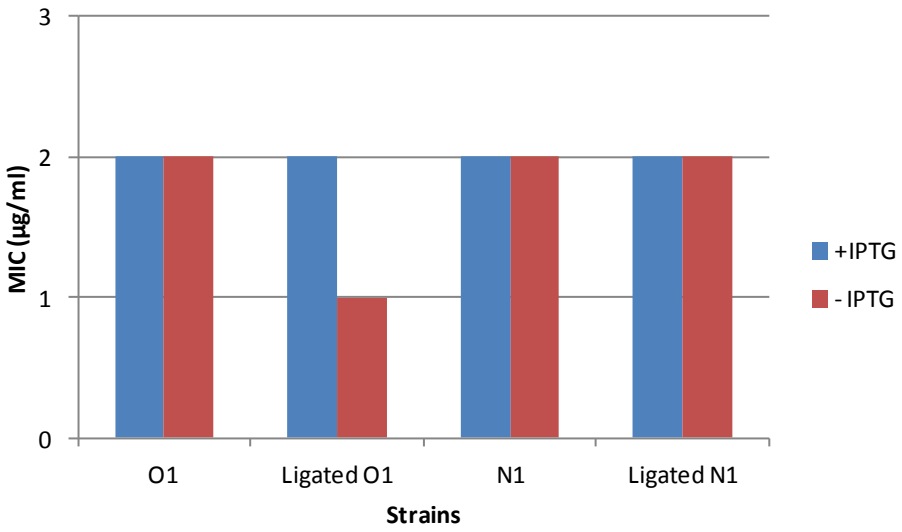

Figure 2.9. Thiomarinol MIC results comparing original *mupM* mutants with re-cloned genes with and without IPTG induction. The MIC values are an average of samples in triplicates. O1 and ligated O1 behaved as expected while N1 and its clone did not.

The unexpected low MIC value of wild-type DH5α (pJH10mupM) in Figure 2.8 was re-visited and compared to the values obtained previously (Table 2.4). The significant decrease in MIC value led to suspicions that the strain used for generating spontaneous mutants was somehow not functioning as it used to. A fresh stock was streaked onto L-agar from the -80°C stock and tested against mupirocin for their resistance phenotype. The new stock showed restored MIC values of 64 µg/ml thiomarinol, highlighting the importance in refreshing L-agar stocks of the strain – as continual re-streaking of the same stock may have caused the loss of the pJH10mupM plasmid.

2.3.3 *mupM* UV mutants

UV was chosen as a method for inducing an increased rate thiomarinol-resistance mutagenesis in the *mupM* gene. UV irradiation causes adjacent thymines to dimerise, which block DNA replication and induce error prone repair across the lesion. The *mupM* gene is rich in TT positions, despite its relatively high GC content of approximately 60 % and therefore UV mutagenesis was deemed a suitable method for generating thiomarinol-resistant mutants (Figure 2.10).

Figure 2.10. Thymine-Thymine positions in mupM DNA sequence and its corresponding amino acid residues (both highlighted in yellow). Adenine-Adenine positions have also been highlighted in blue as they correspond to Thymine-Thymine positions on the other DNA strand. EMBOSS Sixpack used to translate DNA sequence to amino acid sequence. The two highly conserved HYGH and KMSKR regions of the active site highlighted in red.

Preliminary experiments were performed by Claire Riemer to find the optimal UV dosage for generating mutants. High, intermediate and low UV intensity sources were used (using a gel imager, UV lightbox and gel cutting board respectively) and the cell death in 1 ml L-broth cultures monitored at 30 second intervals for up 12 minutes. The UV lightbox was deemed most appropriate for generating mutants (with 50% death rate at 10 minutes irradiation). Due to time constraints, no further tests were performed on the mutants.

The protocol outlined in the Methods for generating UV mutants was thus based on Claire Riemer's preliminary results. Sampling was altered from 30 second intervals to 60, reducing the number of samples handled at the increased irradiation period of 14 minutes. Confluent growth was observed at up to 3 minutes irradiation and decreasing numbers of visible single colonies between 4 to 14 minutes. Single colonies were chosen from time intervals of 8 minutes and above and tested for thiomarinol resistance phenotype by streak testing.

Unfortunately, the same results were observed with the *mupM* mutants irradiated with UV as with the spontaneous mutants (Figure 2.11; Figure 2.12). Although the original mutants from the culture irradiated with UV displayed thiomarinol resistance in the streak test, sequencing results indicated no changes to be found in the *mupM* gene. The UV mutants were not checked for plasmid and gene-mediated resistance phenotype as a time saving exercise. Instead, the potential mutant *mupM* genes were directly cloned into pUC18 vectors and sequenced.

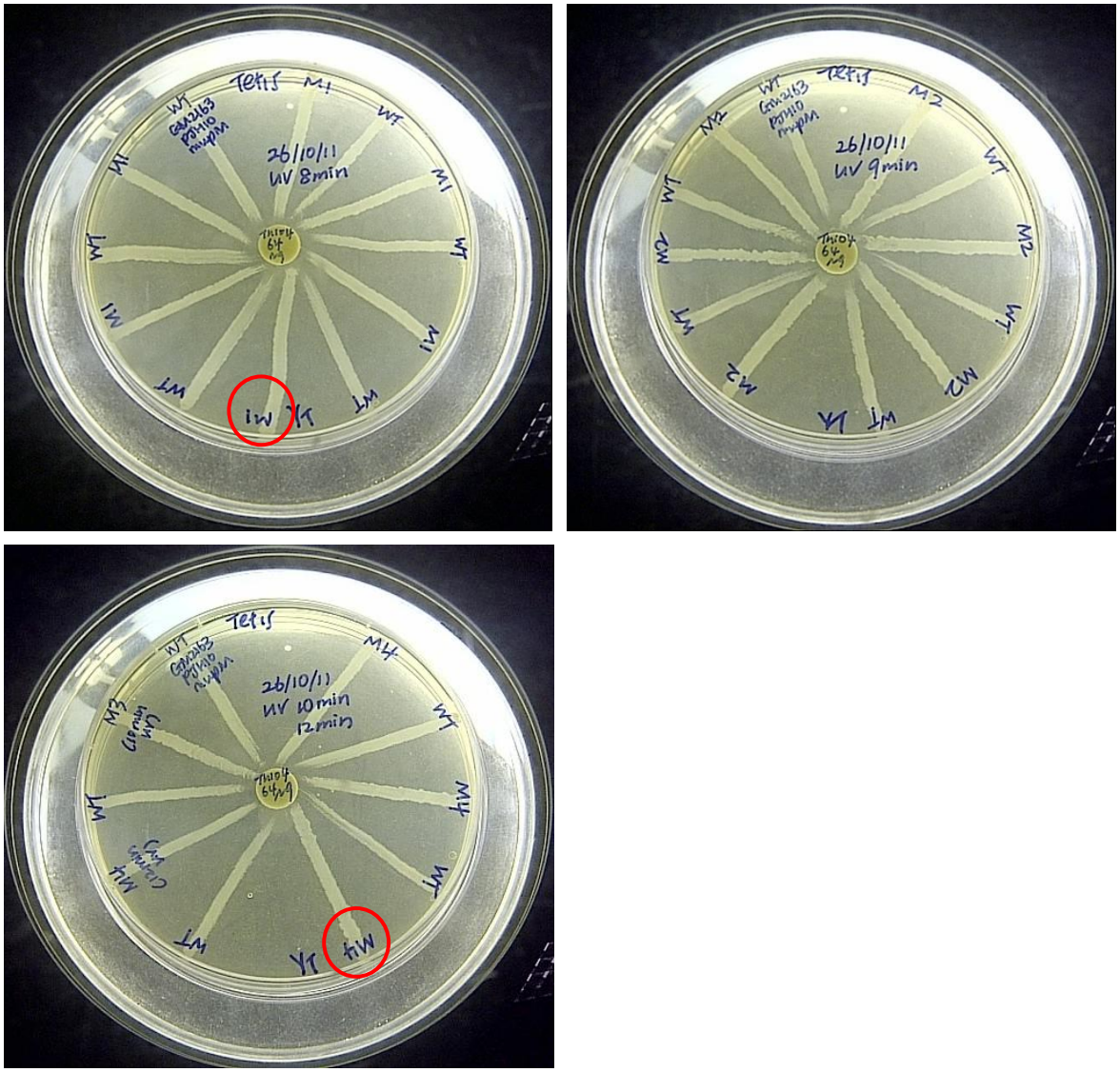

Figure 2.11. Streak tests of potential mutants obtained from UV mutagenesis Trial 1. M1 taken at 8 min UV interval and M4 taken at 12 min UV interval were selected for sequencing (circled in red).

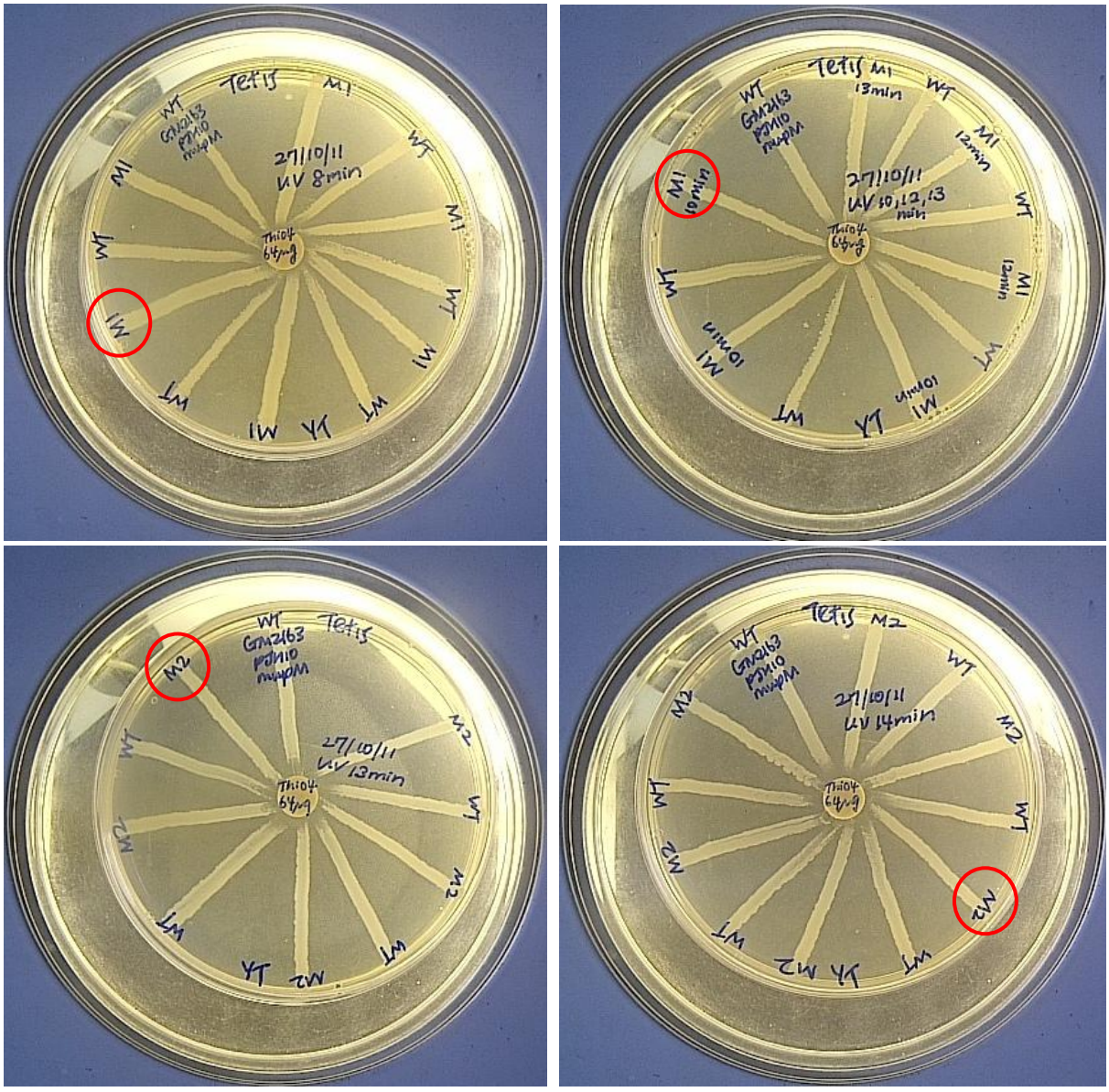

Figure 2.12. Streak tests of potential mutants yielded from UV mutagenesis. M1 taken at 8 min and 10 min UV intervals and M2 taken at 13 min and 14 min UV intervals were selected for sequencing (circled in red).

2.4 Discussion

This study aimed to firstly identify the MIC of thiomarinol against wild-type DH5α carrying the empty pJH10 vector, pJH10mupM, pJH10mupA and pJH10tmlM. Secondly, it attempted to generate thiomarinol-resistant *mupM* mutants by spontaneous and UV mutagenesis. By sequencing these mutants, it was hoped that the amino acids responsible for this resistance phenotype would be highlighted and elucidate the site of pyrrothine binding for increased binding affinity and a mechanism for thiomarinol potency.

2.4.1 Assessing MIC method for mutant characterisation

Using two different inoculum sizes for the MIC test has shown that cell density affects overall MICs. Relatively, a higher cell density would require a higher concentration of thiomarinol to achieve inhibition of growth. Therefore, future MIC values taken from various studies and literature should only be compared once their inoculum sizes have been determined to be the same. In this study, the MIC values identified from the higher inoculum (recommended by BSAC) was selected over the lower inoculum, as following a standard would allow future comparisons with other MIC values.

2.4.2 Thiomarinol resistance conferred by *mupM* overexpression

The hypothesis that thiomarinol tolerance can be conferred by the overexpression of *mupM* is consistent with the data but needs further tests to confirm whether the mutations are indeed in the *tac* promoter or *lac* repressor. One of the methods to consider is using PCR to amplify the promoter and repressor regions and to sequence them for identification of any mutations. Other methods would be to measure the gene expression of *mupM* by

measuring the level of *mupM* mRNA by RT-PCR, Northern blotting or using a reporter gene to measure *mupM* expression.

Alternatively, a simpler method would have been to include a key control DH5α strain expressing its native *ileS* in pJH10 in the initial MIC tests. If the MIC of thiomarinol increased against this control strain compared to DH5α pJH10, it would suggest that overexpression of IleS is a mechanism of thiomarinol resistance.

Induced antibiotic resistance caused by overexpression of the target is a well-documented phenomenon, as discussed in Chapter 1. A recent study found sub-lethal concentrations of methionyl-tRNA synthetase inhibitors to induce resistance in the protozoan *Trypanosoma brucei* by overexpression of the target (Ranade *et al*., 2013). Overexpression was shown by the higher levels of MetRS mRNA on Northern blots and increased gene expression on Southern blots. Interestingly, overexpression came at a fitness cost to the parasites and no mutations were observed on the MetRS enzyme – similar to the results obtained in this study, although fitness cost was not considered. It will be of great interest to continue the work carried out in this study to confirm whether thiomarinol resistance is truly conferred by overexpression of the target enzyme.

2.4.3 Spontaneous and UV mutants may be difficult to obtain

Results from this study indicate thiomarinol resistance may not arise frequently by spontaneous and UV mutagenesis causing changes in the structural gene. In terms of resistance developing in the clinical setting after thiomarinol usage, this is an advantage, as drugs that yield resistant microorganisms too quickly have a limited shelf-life. However, the mutagenesis method needs to be revised to prove that resistance is difficult to obtain.

Investigation of the available literature suggests that sub-inhibitory (SI) concentrations of antibiotics are effective in selecting for antibiotic tolerant mutants (Baquero, 2001; Girgis *et al*., 2009). This would make sense, as in the environment and even in clinical settings, microorganisms are constantly subjected to SI concentrations of various bioactive compounds produced by other living organisms. In the clinical context, antibiotics that are administered to patients enter the body and form a concentration gradient, before reaching the effective dose. At times, this effective dose is never reached, with patients neglecting to finish their prescribed course or limitations in the drugs to access certain tissues (Kohanski *et al*., 2010). Clinical resistance is thought to develop in the same gradual manner, with some bacteria surviving the initial antibiotic exposure and allowing the population to accumulate enough low level mutations that lead to higher tolerance and finally, clinically significant high level resistance (Baquero, 2001; Drlica and Zhao, 2007). Low level selection pressure appears to be key in allowing changes that are beneficial but low in fitness cost.

However, SI concentrations of bactericidal antibiotics have been shown to cause a wide range of responses other than resistance to that particular selection pressure. Kohanski *et al*. (2010) found that sub-lethal levels of antibiotics can act as mutagens and affect a variety of drug targets, causing multidrug resistance and not always including resistance against the antibiotics used. Other studies have observed more general cellular responses such as the production of reactive oxygen species (ROS) that directly damage DNA and cause mutation (Demple and Harrison, 1994; Freiberg *et al*., 2004; Imlay and Linn, 1988; Kohanski *et al*., 2010). The literature highlights the importance and advantages of understanding SI

antibiotic concentrations in relation to not only tolerance and resistance but also to the effect they have on whole genomes.

A popular approach to understanding the mode of action of antibiotics (and how organisms confer resistance) is by profiling whole genome expression at an mRNA and/or protein level (Brazas and Hancock, 2005; Freiberg *et al*., 2004). For a snapshot of a bacterial transcriptome, DNA microarray is commonly used. Microarray surfaces (such as chips or beads) are fixed with DNA probes for every open reading frame of the organism of interest, so for the purpose of this study, they could be set up from *P. fluorescens*. The microorganism can then be separately grown at sub-inhibitory concentrations of thiomarinol and its mRNA purified to generate cDNA using reverse transcriptase. The cDNA is then labelled, such as with fluorescence dye, and hybridised to the microarray. The fluorescence or signal detected can be analysed to map out the whole genome response of *P. fluorescens* to thiomarinol, including any changes in expression of *mupM*.

For proteomic analysis, two-dimensional gel electrophoresis (2-DE) is commonly used to separate proteins, first by their isoelectric point (i.e. the pH at which the protein has no net electrical charge) and second by their protein mass. The first step, called isoelectric focusing (IEF), utilises a pH gradient to separate proteins. An electric potential is applied across the gel and proteins accumulate at their isoelectric point. In the second step, the proteins are denatured and bound to negatively charged SDS molecules and separated by application of again an electric potential by their mass but at a 90 degree angle from the first step. The gel is then stained either by silver or Coomassie Brilliant Blue. Therefore, a proteomic analysis of *P. fluorescens* can be performed to also determine whether MupM is

over-expressed during thiomarinol exposure and whether any other proteins are up-regulated for resistance/tolerance to the antibiotic.

It would be of interest to compare various bacterial transcriptome and proteome profiles in response to thiomarinol and mupirocin, as these techniques may elucidate whether any targets other than IleS are expressed and/or upregulated by thiomarinol but perhaps not mupirocin. This technique could also, in theory, be used to elucidate the cause of the loss in thiomarinol resistance phenotype when mutant *mupM* genes in this study were cloned into fresh pJH10 vectors. The transcriptome analysis may elucidate whether this was due to a defective LacI in the construct or perhaps other changes in the host DH5α bacterial gene expression.

In this study, thiomarinol concentrations of 32, 64 and 128 µg/ml were used in attempt to yield resistant mutants. The lower concentrations were initially tested but did not always yield growth in the cultures after 2 days of incubation. The highest concentration, on the other hand, guaranteed growth after 2 days and was chosen as the set concentration for yielding spontaneous mutants. However, 128 µg/ml is approximately 2 to 4-fold greater in concentration than the MIC against DH5α (pJH10mupM) (32-64 µg/ml). It is plausible that many of the cultures that grew in this high thiomarinol concentration for two days but failed to grow at subsequent inoculation onto L-agar with the thiomarinol impregnated discs were persister cells. Persisters were first noted by Bigger in 1944 and have since then been linked to high tolerance levels against antibiotics, although they are non-replicating, not resistant to antibiotics and do not exhibit high MIC values (Keren *et al*., 2004; Kester and Fortune, 2014). This, however, does not provide an explanation for the mutants that maintained their

resistance phenotype in the original streak tests but not when the *mupM* genes were cloned into fresh pJH10 vectors.

This study's use of high thiomarinol concentrations (> MIC) has failed to generate true *mupM* mutants. Although the use of SI concentrations appears to generate genome-wide mutations other than solely those related to the primary target(s), it is undeniable that the SI methodology also yields true resistant mutants. SI levels of thiomarinol may be the better choice for selecting mutations in *mupM*, with gradual incremental increases in the antibiotic concentration as low tolerance accumulates in the population (Ranade *et al*., 2013). Alternatively, direct approaches such as mutagenic PCR could also be beneficial and time efficient, and allow mutations to be focused on only the structural gene (Cadwell and Joyce, 1994).

Other methods to consider are using pre-existing mupirocin resistant mutants to derive thiomarinol resistant mutants or changing the heterologous host of the plasmids in this study from *E. coli* to *S. aureus*. Mupirocin resistant *S. aureus* IleS mutants were spontaneously selected by Hurdle *et al.* (2004) using four times the MIC of mupirocin. These mutants could have been tested for thiomarinol resistance and/or used as a template for selecting thiomarinol resistant mutants by passaging with gradually increasing antibiotic concentrations. *S. aureus* may have also been the better host for the plasmids used in this study instead of *E. coli*, as MIC tests show the former to be more susceptible to thiomarinol than the latter (Table 1.5). The difference in susceptibility is yet to be understood but more efficient efflux of the antibiotic in *E. coli* may play a role in its reduced susceptibility.

Therefore, using *S. aureus* instead of *E. coli* may avoid the possible complications of efflux and show clearer thiomarinol resistance phenotypes of the mutated IleSs.

In summary, this study has highlighted the importance of selecting the optimal inoculum size and antibiotic concentration for generating antibiotic resistant mutants. It would be of interest to optimise the methodology with the above suggestions and to elucidate the sites of MupM that are important for its mupirocin resistance phenotype, as well as its sensitivity against thiomarinol. Once optimised using *mupM*, it would also be of interest to resume the same work on *mupA* as an additional means to understand if the sites for resistance and susceptibility is conserved across these mupirocin-resistant IleSs.

CHAPTER 3

3 IDENTIFYING AMINO ACID RESIDUES OF INTEREST ON MUPM AND TMLM USING STRUCTURAL MODELLING

3.1 Introduction

Thiomarinols (A-G) are a group of hybrid polyketide antibiotics produced by the marine bacterium *Pseudoalteromonas rava* sp. nov. SANK 73390. As discussed in Chapter 1, they share structural similarity to mupirocin (or pseudomonic acid A) but have an additional pyrrothine moiety. While mupirocin is widely used in hospitals, thiomarinol is not clinically available but has demonstrated activity against a range of Gram-positive and negative organisms (Shiozawa *et al*., 1993). Understanding what potentiates the activity of thiomarinol compared to mupirocin is of interest, as it may elucidate ways to synthesise better analogues of mupirocin and to counter the rising trend of mupirocin resistance in the clinical setting.

In this study, the mode of action of thiomarinol is investigated based on what is already known about mupirocin. The target of mupirocin is the isoleucyl-tRNA synthetase (IleS), a Class I aminoacyl-tRNA synthetase characterised by its Rossman fold catalytic domain and conserved HIGH and KMSKS signature motifs. Structural studies of *Staphylococcus aureus* mupirocin-sensitive IleS complexed with mupirocin has revealed that the antibiotic targets this catalytic domain; as discussed in Chapter 1, the C14 end of the monic acid imitates the isoleucine side chain, the pyran ring sits where ATP normally binds and the 9-hydroxynonanoic acid stabilizes the entire complex via the

carboxylate tail binding to the second lysine of the KMSKS motif (Nakama *et al*., 2001; Silvian *et al.*, 1999).

When organisms such as *S. aureus* and *Escherichia coli* gain a single amino acid change in the Rossman fold (valine to phenylalanine V588F and leucine to phenylalanine L594F respectively), they develop low level mupirocin resistance (Antonio *et al*., 2002; Yanagisawa *et al*., 1994). With the Rossman fold altered, the 9-hydroxynonanoic acid of mupirocin can no longer bind and stabilise the antibiotic, allowing the organism to gain low level resistance at a low fitness cost. On the contrary, high level mupirocin resistance has been observed to be conferred by the presence of IleSs that are similar to the eukaryotic enzymes, likely acquired by horizontal gene transfer. For example, the mupirocin-producing strain *Pseudomonas fluorescens* has been shown to express two different chromosomal IleSs, one of which is similar to eukaryotic IleSs called MupM (El-Sayed *et al*., 2003; Yanagisawa and Kawakami, 2003).

Thiomarinol is also proposed to target IleS because of its structural similarity to mupirocin but also from observation that *E. coli* becomes highly thiomarinol resistant when it expresses the thiomarinol resistant IleS gene *tmlM* from *P. rava* (Fukuda *et al*., 2011). The pyrrothine moiety is of particular interest, as a previous study observed marinolic acid (thiomarinol without the pyrrothine moiety) to be less active against *S. aureus* than mupirocin, indicating pyrrothine to be important for the increased potency of thiomarinol (Fukuda *et al*., 2011). Although yet to be determined experimentally, structural similarity between the two antibiotics suggests that thiomarinol should bind to IleS in the same orientation as mupirocin.

Based on the above proposal, this study homology modelled MupM and TmlM using the solved crystal structure of mupirocin-sensitive *S. aureus* IleS complexed with mupirocin (PDB: 1QU2) as a template. The aim was to use these models to investigate the structural basis for thiomarinol's potency via the hypothesised enhanced binding affinity. In addition, the residues on the active site that may constitute the resistance phenotype of TmlM against thiomarinol was also investigated.

3.2 Materials and Methods

3.2.1 Homology Modelling MupM, MupA and TmlM

Template structures were selected by performing BLAST searches of MupM, MupA and TmlM sequences individually against solved protein structures in the PDB, using the web interface at the NCBI with default settings (http://www.ncbi.nlm.nih.gov/). The best template candidate was selected by choosing the structure with the lowest E-value, which represents the number of PDB hits expected by chance. The template structure was also required to have a high resolution of ≤ 2.5Å. An IleS structure from *S. aureus* complexed with isoleucyl-tRNA ($tRNA^{Ile}$) and mupirocin (PDB: 1QU2) was chosen as the best template for all three proteins. The template, query (MupM, MupA and TmlM) and homologous sequences were automatically aligned using ClustalX (Larkin *et al*., 2007) and further aligned manually using SeaView (Gouy *et al*., 2010). The secondary structures of the query sequences were obtained by the DSSP algorithm and taken into account during manual alignment (Kabsch and Sander, 1983).

Once the chosen templates were deemed appropriate and the sequences all aligned, the alignments and structure were read by Modeller (Eswar *et al*., 2006) and 25 models

generated for evaluation. The best model was chosen based on its discrete optimised protein energy (DOPE) (Shen and Sali, 2006) and genetic algorithm (GA) score (John and Sali, 2003; Melo *et al.*, 2002). The DOPE score indicates the threading potential or the energetic measure between two amino acids next to each other and the more negative the value, the better. The GA score assesses the overall fold quality of the model and a value closer to 1 is deemed more native-like than a value closer to 0. Therefore, the model with the lowest DOPE and highest GA score was chosen.

3.2.2 Active site characterisation

The Builder function on PyMOL, Version 1.7 was used to modify the mupirocin structure from the PDB structure 1QU2 by adding the pyrrothine moiety to generate a thiomarinol A structure. UCSF Chimera (Pettersen *et al*., 2004) was then used to energy-minimise the newly drawn thiomarinol structure (complexed in IleS) using the Minimise Structure function (with default Amber and Antechamber force field parameters). This function is intended for cleaning up small molecule structures and improves localised interactions within larger systems; hence it is appropriate for resolving minimal distortions in the drawn pyrrothine ring.

Pocket v.2 (Chen and Lai, 2006) was used to derive pharmacophore models (that is, key interaction sites) of 1QU2, MupM and TmlM respectively. Mupirocin and thiomarinol were used separately as the known ligand for each of the three structures, giving six results in total. The binding features of each protein were then compared against each other.

3.2.3 Identifying amino acid residues of interest

The LIGPLOT programme (Wallace *et al*., 1995) was used as the starting point for identifying amino acids that may be of interest in protein-ligand interactions of 1QU2. This programme automatically generates schematic 2D diagrams of protein-ligand complexes and highlights the intermolecular interactions which include hydrogen bonds, hydrophobic interactions and atom accessibility to solvent (Wallace *et al*., 1995). Any interesting residues highlighted by LIGPLOT were further studied on the 3D structural models.

The Evolutionary Trace (ET) programme (Lichtarge *et al*., 1996) was also utilised to identify functional amino acid residues. This programme was developed to provide an alternative to experimental mutagenesis for characterising protein functional sites. It analyses evolutionary patterns in amino acid sequences, i.e. their conservation within clades, and ranks every residue in the query protein's sequence by their likely importance for structure and function. The ET results, in conjunction with the LIGPLOT results allowed better analysis of the amino acid residues of interest.

Finally, PyMOL was used to identify residues within an 8 Å radius of the mupirocin ligand. Residues of potential interest were selected manually by comparing the residues between 1QU2, MupM and TmlM.

3.3 Results

3.3.1 Pharmacophore models of 1QU2, MupM and TmlM

Pocket v.2 relies on a known ligand in the query protein to help with the identification of crucial features in the active site (Chen and Lai, 2006). Since 1QU2

complexed with mupirocin was used as the template during the homology modelling of MupM and TmlM, mupirocin was used as the ligand of choice for the running of Pocket v.2 for the latter proteins. To ensure that the results from the programme are not sensitive to the choice of ligand used, i.e. the computer algorithm and its implementation are robust, MupM was run twice with mupirocin and thiomarinol individually (Figure 3.1). As hoped, the models generated were similar, indicating that the use of mupirocin as the known ligand should not influence the results (Figure 3.2).

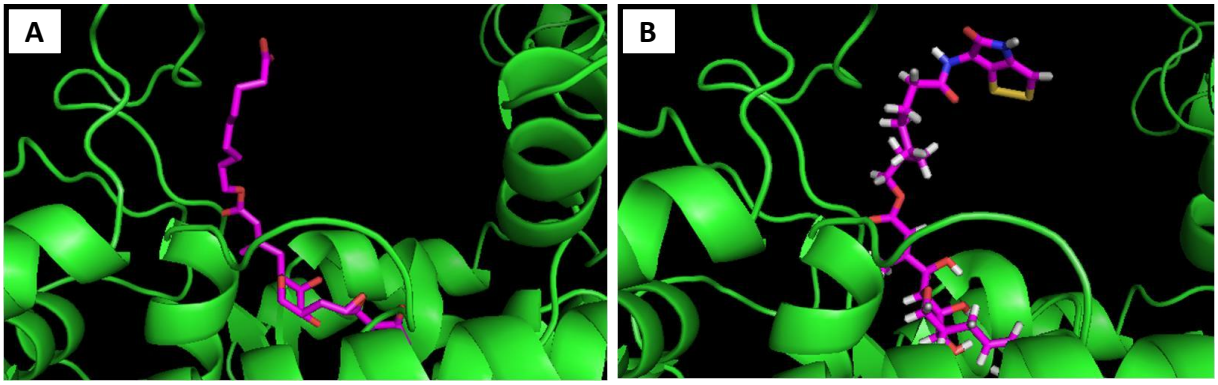

MupM with mupirocin MupM with thiomarinol

Figure 3.1. Close-up of MupM structure complexed with (A) mupirocin from PDB structure 1QU2 and (B) thiomarinol generated using PyMOL. The thiomarinol structure is sub-optimal with no reliable parameters available to describe the peptide-linked pyrrothine moiety. It was intended for geometric speculation as to where the pyrrothine moiety may interact with other residues on the protein.

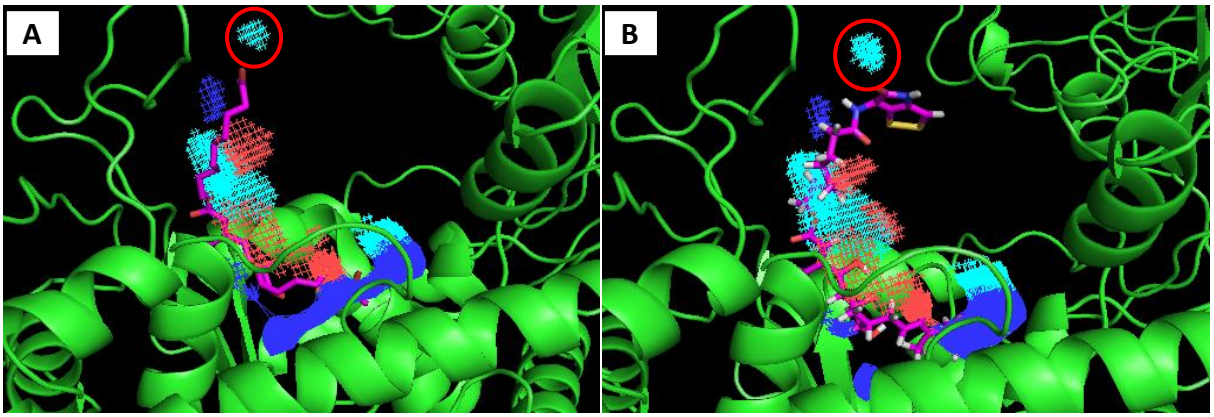

MupM with mupirocin MupM with thiomarinol

Figure 3.2. Pocket v.2 results of MupM complexed with (A) mupirocin and (B) thiomarinol. Both pharmacophore models are similar to each other, including the hydrophobic patch highlighted by the red circles. The three differently coloured areas represent the following: light blue = hydrophobic sites; dark blue = hydrogen-bond donor sites; red = hydrogen-bond acceptor sites. All these sites are created by single or multiple amino acid residues on the query enzyme (in this case MupM). (B) Thiomarinol is depicted with hydrogens while mupirocin is not. This is because the hydrogens were placed on the sub-optimal thiomarinol structure using PyMOL in order to minimise the structure on UCSF Chimera.

The pharmacophore profiles of mupirocin-sensitive IleS 1QU2 and mupirocin-resistant MupM were more similar to each other than to that of thiomarinol-resistant TmlM (Figure 3.3). TmlM appears to be much more hydrophobic around the fatty acid binding site. General similarity of MupM to 1QU2 was supported by the results of running a BLAST analysis with TmlM, which showed its closer homology to mammalian IleS from rat, mouse and human than MupM, which showed closer homology to bacterial IleS (Figure 3.4).

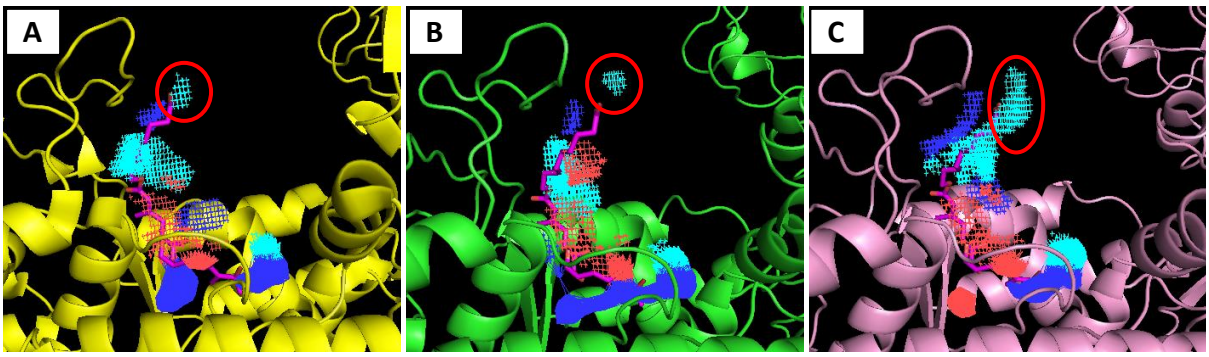

1QU2 with mupirocin | MupM with mupirocin | TmlM with mupirocin

Figure 3.3. Pocket v.2 results of (A) 1QU2, (B) MupM and (C) TmlM all complexed with mupirocin (in purple). The hydrophobic patches of interest are highlighted by the red circles. Colour scheme as described above.

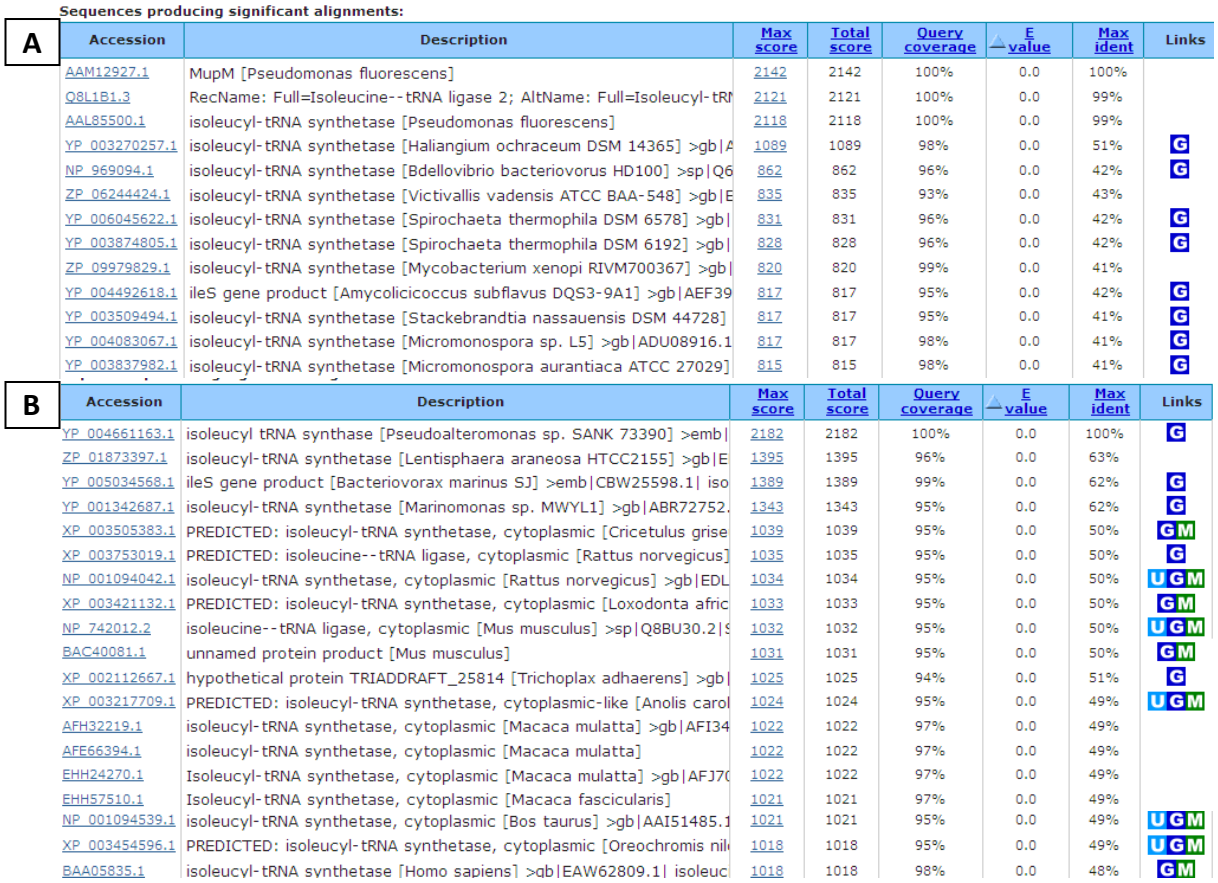

Sequences producing significant alignments:

A

Accession	Description	Max score	Total score	Query coverage	E value	Max ident	Links
AAM12927.1	MupM [Pseudomonas fluorescens]	2142	2142	100%	0.0	100%	
Q8L1B1.3	RecName: Full=Isoleucine--tRNA ligase 2; AltName: Full=Isoleucyl-tR	2121	2121	100%	0.0	99%	
AAL85500.1	isoleucyl-tRNA synthetase [Pseudomonas fluorescens]	2118	2118	100%	0.0	99%	
YP_003270257.1	isoleucyl-tRNA synthetase [Haliangium ochraceum DSM 14365] >gb|A	1089	1089	98%	0.0	51%	G
NP_969094.1	isoleucyl-tRNA synthetase [Bdellovibrio bacteriovorus HD100] >sp|Q6	862	862	96%	0.0	42%	G
ZP_06244424.1	isoleucyl-tRNA synthetase [Victivallis vadensis ATCC BAA-548] >gb|E	835	835	93%	0.0	43%	
YP_006045622.1	isoleucyl-tRNA synthetase [Spirochaeta thermophila DSM 6578] >gb|	831	831	96%	0.0	42%	G
YP_003874805.1	isoleucyl-tRNA synthetase [Spirochaeta thermophila DSM 6192] >gb|	828	828	96%	0.0	42%	G
ZP_09979829.1	isoleucyl-tRNA synthetase [Mycobacterium xenopi RIVM700367] >gb|	820	820	99%	0.0	41%	
YP_004492618.1	ileS gene product [Amycolicicoccus subflavus DQS3-9A1] >gb|AEF39	817	817	95%	0.0	42%	G
YP_003509494.1	isoleucyl-tRNA synthetase [Stackebrandtia nassauensis DSM 44728]	817	817	95%	0.0	41%	G
YP_004083067.1	isoleucyl-tRNA synthetase [Micromonospora sp. L5] >gb|ADU08916.1	817	817	98%	0.0	41%	G
YP_003837982.1	isoleucyl-tRNA synthetase [Micromonospora aurantiaca ATCC 27029]	815	815	98%	0.0	41%	G

B

Accession	Description	Max score	Total score	Query coverage	E value	Max ident	Links
YP_004661163.1	isoleucyl tRNA synthase [Pseudoalteromonas sp. SANK 73390] >emb|	2182	2182	100%	0.0	100%	G
ZP_01873397.1	isoleucyl-tRNA synthetase [Lentisphaera araneosa HTCC2155] >gb|E	1395	1395	96%	0.0	63%	
YP_005034568.1	ileS gene product [Bacteriovorax marinus SJ] >emb|CBW25598.1| iso	1389	1389	99%	0.0	62%	G
YP_001342687.1	isoleucyl-tRNA synthetase [Marinomonas sp. MWYL1] >gb|ABR72752.	1343	1343	95%	0.0	62%	G
XP_003505383.1	PREDICTED: isoleucyl-tRNA synthetase, cytoplasmic [Cricetulus grise	1039	1039	95%	0.0	50%	GM
XP_003753019.1	PREDICTED: isoleucine--tRNA ligase, cytoplasmic [Rattus norvegicus]	1035	1035	95%	0.0	50%	G
NP_001094042.1	isoleucyl-tRNA synthetase, cytoplasmic [Rattus norvegicus] >gb|EDL	1034	1034	95%	0.0	50%	UGM
XP_003421132.1	PREDICTED: isoleucyl-tRNA synthetase, cytoplasmic [Loxodonta afric	1033	1033	95%	0.0	50%	GM
NP_742012.2	isoleucine--tRNA ligase, cytoplasmic [Mus musculus] >sp|Q8BU30.2|S	1032	1032	95%	0.0	50%	UGM
BAC40081.1	unnamed protein product [Mus musculus]	1031	1031	95%	0.0	50%	GM
XP_002112667.1	hypothetical protein TRIADDRAFT_25814 [Trichoplax adhaerens] >gb|	1025	1025	94%	0.0	51%	G
XP_003217709.1	PREDICTED: isoleucyl-tRNA synthetase, cytoplasmic-like [Anolis carol	1024	1024	95%	0.0	49%	UGM
AFH32219.1	isoleucyl-tRNA synthetase, cytoplasmic [Macaca mulatta] >gb|AFI34	1022	1022	97%	0.0	49%	
AFE66394.1	isoleucyl-tRNA synthetase, cytoplasmic [Macaca mulatta]	1022	1022	97%	0.0	49%	
EHH24270.1	Isoleucyl-tRNA synthetase, cytoplasmic [Macaca mulatta] >gb|AFJ7(	1022	1022	97%	0.0	49%	
EHH57510.1	Isoleucyl-tRNA synthetase, cytoplasmic [Macaca fascicularis]	1021	1021	97%	0.0	49%	
NP_001094539.1	isoleucyl-tRNA synthetase, cytoplasmic [Bos taurus] >gb|AAI51485.1	1021	1021	95%	0.0	49%	UGM
XP_003454596.1	PREDICTED: isoleucyl-tRNA synthetase, cytoplasmic [Oreochromis nil	1018	1018	95%	0.0	49%	UGM
BAA05835.1	isoleucyl-tRNA synthetase [Homo sapiens] >gb|EAW62809.1| isoleuc	1018	1018	98%	0.0	48%	GM

Figure 3.4. Snapshot of BLAST results of (A) MupM and (B) TmlM.

The most striking characteristic of these profiles was the hydrophobic patch at the 9-hydroxynonanoic tail of mupirocin for all three IleSs. This hydrophobic region appears geometrically in a place where the pyrrothine moiety can interact with the KMSKS loop (Figure 3.2 and Figure 3.3). The two amino acid residues responsible for this hydrophobicity were the aliphatic parts of lysine and arginine in MupM and TmlM, and only lysine in 1QU2 (Figure 3.5). This lysine is the second lysine in the KMSKS motif in Class I aminoacyl-tRNA synthetases and associated with ATP hydrolysis and/or tRNA stabilisation in *E. coli* IleS (Baouz *et al*., 2009) (Figure 3.6).

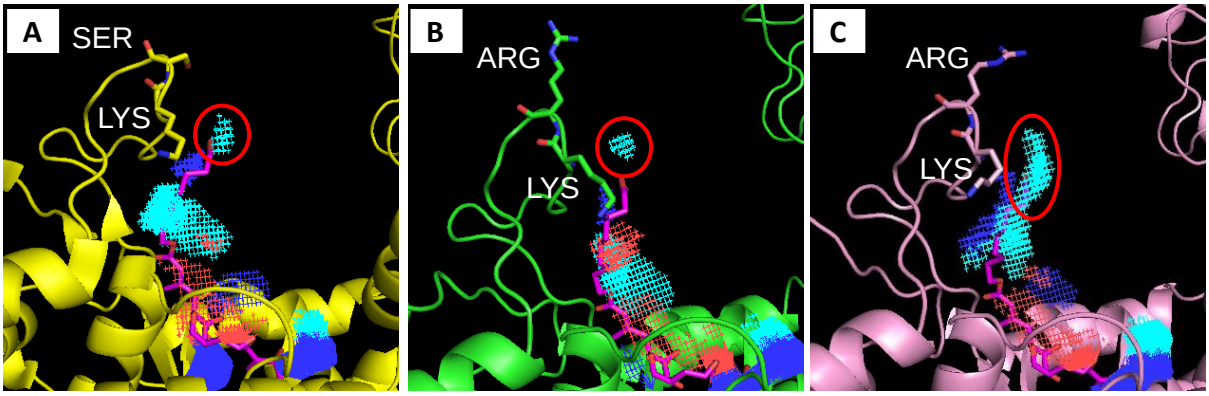

1QU2 with mupirocin | MupM with mupirocin | TmlM with mupirocin

Figure 3.5. The aliphatic chains of lysine and/or arginine that are responsible for the hydrophobic patches (highlighted in red circles) in (A) 1QU2, (B) MupM and (C) TmlM. Colour scheme as described above.

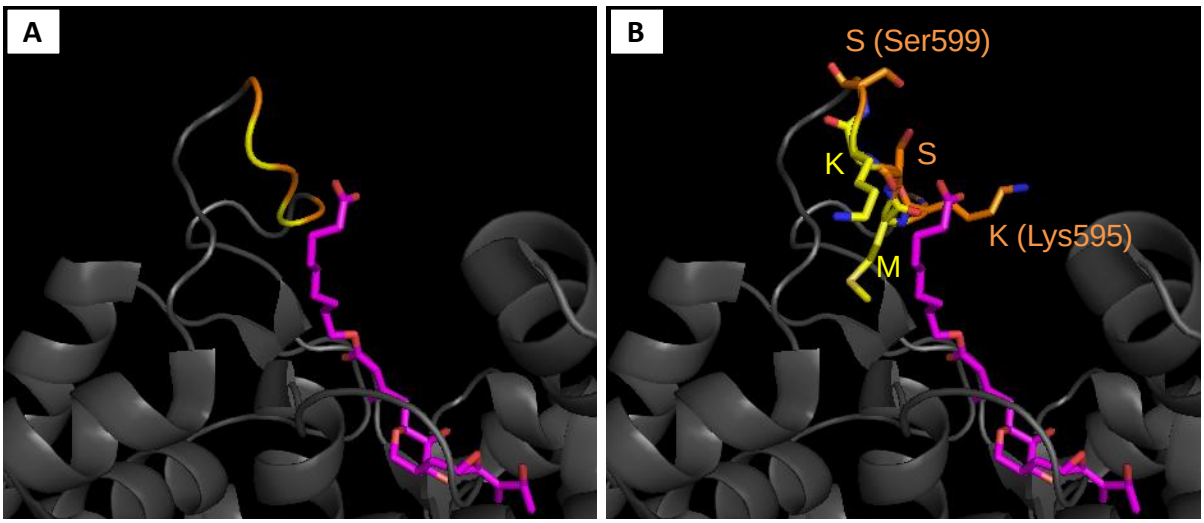

Figure 3.6. KMSKS loop highlighted on 1QU2 in (A) cartoon and (B) sticks format. The second lysine (in yellow) is the critical residue for ATP interaction.

In addition to the possibility of the pyrrothine binding to this hydrophobic patch, the moiety also has the capacity to hydrogen bond (subject to distance) with the residues on the KMSKS loop of the susceptible IleS enzyme. The pyrrothine has two amide groups, one in the heterocycle and one linking the moiety to the rest of the thiomarinol structure. Each amide has the potential to accept a hydrogen bond via the carbonyl group (C=O) and donate one

via the amine group (NH). The KMSKS residues on the loop appear unburied and likely to interact with the surrounding solvent (Figure 3.6) and therefore, the amide groups on the pyrrothine may interact with the side chains as well as the backbones of the amino acid residues. For example, the carbonyl group on the heterocycle of pyrrothine moiety may hydrogen bond with the amine group from the side chain or backbone of the second lysine of the KMSKS loop. Alternatively, the amide groups on the pyrrothine moiety may simply interact with the solvent while the ring binds to the hydrophobic patch.

In comparison, mupirocin has a carboxylate tail which appears to form a salt bridge with the second lysine residue (Silvian *et al.*, 1999). (Silvian *et al.* only noted lysine to bind to the carboxylate tail but Marion *et al.* (2009) also highlighted the neighbouring methionine to hydrogen bond with the terminus (Figure 3.11)). These possible differences in interaction of mupirocin and thiomarinol with 1) the KMSKS loop (from forming a salt bridge or two potential hydrogen bonds to several hydrogen bonds respectively) and 2) the latter having the additional interaction with the hydrophobic patch may be important factors in the increased binding affinity of the latter antibiotic to susceptible IleS.

3.3.2 Active site residues that may contribute to increased binding of mupirocin/thiomarinol or to individual resistance phenotypes

The important interactions taking place between 1QU2 and its known ligand mupirocin were deduced using Ligplot (Figure 3.7) and verified for their conserved importance using Evolutionary Trace (ET). The equivalent residues were then sought out on the 3D structures of MupM and TmlM using PyMOL. Residues that were identical in all three proteins were ignored, while residues that were different were investigated further. On the

3D structures of 1QU2, MupM and TmlM, the distances between the residues of interest and mupirocin were also noted to determine whether interactions were likely.

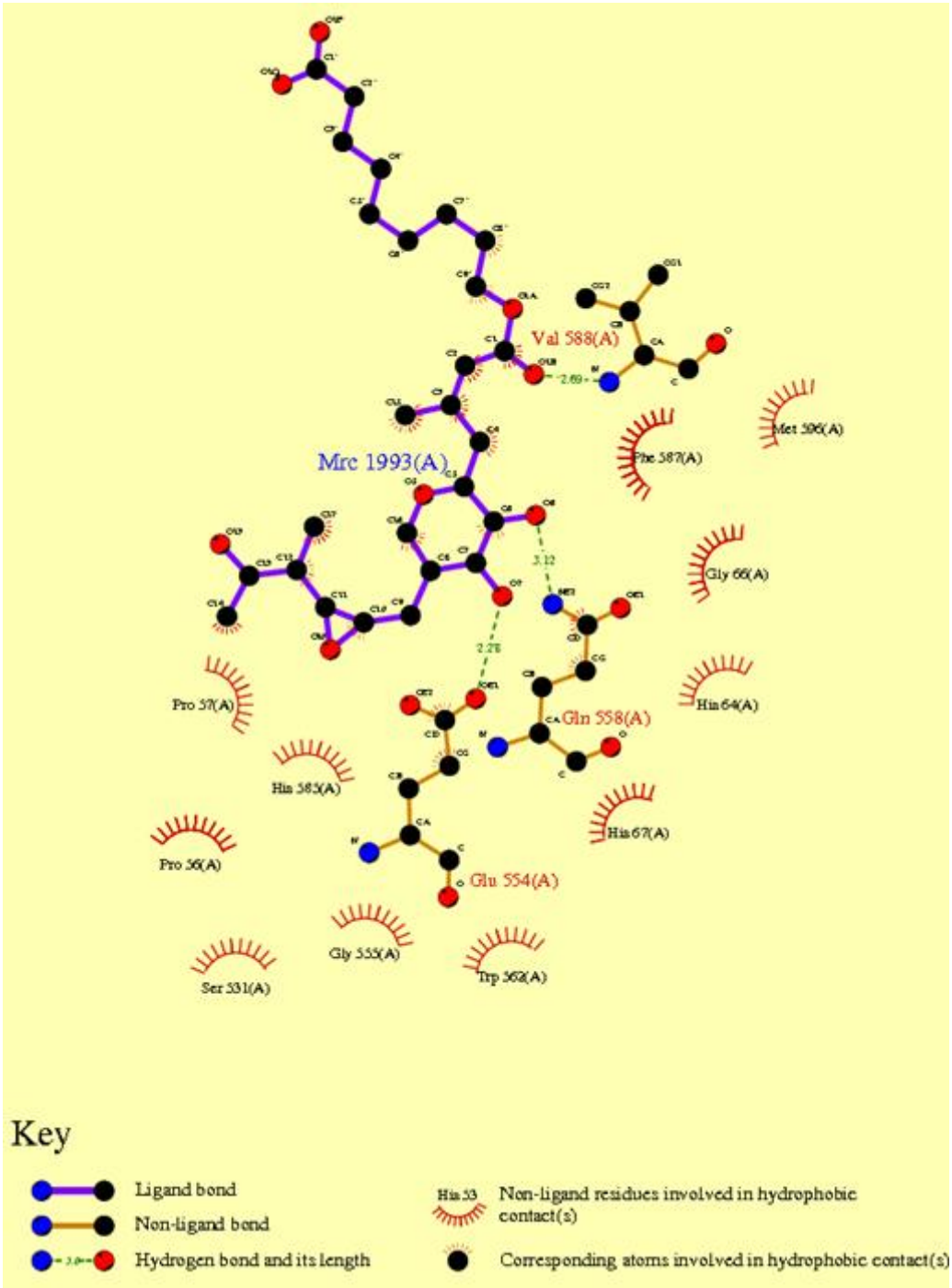

Figure 3.7. Ligplot result of PDB structure 1QU2 complexed with mupirocin.

In addition to the residues identified by Ligplot and ET, residues within 8 Å of mupirocin were highlighted on the 1QU2, MupM and TmlM structures using PyMOL. The residues were then manually compared and those that appeared to interact with the ligand also selected for further work. The selected residues from the Ligplot, ET and PyMOL results are summarised in Table 3.1, Figure 3.8 and Figure 3.14. The residues highlighted in Figure 3.8 will be discussed first in detail.

Phe587 in the mupirocin-sensitive 1QU2 is a bulkier residue than Val581 and Ile590 in MupM and TmlM respectively. It may allow better hydrophobic interaction with mupirocin, or due to the residue's position at the base of the KMSKS loop, it may affect the loop's dynamics. Tyr44 and Tyr48 in MupM and TmlM respectively are slightly bulkier than His53 in 1QU2 but seem too distant from the ligand to play any particular role.

Tyr597 and Tyr606 in MupM and TmlM respectively are bulkier residues than Val603 in 1QU2. ET results of MupM and the multiple sequence alignment from the BLAST results indicate this residue to vary from aromatic residues tyrosine and phenylalanine to non-bulky residues valine and alanine depending on the organism (Figure 3.9). The amino acid sequence of MupA, a highly mupirocin-resistant protein (Hodgson *et al*., 1994) carries a valine instead of tyrosine. However, further scrutiny of the structures and multiple sequence alignment reveal that the IleSs represented in the multiple sequence alignment have a bulky residue at one of the equivalent positions of Val581 and Tyr597 in MupM (except *Thermus thermophilus* IleS (PDB 1JZQ), which has a leucine and valine respectively). This indicates that the Tyr597 and Tyr606 in MupM and TmlM respectively may only be compensating for the

lack of bulky residue in the position of Val581 and Ile590 and are not functionally important to mupirocin/thiomarinol resistance.

Table 3.1. Summary of the amino acid residues of interest that may be important in interacting with mupirocin/thiomarinol and conferring the thiomarinol sensitive phenotype*.

1QU2	MupM	TmlM
Phe587	Val581	Ile590
His53	Tyr44	Tyr48
Asn70	Thr61	Ala65
Val603	Tyr597	Tyr606
Gly601	Lys595	Arg604
Asp557	Ala551	Asp560
His585	His579	Asn588
Gly555	Tyr549	Gly558
Tyr58	Phe49	Phe53

*The residues were selected from Ligplot, Evolutionary Trace (ET) and manual visualisation on PyMOL. A total of 18 residues were initially identified by Ligplot and ET, while manual visualisation on PyMOL identified an additional 36 residues. Any identical residues across 1QU2, MupM and TmlM were discarded. The remaining residues were carefully considered using PyMOL and the residues most likely to interact with mupirocin/thiomarinol and thus influence the resistance/susceptible phenotype were selected for the above table. The residues in red are highlighted in Figure 3.8. The residues in black are highlighted in Figure 3.14.

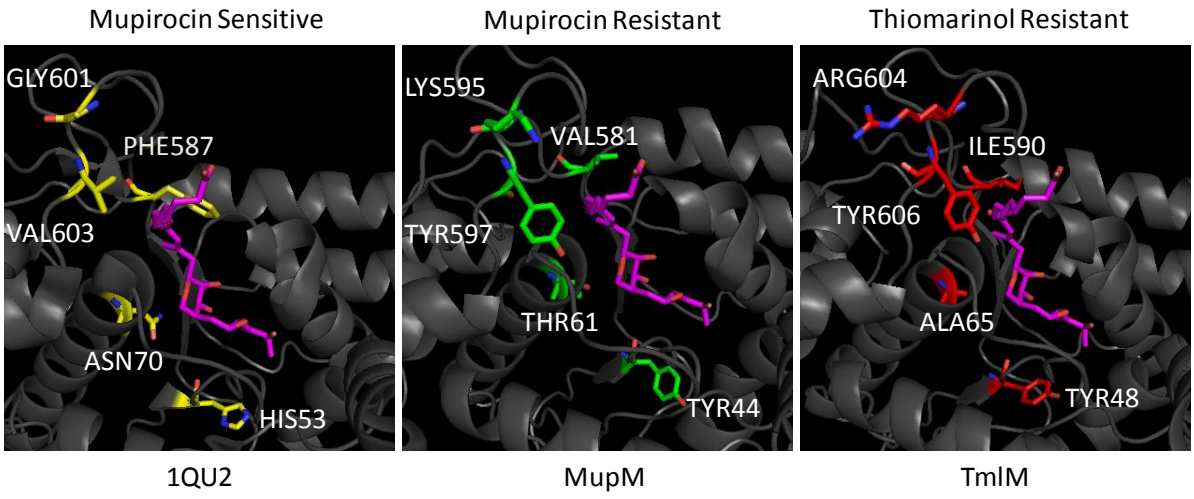

Figure 3.8. Amino acid residues of interest from Table 3.1 highlighted on structures 1QU2, MupM and TmlM. Mupirocin is highlighted in purple. The equivalence between residues is summarised in Table 3.1 (in red).

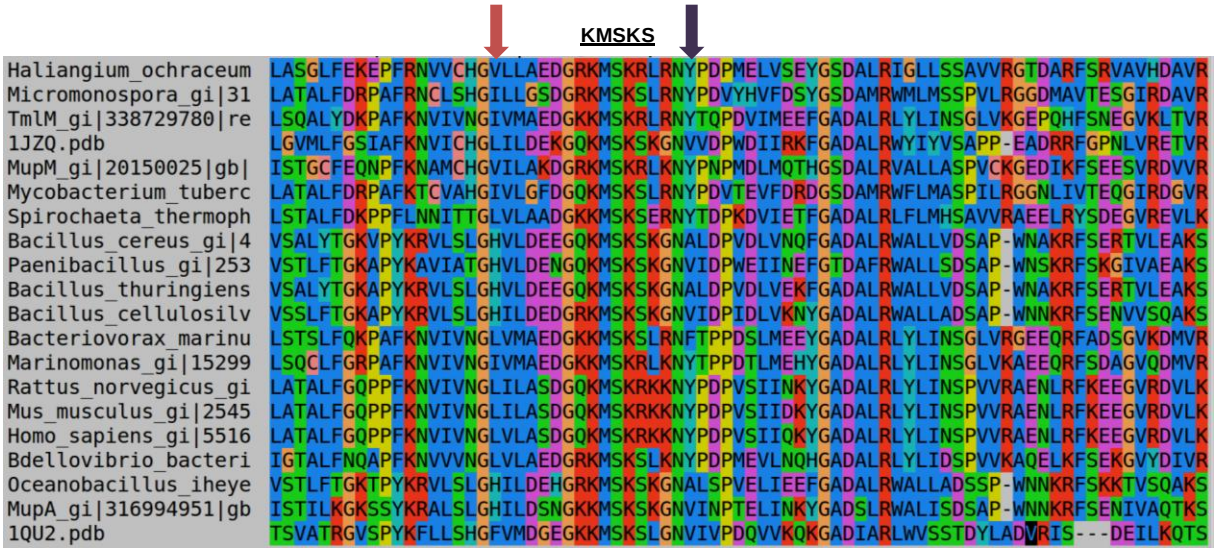

Figure 3.9. Multiple sequence alignment of 1QU2, MupM, MupA, TmlM and their homologues around the KMSKS motif. The purple arrow is highlighting Tyr597 from MupM and the equivalent residues in all other aligned IleSs. The red arrow is highlighting Val581 from MupM and the equivalent residues in all other aligned IleSs. Where there is an aliphatic residue at the position of the red arrow, there is an aromatic residue at the position of the purple arrow and vice versa, with the exception of 1JZQ, suggesting the difference noted in 1QU2 (Val603, Phe587) and MupM/TmlM (Tyr597, Val581 and Tyr606, Ile590 respectively) to be a compensatory change.

The residues of particular interest are Asn70 and Gly601 in 1QU2 (Figure 3.8). Asn70 in 1QU2 is approximately 4 Å from the pyran ring of mupirocin (Figure 3.10). This suggests that Asn70 may interact via hydrogen bonding with the ligand, although the observation was not highlighted in the Ligplot results. The equivalent residues on MupM and TmlM (Thr61 and Ala65 respectively) are smaller and therefore may not be able to interact with the pyran ring. This may significantly reduce mupirocin/thiomarinol binding stability, allowing MupM and TmlM to be highly mupirocin/thiomarinol resistant. This hypothesis is supported by the map of main molecular interactions published by Marion *et al*., based on the X-ray crystal structure of mupirocin complexed with IleS and tRNA solved by Silvian *et al*. (Figure 3.11) (Marion *et al*., 2009; Silvian *et al.*, 1999). They predicted both Asn70 and also its neighbouring Glu554 to interact with the second hydroxyl group on the pyran ring of

mupirocin. The equivalent residues to Glu554 on MupM and TmlM are also glutamic acids (Glu548 and Glu557 respectively, Figure 3.10).

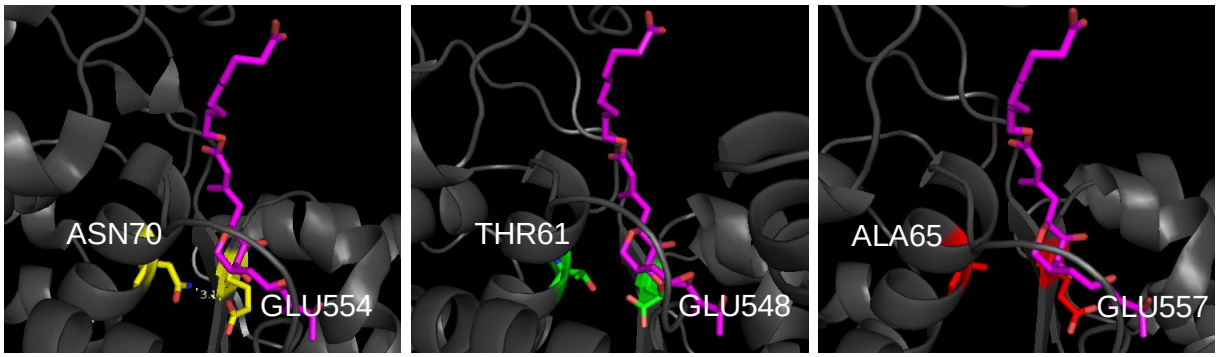

1QU2 with mupirocin | MupM with mupirocin | TmlM with mupirocin

Figure 3.10. The proximity of Asn70, Thr61 and Ala65 and their respective glutamic acid residues to the pyran ring of mupirocin. Asn70 on 1QU2 appears to be favourably placed to interact with the ligand, while the equivalent Thr61 and Ala65 on MupM and TmlM respectively appear to be too distant from the ligand for any interaction (>4 Å). A typical hydrogen bond (measured from the hydrogen) is between 1.5 to 2.6 Å (Berg *et al*., 2002).

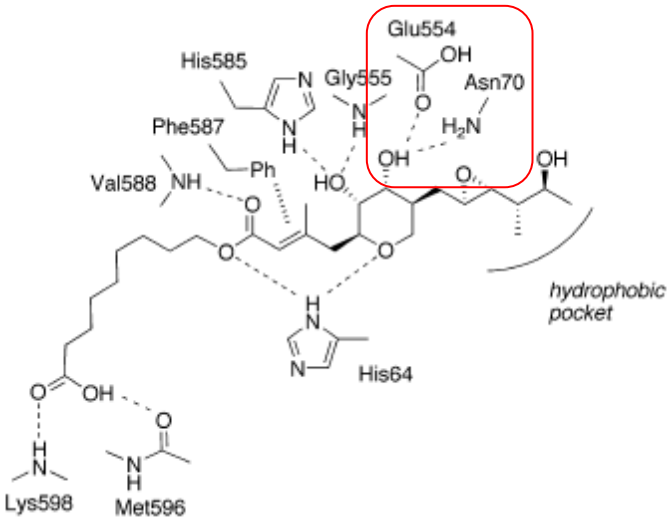

Figure 3.11. Main molecular interactions of mupirocin and 1QU2 solved by Silvian *et al*. (1999), adapted from Marion *et al*. (2009). Interactions of Glu554 and Asn70 with the hydroxyl group in the pyran ring are highlighted in the red box.

Further inspection of the IleS models identified Lys74 and Asp54 in 1QU2 to be favourably placed to interact with Glu554 instead of the pyran ring to create a salt bridge (Figure 3.12).

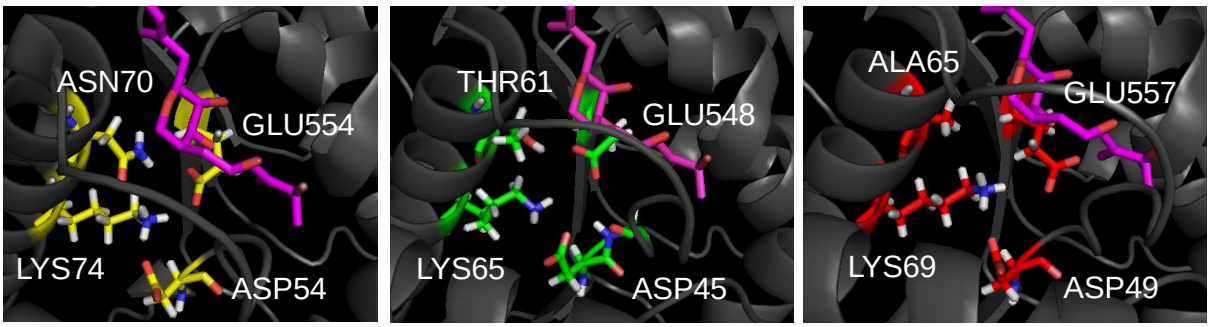

1QU2 with mupirocin | MupM with mupirocin | TmlM with mupirocin

Figure 3.12. The positioning of glutamic acid, lysine and aspartic acid on 1QU2, MupM and TmlM. In 1QU2, Asp54 interacts with Lys74 which interacts with Glu554 rather than with Asn70, allowing the latter residue to interact with the pyran ring of mupirocin. Thr61 and Ala65 on MupM and TmlM respectively are positioned to be more likely to interact with the neighbouring glutamic acids.

These residues can create an overall network of electrostatic charges and hydrogen bonding that may stabilise the site for mupirocin to bind with Asn70. This network is also conserved in MupM and TmlM. However in MupM, Asn70 is replaced with Thr61 and the latter residue appears to be placed favourably for interaction with Glu548 instead of the pyran ring of mupirocin. With Thr61 too far away to interact with the pyran ring, mupirocin may be prevented from effectively binding to the active site, allowing MupM to be resistant to mupirocin. In TmlM, the methyl group of Ala65 is non-polar and incapable of hydrogen bonding with the pyran ring or neighbouring residues. Glu557 appears buried and unlikely to interact in this model (although the orientation of these residues may be an artefact of the model). This may play a role in mupirocin/thiomarinol resistance by creating an

unfavourable environment where the ligand should bind, compared to the stable environment created by Asn70, Glu554, Lys74 and Asp54 in mupirocin-sensitive 1QU2.

Finally, Gly601 in 1QU2 may play a role in the flexibility of the KMSKS loop, while MupM and TmlM have non-flexible residues Lys595 and Arg604 respectively at the equivalent position (Figure 3.8). Three separate ET analyses were run on 1QU2, MupM and TmlM using individual multiple sequence alignments generated by default (a FASTA search of each proteins over the Swiss Protein Databank). ET results ranked Gly601 to be highly conserved within 1QU2 and its homologues, while Lys595 and Arg604 were ranked not as functionally important (Table 3.2). With less flexibility, the resistant proteins may prevent the loop from stabilising the mupirocin/thiomarinol complex.

Table 3.2. Residue variation of Gly601 (1QU2), Lys595 (MupM) and Arg604 (TmlM) from three separate ET analyses*.

Protein	Alignment#	Residue#	AA type	Coverage	Variability	Score (rvET)
1QU2	667	601	G	3	GWQ	3.26
MupM	869	595	K	5	KRQNG	19.02
TmlM	936	604	R	6	RGKQND	21.64

*Alignment# is the alignment position in the multiple sequence analysis (MSA). Residue# is the residue position in the query protein. Type is the one letter amino acid name in the query protein. Coverage is the relative importance position for each residue. Low coverage implies evolutionary importance. Variability shows the residue variation in the column of the MSA. Evolutionary scores for residues are calculated with rvET method. Low score implied evolutionary importance. (Column key reproduced from Mihalek *et al*., 2004).

3.3.3 Residues near the key structural differences of mupirocin and thiomarinol

There are a few structural differences between mupirocin and thiomarinol. The main and most obvious difference is the addition of the pyrrothine moiety on thiomarinol. However, there are other smaller differences to note. Firstly the fatty acid chain attached to

the monic acid backbone of mupirocin is one carbon longer than that on the marinolic acid of thiomarinol. Secondly, thiomarinol has a hydroxyl group at position C4 and finally, the C10-11 epoxide bond on mupirocin is replaced with an E alkene in thiomarinol. Based on the hypothesis that thiomarinol binds in the same orientation as mupirocin, the active site near the differing residues of the marinolic acid was investigated for any residues that may be further interacting with thiomarinol to allow the antibiotic to bind more strongly to the enzyme. Asp557 in 1QU2 was identified as potentially interacting with the C4 hydroxyl group of thiomarinol (Figure 3.13). This observation was also made by Marion and colleagues, although they also identified His64 to potentially interact with the C4 hydroxyl group (Marion *et al*., 2009). The corresponding residue of Asp557 in MupM is Ala551 and unlikely to interact due to its lack of hydrogen bonding capacity in the main chain as well as the distance (>4 Å). However on TmlM, the residue is also an aspartic acid (Asp560) which goes against the hypothesis that an aspartic acid residue could contribute to stronger binding of thiomarinol to susceptible targets unless there are sufficient other changes to decrease binding. All other residues identified near the differing residues did not appear to contribute to further interaction with thiomarinol.

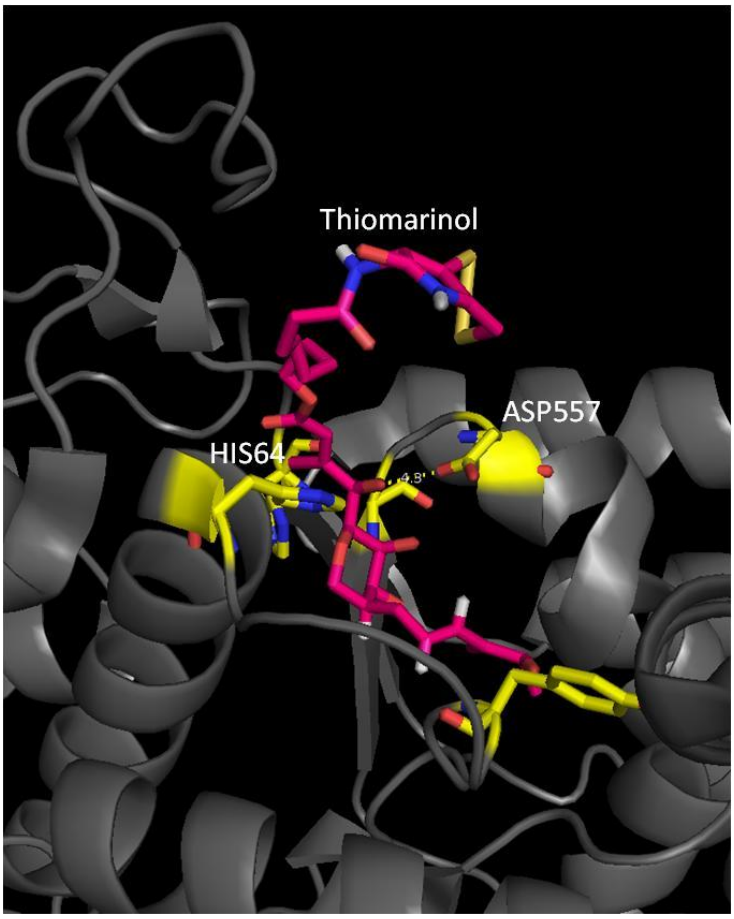

Figure 3.13. Residues near the C4 hydroxyl and C10-11 E alkene groups on thiomarinol highlighted in yellow on 1QU2. Thiomarinol is highlighted in pink. The distance between Asp557 and the C4 hydroxyl group in this model is 4.3 Å and theoretically too distant for interaction. However, within the uncertainty of the model and the known flexibility of the enzyme, Asp557 may still interact with the C4 hydroxyl group at a closed confirmation. Marion *et al*. (2009) has predicted His64 to also interact with the hydroxyl group.

3.3.4 Residues highlighted in the literature

Residues identified by previous literature such as Asp557 in 1QU2 were also highlighted on the IleS structures and included in further studies (Figure 3.14). Marion *et al*. (2009) also noted the amine group from Gly555 may interact with the hydroxyl group on C6 of the pyran ring of mupirocin. The corresponding residue in MupM is Tyr549, which may not interact and thus may confer the mupirocin resistance phenotype. However on TmlM, this residue is also a Gly558 as with Gly555 in 1QU2, so it would be interesting to see

whether changing Tyr549 in MupM to a glycine residue would confer the phenotype of 1QU2 or TmlM i.e. whether it would improve or worsen the enzyme's resistance against mupirocin and thiomarinol (see Chapter 4 for results).

Nakama and colleagues identified His581 and Thr48 on the mupirocin sensitive *Thermus thermophilus* (*T. thermophilus*) IleS to be important residues for conferring its sensitive phenotype. They proposed His581 to interact with the pyran ring via hydrophobic stacking interactions. However in eukaryotic IleSs, they noted this residue to be replaced with an asparagine or serine and suggest this change to weaken the hydrophobic interaction with the pyran ring. Regarding Thr48, no specific interactions were proposed but they noted this residue to be replaced with phenylalanine in eukaryotic IleSs. They created a double mutant, replacing these residues with asparagine and phenylalanine respectively to mimic a eukaryotic IleS and found the K_i value to increase by one order of magnitude compared to the wild type *T. thermophilus* (Nakama *et al*., 2001). The corresponding residues on MupM are His579 and Phe49 respectively, which partially support Nakama's observations on phenylalanine conferring weaker binding by the enzyme. On TmlM, the residues are Asn588 and Phe53 (Figure 3.14), which may be an important factor in preventing auto-toxicity in the producer and conferring the thiomarinol resistance phenotype.

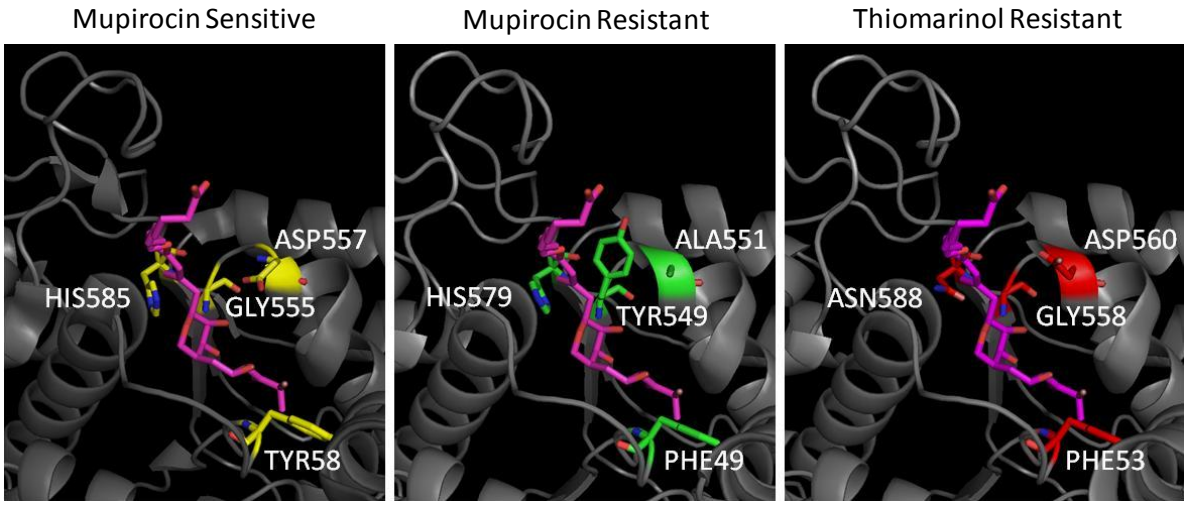

Figure 3.14 Amino acid residues of interested highlighted by Marion *et al*. (2009) and Nakama *et al.* (2001). Mupirocin is highlighted in purple. The equivalence between residues is summarised in Table 3.1 (in black).

3.4 Discussion

This study modelled MupM and TmlM by homology with the structure of a mupirocin-sensitive IleS complexed with mupirocin (PDB: 1QU2) and performed active site analyses, in an attempt to understand the interactions taking place between specific amino acid residues and thiomarinol that render this antibiotic more potent than mupirocin. In particular, this study aimed to understand what additional interactions, if any, the pyrrothine moiety may bring to increase the binding affinity of thiomarinol to susceptible IleS.

This study also reviewed previous studies conducted by Marion *et al*. (2009) and Nakama *et al*. (2001) and with the active site analysis findings, concluded that a total of eight residues in the mupirocin-sensitive active site of IleS1 (Phe587, Asn70, Val603, Gly601, His585, Asp577, Gly555 and Tyr58) may interact with mupirocin and/or thiomarinol and render the enzyme sensitive (Figure 3.8; Figure 3.14). Four out of the eight residues on

mupirocin and thiomarinol-resistant TmlM (Arg604, Ala65, Asn588 and Phe53) were hypothesised to confer the thiomarinol resistance phenotype through a combination of reducing (i) flexibility of the IleS enzyme and (ii) the molecular interaction of marinolic acid in the active site (Figure 3.15).

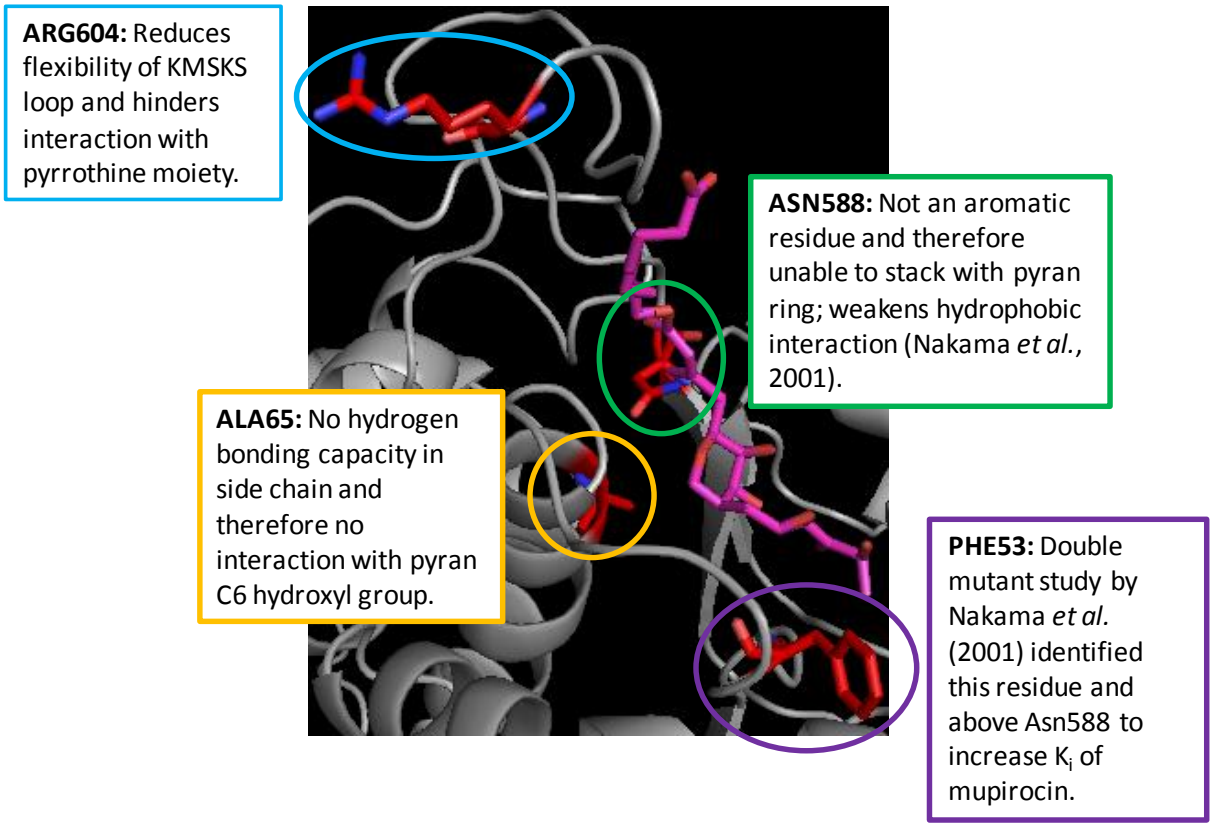

Figure 3.15. Summary of hypothesised amino acids responsible for TmlM thiomarinol resistance phenotype. Mupirocin is highlighted in pink.

3.4.1 Reduced flexibility of the KMSKS loop

The flexibility conferred by the glycine residue (Gly601) at the base of the KMSKS motif in 1QU2 is proposed to be important for binding of mupirocin and thiomarinol and part of the resistance to these antibiotics in MupM and TmlM is thought to be due to this position being occupied by amino acids that confer less flexibility (Lys595 and Arg604

respectively). This difference in amino acid may restrict the movement of the loop and prevent interactions between the protein and mupirocin/thiomarinol. The aromatic Phe587 residue at the base of 1QU2's KMSKS loop may restrict movement but may also hold the mupirocin in place. This conserved KMSKS motif has been structurally observed to undergo conformational rearrangement during catalysis of aminoacyl-adenylate in TyrS, TrpS and LeuS, including the change in positioning of the critical second lysine in the conserved motif to interact with the α-phosphate of the ATP in the transition state (Cusack *et al*., 2000; Ilyin *et al*., 2000; Yaremchuk *et al*., 2002). The crystal structure of mupirocin-sensitive *S. aureus* IleS complexed with $tRNA^{Ile}$ and mupirocin also shows the carboxylate tail of mupirocin to bind to the second lysine (Lys598) of the KMSKS motif instead of the α-phosphate of ATP (Silvian *et al.*, 1999). Additionally, the backbone amide of the first lysine (Lys595) and the backbone carbonyl of Gly593 (upstream KMSKS) binds to the tRNA backbone, stabilising tRNA onto IleS and opening the IleS active site. The lack of glycine downstream from the KMSKS motif may restrict the flexibility of the loop just enough to prevent the second lysine from binding to the mupirocin tail, giving rise to mupirocin and/or thiomarinol resistance. However, this restriction should be at a low fitness cost and not disable aminoacylation completely.

3.4.2 Difference in binding of marinolic acid versus mupirocin

The possible reduction of flexibility of the KMSKS loop does not appear to be the only changes found in MupM and TmlM compared to 1QU2 to render the first two enzymes resistant to mupirocin and/or thiomarinol. Comparison of the three enzymes has revealed eight amino acid differences between the active sites and suggests a collective change in

active site residues confers the resistance phenotype against mupirocin and thiomarinol. In particular, four residues appear to be involved in the thiomarinol resistance phenotype of TmlM (Figure 3.15). Observations by Nakama *et al*. (2001) and this study suggest that the residues in the binding pocket of mupirocin and marinolic acid are important in determining the resistance phenotype of the enzyme. Their *T. thermophilus* double mutant suggests that resistance in TmlM is conferred by multiple changes in the active site, instead of one point mutation as seen in low mupirocin resistant *S. aureus* enzymes (Antonio *et al*., 2002).

As for the susceptible enzymes, the marinolic acid must bind strongly to the Rossman fold. However, a previous study observed marinolic acid to inhibit growth of *S. aureus* but less well than mupirocin (MIC of 0.125 µg/ml and 1 µg/ml respectively) (Fukuda *et al*., 2011). The implication of this was that marinolic acid does not bind as well to IleS as mupirocin, and that the increased potency of thiomarinol is solely due to the addition of the pyrrothine moiety. However, this may be due to the fact that the marinolic acid moiety is one carbon shorter than mupirocin and the shortening of the polyketide chain prevents the second lysine of KMSKS from binding to the ligand.

All IleS residues in the proximity of where marinolic acid and mupirocin differ were carefully considered. However, only Asp557 in 1QU2 was observed to be within interacting distance of the C4 hydroxyl group on thiomarinol. The equivalent residue is Ala551 in MupM and therefore it was hypothesised that the C4 hydroxyl group may contribute to stronger binding to susceptible IleS. However, the same aspartic acid residue was found on TmlM which went against the hypothesis. Since no other notable residues were identified in this

study, there appears to be no molecular explanation for better mupirocin binding than marinolic acid, except for the suggested difference in carbon chain length.

Site-directed mutagenesis studies have been conducted to confirm the importance of the amino acids highlighted in this work as well as from the literature (Chapter 4). It was hypothesised that by changing single amino acids on the active site of MupM to mimic that of TmlM, the mutant enzyme will gain increased tolerance or even resistance against mupirocin and thiomarinol. Likewise, altering residues on MupM to corresponding residues of 1QU2 was hypothesised to decrease tolerance against mupirocin and thiomarinol. Multiple mutants were also constructed to see whether the resistance phenotype was dramatically improved or weakened by multiple amino acid changes.

3.4.3 Does pyrrothine increase binding to the hydrophobic patch?

The above observations of likely reduced flexibility and multiple amino acid changes in the active site may explain the resistance mechanism of TmlM against thiomarinol and also the increased potency of the drug against susceptible targets via increased affinity to the active sites. However, the role of pyrrothine in the potency of thiomarinol is yet to be understood. Pocket v.2 has identified a hydrophobic patch created by the aliphatic chains of the highly conserved second lysine of the KMSKS motif in 1QU2 and the additional arginine residue in MupM and TmlM. This could be the site where the pyrrothine moiety sits to increase overall binding of the antibiotic to the target IleS.

As mentioned in the Results, there is also the potential of pyrrothine to form several hydrogen bonds with the IleS enzyme (although this may also be only to solution). The two amide groups on the pyrrothine moiety may hydrogen bond with residues on the KMSKS

loop and increase overall binding of thiomarinol to susceptible IleS. According to computation work performed by Maddipati (2007), it is energetically unfavourable to embed a salt bridge in a hydrophobic environment, as a salt bridge is highly polar and hence, difficult to completely displace all water molecules that interact with it. On the contrary, dehydration of a hydrogen bond is spontaneous and when fully embedded in a hydrophobic environment, the bond becomes stabilised (Maddipati, 2007). Therefore, compared to the salt bridge interaction between the carboxylate tail of mupirocin and the IleS enzyme, the hydrogen bonding of amides in the pyrrothine moiety may allow a more stabilised interaction with the KMSKS loop when it is fully embedded in the hydrophobic patch, made accessible by the eight carbon length fatty acid chain.

This study also proposes that the length of the eight carbon chain of marinolic acid is important for the pyrrothine moiety to fit in the hydrophobic patch. An additional carbon on the marinolic acid may disrupt the interaction between pyrrothine and the target IleS – by moving the moiety out of the hydrophobic zone and into solution. The pyrrothine moiety does not sit in the hydrophobic patch in Figure 3.2 but this is most probably due to the sub-optimal thiomarinol structure used. The available structure of thiomarinol B in the Daresbury Chemical Database (https://cds.dl.ac.uk/) confirms the planarity of the pyrrothine moiety in relation to the rest of the thiomarinol structure. Quantum mechanics calculations were performed using MolPro (Werner *et al.*, 2012) on the pyrrothine moiety constructed in this study to fix its rotation. (The entire thiomarinol A structure could not be optimised by MolPro due to its size.) Further work is required to attach this optimised pyrrothine moiety on the marinolic acid and to confirm that the amide groups of the former is proximal for interacting with the the KMSKS loop within the hydrophobic patch. The length of a

mupirocin/thiomarinol analogue may be crucial in determining its activity against IleS. This may also be of interest in future mutasynthesis and molecular dynamics simulation studies.

It can also be hypothesised that pyrrothine binding to the enzyme would be lethal, as the moiety would block the enzyme from undergoing conformational changes to activate isoleucine with ATP. However, this hydrophobic patch is also present in MupM and TmlM, the latter enzyme conferring high level resistance to thiomarinol.

The current hypothesis is that the pyrrothine moiety does increase the potency of thiomarinol against 1QU2 and MupM by better interaction with the KMSKS loop within the hydrophobic patch. This interaction is made possible by the specific 8 carbon length of the 8-hydroxyoctanoic acid (Figure 3.16).

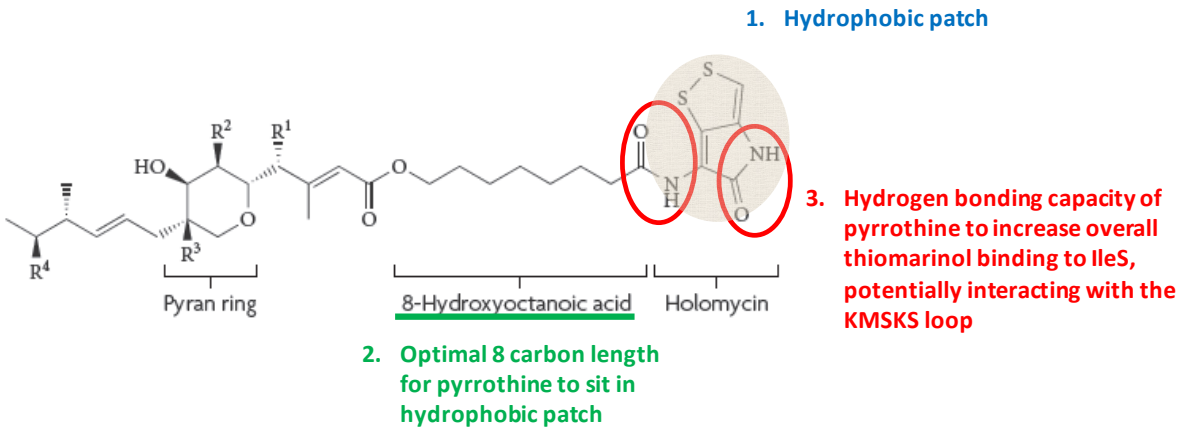

Figure 3.16. The hypothesised mechanism of thiomarinol A potency via increased binding to target IleS (adapted from Thomas *et al.*, 2010). R^1 = OH, R^2 = OH, R^3 = H, R^4 = OH.

In TmlM, the pyrrothine may also able to interact with the same hydrophobicity; however, multiple changes elsewhere in the active site of TmlM (as proposed in Figure 3.15) prevent the marinolic acid from binding and consequently confer thiomarinol resistance. This is difficult to prove experimentally because the hydrophobic area is created mainly by lysine, a

highly conserved residue of the KMSKS motif. Mutating or replacing this residue may compromise the functionality of the IleS enzyme and hence this was not pursued in Chapter 4.

A possible future experiment would be to generate a thiomarinol analogue but with a shorter marinolic acid chain (such as a three or five carbon tail instead of the original seven). The shorter chain should prevent the pyrrothine moiety from sitting in the hydrophobic patch, if this analogue binds to the active site in the same manner as the wild-type marinolic acid. The K_i value of the shorter analogue should be higher, indicating less binding to the enzyme. Various analogues have been created and tested for their biological activity against *Bacillus subtilis* and MRSA by Murphy and colleagues (Murphy *et al*., 2011). However, all analogues have been drastically altered from the original thiomarinol structure such as analogues with an intact pyrrothine moiety but the marinolic acid exchanged with MeCO. An analogue with a fully intact marinolic acid, but with a shorter carbon tail, may elucidate more on whether the hydrophobic patch is important in increasing the overall binding affinity of thiomarinol via the pyrrothine moiety in susceptible enzymes.

CHAPTER 4

4 CHARACTERISING THE RESIDUES IN THE ILES ACTIVE SITE

4.1 Introduction

As explained in Chapter 1, thiomarinol is of interest as it exhibits higher potency than mupirocin against a wide range of microorganisms (Table 1.5). One of the hypotheses to explain this potency is that the pyrrothine moiety and the small differences between marinolic acid and mupirocin increase the binding affinity of thiomarinol for its target enzyme, isoleucyl-tRNA synthetase (IleS). The active site of mupirocin-sensitive IleS1 was compared to that of mupirocin-resistant MupM and mupirocin/thiomarinol-resistant TmlM in the previous computational study (Chapter 3) and several amino acid residues highlighted for their possible involvement in greater or lesser binding to mupirocin and/or thiomarinol (Figure 3.8).

Also discussed in Chapter 3 are residues suggested by other studies that may be increasing the binding affinity of susceptible IleS to mupirocin and/or thiomarinol (Marion *et al*., 2009; Nakama *et al*., 2001; Silvian *et al.*, 1999) (Figure 3.14). Most notable were residues His581 and Thr48 identified in the mupirocin-sensitive *T. thermophilus* IleS by Nakama *et al*. (2001), in which they created a double mutant replacing these residues to mimic those of an eukaryotic IleS. They found the K_i value of mupirocin was increased by one order of magnitude compared to the wild-type IleS. All other residues reviewed in the previous chapter were suggestions from computational analyses and yet to be experimentally supported.

In this study, I describe studies in which the residues identified computationally were substituted in MupM to determine their importance in conferring the mupirocin/thiomarinol resistance or sensitivity phenotype. Both single and multiple changes were made to mimic the active site of IleS1 or TmlM and it was hypothesised that any changes made to important residues would change the minimal inhibitory concentration (MIC) of mupirocin and thiomarinol compared to wild-type MupM. Two methodologies were also used in an attempt to confirm the functionality of these MupM mutants by (1) protein purification for subsequent use in aminoacylation assays and (2) expressing them in *P. fluorescens* with *ileS1* and *mupM* deleted by suicide mutagenesis.

4.2 Materials and Methods

4.2.1 Bacterial strains, plasmids and growth conditions

All bacterial strains and plasmids used in this study are listed in Table 4.1 and Table 4.2.

Table 4.1. Bacterial strains used in this study.

Bacterial Strain	Genotype	Phenotype	Source/Reference
E. coli BL21 (DE3)	F^- *ompT hsdSB gal dcm* (DE3)	Strain for inducing high protein expression. Contains the DE3 lysogen that carries the gene for T7 RNA polymerase under the control of the lacUV5 promoter.	Invitrogen
E. coli BL21 C41 (DE3)	F^- *ompT hsdSB (rB- mB-) gal dcm* (DE3)	Derived from BL21 (DE3). Contains mutations in the lacUV5 promoter that drives expression of T7 RNA Pol and prevents cell death associated with toxic recombinant protein expression.	Miroux and Walker, 1996; Wagner *et al.,* 2008; Y. Sevastsyanovich
E. coli BL21 C43 (DE3)	F^- *ompT hsdSB (rB- mB-) gal dcm* (DE3)	Derived from Bl21 C41 (DE3). Contains mutations in the lacUV5 promoter that drives expression of T7 RNA Pol and prevents cell death associated with toxic recombinant protein expression.	Miroux and Walker, 1996; Wagner *et al.,* 2008; Y. Sevastsyanovich
E. coli DH5α	*endA1 recA hsdR17 lacZΔM15 supE44 gyrA96 thi-I relA1* F^-	High transformation efficiency strain.	Gibco BRL
E. coli S17-1	*thi pro* res^- mod^+ *recA1 RP-4-2 [Tc::Mu; Km::Tn7]*	Donor strain with sex pilli for bacterial conjugation.	Simon *et al.,* 1983
P. fluorescens NCIMB 10586	-	Mupirocin-producer wild type (WT). Inherently ampicillin resistant.	G.T. Banks
P. fluorescens NCIMB 10586 *Δ mupM*	*ΔmupM*	Mupirocin-producer with mupM deletion. Ampicillin resistant.	El-Sayed *et al.,* 2001

Table 4.2. Plasmids used in this study (continued to the next page).

Plasmid	Size (kb)	Properties	Source/Reference
pAKE604	7.2	pMB1 replicon. Amp^R, Kan^R, oriT, lacZα, sacB	El-Sayed *et al.,* 2001
pET28a	5.4	Kan^R, T7lac promoter, N-terminus His•Tag	Novagen
pET28amupM	8.4	pET28a derivative with cloned 3092 bp *mupM* fragment (EcoRI-HindIII)	This study
pGBT30	6.3	pMB1 replicon, AmpR, $lacI^Q$ tacp-galK, expression vector	Jagura-Burdzy *et al.,* 1991
pGBT30mupM	9.3	pGBT30 derivative with cloned 3092 bp *mupM* fragment (EcoRI-XbaI)	This study
pGBT30mupM1	9.3	pGBT30mupM derivative with mutation in *mupM* (Thr61Ala)	This study
pGBT30mupM2	9.3	pGBT31mupM derivative with mutation in *mupM* (Thr61Asn)	This study
pGBT30mupM3	9.3	pGBT31mupM derivative with mutation in *mupM* (Phe49Tyr)	This study
pGBT30mupM4	9.3	pGBT31mupM derivative with mutations in *mupM* (Tyr549Gly/Ala551Asp)	This study
pGBT30mupM5	9.3	pGBT31mupM derivative with mutations in *mupM* (Val581Ile/His579Asn)	This study
pGBT30mupM6	9.3	pGBT31mupM derivative with mutation in *mupM* (Val581Phe)	This study
pGBT30mupM7	9.3	pGBT31mupM derivative with mutation in *mupM* (Lys595Arg)	This study
pGBT30mupM8	9.3	pGBT31mupM derivative with mutations in *mupM* (Lys595Gly/Tyr597Val)	This study
pGBT30mupM1+7	9.3	pGBT31mupM derivative with mutations in *mupM* (Thr61Ala/Lys595Arg)	This study
pGBT30mupM3+4	9.3	pGBT31mupM derivative with mutations in *mupM* (Phe49Tyr/Tyr549Gly/Ala551Asp)	This study

Plasmid	Size (kb)	Properties	Source/Reference
pJHIle01	6.9	pAKE with BamHI-EcoRI 960 bp PCR fragment creating 1890 bp in-frame deltion in *ileS*	J. Hothersall
pJH10	14.5	IncQ replicon, pOLE1 IncC1 deleted, with EcoRI-SacI polycloning site, Tc^R from pDM1.2	El-Sayed *et al.,* 2003
pJH10mupM	17.5	pJH10 derivative with cloned 3092 bp *mupM* fragment (EcoRI-XbaI)	El-Sayed *et al.,* 2003
pJH10mupM1	17.5	pJH10mupM derivative with mutation in *mupM* (Thr61Ala)	This study
pJH10mupM2	17.5	pJH10mupM derivative with mutation in *mupM* (Thr61Asn)	This study
pJH10mupM3	17.5	pJH10mupM derivative with mutation in *mupM* (Phe49Tyr)	This study
pJH10mupM4	17.5	pJH10mupM derivative with mutations in *mupM* (Tyr549Gly/Ala551Asp)	This study
pJH10mupM5	17.5	pJH10mupM derivative with mutations in *mupM* (Val581Ile/His579Asn)	This study
pJH10mupM6	17.5	pJH10mupM derivative with mutation in *mupM* (Val581Phe)	This study
pJH10mupM7	17.5	pJH10mupM derivative with mutation in *mupM* (Lys595Arg)	This study
pJH10mupM8	17.5	pJH10mupM derivative with mutations in *mupM* (Lys595Gly/Tyr597Val)	This study
pJH10mupM1+7	17.5	pJH10mupM derivative with mutations in *mupM* (Thr61Ala/Lys595Arg)	This study
pJH10mupM3+4	17.5	pJH10mupM derivative with mutations in *mupM* (Phe49Tyr/Tyr549Gly/Ala551Asp)	This study
pJH10tmlM	17.6	pJH10 derivative with cloned 3146 bp *tmlM* fragment (EcoRI-XbaI)	Fukuda *et al.,* 2010

For the construction of all *mupM* mutants, pGBT30mupM was used as the starting point and *E. coli* DH5α used as the bacterial host. The mutants' mupirocin and thiomarinol resistance phenotypes were characterised in *E. coli* DH5α pJH10 by Minimal Inhibitory Concentration (MIC) tests with 1 mM IPTG induction as described in Chapter 2.

For protein purification, various IleSs were individually expressed in *E. coli* BL21, C41 (DE3) or C43 (DE3) cells carrying plasmid pET28a (Novagen, United Kingdom). This pET28a vector carries a kanamycin resistance gene, a T7 *lac* promoter and N-terminus His Tag and is therefore inducible by the addition of isopropyl-β-D-thiogalactoside (IPTG) in the cell culture. Plasmid pJH10 carries a tetracycline resistance gene, a *tac* promoter, an *oriT* region and a multiple cloning site, thus being selectable and also inducible by IPTG. All strains were grown in L-broth or Overnight Express^{TM} Instant Terrific Broth (TB) medium (Novagen, United Kingdom) at 200 rpm, with the appropriate selection antibiotic, with or without IPTG and incubated at appropriate temperature and duration.

4.2.2 Generating and characterising *mupM* mutants

QuikChange Lightning Site-Directed Mutagenesis kit (Agilent, United Kingdom) was used to create all *mupM* mutants. Primers were designed using the QuikChange Primer Design tool (Agilent, United Kingdom) to introduce mutations at the residues of interest identified computationally in Chapter 3 (Table 4.3). A total reaction volume of 50 µl was made per mutation containing 5 µl of buffer, 0.6 µl of dsDNA template, 1.7 µl of primers (10 pmole/µl) each, 1 µl dNTP (10 mM), 1.5 µl of QuikSolution, 37.5 µl of ddH_2O and 1 µl of QuikChange DNA polymerase. The recommended PCR programme for the kit was used (Table 4.4). Once amplified, the reaction was digested with 2 µl of DpnI, in order to degrade

the unwanted parental template (without the mutation). All initial mutants were sequenced to ensure only the desired changes were present in the gene.

Table 4.3. Oligonucleotide primers designed and used for QuikChange mutagenesis*.

Mutant Name	Mutation	Primer
M1	THR61ALA	5'-gcactacggccatattctg**g**cttcctatatcaaagacg-3' 5'-cgtctttgatataggaag**c**cagaatatggccgtagtgc-3'
M2	THR61ASN	5'-cactacggccatattctga**a**ttcctatatcaaagacgtc-3' 5'-gacgtctttgatataggaa**t**tcagaatatggccgtagtg-3'
M3	PHE49TYR	5'-gacggcccgccgt**a**tgctaccgg-3' 5'-ccggtagca**t**acggcgggccgtc-3'
M4	TYR549GLY/ALA551ASP	5'-ccgacttcatcgtcgag**gg**ccttg**at**cagacccgcggttggtt-3' 5'-aaccaaccgcgggtctg**at**caagg**cc**ctcgacgatgaagtcgg-3'
M5	HIS579ASN/VAL581ILE	5'-caagaacgccatgtgc**a**acggg**att**attctggccaaggacg-3' 5'-cgtccttggccagaat**a**at**c**ccgtt**g**cacatggcgttcttg-3'
M6	VAL581PHE	5'-gccatgtgccacggg**ttt**attctggccaaggac-3' 5'-gtccttggccagaat**a**a**a**acccgtggcacatggc-3'
M7	LYS595ARG	5'-gtccaagcgcctga**g**gaactaccccaacc-3' 5'-ggttggggtagttc**c**tcaggcgcttggac-3'
M8	LYS595GLY/TYR597VAL	5'-caagatgtccaagcgcctg**gg**gaac**gt**ccccaacccgatggatctc-3' 5'-gagatccatcgggttgggg**ac**gttc**cc**caggcgcttggacatcttg-3'

*Bases that have been altered from the original MupM sequence are highlighted in red.

Table 4.4. PCR programme for QuikChange mutagenesis as recommended by the supplier.

Cycles	Temperature	Time
1	95°C	2 minutes
18	95°C	20 seconds
	60°C	10 seconds
	68°C	30 seconds/kb of plasmid length*
1	68°C	5 minutes

*In this study, 4.5 minutes was used for the 6 kb-sized pGBT30 *mupM*.

Once the mutants were confirmed by sequencing, the plasmids were transformed into *E. coli* GM2163 to yield DNA with no dam methylated sites. The mutant *mupM* genes were then digested with EcoRI and XbaI, ligated with the expression vector pJH10 and transformed into DH5α for biological characterisation. Further combinations (double and multiple mutants) were generated by digesting gene fragments containing the desired single mutations from the individual pGBT30 *mupM* mutants using EcoRI and KpnI. Corresponding

EcoRI-KpnI fragments were digested out from another set of pGBT30 *mupM* mutants carrying the desired secondary/tertiary mutations and the former fragments (with the primary mutation) ligated to form complete pGBT30 constructs carrying multiple mutations in the *mupM* gene. Once successfully cloned into pGT30, the same process outlined above was performed to transfer the genes into pJH10.

All mutants were characterised by performing MIC tests using thiomarinol and mupirocin as outlined in Chapter 2. An inoculum size of 5 x 10^5 cfu/ml (as recommended by the British Society for Antimicrobial Chemotherapy or BSAC) was used.

4.2.3 Suicide mutagenesis

Biparental mating was performed by vortexing 500 µl of overnight culture of S17-1 carrying the appropriate plasmid with 500 µl of *P. fluorescens ΔmupM* overnight culture, filtered onto a nylon membrane which was then placed on an L-agar plate for up to six hours at 30°C to ensure conjugation. Once incubated, the filter was transferred into a universal bottle with 1 ml saline and vortexed to remove the bacteria from the filter. This mixture was then serially diluted from 10^{-1} to 10^{-5} with saline and 200 µl of each dilution spread on minimal media (MM) agar (Table 4.5) with 15 µg/ml tetracycline and 100 µg/ml ampicillin for selection of *P. fluorescens* carrying pJH10mupM wild-type or mutants. The plates were left at 30°C for up to four days to give single colonies. At least 10 single colonies were then streaked individually onto MM agar with tetracycline and ampicillin and again incubated for up to four days at 30°C. At least 10 single colonies were then streaked onto L-agar plates with the same antibiotics.

For selection of *P. fluorescens ΔmupM* pJH10mupM carrying suicide plasmid pJHIle01, MM agar and L-agar containing 15 µg/ml tetracycline and 50 µg/ml kanamycin were used instead. For removal of the suicide plasmid, single colonies of *P. fluorescens ΔmupM* pJH10mupM carrying pJHIle01 were grown in 5 ml L-broth overnight cultures and streaked onto L-agar with 15 µg/ml tetracycline and 5% sucrose.

Table 4.5. Preparation of minimal media (MM) agar.

Minimal Media Agar Preparation
200 ml 3 % agar
200 ml M9 x 2 (Prewarmed at 48°C)
400 µl 1M $MgSO_4$
400 µl Thiamine HCl
400 µl 0.1M $CaCl_2$
2 ml 40% glucose
400 µl required antibiotic

4.2.4 Protein expression and purification of IleS proteins

Total protein expression. Overnight cultures of strains expressing the protein of interest in appropriate plasmids were prepared by inoculating 5 ml L-broth with a single colony and the antibiotic for selection. The overnight cultures were then diluted 1:50 into fresh L-broth containing the selection antibiotic and grown to an OD_{600nm} 0.4. Once the required cell density was reached, the appropriate amount of IPTG was added and incubated for the desired length of time at the desired temperature. 1 ml samples were taken at appropriate intervals and the bacteria harvested by centrifugation at 4°C at 14,000 x*g* for 5 min. The supernatant was removed and 500 µl of STE buffer (10mM Tris-Cl pH 8.0, 0.1M NaCl, 1mM EDTA pH 8.0) added before the centrifugation was repeated with the same

conditions. The supernatant was again removed and the cell pellet resuspended by vortexting into a slurry before storage at -20°C. For analysis by sodium dodecyl sulfate polyacrylamide gel electrophoresis (SDS-PAGE), the samples were defrosted and the slurry re-suspended in 20 µl of 1xSDS loading buffer (50mM Tris-Cl pH 6.8, 2% w/v SDS, 0.1% bromophenol blue, 10% v/v glycerol and an addition of 100mM dithiotheitol (DTT) before use) and boiled for 3 min.

Soluble and insoluble protein expression. The protocol for "total protein expression" (above) was followed with harvesting of 1 ml samples for storage at -20°C until future use. The slurry was defrosted and re-suspended with 100 µl of BugBuster™ Protein Extraction Reagent (Novagen, United Kingdom) before incubation at room temperature with rocking for 20 min. The sample was centrifuged at 4°C at 14,000 x*g* for 5 min and the supernatant (containing soluble protein) transferred into a fresh microfuge tube. 100 µl of 2xSDS loading buffer was added. The remaining cell pellet was re-suspended in 100 µl 1% SDS and 100 µl of 2xSDS loading buffer added. All samples were boiled for 3 min prior to running on SDS-PAGE.

As an alternative method for lysing cells, the cell pellet was resuspended in 1 ml 0.1 M Tris-HCl (pH7.6) and sonicated for 6x 10 second bursts at an amplitude of 15 while kept on ice. The sample was then centrifuged for 5 minutes at 18,000 x*g* and the supernatant transferred into a fresh microfuge tube. 100 µl of supernatant was added to 100 µl of 2xSDS loading buffer. The remaining cell pellet was re-suspended in 1 ml 1% SDS and 100 µl of the mixture added to 100 µl of 2xSDS loading buffer. All samples were boiled for 3 min prior to running 10 µl on SDS-PAGE.

SDS-PAGE. The recipes for the SDS-PAGE gels are summarised below (Table 4.6). Dependent on the size of the protein of interest, the proportions of ingredients in the resolving gel were altered. The resolving and stacking gels were made according to Table 4.6. Ammonium persulphate (APS) was made fresh before use or taken from a frozen aliquot. Tetramethylethylenediamine (TEMED) was added immediately prior to pouring to catalyse polymerisation of the gel. A BIO-RAD Mini-PROTEAN® electrophoresis system (BIO-RAD, United Kingdom) was used for pouring and running the gels and these were assembled according to the manufacturer's instructions. TEMED was added to the resolving gel solution, mixed quickly and pipetted in-between the gel plates up to approximately 1 cm from the top. A layer of isopropanol was pipetted on top of the resolving gel and left to set for approximately 30 min. Isopropanol was removed and the top of the gel washed with two volumes of water. All traces of water were removed from the top before adding the stacking gel solution. TEMED was added to the stacking gel, quickly mixed and pipetted on top of the set resolving gel. An SDS-PAGE comb was inserted and TEMED pippetted into any visible gaps to seal it. The gel was left to set for another 30 min. Once set, the gels were removed from the holders and assembled in the gel tank by clipping the gels into the white electrode piece holder and placed into the clear tank. Tris-glycine electrophoresis buffer (5x concentrated solution consisting of 25mM Tris pH 8.3, 250mM glycine, 0.1% w/v SDS, diluted to 1x before use) was added to the gel tank before the combs in the gels were removed. The boiled protein samples were then loaded into the wells using longer gel tips (Alpha Laboratories, United Kingdom) and the gel run at 100 volts, 20 mA for approximately 4 hrs. Once complete, the gels were removed from the equipment and submerged in Coomassie Blue stain (Phastgel® Blue R (Sigma-Aldrich, United Kingdom) tablets dissolved in water and

methanol as recommended by supplier) for at least 1 hr. The Coomassie Blue stain was poured back into the bottle and the gels rinsed with water before being placed in destain (30% methanol, 10% glacial acetic acid, made up to total volume with water) for a minimum of 1 hr on the rocker at room temperature. The destain was then replaced with fresh solution and left overnight in the fume cupboard covered with aluminium foil. The gels were sandwiched between two clear cellophane films and dried for storage.

Table 4.6. Preparation of SDS-PAGE gels*.

	10% Resolving Gel	15% Resolving Gel	3% Stacking Gel
Standard Distilled Water (SDW)	4 ml	2.3 ml	3.24 ml
Tris	2.5 ml Lower	2.5 ml Lower	1.25 ml Upper
10% Ammonium persulphate	240 µl	240 µl	120 µl
Acrylamide	3.35 ml	5 ml	0.6 ml
TEMED	8 µl	8 µl	15 µl
10% SDS	50 µl	100 µl	-

*Lower Tris consists of 1.5M Tris-Cl pH 8.8, 0.4% SDS. Upper Tris consists of 0.5M Tris-Cl pH 6,8, 0.4% SDS. 10% resolving gel is for separation of protein size 20-80 kDa. 15% resolving gel is for 10-43 kDa.

Protein purification by nickel affinity chromatography. Soluble protein samples were prepared, following the same protocol as above with insoluble and soluble protein expression but at larger culture volumes. Therefore, the cultures grown at appropriate IPTG concentration, temperature and duration were washed in 20 ml STE buffer and centrifuged for 10 min at 11,000 x*g* at 4°C. The pellets were stored in the same slurry condition at -20°C until required.

The slurry samples were defrosted and re-suspended in 5 ml BugBuster^{TM} per gram of wet pellet and incubated at room temperature with rocking for 1 hr. The cultures were then centrifuged at 11,000 x*g* for 20 min at 4°C to separate the cell debris from the soluble protein fraction. The supernatant was transferred to a fresh microfuge tube and 20 µl saved

for analysis. The cell pellet was also kept for analysis and re-suspended in an equal volume (of the initial total volume of culture with BugBuster™) of 1% SDS. 1 ml of Ni-NTA Agarose (QIAGEN, United Kingdom) per 4 ml of lysate was added and the mixture rotated for 1 hr at 4°C before being transferred to a 5 ml polypropylene column (QIAGEN, United Kingdom). The flow-through was collected for analysis before washing the column three times with Wash Buffer A (50mM sodium phosphate buffer pH 6.0, 300mM NaCl, 10% glycerol). A 1 ml sample was collected from the final wash. Soluble proteins were eluted with 1 ml of each elution buffer (consisting of Wash Buffer A with increasing concentrations of imidazole) and all samples collected for analysis. 20 µl of all samples were then mixed with 2xSDS loading buffer on a 1:1 ratio and boiled for 3 min prior to running on SDS-PAGE.

Dialysis. Fractions containing the soluble protein of interest were collected from nickel affinity chromatography and pooled together. Spectra/Por 1 dialysis membrane (Spectrum® Laboratories, Inc., Europe) was cleaned as specified by the manufacturer, prior to dialysis to remove sulphide and metal residues. Sulphide was firstly removed by washing the membrane for one minute at 80°C in two part dH_2O and one part Solution A (1 g sodium sulphite in 100 ml H_20). The membrane was then washed with dH_2O at 60°C for two minutes before adding 2 ml of Solution B (0.4 ml sulphuric acid (99.999%) in 100 ml dH_2O) per 50 ml of total solution. The solution was mixed thoroughly for one minute before rinsing with dH_2O for several minutes. Metal residues were then removed by washing the membrane with 0.05M EDTA (pH 8.0) for 10 minutes before rinsing with dH_2O. The pooled fractions of soluble protein were pipetted into the prepared dialysis membrane, clipped at both ends and left stirring overnight at 4°C in 100 times the volume of soluble protein of Tris-HCl

(50mM, pH7.9). Contents of the dialysis tube were transferred into a falcon tube and stored at 4°C until further use.

4.3 Results

4.3.1 Phenotypic effects of mutations in *mupM*

Ten QuikChange *mupM* mutants were constructed to investigate whether changing single and double amino acids to resemble the active site of a) TmlM would confer the thiomarinol resistance phenotype and b) IleS1 (PDB:1QU2) would confer mupirocin and thiomarinol sensitivity (Table 4.7). The only exception was Mutant 4 (M4) with changes mimicking both TmlM and IleS1. This double mutant was constructed to observe which phenotype will be conferred, resistance or sensitivity. A recapitulation of the residues chosen in Chapter 3 for QuikChange mutagenesis in this study is shown in the next figure (Figure 4.1).

Table 4.7. Summary of all amino acid changes performed using QuikChange Lightning Site-Directed Mutagenesis kit (Agilent, United Kingdom) on pGBT30mupM.

		Residues							
Thiomarinol Resistance ?	TmlM	ALA	PHE	GLY	ASP	ASN	ILE	ARG	TYR
	Mutant #	M1		M4		M5		M7	
Thiomarinol/ Mupirocin Sensitivity ?	MupM	THR_{61}	PHE_{49}	TYR_{549}	ALA_{551}	HIS_{579}	VAL_{581}	LYS_{595}	TYR_{597}
	Mutant #	M2	M3	M4			M6	M8	
	IleS1	ASN	TYR	GLY	ASP	HIS	PHE	GLY	VAL

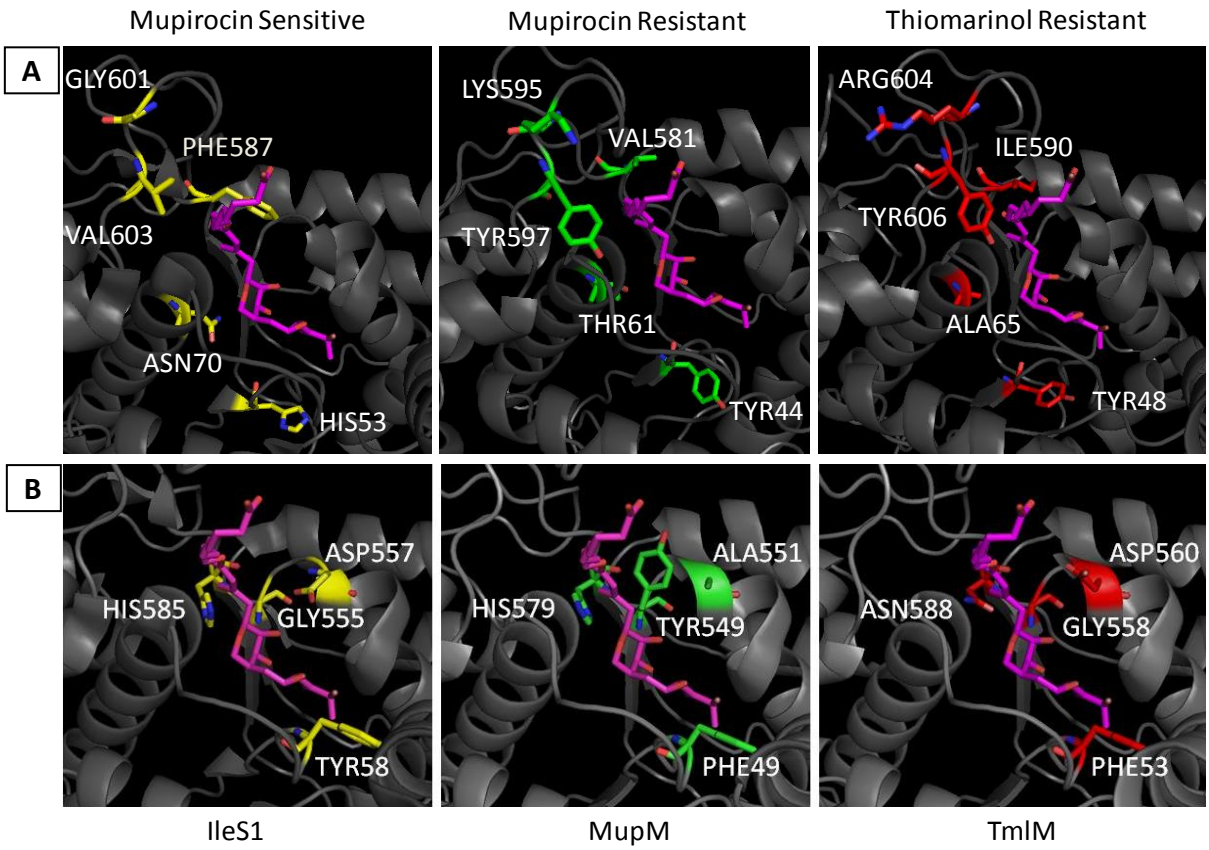

Figure 4.1. Summary of residues selected in Chapter 3 for QuikChange mutagenesis. (A) Residues highlighted in the computational study (Chapter 3). (B) Residues highlighted previously in literature.

Wild type *mupM* (EcoRI-XbaI fragment) was cloned into pGBT30 to provide a template for construction of further QuikChange mutagenesis to produce M1-8. M1+7 and M3+4 were constructed by digesting the relevant fragment carrying the mutation from the respective mutants (pGBT30 M1, 7, 3 and 4) with EcoRI and KpnI and ligating them together to create further double and triple mutants. Several unsuccessful attempts were also made to construct M2+6, until it was later realised that when creating M2 using QuikChange, an additional EcoRI site was introduced by changing Thr61 (DNA sequence: act) to asparagine (aat). With two EcoRI sites, the initial digestion using EcoRI and KpnI enzymes was releasing two fragments and yielding a smaller ligated product compared to the successful M1+7 and M3+4. Due to time constraints, attempting to get this mutant was aborted and the remaining ten mutants were subjected to MIC tests.

M1 and M2 (Thr61Ala and Thr61Asn respectively) were constructed to test whether Asn70 in IleS1 is important for interaction with the 6-hydroxyl group on the pyran ring of mupirocin and thiomarinol as proposed from the in silico modelling. M3 (Phe49Tyr) was constructed to investigate whether the phenylalanine is as important as proposed by Nakama and colleagues to confer mupirocin and/or thiomarinol resistance (Nakama *et al*., 2001).

M4 (Tyr549Gly/Ala551Asp) is a double mutant that introduces the same residues found in both IleS1 and TmlM. Asp557 and Gly555 in IleS1 were proposed by Marion *et al*. (2009) to interact with the hydroxyl group on C4 of the marinolic acid and C6 of the pyran ring of mupirocin respectively. Since both residues are also found in TmlM, these changes should retain function and not make any difference to the resistance phenotype.

M5 (His579Asn/Val581Ile) is also a TmlM-like double mutant. The role of His579 in mupirocin susceptibility was investigated by Nakama *et al*. (2001), by constructing a double mutant of mupirocin sensitive *T. thermophilus* His581Asn/Thr48Phe. His581 is equivalent to His579 and Thr48 to Phe49 on MupM respectively. They found that these two amino acid changes increased the K_i value for mupirocin by one order of magnitude. M5 mimics the same change of histidine to asparagine while retaining its wild-type phenylalanine residue. Nakama *et al*. (2001)'s findings suggest that the mupirocin and/or thiomarinol resistance phenotype should increase for M5.

The mutation Val581Ile was also created in M5 because the residue's close proximity to the first mutation (His579 to asparagine) made it experimentally easy to create a double mutant. A single mutation of valine to isoleucine was not expected to confer any significant changes in phenotype because sequence results in Chapter 3 suggest that this Val581 position and Tyr597 position (in MupM) alternated in having one bulky residue, presumably to maintain the hydrophobic pocket of the active site (Chapter 3, Figure 3.9). This change was included in the double mutant to confirm the above hypothesis.

To further test the importance of one bulky residue at this site, M6 was created so that the mutant protein would now carry two bulky residues. Therefore Val581 in MupM was mutated to phenylalanine, to mimic IleS1. It was hypothesised that having two bulky residues would create a larger hydrophobic patch for the antibiotics to bind more strongly to the active site and this would render the enzyme more susceptible to mupirocin and/or thiomarinol.

Finally, Lys595 was mutated to arginine in M7 to determine whether reduced flexibility of the KMSKS loop would increase resistance to mupirocin and thiomarinol. A double mutant M8 was created to firstly replace Lys595 with the flexible residue glycine to determine whether increased flexibility would render the enzyme more susceptible to both antibiotics. Tyr597 was also exchanged with valine to abolish the important hydrophobic patch created by altering the bulky residue mentioned for M6. Although these two mutations render the active site of M8 more like IleS1, the lack of bulky residues may allow the enzyme to become more tolerant/resistant to mupirocin and/or thiomarinol.

Double and triple mutants M1+7 and M3+4 respectively were constructed to create mutants with possibly more significant phenotypic changes than the single and double mutants M1-8. M1+7 was hypothesised to be more thiomarinol resistant due to its inflexible KMSKS loop and the alanine residue having no hydrogen bonding capacity in its side chain to form the important interaction with the pyran ring. M3+4 was hypothesised to show more susceptibility to mupirocin and/or thiomarinol, with three residues mimicking IleS1.

MIC tests were performed on the QuikChange mutants using a range of mupirocin and thiomarinol concentrations. Results were not all as hypothesised. While the IleS1-like mutants (M2, 3, 6, 8 and 3+4) all showed a decrease in thiomarinol and mupirocin MICs compared to wild-type as hypothesised, most of the TmlM-like mutants (M1, 5, 7, 1+7) also had unexpected MIC decreases (Figure 4.2). Of the above mentioned decreases, only M2, 3+4, 5 and 1+7 mutants showed over two fold decrease in the MIC of thiomarinol compared to wild-type and thus deemed significant. Likewise, M6, 3+4, 5 and 1+7 had significant decreases in the MIC of mupirocin. The only mutant to show increased resistance against

thiomarinol was M7, although this was not considered significant. Against mupirocin, only M1 showed an increase in resistance but again, this was considered insignificant in terms of fold increase.

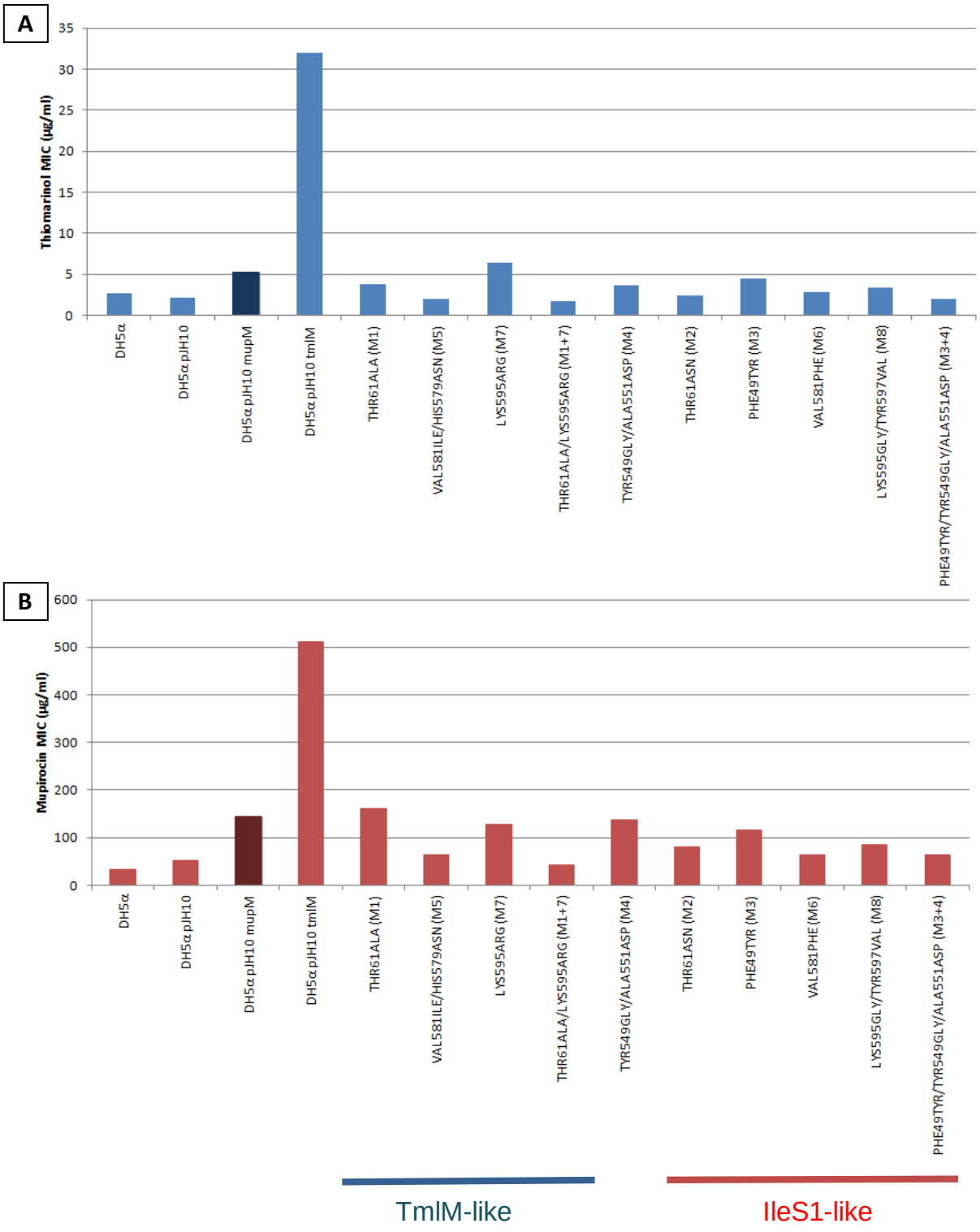

Figure 4.2. MIC of (A) thiomarinol and (B) mupirocin against wild-type DH5α pJH10mupM and QuikChange mutants. The wild-type *mupM* is highlighted by a darker shade of colour. M1, 5, 7 and 1+7 carry TmlM-like mutation(s) and M2, 3, 6, 8 and 3+4 carry IleS1-like mutation(s). M4 have changes that mimic both corresponding TmlM and IleS1 residues. MIC values are an average taken from a single experimental set of triplicates to 10 sets (total of 33 replicates).

M7 (Lys595Arg), as discussed above, has a bulkier residue at the base of the KMSKS loop and this change was hypothesised to reduce the flexibility of the loop and consequently the ability of the enzyme to interact with the pyrrothine, increasing its resistance phenotype against thiomarinol. Although it appears to have a slight increase in MIC of thiomarinol, this is less than a two fold increase and thus insignificant, just as its decrease in MIC of mupirocin. This is peculiar, as it was speculated that by reducing the flexibility of the loop, it may prevent the carboxylate tail of mupirocin interacting with the second lysine of the KMSKS loop and weaken the overall binding strength of mupirocin to M7.

M1 (Thr61Ala) was hypothesised to lose the ability to interact with the 6-hydroxyl group on the pyran ring of both mupirocin and thiomarinol, causing the mutant to become more resistant to both antibiotics. However, this change only increased the mutant's MIC of mupirocin and decreased its MIC of thiomarinol (although both again insignificant). Interestingly, double mutant M1+7, which combines the above two changes, had a significant and unexpected decrease in resistance against both antibiotics.

M4 (Tyr549Gly/Ala551Asp) has altered residues found in both IleS1 and TmlM and hence hypothesised to show no change in phenotype against mupirocin and thiomarinol. Interestingly, there was a decrease in MIC of both antibiotics, although not within the significant fold change.

The MIC results are conflicting, as well as unexpected with some of the mutants. A possible cause for this is that the functionality of these mutant MupMs has been compromised by changing important active site residues and that an optimal combination of changes must be made for the advantageous resistance phenotype to be conferred. This

may be an explanation for the significant decrease in resistance phenotype of double mutant M1+7, compared to the individual single mutants M1 and M7. If too many drastic alterations are made, it may instead impose a fitness cost on the mutants and render them susceptible to the antibiotics.

Alternatively, there may have been a problem with the template *mupM* used to generate these mutants – the average MIC value of pJH10mupM was 5 µg/ml thiomarinol in this study and lower than the 32-64 µg/ml identified in Chapter 2, Table 2.4. A similar issue with lower MIC against pJH10mupM was observed in Chapter 2, which suggests that perhaps the functionality of the template *mupM* was already reduced before mutations were introduced.

4.3.2 Functionality of the *mupM* mutants

In order to check the functionality of the *mupM* mutants, two approaches were undertaken. Firstly, the wild-type *mupM* gene was cloned into pET28a for protein expression and purification. Once the optimal conditions for soluble MupM expression were found, the plan was to purify all mutant MupMs and test their functionality by using them in the aminoacylation assay. The second method for checking functionality was to express the mutants in *P. fluorescens ΔileS1 ΔmupM*.

4.3.3 Insolubility of MupM in heterologous BL21 pET28a system

The pGBT30mupM construct was digested at restriction sites EcoRI and HindIII, and cloned into BL21 pET28a for protein expression and purification. 5 ml and 100 ml cultures were grown in L-broth at 37°C up to OD_{600nm} 0.4, before protein expression was induced at

IPTG concentrations of 0.001, 0.01, 0.05, 0.1, 0.5 and 1 mM and temperatures of 16, 18, 30 and 37°C. 1 ml samples were taken at 4 and 6 hours IPTG induction and overnight at the lower temperatures (16 and 18°C) and checked on SDS-PAGE gels for total and soluble protein expression. The various conditions tested did not yield soluble protein in the sample supernatants (Figure 4.3; Figure 4.4).

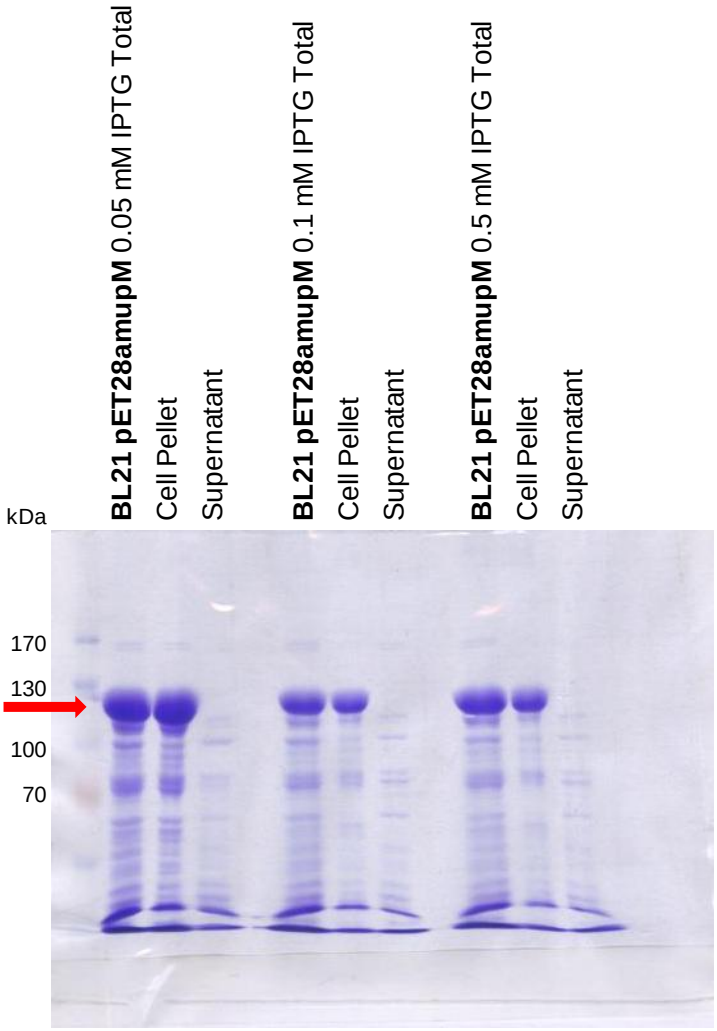

Figure 4.3. SDS-PAGE gel of BL21 (pET28amupM) total, insoluble (cell pellet) and soluble (supernatant) protein expression at various IPTG concentrations. 100 ml cultures were induced with 0.05, 0.1 and 0.5 mM IPTG for 4 hours at 37°C. There are comparable MupM bands in the total and cell pellet lanes but none in the supernatant lane, indicating no soluble MupM was produced under these conditions. The position of the MupM band is indicated by the red arrow.

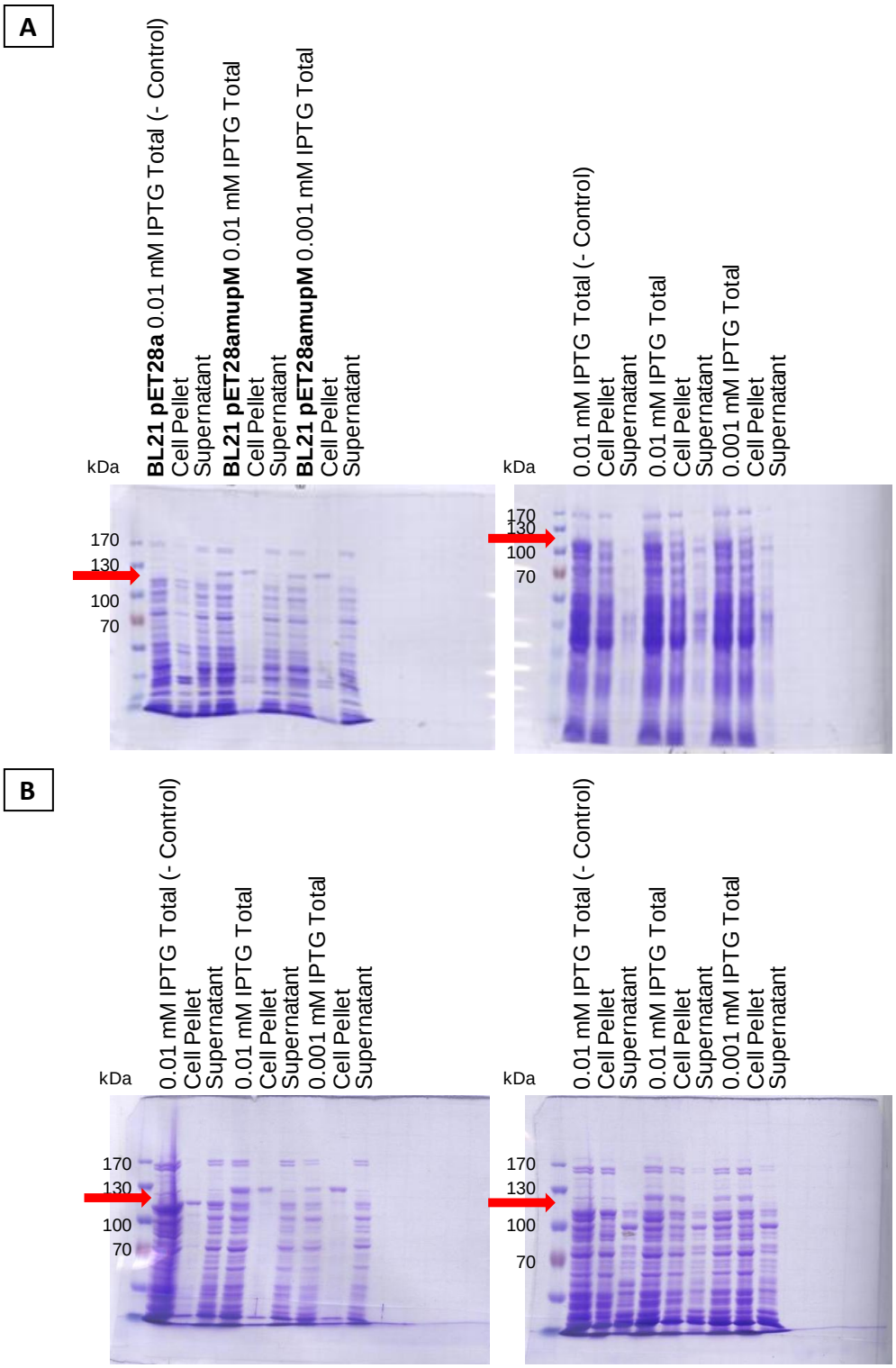

Figure 4.4. SDS-PAGE gels of BL21 (pET28a) and (pET28amupM) total, insoluble (cell pellet) and soluble (supernatant) protein expression at various conditions. 100 ml cultures were induced with 0.01 and 0.001 mM IPTG for 4 hours and overnight at (A) 18°C and (B) 16°C. No MupM band is seen on the BL21 (pET28a) lane (negative control). No significant soluble MupM bands are visible in these conditions. The position of the MupM band is indicated by the red arrow.

Overnight Express™ Instant TB media (Novagen, United Kingdom) was used instead of L-broth in an attempt to promote soluble protein production. Instant TB is an autoinduction (AI) culture media formulated to automatically express IPTG-inducible protein once the culture reaches high cell density. The culture uses the available glucose in the media until it is depleted, and then switches to lactose – which in turn is converted to the inducer allolactose by β-galactosidase. Allolactose de-represses the lac repressor and induces T7 RNA polymerase-dependent protein expression. The media therefore would provide an alternative method to express soluble MupM without the need to check cell density or optimise IPTG induction levels. 5 ml cultures were grown at 22, 30, and 37°C for 24 hours and samples treated in two different methods, using Bugbuster™ and sonication. The results were similar to that of the L-broth cultures. No soluble protein was produced in the AI media (Figure 4.5).

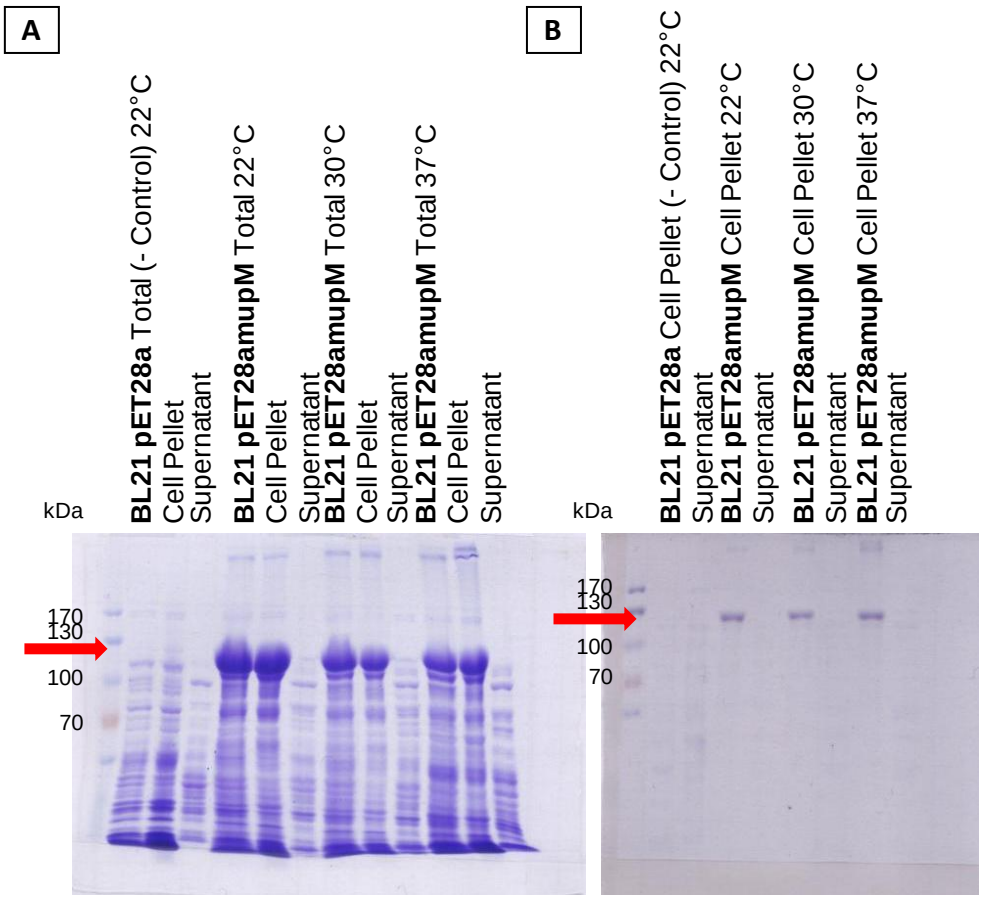

Figure 4.5 SDS-PAGE gels of BL21 (pET28a) and (pET28amupM) grown at various temperatures and treated by (A) Bugbuster and (B) sonication. No soluble MupM was yielded from either methods. The position of the MupM band is indicated by the red arrow.

The pET28amupM plasmid was transformed individually into C41 (DE3) and C43 (DE3) strains, which were kindly donated by Dr. Yanina R. Sevastsyanovich, University of Birmingham. These strains were chosen for their effectiveness in overexpressing toxic proteins. C41 (DE3) was derived from BL21 (DE3) (Miroux and Walker, 1996) and has at least one uncharacterised mutation that prevents autotoxicity from toxic protein expression. C43 (DE3) is a further derivative from C41 (DE3) which contains no plasmid (Miroux and Walker, 1996). 100 ml cultures were grown at 25°C to OD_{600nm} 0.6, before inducing expression with 0.01 mM IPTG overnight. As with the other conditions tested, no soluble MupM protein was yielded using these strains (Figure 4.6).

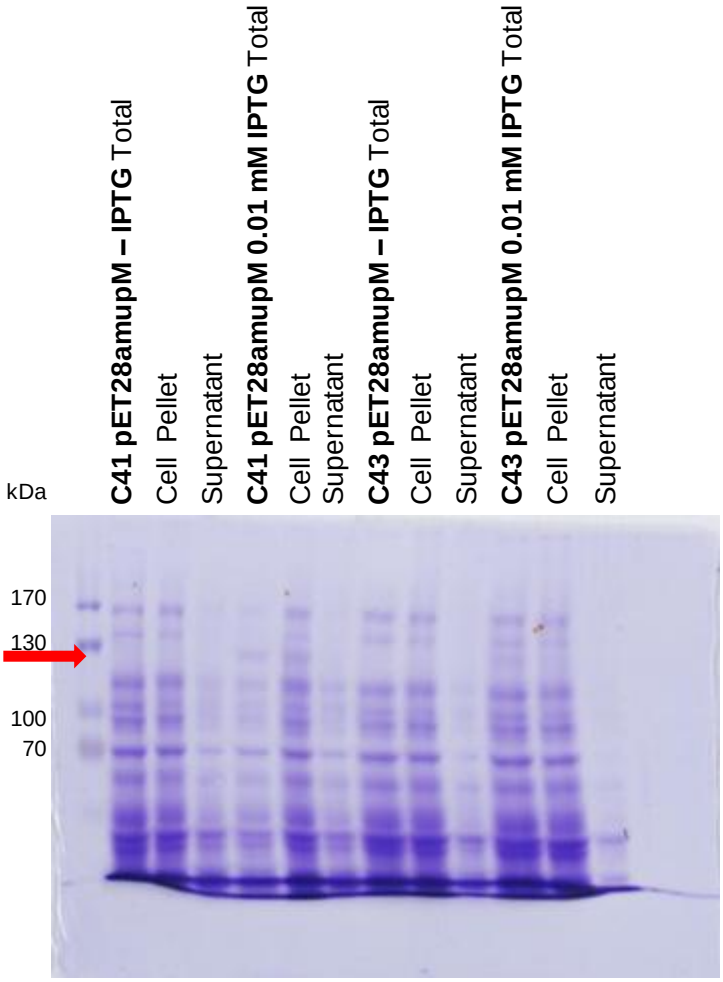

Figure 4.6. SDS-PAGE gel of C41 and C43 (pET28amupM) total and soluble protein expression. The red arrow indicates the size of MupM (117.81 kDa). A faint band of MupM is visible in C41 and C43 total and cell pellet samples at 0.01 mM IPTG induction. The position of the MupM band is indicated by the red arrow.

With no success in yielding soluble MupM, it was hypothesised that the mutant MupMs would also be insoluble using the pET28a system. Attention was therefore concentrated on testing function by complementing a strain lacking *ileS* gene activity.

4.3.4 Expressing *mupM* mutants in *P. fluorescens ΔileS1 ΔmupM*

For creating *P. fluorescens ΔmupM ΔileS1* pJH10mupM, a two part strategy was chosen to maximise the success rate. The wild-type and mutant pJH10mupM constructs were transferred into *P. fluorescens ΔmupM* first, before deleting the chromosomal *ileS1* copy. This would allow *P. fluorescens ΔmupM* to rely on the wild-type or mutant *mupM* copy when it loses its chromosomal *ileS1*. Jo Hothersall and Elton Stephens (University of Birmingham) had previously constructed the suicide plasmid pJHIle01 and shown that *ileS1* can be deleted from *P. fluorescens* with a functional *mupM* gene without affecting the viability of the strain. However, an attempt to construct *P. fluorescens ΔmupM ΔileS1* yielded no colonies (unpublished) showing that *ileS1* and *mupM* are the only genes present encoding isoleucyl-tRNA synthetase activity. Therefore, to test for *mupM* function, it was proposed to transfer wild-type/mutant pJH10mupM into *P. fluorescens ΔmupM* before attempting to delete *ileS1*. If it were possible to do this, then it would show that *mupM* was still active.

Wild-type and all pJH10mupM mutants were first transformed into *E. coli* S17-1, in preparation for mating with *P. fluorescens ΔmupM* (previously constructed by Elton Stephens, University of Birmingham). Conjugation of the wild-type and mutant pJH10mupM plasmids into *P. fluorescens ΔmupM* was successful except for pJH10mupM5. The transconjugants were purified by streaking to single colonies on L-agar plates with ampicillin and tetracycline.

In the second stage, *E. coli* S17-1 with the suicide plasmid pJHIle01 was mated with *P. fluorescens ΔmupM* pJH10mupM (all mutants were mated first because it was assumed that at least some of the mutants would still be functional). Unexpected difficulties were noted in this step because liquid overnight cultures of *P. fluorescens* strains did not grow consistently well in the presence of tetracycline at either 7.5 or 15 µg/ml despite a variety of attempts to diagnose the problem. These discrepancies suggest that tetracycline concentrations must be carefully controlled.

P. fluorescens ΔmupM pJH10mupM M1-8 (except M5) that had grown were mated with S17-1 carrying the suicide vector pJHIle01 and serial dilutions of the cultures grown on MM agar plates with 50 µg/ml kanamycin (to select for the suicide vector) and 15 µg/ml tetracycline. The cultures were grown for 6 days at 30°C but no colonies were yielded.

It was unexpected for the mating of *P. fluorescens ΔmupM* pJH10mupM1-8 and S17-1 pJHIle01 to fail at this stage as only the first recombination step (integration) would have occurred and the *ileS1* would still be intact. The cultures were then to be streaked out onto L-agar plates with tetracycline and 5% sucrose to remove the suicide vector. Therefore, if the functionality of the *mupM* mutants was compromised from the QuikChange mutagenesis, it was hypothesised that no colonies would be yielded at the later stage when the suicide plasmid was excised from the chromosome.

To ensure the basic replacement strategy was working, the process was repeated using wild-type *mupM* and all the variants of the antibiotic selection procedure worked out in trying the replacement with the mutants (MM agar with 15 µg/ml tetracycline and 50 µg/ml kanamycin; 7 µg/ml tetracycline and 50 µg/ml kanamycin; and 50 µg/ml kanamycin

only). Kanamycin selection was maintained at 50 μg/ml for all three variations because of observations made from the preliminary matings of *P. fluorescens ΔmupM* pJH10mupM2 and S17-1 pJHIle01. Although colonies were obtained from these matings, none grew well on re-streaking and so appear to have been false positives.

To test whether the presence of a pJH10 plasmid affects the ability of *P. fluorescens* to accept a suicide plasmid (indicating a technical issue), *P. fluorescens* pJH10 was mated with S17-1 pJHIle01. Mating appeared to be unsuccessful with no true *P. fluorescens* pJH10 pJHIle01 colonies. Due to time constraints, testing the functionality of the *mupM* mutants was not continued. Further work is required to understand whether it is technically possible to conjugate more than one plasmid into *P. fluorescens*.

4.4 Discussion

4.4.1 Functionality of *mupM* mutants

The MIC results of the *mupM* mutants were interesting, although not all as hypothesised. All IleS1-like mutants showed a decrease in MIC values of thiomarinol and mupirocin, although only M2 and 3+4 for the former and M6 and 3+4 for the latter showed significant shifts above the two fold cut off point. Amongst the TmlM-like mutants, M1 and M7 were the only two to show improvement in their MIC values of mupirocin and thiomarinol respectively, although this was not considered significant based on their less than two fold change. This may still suggest that Ala65 and Arg604 are important residues that confer the resistance phenotype of TmlM; however, it is interesting that when these two changes are combined in M1+7, its resistance is noticeably and significantly reduced

against both antibiotics. Likewise, TmlM-like double mutant M5 also showed a similar decrease in phenotype. There appears to be a trend amongst the majority of the *mupM* mutants; there is a decrease in resistance against thiomarinol and mupirocin when residues are altered in the active site. This observation is also applicable to a certain extent to M1 and M7, as they only show improvement against one of the tested antibiotics and not both.

Therefore, it is essential to confirm that the functionality of the *mupM* mutants has not been compromised, before any further conclusions can be drawn from the MIC results. The parent *mupM* gene was initially thought to be functioning correctly, as the gene was cloned from the template used in the QuikChange mutagenesis (pGBT30mupM) back to the expression vector pJH10 for all further MIC tests. The wild-type pJH10mupM had a mupirocin MIC value comparable to that identified before the start of this study, when original -80°C stock was used (64-128 µg/ml).

However, revisiting the literature suggests that the pJH10mupM plasmid stock is behaving differently from the wild-type *mupM* gene in the *P. fluorescens* strain. While MIC values of 64-128 µg/ml mupirocin were consistently yielded against DH5α carrying pJH10mupM in this thesis, Yanagisawa and Kawakami reported values of 800-1,000 µg/ml against their DH5α strain carrying pEXR2 vector (expressing *mupM*) at cell densities of 10^6 cells (Yanagisawa and Kawakami, 2003). They also showed the producer *P. fluorescens* to be resistant to > 1,000 µg/ml of mupirocin. Similarly, El-Sayed *et al*. (2003) reported an MIC of 30 to 250 µg/ml when *mupM* was expressed in the pAKE900 construct in *E. coli* DH5α (Materials and Methods not specified). The MIC methodology and cell densities used in this study and by Yanagisawa and Kawakami differ slightly (broth dilution MIC with 5 x 10^5 cfu/ml

and agar dilution with 10^6 cells per 2 µl spots respectively); however the MIC breakpoint yielded in this study appear to be too low, suggesting two of the following: (1) that the *mupM* gene used is somehow compromised or (2) there is great difference in the level of *mupM* expression in the various pEXR2, pAKE900 and pJH10 plasmids due to difference in promoter sequence, ribosome binding site and/or plasmid replicon and copy number. Details of the pEXR2 expression vector, pEXPCR could not be found in the literature. However, the pAKE900 construct is based on the pGEM-TEasy vector, which is a high copy number vector containing the origin of replication pMB1 and it is under the control of T7 and SP6 RNA polymerase promoters (Promega, United Kingdom). pJH10, on the other hand contains an IncQ replicon and is a medium copy number vector. Although induced with IPTG, pAKE900 may express more MupM than pJH10, conferring high thiomarinol resistance than what was observed in this study. (See Chapter 2 for more discussion on *mupM* overexpression possibly conferring thiomarinol resistance.)

After completion of the experimental procedures in this study, discrepancies between the published and recently re-sequenced *mupM* sequences were identified by Anthony Haines, University of Birmingham and updated on the NCBI database on the 14th February 2014. A total of seven mutations were found on the *mupM* gene used in this study and in Chapters 2 and 3 (Table 4.8).

Table 4.8. Summary of mutations identified on MupM used in this study, Chapter 2 and 3*.

	MupM Residues	
Position No.	Used in this study	Wild-Type
400	Thr	Ala
667	Pro	Leu
671	Pro	Leu
717	His	Tyr
805	Cys	Arg
885	Val	Ala
939	Pro	Ser

*Residues highlighted in red are those identified in Chapter 2 and initially thought of as sequencing errors.

It is suspected that five of the seven mutations were introduced by PCR when the gene was initially cloned out of *P. fluorescens* by A. Kassam El-Sayed (2003). This copy was then sequenced and the results published on the NCBI database (Accession number: AAM12927.1) and used for the purpose of this study, Chapter 2 and 3. This would explain the reason for the five mutations not being identified when spontaneous and UV mutants from Chapter 2 and QuikChange mutants from this study were sequenced. The additional two mutations identified in Chapter 2 are thought to have been introduced when *mupM* was subsequently cloned into pJH10 and pUC18 by Jo Hothersall and Elton Stephens, and hence noticeable when pairwise aligned with the published sequence.

These additional seven mutations that were unknown during the duration of these studies may explain the low MIC values and the decrease in thiomarinol and mupirocin tolerance amongst the QuikChange mutants. The mutations were located on the MupM structure previously modelled in Chapter 2 using PyMOL (Figure 4.7). The structure revealed five out of seven mutations to be located away from the active site. The last two residues

were at the N-terminus end of the protein (after Cys805) and not modelled as it appeared to be part of the linker region.

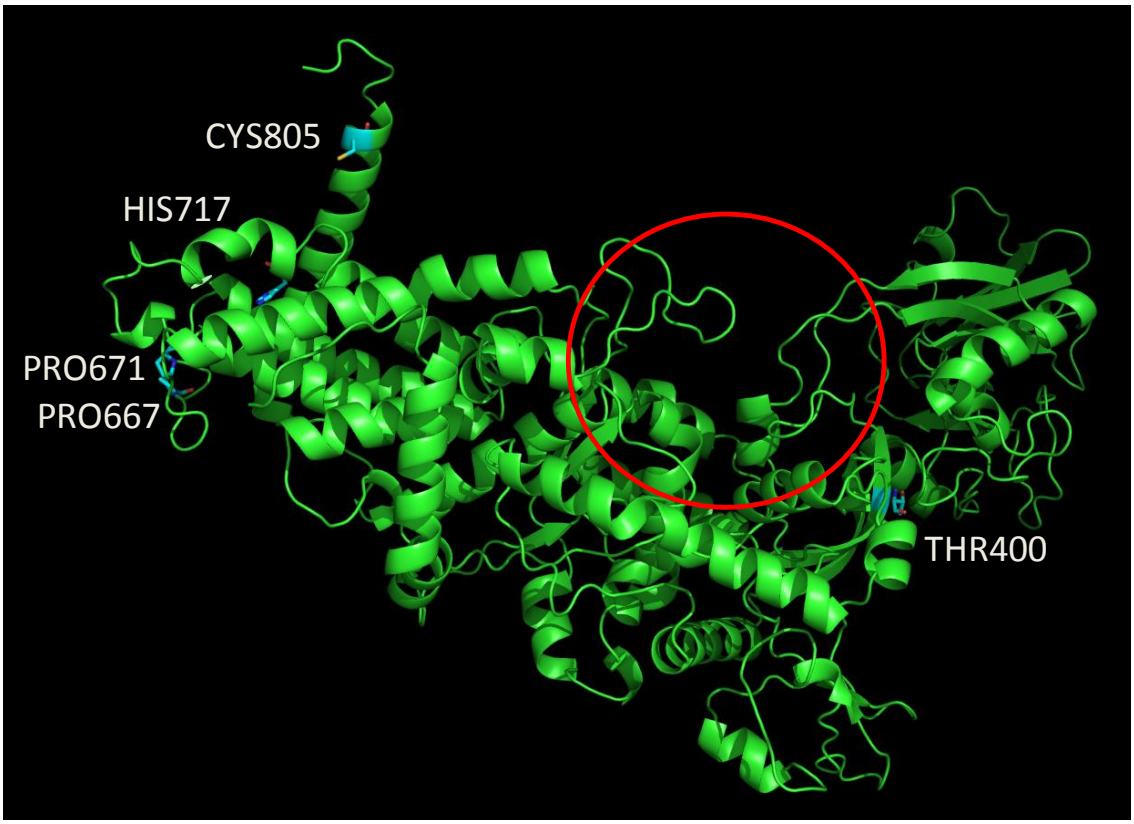

Figure 4.7. Mutations on the MupM copy used in this study and in Chapter 2. The mutated residues are highlighted in blue. The active site is highlighted by the red circle.

Although the mutations were not located in the active site of MupM, the multiple mutations may have had a fitness cost on the enzyme and caused decrease in functionality and mupirocin-resistance. Some of the amino acid changes are quite drastic, such as the leucines in position 667 and 671 mutated to flexible proline residues. These changes may alter how the enzyme folds and/or behaves compared to the wild-type. This may also affect the solubility of MupM. Adding further mutations during this study may have further dampened the functionality of this enzyme. To test these theories, the correct *mupM* gene needs to be re-cloned into pJH10 and its MIC value verified. If the resistance phenotype is

similar to that reported by Yanagisawa and Kawakami, it would be of interest to repeat the QuikChange mutagenesis using the correct *mupM* gene to see if the residues identified in Chapter 2 are truly important in conferring the thiomarinol resistance phenotype.

Once the correct *mupM* gene is cloned into pJH10, there may also be advantages in repeating the mating experiment of *P. fluorescens* pJH10 and S17-1 *pAKE604ΔileS1*. Colonies were yielded in the initial experiment, although the identity of these colonies needed to be confirmed as true *P. fluorescens* pJH10 pJHIle01 and not contaminants or *P. fluorescens* carrying one plasmid only.

4.4.2 Mimicking TmlM does not necessarily increase thiomarinol resistance

If the MupM mutants are functional yet have decreased mupirocin and thiomarinol resistance, it suggests that simply mimicking the active site of TmlM is not enough to gain thiomarinol resistance and that while changing Lys595 in MupM to an arginine may increase thiomarinol tolerance, perhaps a specific combination of changes is required to create the resistance phenotype. Furthermore, mimicking the active site of TmlM does not necessarily increase mupirocin resistance (as demonstrated by M7).

Perhaps a better strategy for understanding the key residues involved in the thiomarinol resistance phenotype would be to substitute amino acids in TmlM to those found in MupM and to look for loss of resistance, rather than gain of resistance. However, it is also worth noting that not seeing an increase or decrease in MIC value does not necessarily mean that less binding is taking place between the ligand and the active site of the mutants, as discussed by Nikaido and Pages (2012). (See Chapter 6, Discussion.)

As discussed in Chapter 3 and in this study, Nakama and colleagues identified two residues (His581 and Thr48) on the mupirocin sensitive *T. thermophilus* to be important in conferring the mupirocin sensitive phenotype. When these residues were mutated to mimic those of an eukaryotic IleS (asparagine and phenylalanine), they found the K_i value to increase by a order of magnitude (Nakama *et al*., 2001). They did not perform MIC tests on their double mutant.

The mutant M5 was created in this study carrying the two important residues asparagine and phenylalanine to mimic TmlM and similarly the eukaryotic IleS mentioned by Nakama *et al*. (2001). However, a decrease in MIC values was seen for both mupirocin and thiomarinol and not what was expected based on the paper by Nakama *et al*. (2001). It would be interesting to measure the K_i for mupirocin and thiomarinol against this mutant to see if Nakama and his colleagues' results are reproducible in MupM.

Overall, it would be useful to have soluble wild-type and mutant MupM protein for further work to understand more of the kinetics of these enzymes instead of relying on their MIC phenotype. It may be worthwhile continuing to troubleshoot for yielding soluble protein by ways of denaturing and re-naturing or changing the expression system.

4.4.3 Insolubility of *P. fluorescens* proteins in heterologous system

Previous protein purification works undertaken by colleagues have all faced difficulty in yielding soluble protein from the mupirocin biosynthesis cluster. By comparison, expressing and purifying IleS1s from *E. coli* DH5α, SBW25 and *B. subtilis* were straightforward and required minimal method optimisation as described in Chapter 5. As mentioned in Chapter 1, mupirocin is produced by a chromosomally encoded Type I

polyketide synthesis cluster called the *mup* cluster (Whatling *et al.*, 1995). The biosynthesis genes are clustered into six multifunctional polypeptide modules. Previous works, including this study have attempted to express single proteins in the pET28a system and never entire modules. It is now hypothesised that soluble proteins may be more effectively yielded by expressing modules of proteins together, as laboratory and computational work are starting to elucidate the important interactions between proteins and their linkers in the same modules (Thomas *et al.*, Unpublished).

Alternative approaches to yielding soluble MupM would be to follow the protocol of Yanagisawa and Kawakami (2003). They were successful in producing soluble IleS1 and MupM (called IleRS-R2 in their publication) by expressing and purifying these proteins directly from *P. fluorescens* using DEAE-Sephacel Chromatography and multiple elutions using various buffers. They were also able to overexpress and purify the proteins by expressing the genes on plasmid pEXR1 (formerly called pPFNB7) in *E. coli* strain Ts331. The cultures were grown in large volumes at 3 L of rich SOB medium with 50 µg/ml ampicillin and 0.5 mM IPTG at 30°C for 10 hours. The cells were harvested by sonication and the purified proteins yielded from a three-step chromatography method using DEAE-Toyopearl or DEAE-Sephacel, *n*-butyl-Toyopearl and hydroxyapatite columns. Their second protocol suggests that increasing overall production volume may allow soluble proteins to be yielded from the pET28a system used in this study.

4.4.4 Concluding remarks

This study has made attempts to understand whether increased binding to the IleS target is an important mechanism behind thiomarinol's potency. QuikChange mutagenesis

was performed in an attempt to confirm the importance of the residues identified in the computer modelling work of Chapter 3, and whether increased binding affinity of thiomarinol to its target IleS confers its potent activity. The underlying issues with the seven mutations in the *mupM* gene used in this study needs to be corrected and the QuikChange mutations repeated. The identification of unwanted mutations at the end of this study highlights the importance of confirming all materials prior to undertaking experiments – this is regardless of experimental repetition and additional costs such as in sequencing. There is great value in confirming the residues involved in the interaction with thiomarinol, as it will provide a comprehensive map of the target enzyme's active site and allow a more informed and tactical approach to producing improved analogues.

CHAPTER 5

5 PURIFICATION AND ENZYME ACTIVITY OF ILES

5.1 Introduction

The aim of the work described in Chapters 3 and 4 was to determine the specific residues in the IleS active site that may allow thiomarinol to bind more strongly than mupirocin to their target enzyme. Although the computational work in Chapter 3 identified eight residues of potential importance, the mutagenesis of these amino acids in Chapter 4 did not confirm their role in increasing or decreasing thiomarinol/mupirocin resistance.

In this section, a more direct approach of enzyme kinetics was taken to determine whether increased binding of thiomarinol to IleS is a major contributor to its potency. The mechanism of mupirocin inhibition of IleS from *Staphylococcus aureus* and *Escherichia coli* has previously been characterised using steady-state kinetics (Hughes and Mellows, 1980; Pope *et al.*, 1998a) but work in characterising the activity of thiomarinol by scientists at Daiichi-Sankyo did not go as far as looking at its activity against purified enzymes (Shiozawa and Takahashi, 1994; Shiozawa *et al.*, 1993, 1995, 1997). The aim of the study was to determine the inhibitor concentration (K_i) for thiomarinol via the aminoacylation assay using IleS1 from *E. coli* DH5α. If thiomarinol is a stronger inhibitor than mupirocin, the former would yield a lower K_i value than mupirocin.

5.2 Materials and Methods

5.2.1 Bacterial strains, growth conditions and plasmids

All bacterial strains and plasmids used in this study are listed in Table 5.1.

For protein purification, various IleSs were individually expressed in *E. coli* BL21 carrying plasmid pET28a (Novagen, United Kingdom) as outlined in Chapter 4. All strains were grown in L-broth at 200 rpm, with the appropriate antibiotic for selection. IPTG was added as appropriate, ranging from 0.1 to 0.001 mM concentrations.

Table 5.1. Bacterial strains and plasmid used in this study.

Bacterial Strain	Genotype	Phenotype	Source/Reference
B. subtilis 1064	*trpC2amyE::(spec Pxyl-gfp-lacI) chr::pSG1196 (rrnD-lacO cat)*	Inherently mupirocin sensitive.	Moir *et al.*, 1979
E. coli BL21 (DE3)	F$^-$ *ompT hsdSB gal dcm* (DE3)	Strain for inducing high protein expression. Contains the DE3 lysogen that carries the gene for T7 RNA polymerase under the control of the lacUV5 promoter.	Invitrogen
E. coli DH5α	*endA1 recA hsdR17 lacZΔM15 supE44 gyrA96 thi-I relA1* F$^-$	High transformation efficiency strain.	Gibco BRL
P. fluorescens SBW25	-	Mupirocin non-producer wild type (WT). Inherently ampicillin resistant.	Rainey and Bailey, 1996
Plasmid	**Properties**	**Size (kb)**	**Source/Reference**
pET28a	KanR, T7*lac* promoter, N-terminus His•Tag	5.4	Novagen

5.2.2 Cloning IleS1 from various microorganisms

IleS1 genes from *E. coli* DH5α, *Pseudomonas fluorescens* SBW25 and *Bacillus subtilis* 1064 were PCR-amplified from boiled cell samples using Q5® High Fidelity DNA Polymerase (New England BioLabs Inc, United Kingdom). 1-2 single colonies were resuspended in 200 µl dH_20 and vortexed before boiling for 10 minutes. The mixture was then centrifuged for 5 minutes at 11,300 x*g* and 2 µl of supernatant used for each PCR reaction. Primers were designed with suitable restriction sites at the 5' ends to allow subsequent cloning of the amplified gene into pET28a (Table 5.2). The PCR reaction (final volume of 50 µl) consisted of 10 µl of 5x Q5® Reaction Buffer, 4 µl of 2.5 mM dNTP mixture, 2.5 µl of 10 µM forward and reverse primer each, 2 µl of boiled template DNA, 0.5 µl of Q5® High-Fidelity DNA polymerase, 10 µl of 5x Q5® High GC Enhancer and 18.5 µl of dH_2O. The PCR programme was

set as recommended by the manufacturer but with 2 initial cycles at a lower annealing temperature optimal for the primer to correctly anneal to the *ileS1* gene. To determine the optimal annealing temperatures, the Tm calculator provided by New England Labs was used. For the 2 initial cycles, the Tm was calculated using the primer sequence excluding the additional restriction site sequence. The remaining 28 cycles were run at the annealing temperature optimal for the whole primer (including the restriction site) (Table 5.3). 5 µl of the PCR reaction was run on 1 % agarose gel to confirm the presence of the correct product before cleaning the remaining reaction using a gel band purification kit (G.E. Healthcare, United Kingdom), digesting with the appropriate restriction enzymes and ligating into pET28a vector. The ligated vector and insert was transformed into *E. coli* BL21 for further protein expression and purification. The sequence of the cloned DH5α *ileS1* gene was checked using primers described in Table 5.2.

Table 5.2. Oligonucleotide primers designed for amplifying and checking the sequence of *ileS1* genes*.

Organism	PCR Primer
E. coli DH5α	5'-aaaGCTAGCatgagtgactataaatcaaccct-3' 5'-aaaCTCGAGtcaggcaaacttacgtttttc-3'
B. subtilis 168	5'-aagGCTAGCatggattttaaagacacgct-3' 5'-aaaCTCGAGttatttttgatagtatttttcaacg-3'
P. fluorescens SBW25	5'-aaaGCTAGCatgaccgactataaagcca-3' 5'-aaaCTCGAGttaggcatagtgacgaacc-3'
Organism	**Sequence Checking Primer**
E. coli DH5α	5'-taatacgactcactataggg-3' (Universal T7 Promoter) 5'-gctagttattgctcagcgg-3' (Universal T7 Terminator) 5'-acctgaccatggacttcaaaact-3' 5'-acttatctgccgggcacttat-3' 5'-tggttcatgtcttccctaat-3'

*All *ileS1* genes were amplified with NheI or XhoI restriction sites at the 5' end. Restriction sites are highlighted in capital letters.

Table 5.3. PCR programme for using Q5® High-Fidelity DNA Polymerase as recommended by supplier[1].

Cycles	Temperature	Time
1	98°C	30 seconds
2	98°C	10 seconds
	x°C	30 seconds
	72°C	30 seconds/kb*
28	98°C	10 seconds
	xx°C	1 minute
	72°C	30 seconds/kb*
1	72°C	2 minutes

[1]The lower annealing temperature was used for x and the higher temperature for xx. Therefore 56°C and 65°C respectively were used for *B. subtilis* and 61°C and 70°C for DH5α and SBW25. *In this study, 90 seconds for the approximately 3 kb length *ileS1* genes.

5.2.3 Protein expression and purification of IleSs

For total and soluble protein expression, SDS-PAGE and protein purification by nickel affinity chromatography, methods outlined in Chapter 4 were followed.

For dialysis, fractions containing the soluble protein of interest were collected from nickel affinity chromatography and pooled together. Spectra/Por 1 dialysis membrane (Spectrum® Laboratories, Inc., Europe) was cleaned as specified by manufacturer, prior to dialysis to remove sulphide and metal residues. Sulphide was firstly removed by washing the membrane for one minute at 80°C in two part dH_2O and one part Solution A (1 g sodium sulphite in 100 ml H_20). The membrane was then washed with dH_2O at 60°C for two minutes before adding 2 ml of Solution B (0.4 ml 99.9% sulphuric acid in 100 ml dH_2O) per 50 ml of total solution. The solution was mixed thoroughly for one minute before rinsing with dH_2O for several minutes. Metal residues were then removed by washing the membrane with 0.05M EDTA (pH 8.0) for 10 minutes before rinsing with dH_2O. The pooled fractions of soluble protein were pipetted into the prepared dialysis membrane, clipped at both ends and left stirring overnight at 4°C in 100x the volume of soluble protein of Tris-HCl (50mM, pH7.9). Contents of the dialysis tube were transferred into a falcon tube and stored at 4°C until further use.

5.2.4 Quantification of active IleS concentration

The concentration of active enzyme in the dialysed IleS1 fraction was determined by the protocol outlined by Francklyn *et al.* (2008). An assay mix consisting of 10 µM [^{14}C] isoleucine (final specific activity of 5 µCi/ml), 2 mM Mg-ATP, 144 mM Tris-HCl, pH 7.78, 10 mM $MgCl_2$, 1 U/ml inorganic pyrophosphatase and 5 mM β-mercaptoethanol was prepared

and equilibrated at the temperature selected for the assay (25°C or 37°C). The assay mix was then separated into individual 15 µl final volume aliquots and 1 µM of dialysed IleS1 (2 µl) added to start the reaction at the chosen temperature. After incubation periods of 5, 10 or 20 minutes, the 15 µl aliquots with enzyme (in triplicates) were spotted onto dry nitrocellulose filters (Sigma-Aldrich, United Kingdom) in 144 mM Tris-HCl pH 7.78 buffer, left for varying periods to allow binding and then washed with 5 ml cold 144 mM Tris-HCl pH 7.78 buffer. The filters were dried at 42°C, vortexed in 10 ml Ultima Gold^{TM} MV scintillation cocktail (Perkin Elmer, United Kingdom) and counted in the scintillation counter. An aliquot of assay mix without the addition of IleS1 (in triplicate) was also spotted onto nitrocellulose filters and dried without washing to determine the specific activity of the assay mix. This specific activity was then used to calculate the concentration of active IleS2 i.e. the amount of IleS1 that contained bound [^{14}C] isoleucyl adenylate. Equations used were as follows:

Specific Activity (CPM/pmol) = Average of no wash (CPM) / Ile in aliquot (pmol)

[Active IleS] (pmol) = Average of washed aliquots (CPM) / Specific Activity (CPM/pmol)

5.2.5 Aminoacylation assay

Aminoacylation assays were set up at a range of enzyme concentrations. The assay mix consisted of 50 mM Tris-HCl (pH 7.9), 10 mM $MgCl_2$, 50 mM KCl, 2 mM dithiothreitol (DTT), 0.2 mg/ml BSA, 1 mM ATP, L-[U-^{14}C] isoleucine (specific activity of 11.5 MBq/mmol) and 4 mg/ml final concentration of *E. coli* tRNA (equivalent to 4 µM $tRNA^{Ile}$) (Sigma-Aldrich, United Kingdom) and was equilibrated at 25°C before separating them into 15 µl final volume aliquots. Active IleS1 was diluted to chosen concentrations with 144 mM Tris-HCl, pH 7.78 and left on ice prior to use. IleS1 was added to the assay mix to start the reaction and at

specific time points, the 15 µl aliquots (in triplicates) were mixed with 15 µl of 10% trichloroacetic acid (TCA) pre-chilled on ice to terminate the reaction and incubated on ice for 10 minutes. The contents were then filtered onto dry glass fibre filters and washed with 5 ml 5% TCA, followed by 5 ml cold ethanol. The filters were dried at 42°C before vortexing in 10 ml Ultima Gold^{TM} MV scintillation cocktail for counting.

5.3 Results

5.3.1 Isolation of soluble IleS1 from DH5α, SBW25 and *B. subtilis*

The *ileS1* genes from *E. coli* DH5α, *P. fluorescens* SBW25 and *B. subtilis* were PCR-amplified using the designed primers (Table 5.2) and each cloned into pET28a vectors as explained in the Materials and Methods. Once transformed into BL21 cells, growth conditions and IPTG concentrations were optimised to give a level of expression that would result in sufficient soluble IleS1. 5 ml LB cultures with 50 µg/ml of kanamycin were grown up to an OD_{600nm} 0.4 at their respective temperatures of 25, 30 and 37°C before being induced with IPTG concentrations of 0.1, 0.01 and 0.001 mM for 4 hours at 37°C and overnight for the two lower temperatures (Figure 5.1; Figure 5.2; Figure 5.3).

For soluble protein expression of IleS1 from DH5α and *B. subtilis*, 37°C growth temperature and 0.1 mM IPTG induction for 4 hours was deemed most suitable. For expression of SBW25 IleS1, growth at 30°C and 0.001 mM IPTG induction overnight was chosen. These conditions were then applied for up-scaling the production cultures to 100 ml. The larger volume cultures were treated with Bugbuster as outlined in the Materials and

Methods and soluble protein fractions collected using nickel affinity chromatography (Figure 5.4).

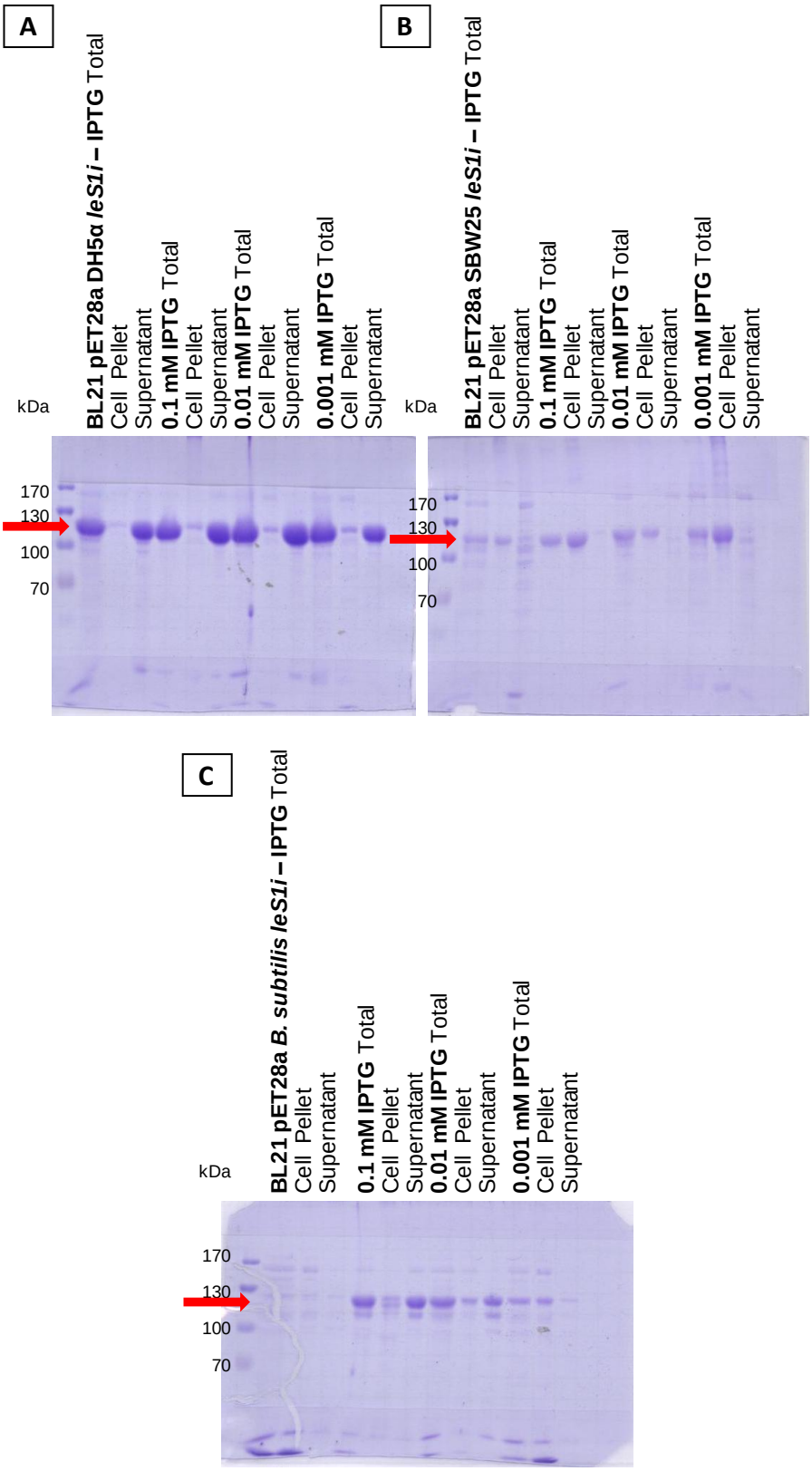

Figure 5.1. SDS-PAGE gels of BL21 pET28a *ileS1* from (A) DH5α, (B) SBW25 and (C) *B. subtilis* induced at various IPTG concentrations for 4 hours at 37°C. The red arrow indicates the position of the IleS1 band.

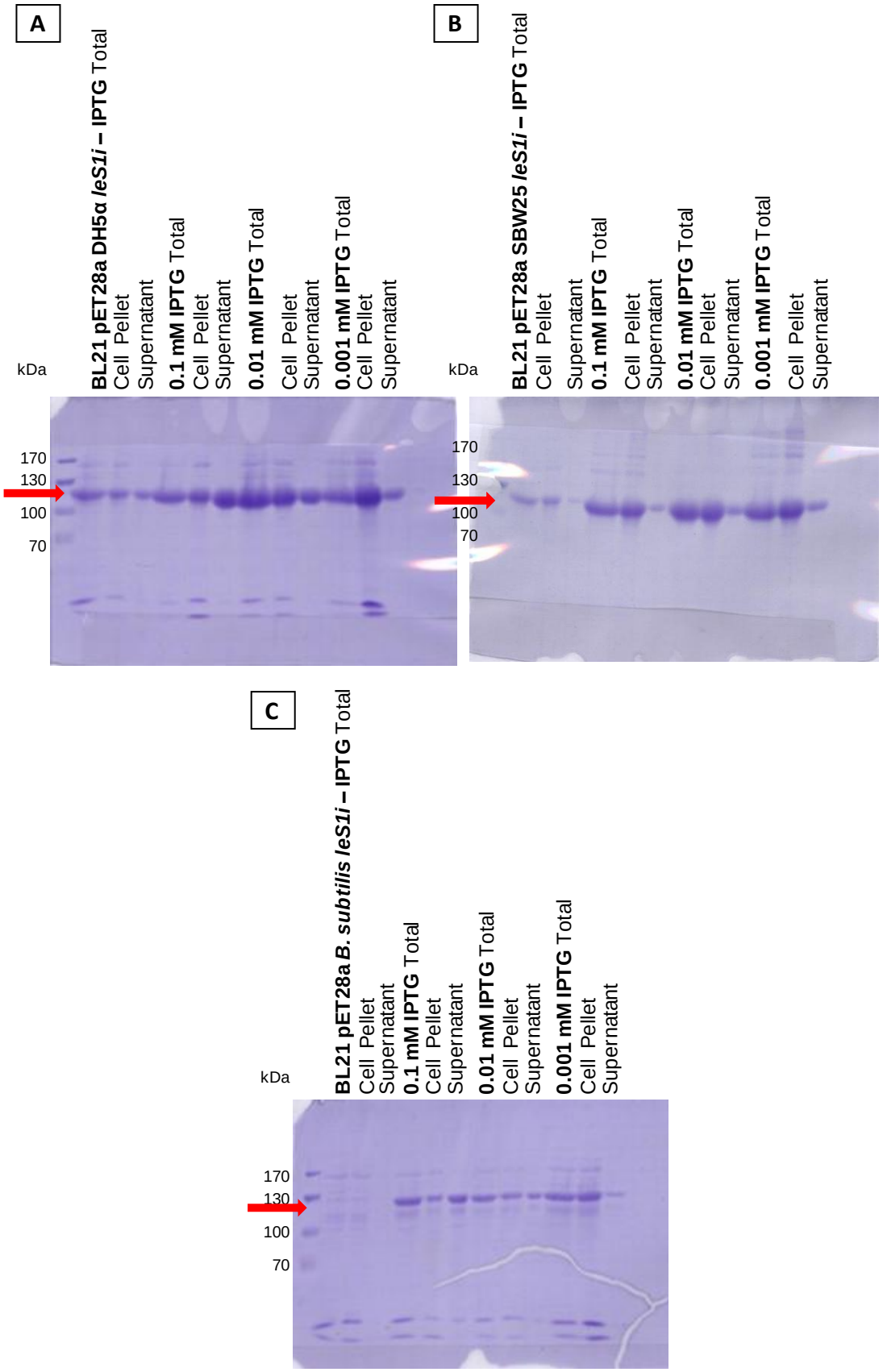

Figure 5.2. SDS-PAGE gels of BL21 pET28a *ileS1* from (A) DH5α, (B) SBW25 and (C) *B. subtilis* induced overnight at various IPTG concentrations at 30°C.

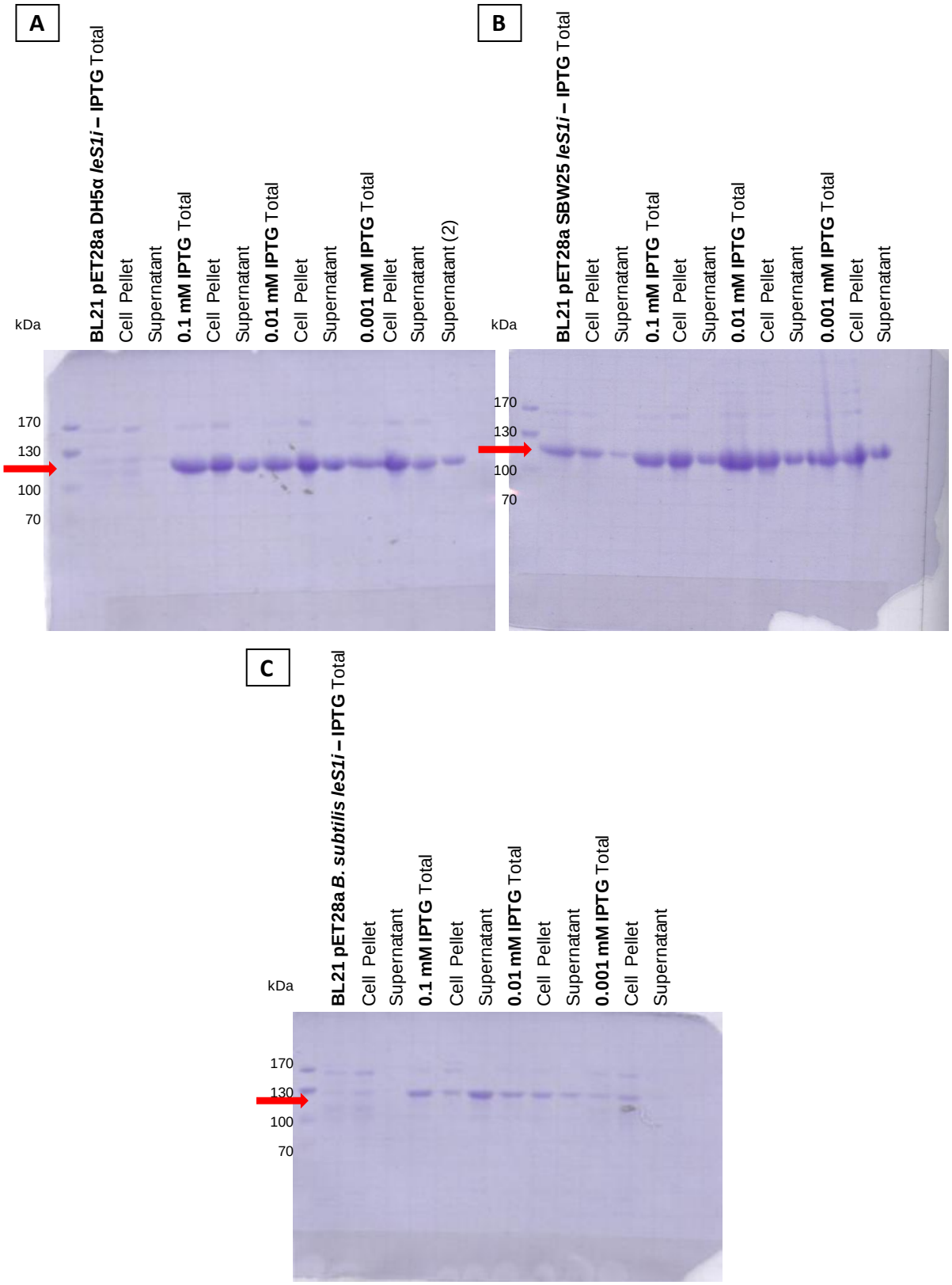

Figure 5.3. SDS-PAGE gels of BL21 pET28a *ileS1* from (A) DH5α, (B) SBW25 and (C) *B. subtilis* induced overnight at various IPTG concentrations at 25°C. (A) Sample supernatant (2) from the DH5α gel is an overspill from the lane on the left.

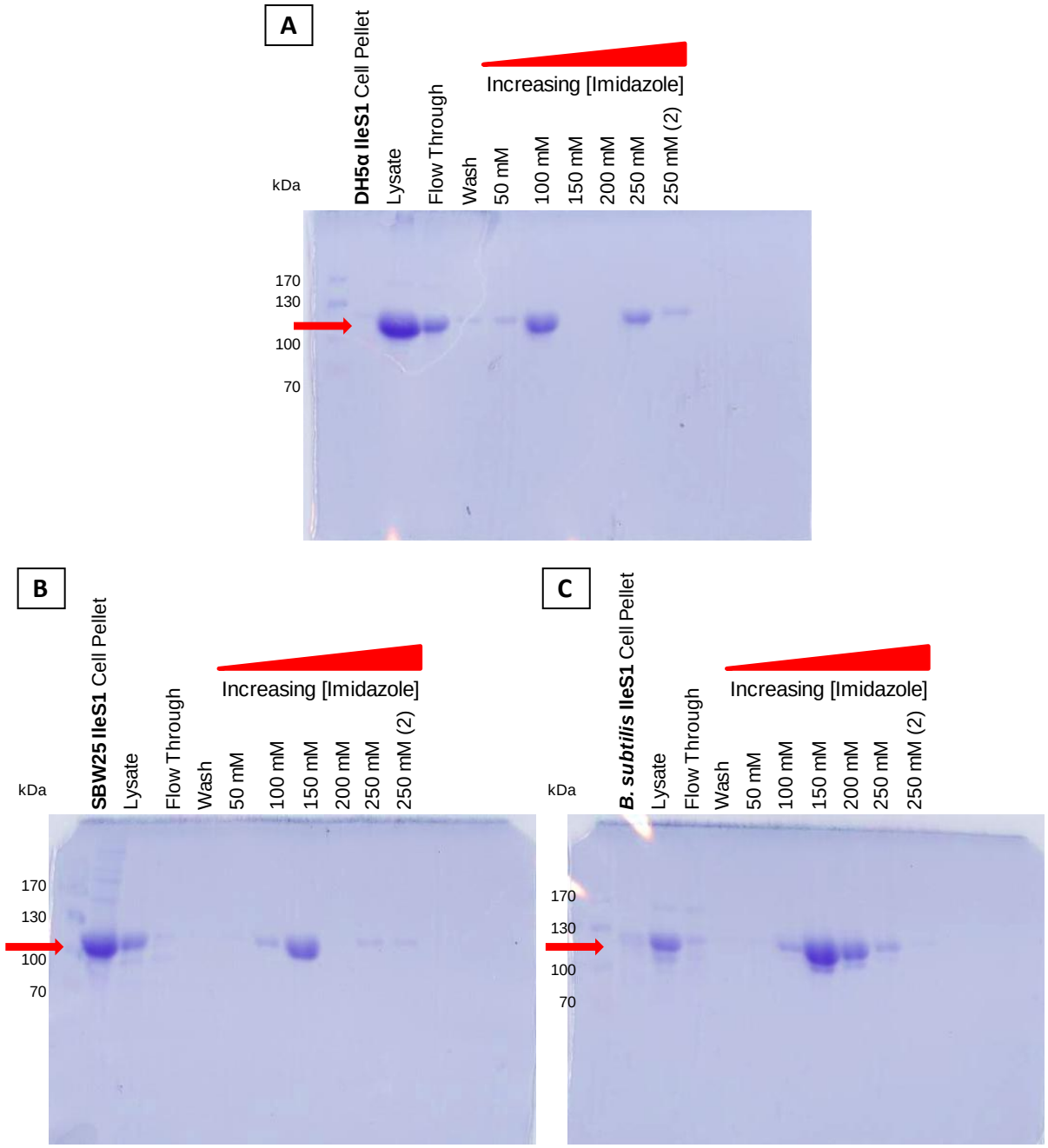

Figure 5.4. SDS-PAGE gels of Nickel Affinity Chromatography fractions from 100 ml production cultures of (A) BL21 *pET28a* DH5α *ileS1*, (B) SBW25 *ileS1* and (C) *B. subtilis ileS1*. 1 ml fractions were collected and 20 µl samples run on SDS-PAGE. The red arrows indicate the position of the IleS1 proteins.

The fractions containing the IleS band were pooled and dialysed to remove imidazole and other solutes that may interfere with downstream applications. The dialysed samples were quantified using the nanodrop for total protein concentration. The active enzyme concentration of IleS1 from DH5α was deduced in the following section for further use in the aminoacylation assay. The PCR-amplified sequence of DH5α was also sequence checked using the designed primers as outlined in the Methods (Table 5.2).

5.3.2 Deducing the concentration of active DH5α IleS1

To determine the amount of active DH5α IleS1 enzyme present in the dialysed sample, a protocol outlined by Francklyn *et al.* (2008) was followed as described in the Methods. As discussed in Chapter 1 (Figure 1.5), IleS is responsible for catalysing a two step process which involves first the activation of the amino acid and second the transfer of the activated amino acid to its cognate tRNA as outlined below:

Step 1: IleS + Ile + ATP → IleS(Ile-AMP) + PP_i

Step 2: IleS(Ile-AMP) + tRNA → Ile-tRNA + AMP + IleS

The protocol used in this study was designed to monitor the amount of IleS(Ile-AMP) formed in the first step of the aminoacylation reaction by using [^{14}C] isoleucine. It also relied on the fact that IleS complexed with the activated [^{14}C] isoleucine has a net positive charge (as most enzymes do) and will be trapped when passed through a nitrocellulose filter, which has a net negative charge. These filters were then counted on the scintillation counter to determine the CPM of the bound IleS([^{14}C]Ile-AMP). Unbound [^{14}C] Ile has a net negative charge and will therefore pass through the nitrocellulose filter.

The assay for quantifying the active concentration of DH5α IleS1 was optimised at various steps and all results summarised in Table 5.4. When a master mix assay was tested at the preliminary stages, in which the reaction was performed in one bulk and 15 µl triplicate samples taken at each time point, inconsistent CPM counts were observed between the triplicates (data not shown). The assay mix was therefore separated into individual 15 µl aliquots before adding the enzyme to start the reaction in Trial 1. This ensured that each sample should have equal amounts of [^{14}C] isoleucine and prevented the introduction of variability when removing 15 µl samples from a master mix assay at different time points.

In the second trial, the assay was equilibrated and performed at 25°C and 37°C to determine the optimum temperature. The samples were also passed through the nitrocellulose filter straight away after 0 or 10 minutes incubation, to see if the inconsistency in CPM values was due to the varying times in which the samples were left on the filters before further processing. The resulting CPM counts were very low compared to that of the initial trial and still inconsistent between the duplicates (Table 5.4). Some of the counts were mostly background, as 1 ml scintillation cocktail had a CPM of 24.

The low counts were proposed to be caused by spotting samples onto nitrocellulose filters straight away without given them enough time to bind to the filters, causing the enzyme to be washed away. To address this possibility, the samples in the final assay were left to bind on dry nitrocellulose filters for five, 10 and 20 minutes after 20 minutes incubation. Additionally, the incubation times of the assay were trialled at 5, 10 and 20 minutes to optimise the incubation period before allowing the samples to bind to the filters for one minute before washing and drying.

Table 5.4. Results of radioactive isoleucine binding to active DH5α IleS1: quantification Trial 1, 2 and 3*.

Trial 1			Trial 2			Trial 3		
Samples	**CPM**	**Average**	**Samples**	**CPM**	**Average**	**Samples**	**CPM**	**Average**
25°C			**25°C**			**25°C**		
Specific Activity 1	179561	**181919.67**	Specific Activity 1	116922	**119610.50**	5 min 1	1140	**1105.50**
Specific Activity 2	183065		Specific Activity 2	122299		5 min 2	1071	
Specific Activity 3	183133		0 min 1	156	**97.50**	10 min 1	2139	**1420.50**
2 min 1	3696	**7754.00**	0 min 2	39		10 min 2	702	
2 min 2	12785		10 min 1	81	**168.50**	20 min 1	543	**495.00**
2 min 3	6781		10 min 2	256		20 min 2	447	
5 min 1	1513	**3236.67**	**37°C**			20 min, 5 min filter 1	2344	**1651.83**
5 min 2	5100		Specific Activity 1	120115	**114559.00**	20 min, 5 min filter 2	1341	
5 min 3	3097		Specific Activity 2	109003		20 min, 10 min filter 1	2243	
10 min 1	5048	**4086.00**	0 min 1	32	**40.50**	20 min, 10 min filter 2	1276	
10 min 2	1327		0 min 2	49		20 min, 20 min filter 1	1282	
10 min 3	5883		10 min 1	90	**117.00**	20 min, 20 min filter 2	1425	
			10 min 2	144				

*The Specific Activity samples are reaction mixes without IleS, spotted directly on the nitrocellulose filters and dried without washing to determine the specific activity of the assay mix. The values used for calculating the active concentration of IleS1 are highlighted in red.

The resulting CPM counts were an improvement from the previous assays, with the duplicate counts higher and more consistent than before. All CPMs from samples that were incubated for 20 minutes and left to bind to the filters at 5, 10 and 20 minutes were averaged to calculate the concentration of active DH5α IleS1. The equations outlined in the Methods were used to calculate the concentration of active DH5α IleS1 and this was 3.11 pmol in 15 µl (Table 5.5), hence 0.207 µM [IleS1].

Table 5.5. Calculations for determining the concentration of active DH5α IleS1 (pmol).

	Value	Units	Calculations
[^{14}C] Ile stock concentration	20	µg/ml	-
[^{14}C] Ile used in 15 µl assay	1.5	µl	-
Molar Concentration of [^{14}C] Ile	0.015	µmol/ml	20 µg/ml x 0.0015 ml = 0.03 µg xM x 131.2 g/mol = 0.03 µg/15 µl xM x 131.2 g/mol = 2 µg/ml x = 0.015 µmol/ml
[^{14}C] Ile per 15 µl assay	225	pmol	0.015 µmol/ml x 0.015 ml = 0.000225 µmol = 225 pmol
Specific activity	531.6	CPM/pmol	119610.50/225 = 531.60
Concentration of active IleS	3.11	pmol	1651.83/531.60 = 3.11

5.3.3 Aminoacylation assay

The aminoacylation reaction catalysed by DH5α IleS1 was investigated by monitoring the formation of final [^{14}C]Ile-tRNA product in a discontinuous steady state assay. Various protocols from previous studies were considered before deciding on the method used in this study. A summary of the assay mixtures is shown in the next table (Table 5.6). The method of Pope *et al.* (1998) was used with slight modifications in ATP and BSA concentrations. The incubation temperature of 25°C was used in this study based on observations that it was optimal during quantification of active IleS enzyme. (Pope *et al.* (1998) had used 22°C for their protocol.)

Table 5.6. Summary of aminoacylation assay mixes from this study (1) and previous literature (2-5).

1	2	3	4	5
Total Reaction Mixture (µl)				
15	100	500	200	-
Temperature (°C)				
25	37	37	22	37
Materials				
50 mM Tris-HCl	100 mM Tris-HCl	20 mM Tris-HCl	50 mM Tris-HCl	50 mM Tris-HCl
pH 7.9	pH 7.5	pH 7.2	pH 7.9	pH 7.5
2 mM dithiothreitol (DTT)	2 mM DTT	10 mM DTT	2 mM DTT	4 mM DTT
4 µM $tRNA^{Ile}$	12 A_{260} units of tRNA	-	4 mg/ml tRNA (approx. 4 µM)	Range
10 mM $MgCl_2$	10 mM $MgCl_2$	10 mM $MgCl_2$	10 mM $MgCl_2$	10 mM $MgCl_2$
50 mM KCl	10 mM KCl	10 mM KCl	50 mM KCl	20 mM KCl
1 mM ATP	1 mM ATP	1 mM ATP	4 mM ATP	Range
15.25 µM [^{14}C] isoleucine	0.01-0.1 mM [^{14}C] isoleucine	0-1 µM [^{14}C] isoleucine	15.25 µM [^{14}C] isoleucine	Range
0-20 nM mupirocin/thiomarinol	0-50 nM mupirocin	0-50 nM mupirocin	0-50 nM mupirocin	Range
5 nM IleS	0.1 µg IleS (approx. 9 µM)	0.33-1.06 nM/µl of cell volume*	0.2-5 nM IleS	1-5 nM IleS
0.2 mg/ml BSA	-	-	1 mg/ml BSA	0.2 mg/ml BSA

[1]Assay used in this study; [2](Dureković *et al.*, 1973; Hughes and Mellows, 1980); [3](Capobianco *et al.*, 1989); [4](Pope *et al.*, 1998b); [5](Francklyn *et al.*, 2008).

*The amount of IleS in column 3 is per µl of cell volume as crude extracts were used. All other studies used purified IleS stock.

This assay essentially recreates the aminoacylation reaction in a microfuge tube and stops the reaction at a suitable time by incubating on ice. Trichloroacetic acid (TCA) is added to precipitate proteins from the assay and then the mixture is passed through a glass fibre filter to trap [^{14}C]Ile-tRNA for scintillation counting. Ethanol is used to remove traces of TCA from the sample. Following the selection of assay mix components and amounts outlined in Table 5.6, the concentration of IleS enzyme, incubation period and overall procedure for yielding consistent CPM counts were optimised before challenging the assay with mupirocin and thiomarinol.

In the preliminary trial of the aminoacylation assay, the concentration of DH5α IleS1 enzyme was varied in 10-fold steps between 20 nM to 0.02 nM, in order to deduce the optimal enzyme concentration. The resulting CPM counts were widely varying between duplicates and it was impossible to deduce which enzyme concentration was optimal for further assays. It was hypothesised that the widely varying results were due to the assay samples being spotted onto the glass fibre filters before putting them through a pulling vacuum for washing. The filters were individually sandwiched between a two-unit filter device and clamped to secure everything in place. This meant that when the vacuum began pulling, only the centre of the filter exposed to the buffers would be washed but not the outer rim of the filters. It was thought plausible that by allowing the samples to diffuse through the entire filter before washing, any sample at the edges was not efficiently washed, including the non-bound [^{14}C] isoleucine.

In order to correct this, samples were spotted on filters already set up to the vacuum filtration apparatus. The counts obtained in this next assay (incubation period of 5 minutes) had reproducible counts between the duplicates (Figure 5.5). The control assays with 20 nM

IleS but no tRNA yielded counts of 1793 and 1238 CPM. These counts suggest non-specific incorporation to be taking place; if these values are true background noise and deducted from the CPM values at 20 nM IleS in Figure 5.5, the remaining CPM is negligible and implies no specific activity in the aminoacylation assay.

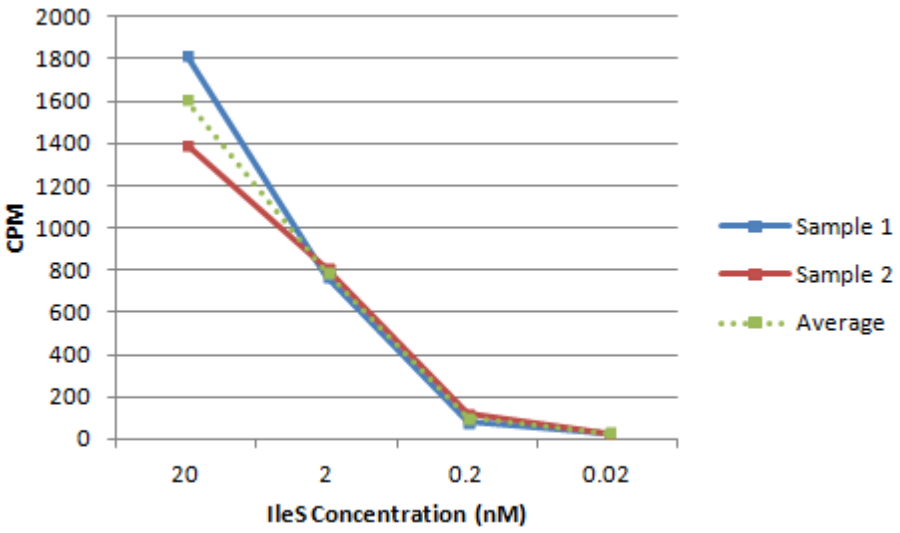

Figure 5.5. Aminoacylation of Ile-tRNA with decreasing concentrations of IleS enzyme. The assays were incubated for 5 minutes before measuring the CPM. The individual data are shown as sample 1 in blue and sample 2 in red. The average of the duplicates is shown by the dotted green line.

The aminoacylation assay was repeated with 2 nM and 5 nM IleS concentrations and at time points of 0, 2, 5 and 10 minutes with and without tRNA (Figure 5.6). The resulting CPM counts with 2 nM IleS and 5 minutes incubation time were lower than from the previous assay (average of 245 and 792.5 CPM respectively), suggesting that the dialysed IleS stock is slowly degrading in the one month storage at 4°C between the two assays. The control assays with no tRNA were all consistently basal CPM of around 30 counts, indicating that non-specific incorporation was not an issue at lower concentrations of the enzyme.

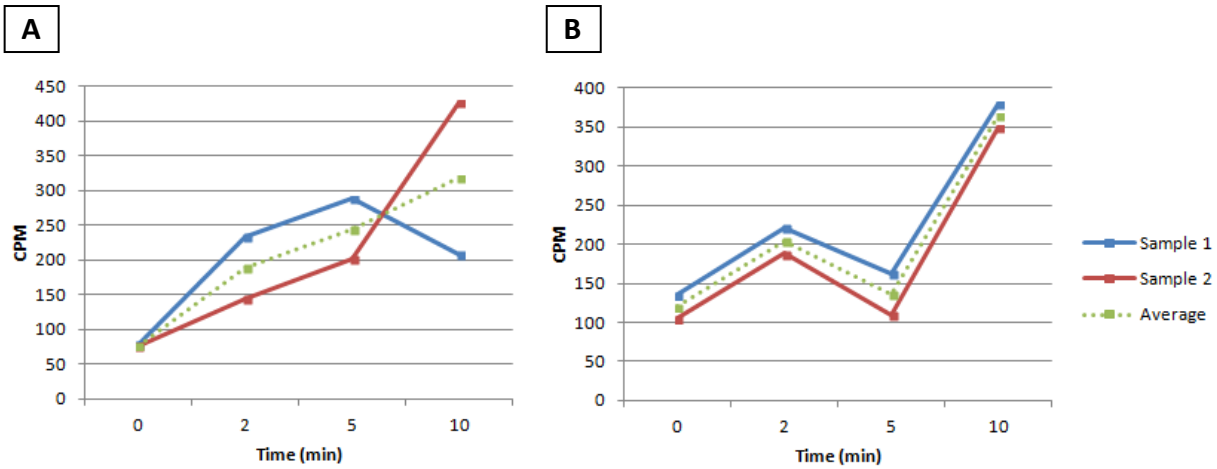

Figure 5.6. Aminoacylation assays performed with (A) 2 nM and (B) 5 nM IleS at different time points. The individual data are shown as sample 1 in blue and sample 2 in red. The averages of the duplicates are shown by the dotted green line.

Although the trendline of the assay performed with 2 nM IleS was as expected – with CPM counts increasing as the assay was left to incubate up to 10 minutes, the variability of counts between the two samples was greater than that of the 5 nM IleS assay. Therefore, the experimental conditions of 5 nM IleS and an incubation period of 10 minutes were chosen, based on their reproducibility between samples, to perform the final aminoacylation assay challenged with various concentrations of mupirocin and thiomarinol (1.25, 2.5, 5, 10 and 20 nM) in duplicates. These concentrations were chosen based on the K_i value for mupirocin previously determined by Hughes and Mellows in 1980 using *E. coli B* IleS. They determined the values for both the activation of isoleucine (the pyrophosphate exchange reaction) and the overall aminoacylation reaction to be K_i 2.5 nM and K_m 11.1 µM (Hughes and Mellows, 1980).

The results were inconclusive, as the CPMs did not decrease as the competitive inhibitor (mupirocin or thiomarinol) concentrations were increased in the assays. On the

contrary, there was a general trend of the CPM values increasing and peaking unexpectedly at 10 nM mupirocin and 2.5 and 20 nM thiomarinol (Figure 5.7).

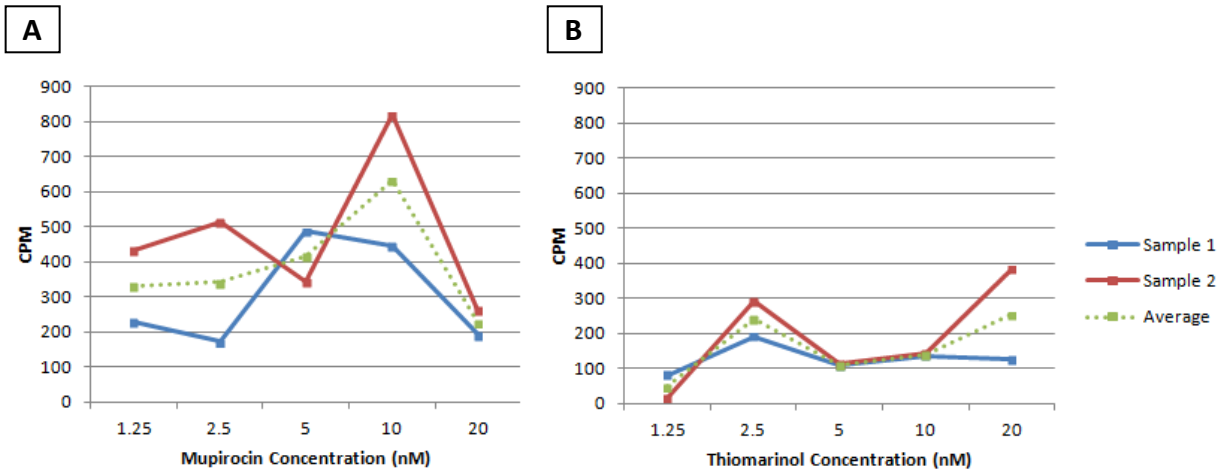

Figure 5.7. Aminoacylation assay challenged with various concentrations of (A) mupirocin and (B) thiomarinol. The individual data are shown as sample 1 in blue and sample 2 in red. The averages of the duplicates are shown by the dotted green line.

Table 5.7. CPM counts of specific activity and control with no antibiotic challenge.

	CPM	
Sample	**Specific Activity**	**No Antibiotics**
1	120274	129
2	124638	305
Average	**122456**	**217**

The control assays that were (1) not washed and (2) had no antibiotic challenge yielded CPM values that were as expected (an average of 122,456 and 217 respectively) (Table 5.7). The average count of the latter control with no antibiotics was comparable to the counts yielded in the previous assay (364 CPM). Considering that the assay produces counts on average 217 and 364 CPM without the addition of antibiotics, it is concerning that at mupirocin concentrations of 5 and 10 nM, the average counts were 417 and 633 CPM respectively. The high counts suggest noise, perhaps introduced by the addition of the antibiotic, making the

data not interpretable. The counts obtained from the assay with thiomarinol are lower than that of mupirocin but again, it is hard to differentiate between background noise and true counts at this stage. However, at the lowest concentration of thiomarinol (1.25 nM), IleS activity appears to be at baseline. If this can be reproduced and a more reliable set of data obtained for mupirocin, comparatively lower counts for thiomarinol would suggest that the antibiotic is indeed the more potent and stronger binding compound than mupirocin. It would be of great interest to continue this work to obtain the K_i value of thiomarinol.

5.4 Discussion

5.4.1 Solubility of the IleS proteins in an heterologous system

Unlike the difficulties faced when attempting to obtain soluble MupM in Chapter 4, soluble IleS1 from *E. coli* DH5α, SBW25 and *B. subtilis* was achieved by a straightforward protocol with minimal optimisation of the growth conditions. As discussed in Chapter 4, this may be because IleS is not part of a modular protein like MupM and therefore easier to express and solubilise in the pET28a system. For future protein solubilisation, it may be advantageous to check first whether the translated protein is singular or modular, in order to select for the optimal heterologous expression system prior to method optimisation.

5.4.2 Future Work on aminoacylation assay

The aminoacylation assay challenged with mupirocin and thiomarinol needs further optimisation before reliable K_i values can be measured for the latter antibiotic. Further troubleshooting is required to understand why the CPM values did not decrease as the concentration of inhibitor was increased by 2-fold steps in this study and why at some

antibiotic concentration, the counts exceeded that yielded in the control assay with no antibiotics. A possible reason for this discrepancy is the gradual degradation of the purified IleS stock. This was observed between the first and second aminoacylation assay performed without inhibitors and the resulting counts were lower for the latter assay. A possible solution to this discrepancy would be to perform the aminoacylation assay in a master mix, instead of individual aliquots, and to remove samples at the required time points. However, the latter was tested during the optimisation stages of deducing the active IleS concentration and it was deemed to cause the large fluctuations between the triplicate samples.

Another possibility is that the 15 µl total volume of each assay is too small and only provides low counts that cause high fluctuation/variability. This was also observed in Chapter 6, where low incorporation of [^{14}C] into pseudomonic acid A and thiomarinol A gave widely variable and inconclusive counts when used in preliminary uptake studies. Perhaps it is worth repeating the assays but at larger sampling volumes of 100-200 µl like in other methods considered in Table 5.6.

Once optimised, the aminoacylation assays will ideally be repeated using increasing concentrations of [^{14}C] isoleucine and thiomarinol to determine the K_i value using the secondary Dixon plot (Hughes and Mellows, 1980). Determining the K_i for thiomarinol would allow better comparison against the binding strength of mupirocin and elucidate whether the former antibiotic is more effective due to its increased binding capabilities.

5.4.3 Concluding remarks

This study has made attempts to optimise the aminoacylation assay for determining the K_i value for thiomarinol. Although no K_i value was obtained in this study for thiomarinol, altering the total volume and concentrations of IleS, [^{14}C] isoleucine and antibiotic may develop a useful standardised assay for future use. Determining the K_i for thiomarinol will assign kinetic parameters to this antibiotic and the optimised assay will allow easier comparison against other analogues in the future.

CHAPTER 6

6 INVESTIGATING THE ROLE OF UPTAKE AND EFFLUX IN THIOMARINOL POTENCY

6.1 Introduction

In the previous sections, the hypothesis that increased binding of thiomarinol (relative to mupirocin) to its target IleS enzyme contributes to the antibiotic's increased efficacy has been investigated. This section focuses on the other hypothesis that efficient transport of thiomarinol into sensitive bacterial cells and/or inefficient efflux by the cells allows the antibiotic to increase its potency on a wider range of Gram-positive and negative microorganisms than occurs with mupirocin.

Antibiotics such as mupirocin that target intracellular enzymes must be able to enter the bacterial cell through its membrane(s). This is more of a challenge for antibiotics that target Gram-negative microorganisms, as they need to overcome the outer membrane as well as the inner membrane. Generally, hydrophobic antibiotics (such as macrolides) penetrate the outer membrane by diffusing through the lipid bi-layer (a mechanism poorly understood) while smaller hydrophilic drugs (such as β-lactams) pass through porins (Delcour, 2009; James *et al.*, 2009). Some antibiotics typically penetrate the inner membrane by forming oligomeric pores that are substrate-selective in electric charge and size; for example, daptomycin forms pores in the presence of calcium and only on membranes containing phosphatidylglycerol (Zhang *et al.*, 2014). It is crucial for the efficacy of the drug that it is delivered rapidly into the cell for timely accumulation to the effective intracellular concentration.

As briefly mentioned in Chapter 1, upregulation or acquisition of efflux transporters is one of the mechanisms of resistance against antimicrobials. In particular, multidrug efflux transporters are an important group associated with intrinsic and acquired resistance in bacteria. This group consists of five families based on their amino acid sequence homology and mode of energy-coupling (Paulsen, 2003) (Figure 6.1).

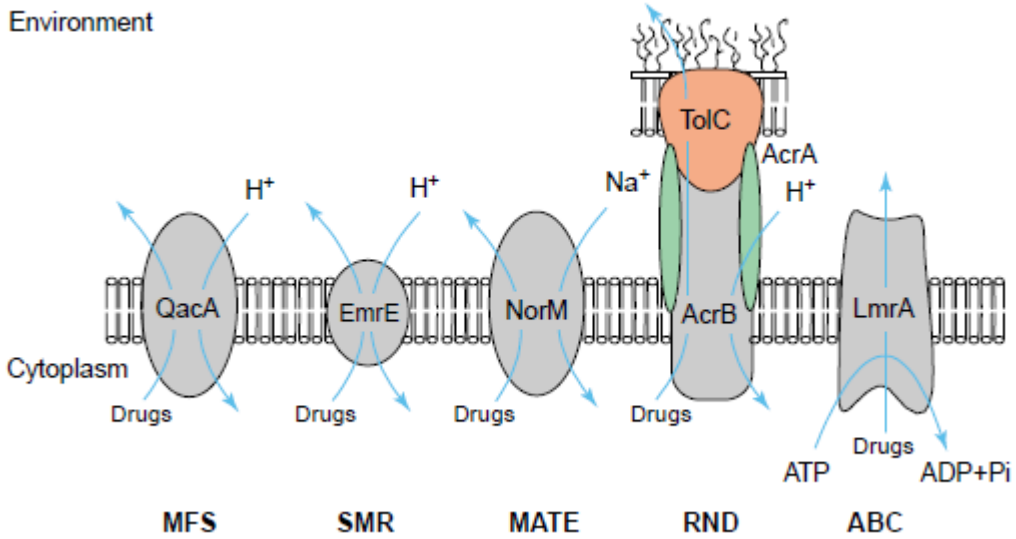

Figure 6.1. The five families of multidrug efflux transporters (reproduced from Paulsen, 2003).

The ATP-binding cassette (ABC) and major facilitator superfamily (MFS) are the largest families within the group and consist of ATP and chemiosmotically-driven uptake/efflux systems respectively. The resistance-nodulation division (RND) and small multidrug resistance (SMR) superfamilies consist of proton-driven systems. Finally, the multidrug and toxic compounds efflux (MATE) transporters are sodium ion-driven. In Gram-negative organisms, RND-type transporters play a significant role in conferring resistance because: (1) their tripartite complex creates a direct efflux pathway from the cytoplasm to the extracellular medium; and (2) they efflux a wide range of substrates from various

antibiotics to detergents (Blair and Piddock, 2009; Yu *et al.*, 2003). It is the combinatory and balancing effect of efflux transporters and the outer membrane slowing the entry of antibiotics that confers this high-level intrinsic and acquired resistance phenotype against many drugs (Cox and Wright, 2013; Webber and Piddock, 2003).

While the transport mechanism of thiomarinol is yet to be elucidated, mupirocin has been observed to indiscriminately enter both sensitive and resistant bacteria by passive diffusion (Capobianco *et al.*, 1989), although not most Gram-negative organisms. The difference that was noted by Capobianco and colleagues was not in the uptake but in accumulation – they noted mupirocin to accumulate in sensitive bacteria (*Staphylococcus aureus* and *Bacillus subtilis*) due to binding to the IleS target. Likewise, they noted that resistant strains restrict this access to the binding site. No efflux mechanism to remove mupirocin from the cells after passive influx was mentioned in their study. Much later, Huang *et al.* (2004) noted mupirocin to be a substrate for the chromosomally-encoded efflux transporter MdeA (part of MFS) in *S. aureus*. When MdeA was overexpressed, an increase in mupirocin tolerance was observed; with the MIC increasing by 16-fold from 0.03 to 0.5 µg/ml. However, Huang *et al.* concluded that the contribution of MdeA to mupirocin resistance was most likely insignificant, as the strain was still susceptible to the antibiotic even after the MIC increase.

As discussed in previous sections, high level mupirocin resistance has been attributed to a eukaryote-like IleS2 such as MupM in the mupirocin-producer *Pseudomonas fluorescens* NCIMB 10586 (El-Sayed *et al.*, 2003; Yanagisawa and Kawakami, 2003). Along with the mupirocin biosynthesis cluster, the expression of *mupM* is also controlled by the *mupI/R*

quorum sensing and occurs at the onset of the log phase (El-Sayed *et al.*, 2001; Hothersall *et al.*, 2007). This gene is thought to play a dominant role in conferring high level mupirocin resistance in the producer because *P. fluorescens* NCIMB 10586 *ΔmupM* exhibited a lower MIC value of mupirocin than *ΔileS* (0.2 mg/ml and > 2 mg/ml respectively) (Hothersall *et al.*, Unpublished). However, high level resistance against mupirocin was also detected during exponential phase, when *mupM* should not be expressed (Hothersall *et al.*, Unpublished). This led to the investigation of additional resistance mechanisms and the identification of a multifunctional efflux transporter that may provide both the resistance phenotype and a transport mechanism for exporting mupirocin from the producer (Whatling *et al.*, 1995). Interestingly, when the homologue of this efflux transporter in *S. aureus* was over-expressed, no increase in resistance was observed against mupirocin in this microorganism (Thomas *et al*., Unpublished).

This study focuses on the possible role of uptake and efflux in bacterial cells in the potency of thiomarinol. It attempts to investigate whether thiomarinol accumulates at a faster rate and/or higher concentration in susceptible cells than mupirocin and whether this is an explanation for the former antibiotic's low MIC against a wider range of microorganisms than the latter (Chapter 1, Table 1.5). As a tool for detecting the accumulation and efflux of thiomarinol and mupirocin in bacterial cells, attempts were made to prepare [^{14}C] thiomarinol A and pseudomonic acid A with high specific activity isotopic labelling. The aim was to use these radioactive ligands to investigate uptake and efflux in *E. coli* as a representative organism for Gram-negative mupirocin resistance and *B. subtilis* for Gram-positive mupirocin sensitivity. This study also investigates the role of efflux transporters (in *Salmonella enterica* serovar Typhimurium or *S. typhimurium*) in

mupirocin/thiomarinol resistance and whether less efficient efflux allows thiomarinol to be a more effective antibiotic than mupirocin.

6.2 Materials and Methods

6.2.1 Bacterial strains and growth conditions

All bacterial strains used in this study are listed in Table 6.1.

Table 6.1. Bacterial strains used in this study.

Bacterial Strain	Genotype	Phenotype	Source/Reference
B. subtilis 1064	*trpC2*	Inherently mupirocin sensitive.	Kunst *et al.,* 1997
E. coli DH5α	*endA1 recA hsdR17 lacZΔM15 supE44 gyrA96 thi-I relA1* F^-	High transformation efficiency strain.	Gibco BRL
P. fluorescens NCIMB 10586 pJH2	Carrying pJH10 containing *mupR*	Mupirocin Overproducer. Ampicillin resistant.	Hothersall *et al.* , 2011
P. rava sp. SANK73390	-	Thiomarinol Producer.	Daiichi-Sankyo
S. enterica serovar Typhimurium ATCC14028s	-	Wild-type (WT).	Fields *et al.* , 1986
ΔtolC	*ΔtolC* ::CmR	ATCC14028s with *tolC* deletion.	Nishino *et al.,* 2006
ΔacrB	*ΔacrB* ::KmR	ATCC14028s with *acrB* deletion.	Nishino *et al.,* 2006
ΔacrD	*ΔacrD* ::CmR	ATCC14028s with *acrD* deletion.	Nishino *et al.,* 2006
ΔacrEF	*ΔacrEF* ::CmR	ATCC14028s with *acrEF* deletion.	Nishino *et al.,* 2006
ΔmdtABC	*ΔmdtABC* ::CmR	ATCC14028s with *mdtABC* deletion.	Nishino *et al.,* 2006
ΔmdsABC	*ΔmdsABC* ::CmR	ATCC14028s with *mdsABC* deletion.	Nishino *et al.,* 2006
ΔemrAB	*ΔemrAB* ::CmR	ATCC14028s with *emrAB* deletion.	Nishino *et al.,* 2006
ΔmdfA	*ΔmdfA* ::CmR	ATCC14028s with *mdfA* deletion.	Nishino *et al.,* 2006
ΔmdtK	*ΔmdtK* ::CmR	ATCC14028s with *mdtK* deletion.	Nishino *et al.,* 2006
ΔmacAB	*ΔmacAB* ::CmR	ATCC14028s with *macAB* deletion.	Nishino *et al.,* 2006

[^{14}C] thiomarinol was produced by inoculating 2 ml of *Pseudoalteromonas rava* sp. SANK 73390 overnight Marine Broth culture into 200 ml of Marine Broth. For production of [^{14}C] mupirocin, a 50 ml seed culture of *P. fluorescens* carrying pJH2 (Hothersall *et al*., 2011) was prepared from a single colony in L-broth and incubated overnight at 25°C shaken at 200 rpm. 10 ml of the seed culture was diluted into 170 ml of Secondary Stage Medium (SSM) with 20 ml of 40% glucose and 0.5 mM IPTG. SSM was prepared as outlined (Table 6.2) and

the pH adjusted to 7.5. The medium was split into 170 ml aliquots in individual bottles and autoclaved. Prior to use, 20 ml of 40% (w/v) glucose (to give 4 % final concentration) and 0.5 mM IPTG were added.

Table 6.2. Preparation of Secondary Stage Media (SSM).

Secondary Stage Media (SSM) Preparation
25 g soya flour
2.5 g spray dried corn liquor
5 g $(NH_4)_2SO_4$
0.5 g $MgSO_4 \cdot 7H_2O$
1 g Na_2HPO_4
1.5 g KH_2PO_4
1 g KCl
6.25 g $CaCO_3$
Volume adjusted to 850 ml with dH_2O

6.2.2 [^{14}C] radioactive feeding of antibiotic production cultures

A total of 4 µCi of [^{14}C] acetate or [^{14}C] methionine (Perkin Elmer, United Kingdom) was fed to the production culture at various time points and incubated at 23°C for *P. rava* and 22°C for *P. fluorescens* at 220 rpm for 48-50 hours. The specific activity of the [^{14}C] acetate stock used was 328 mCi/mmol (12.136 GBq/mmol) and for [^{14}C] methionine, 56.3 mCi/mmol (2.083 GBq/mmol).

6.2.3 Solvent extraction and HPLC quantification of [^{14}C] thiomarinol A and pseudomonic acid A

The process of extracting [^{14}C] thiomarinol and pseudomonic acid A was based on the method for thiomarinol extraction and quantification outlined in Chapter 2 with minor

alterations. For [^{14}C] thiomarinol, 200 ml acetone and ethyl acetate were used for the solvent extraction steps and the final antibiotic dissolved in 2 ml methanol. For [^{14}C] mupirocin, the cells and SSM residues were first separated by centrifugation at 5,000 x*g* for 20 minutes. The supernatant was then acidified to pH4.5 using 2 M HCl and extracted twice with equal volume of ethyl acetate (200 ml). For double extraction, the upper phase of the first ethyl acetate extraction was collected. The lower phase was then treated with another 200 ml ethyl acetate and the upper phase collected. The two upper phases were then pooled, evaporated and dissolved in 2 ml methanol.

The labelled antibiotics were quantified by HPLC. [^{14}C] thiomarinol was quantified as outlined in Chapter 2. [^{14}C] mupirocin was quantified on the same HPLC system but at a UV detection of 233 nm and a mobile phase water/acetonitrile gradient of 30% and 70% respectively. The programme was run for 60 minutes at a flow rate of 1 ml/min and pseudomonic acid A detected at around 20 minutes.

6.2.4 Fraction collection

Fraction collection was performed using the Gilson system to isolate [^{14}C] thiomarinol A and pseudomonic acid A. The same Unipoint LC system software, column and conditions were used as with the HPLC programmes for detecting thiomarinol and mupirocin but with additional fraction collecting steps at various time points. Due to restrictions in volume size of the analytical column and tubes, multiple 100 µl samples were injected into the Gilson system for fraction collection of [^{14}C] thiomarinol A and pseudomonic acid A.

The fractionated [^{14}C] thiomarinol A and pseudomonic acid A samples were pooled and the acetonitrile and water evaporated using the speed vac. The remaining [^{14}C]

thiomarinol A and pseudomonic acid A residues were re-dissolved in absolute methanol and quantified using the HPLC as previously described.

6.2.5 Scintillation counting

The amount of total [^{14}C] incorporation was measured using a scintillation counter (Packard 1600 TR and Perkin Elmer Tri-Carb 2810 TR). 10 or 20 µl of [^{14}C] thiomarinol and mupirocin were mixed in a final volume of 1 ml Instagel (Perkin Elmer, United Kingdom) and counted for 1 or 10 minutes.

6.2.6 Monitoring the window of thiomarinol/mupirocin production

Production cultures (200 ml) of thiomarinol and mupirocin were set up as described above and grown for up to 24 hours. At 1 hour intervals, 100 µl samples were taken and diluted with 900 µl L-broth for measuring cell growth at an absorbance of 600 nm. Samples (1 ml) were also taken at the same intervals for thiomarinol/mupirocin quantification. *P. fluorescens* pJH2 samples were centrifuged at 14,000 x*g* for 5 minutes before passing the supernatant through a filter for HPLC quantification. *P. rava* samples were treated with 1 ml acetone and ethyl acetate as previously described to extract thiomarinol before HPLC quantification.

6.2.7 Uptake Study

Various volumes of *E. coli* and *B. subtilis* overnight cultures were set up from single colony inoculation and incubated overnight at 37°C, 200 rpm to yield appropriate cell densities. The cultures were then centrifuged at 5,000 x*g* for 10 minutes and the cell pellets re-suspended in various volumes of L-broth before dividing into aliquots for addition of [^{14}C]

antibiotics or as control background counts. 100 µl samples were also taken at this stage for 10-fold serial dilutions and plating out 100 µl of each dilution onto L-agar plates to determine the viable cell counts of each culture.

[^{14}C] thiomarinol A or pseudomonic acid A was added to the re-suspended samples and incubated at 22 or 30°C, 200 rpm for various incubation periods. 100 µl samples were taken at various time points and mixed with 900 µl Instagel for scintillation counting. This was to determine the overall total radioactivity in the sample. Other 100 µl samples were centrifuged at 12,200 x*g* for 1 minute and the supernatant mixed with 900 µl Instagel to determine the radioactivity outside the bacterial cells in the L-broth. The cell pellets were re-suspended in 100 µl standard distilled water (SDW) before mixed with 900 µl Instagel to determine the amount of intracellular radioactivity. The same procedure was performed on the background samples with no addition of [^{14}C] antibiotics.

6.2.8 Transport Study

100 µl samples were taken in triplicates for *B. subtilis* (a total of four samples including the background control sample) and single for *E. coli* after 30 or 60 minutes incubation at 30°C from the uptake study and immediately centrifuged at 12,200 x*g* for 1 minute to separate the cells from the L-broth. The cell pellets were re-suspended individually in 2 ml L-broth and incubated at 30°C. 100 µl samples were taken at 2, 5, 10 and 20 minute intervals and centrifuged at 12,200 x*g* for 1 minute. The cell pellets, supernatants and total samples were processed and mixed with Instagel as outlined in the uptake study and counted on the scintillation counter for 10 minutes to obtain intracellular, extracellular and total counts.

6.2.9 MIC Test

Ten efflux transporter deletion mutants of *Salmonella typhimurium* ATCC 14028s were tested for their sensitivity to mupirocin and thiomarinol as outlined in Chapter 2.

6.3 Results

6.3.1 Optimisation of [^{14}C] thiomarinol and mupirocin radioactive incorporation, extraction and quantification

Various materials and methods were tested in an attempt to extract highly ^{14}C-incorporated thiomarinol A and pseudomonic acid A for their downstream applications. Firstly, [^{14}C] acetate was fed to the 200 ml producer cultures in three separate feeds as advised by Dr. Zhongshu Song, University of Bristol. The first feed was given to the cultures at late afternoon on the day of the production medium inoculation (13 µl of [^{14}C] acetate after four hours incubation), followed by a feed early the next morning (14 µl after 20 hours) and late afternoon (13 µl after 27 hours). After a total of 50 hours incubation, the cultures were harvested as described in the Materials and Methods. From the re-dissolved 2 ml stocks of [^{14}C] thiomarinol and mupirocin in absolute methanol, 100 µl of each sample was quantified by HPLC. The resulting chromatograms showed the expected yields of [^{14}C] thiomarinol A at a retention time of 8.28 minutes (Figure 6.2). However, the yield of pseudomonic acid A was higher than expected and so the [^{14}C] mupirocin stock was diluted 10-fold and re-run, giving a peak of [^{14}C] pseudomonic acid A at 20.10 as expected (Figure 6.3).

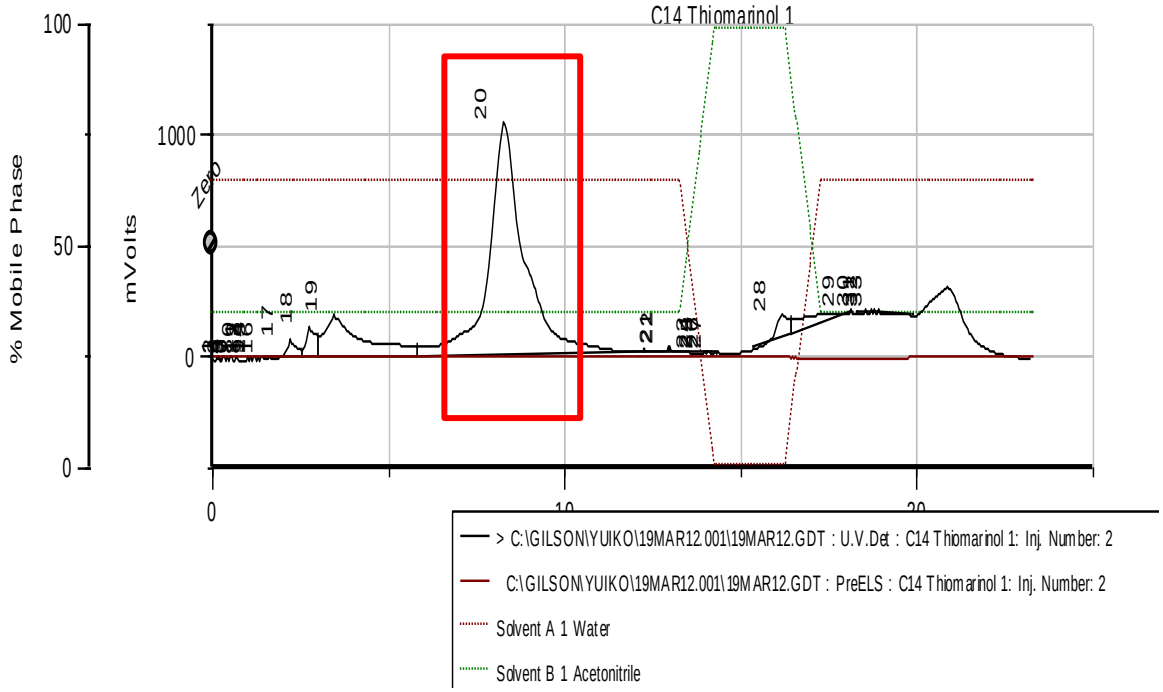

Figure 6.2. HPLC chromatogram of [^{14}C] thiomarinol A (in red). The x-axis represents the time lapsed in minutes on the HPLC programme. The retention area of [^{14}C] thiomarinol A is 1.29 x 10^8.

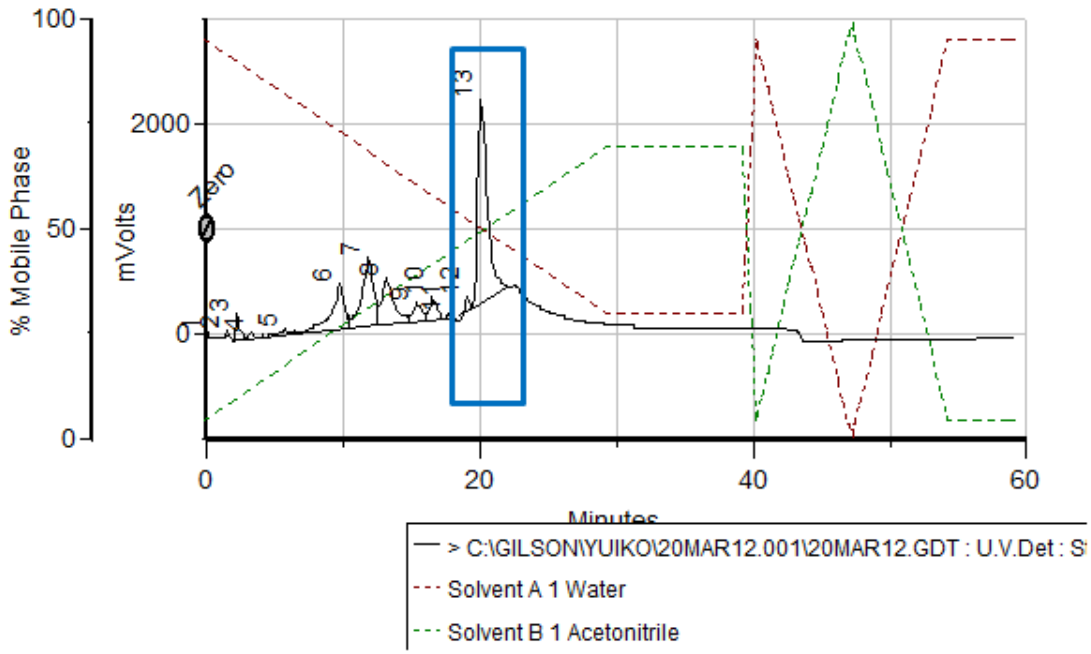

Figure 6.3. HPLC chromatogram of [^{14}C] mupirocin re-run with 10-folds diluted stock for improved detection of pseudomonic acid A (in blue). Peak detected at 20.10 minutes. The retention area of Peak 13 is 1.67 x 10^8.

This greater yield of mupirocin compared to thiomarinol was as expected, as the mupirocin producer *P. fluorescens* used in this study carried the *mupR* gene in the pJH10 vector. The *mupR* gene encodes a transcriptional regulator and together with *mupI*, it is responsible for quorum regulating mupirocin biosynthesis in the exponential and stationary phases (El-Sayed *et al*., 2001). Hothersall *et al.* (2011) showed that expression of *mupR* in trans increases mupirocin production by up to 17-fold. All future mupirocin and pseudomonic acid A stocks were diluted 10-folds prior to HPLC quantification.

Total concentrations obtained were 4.4 mg/ml and 6.9 mg/ml [^{14}C] thiomarinol A and pseudomonic acid A respectively. The overall incorporation of ^{14}C in the thiomarinol and mupirocin stocks was measured by counting 10 and 20 µl of the samples in 990 and 980 µl of Instagel respectively in the scintillation counter (Packard 1600 TR). The two volumes of antibiotics were used as a control to check the radioactive counts doubled accordingly and showed no great variability based on sample size. Non-^{14}C labelled thiomarinol and mupirocin were used as negative controls and 1 ml of Instagel as a blank control for detecting the background CPM. All ^{14}C samples were counted for 1, 3 and 10 minutes to determine the optimal length of scintillation counting for accurate CPMs.

The CPM results were encouraging; values across the different counting times were consistent and approximately double when 20 µl of each antibiotic was counted (Table 6.3). One minute counting time was used for all further scintillation analysis in this study.

Table 6.3. CPM of [^{14}C] mupirocin and thiomarinol at 1, 3 and 10 minutes.

	CPM			
	1 min	3 min	10 min	Average
Scintillant (Blank)	21.00	22.00	19.90	**20.97**
Thiomarinol 10 µl (Control)	9.00	-	-	-
Mupirocin 10 µl (Control)	19.00	-	-	-
[^{14}C] Thiomarinol 10 µl	1153.00	1205.33	1174.60	**1177.64**
[^{14}C] Thiomarinol 20 µl	1924.00	1875.33	1896.10	**1898.48**
[^{14}C] Mupirocin 10 µl	629.00	614.33	609.50	**617.61**
[^{14}C] Mupirocin 20 µl	1517.00	1498.33	1530.60	**1515.31**

6.3.2 Optimisation of fraction collection and further processing of [^{14}C] thiomarinol A

The method for [^{14}C] thiomarinol A and pseudomonic acid A fraction collection and processing to yield final products was firstly optimised using non-^{14}C labelled antibiotics. This was done as a safety measure as well as a way to conserve the available [^{14}C] acetate and methionine stocks. Non-labelled thiomarinol and mupirocin were obtained following the same procedure as with the labelled antibiotics but at a larger production culture volume of 500 ml and without the ^{14}C feeding. The final extraction of thiomarinol and mupirocin were dissolved in 5 ml absolute methanol.

The UniPoint LC programmes used for quantifying thiomarinol was altered to include the fraction collection steps. Fraction collection of thiomarinol A was attempted first, with a collection window set from 7 to 11 minutes. Samples were collected at one minute intervals per tube. The window for collection was kept relatively wide to ensure no thiomarinol A was lost in the initial optimisation of the parameters. 100 µl of thiomarinol stock was injected into the HPLC column and five samples consisting of the thiomarinol A peak obtained at a

retention time of 7.03 minutes (Figure 6.4). The chromatogram confirmed that the first two fractions collected consist of the thiomarinol A peak; therefore these two samples were pooled together with two more samples from another run (data not shown) to a total volume of 4 ml.

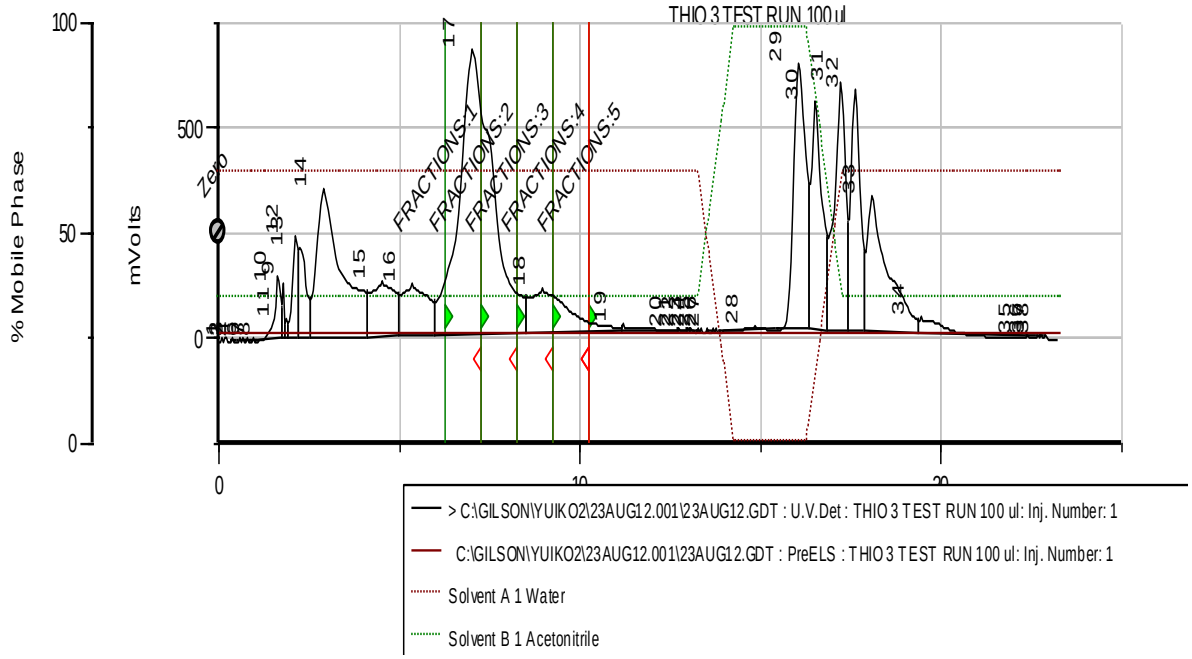

Figure 6.4. HPLC chromatogram of non-radiolabelled thiomarinol A (Peak 17) fractionated at 7, 8, 9, 10 and 11 minutes (shown by the green and red lines).

The samples collected by this method consist of thiomarinol A dissolved in 35% acetonitrile, 65% water and negligible amounts of methanol (as the carrier of the injection sample) and formic acid. Before processing the 4 ml sample obtained, the appropriate method for removing the solvents was established by a series of small scale experiments as indicated in Table 6.4 to determine whether it is better to (1) evaporate the acetonitrile before ethyl acetate extraction of thiomarinol A; or (2) add ethyl acetate directly into the pooled fractions for thiomarinol A extraction.

Table 6.4. Materials used to determine the optimal processing method of fractionated thiomarinol A samples.

Trial	Water (µl)	Acetonitrile (µl)	Thiomarinol (10 mg/ml) (µl)	Ethyl Acetate (µl)	Methanol (µl)
1*	100	100	5	800	-
2	650	350	10	2000	-
3a	650	350	-	2000	10
3b	650	350	10	2000	-

*In Trial 1, an unrepresentative water to acetonitrile ratio of 1:1 (100 µl:100 µl) was used. During HPLC and fraction collection, a ratio of 65:35 (water to acetonitrile) is used and therefore, all further trials were 650 µl:350 µl respectively.

Trial 1 showed that if extraction is done on too small a scale, it is very hard to distinguish the two phases. Trial 2 showed that a total volume of 3 ml facilitated the phase separation but showed that analysis of the phases by HPLC required much more thiomarinol to be present. Trial 3a started from a mix consisting of just water, acetonitrile, ethyl acetate and methanol in the absence of thiomarinol to read the background OD_{385nm} of 1 ml of the ethyl acetate and water emulsion layer. Following this, Trial 3b added 10 µl thiomarinol and determined the OD_{385nm} of the upper layer. The difference in OD_{385nm} values of Trial 3a and 3b allowed the thiomarinol concentration in the upper ethyl acetate and water emulsion to be determined. The results are summarised below in Table 6.5.

Table 6.5. Summary of Trials 1-4 results from Table 6.4.

Trial	Aim	Results/Issues
1	Separate soluble (ethyl acetate) and aqueous layers to detect thiomarinol by measuring absorbance of soluble phase at OD_{385nm}.	Volumes too small for handling and thiomarinol detection.
2	Increased volumes, same aim as above.	Clearer separation of phases observed, however upper phase consisted of ethyl acetate with emulsions which caused background problems during thiomarinol absorbance reading.
3a	Sample excluding thiomarinol to obtain background absorbance reading of emulsion.	OD_{385nm} of 0.678.
3b	Repeat of Trial 2 but with background absorbance deduced from overall reading of upper phase.	OD_{385nm} of 0.850 and therefore thiomarinol detected in upper phase.

These small experiments proved the importance of evaporating acetonitrile from the fraction collections prior to the addition of ethyl acetate for thiomarinol A extraction. Furthermore, the residual amount of methanol was not expected to interfere with the overall process of isolating thiomarinol A from the fractions, as it has the lowest boiling point amongst all solvents (64.7°C) and would evaporate before the acetonitrile.

6.3.3 Is thiomarinol A stable in prolonged heat treatment during isolation from fraction collections?

The above observations, that prior acetonitrile evaporation is important for successful ethyl acetate extraction, raised a question about the thermal stability of thiomarinol A. During standard thiomarinol extraction as outlined in Chapter 2, a 45°C water bath was used to evaporate ethyl acetate from the thiomarinol-ethyl acetate mixture in a vacuum sealed glass flask. The vacuum allows the solvent (with a boiling point of 77.1°C) to evaporate at the lower water bath temperature. The boiling point of acetonitrile is slightly higher than that of ethyl acetate and evaporates at 82°C. This suggested a possible requirement for treatment of the collected fractions with higher temperature but the level of heat stability of thiomarinol was not known or documented in the literature. Therefore, small scale experiments were set up to determine the heat stability of thiomarinol A and if stable, to determine whether all solvents could be removed from the fractions by evaporation instead of ethyl acetate extraction.

The 4 ml pooled sample of thiomarinol A fraction collections was transferred into a glass flask and placed under vacuum for evaporation in a 50°C water bath. Approximately 30 minutes was required to evaporate 1.4 ml acetonitrile from the sample. At this stage, 100 µl

of the sample was removed and analysed by HPLC to quantify the pre-existing amount of intact marinolic acid before increased heat treatment (using the mupirocin detection programme) (Figure 6.5). Following this, the water bath temperature was increased to 60°C and eventually 70°C to evaporate the remaining water. The remaining residue was dissolved in methanol and 100 µl of the sample run on the HPLC for any detection of marinolic acid hydrolysis (Figure 6.6).

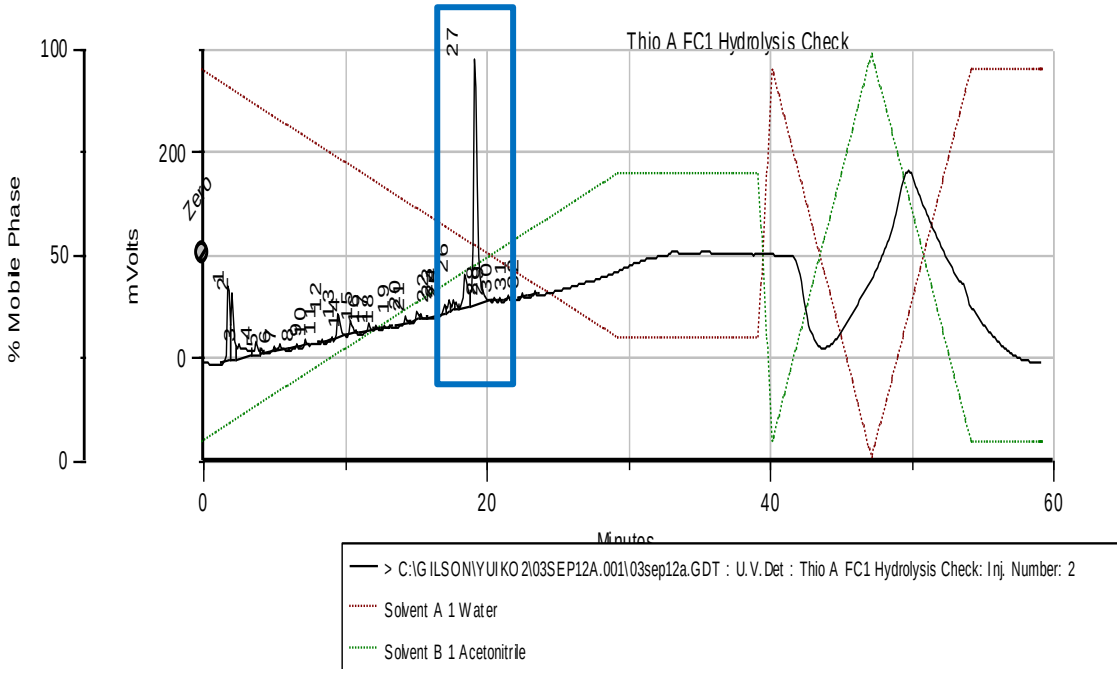

Figure 6.5. HPLC chromatogram of fractionated thiomarinol A after heat treatment under vacuum in 50°C water bath for 30 minutes. The programme for detecting mupirocin was used to quantify the amount of marinolic acid (Peak 27, highlighted in blue), as they share structure similarity and hence the same absorbance at 233 nm. The retention area of Peak 27 is 7.70 x 10^6.

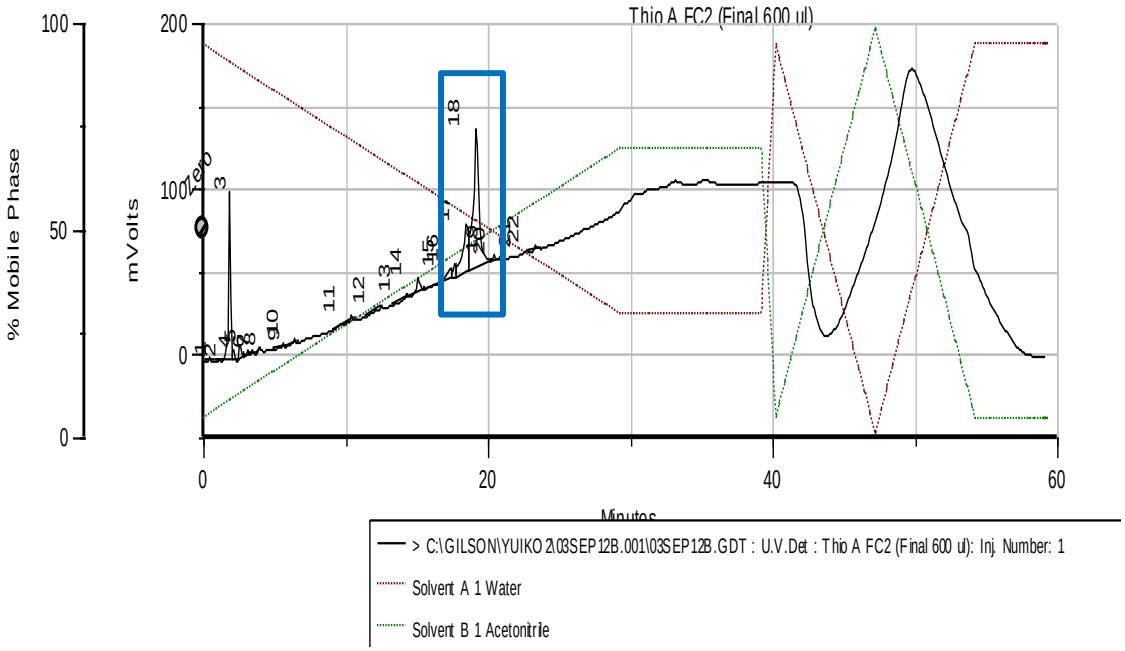

Figure 6.6. HPLC chromatogram of final fractionated thiomarinol A product in methanol, after 60-70°C water bath evaporation, ethyl acetate extraction and speedvac evaporation. Marinolic acid A is detected by the mupirocin HPLC programme (Peak 18 highlighted in blue). The retention area of Peak 18 is 4.00 x 10^6.

The results showed no significant decrease, indicating that thiomarinol A can withstand high temperature treatments. These results were encouraging and indicated that thiomarinol A could be isolated from the fraction collection solvents without the ethyl acetate extraction step. To test this, 100 µl of thiomarinol was fractionated (Figure 6.7) and the four fractions evaporated using the speedvac.

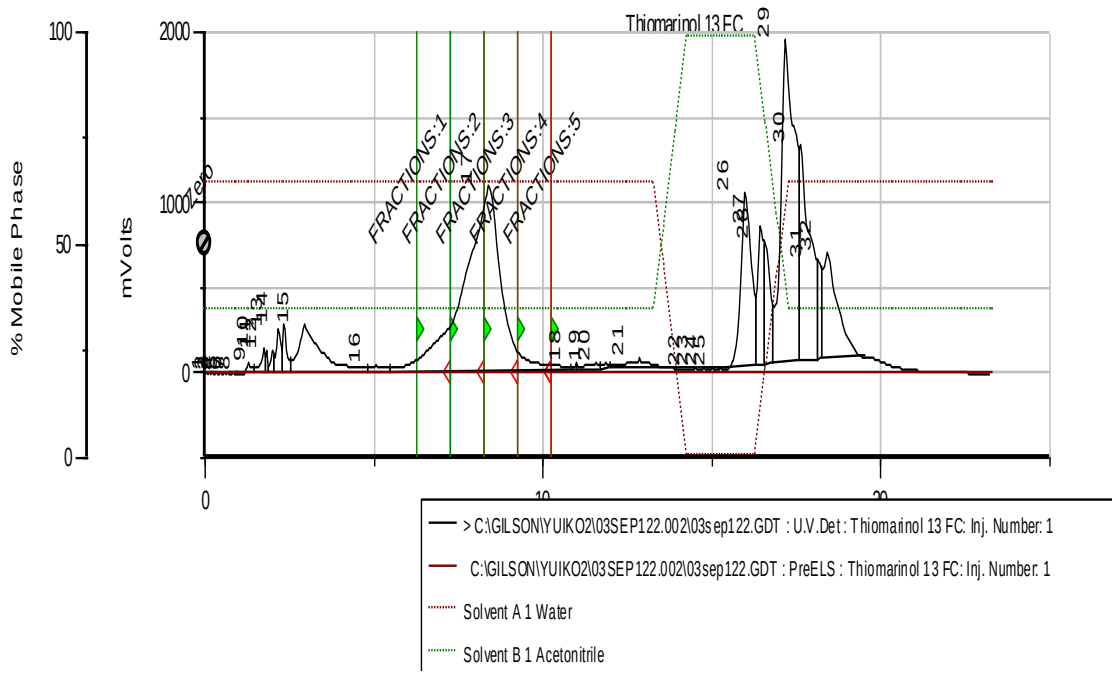

Figure 6.7. HPLC chromatogram of 100 µl thiomarinol A sample fractionated (Peak 17). The retention area of Peak 17 is 1.46 x 10^8.

A total of 4 hours was required to completely evaporate all solutions. The sample was re-dissolved in 200 µl methanol and half of the sample run on the HPLC for detection of fractionated thiomarinol A (Figure 6.8).

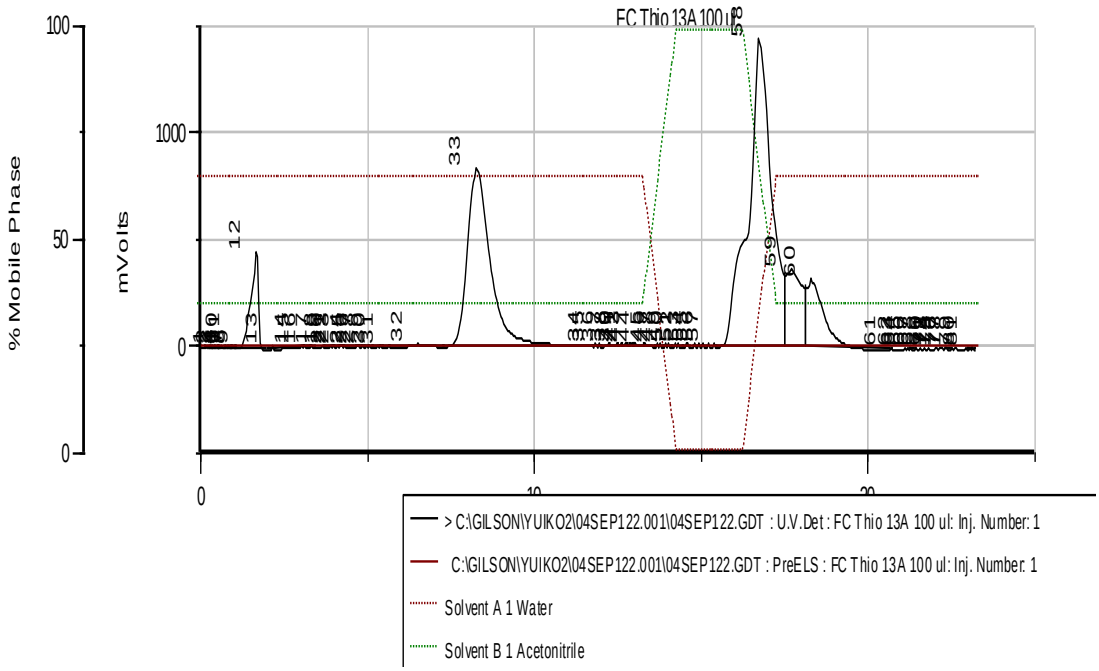

Figure 6.8. HPLC chromatogram of fractionated and processed thiomarinol A (Peak 33). The retention area of Peak 33 is 6.89 x 10^7.

The peak area before and after fraction collecting thiomarinol A showed no significant loss in yield during fraction collection. In conclusion, multiple 100 µl injections for fractionation and speedvac evaporation of the pooled samples were deemed an appropriate method for the isolation of [^{14}C] thiomarinol A.

6.3.4 Fraction collection of [^{14}C] thiomarinol A

Using the optimised protocol above, 10 individual 100 µl [^{14}C] thiomarinol injections (from the 2 ml total stock) were fractionated. A representative chromatogram is shown in Figure 6.9.

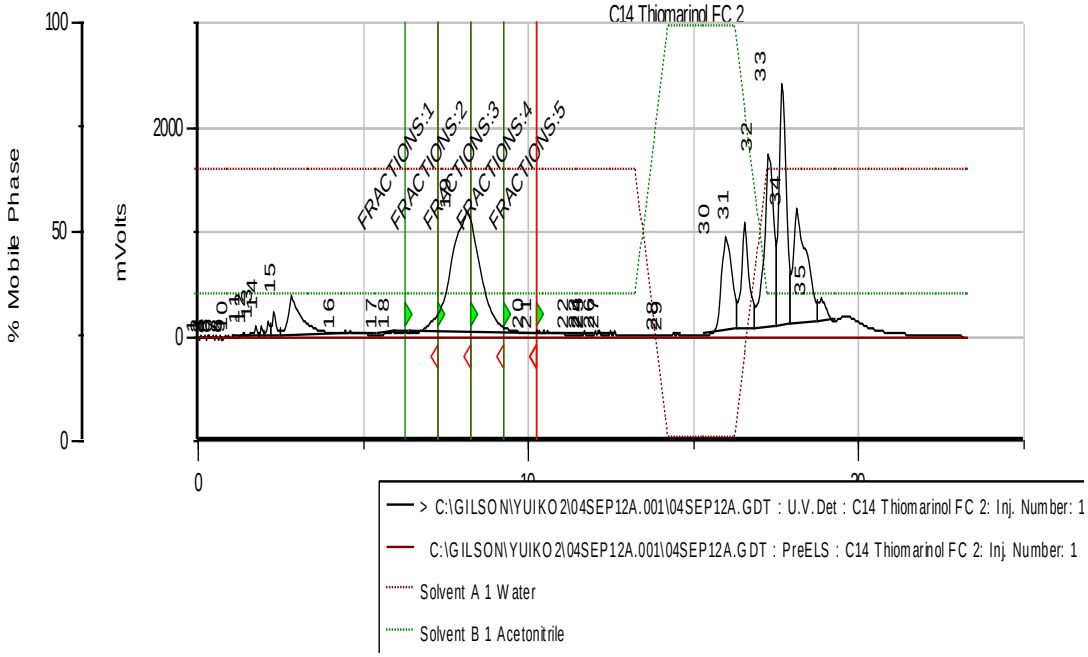

Figure 6.9. One of the ten HPLC chromatograms of 100 µl [^{14}C] thiomarinol A fraction collection (Peak 19). Fraction 1, 2 and 3 were pooled for evaporation and pooling for the final 1 ml [^{14}C] thiomarinol A stock. The retention area of Peak 19 is 1.24 x 10^{8}.

The fractions containing thiomarinol A were all evaporated on the speedvac for 23.5 hours and re-dissolved in a total of 1 ml methanol. A final 1 ml [^{14}C] thiomarinol A stock of 357 µg/ml (Figure 6.10) was obtained from half the original 2 ml (542 µg/ml) non-fractioned stock.

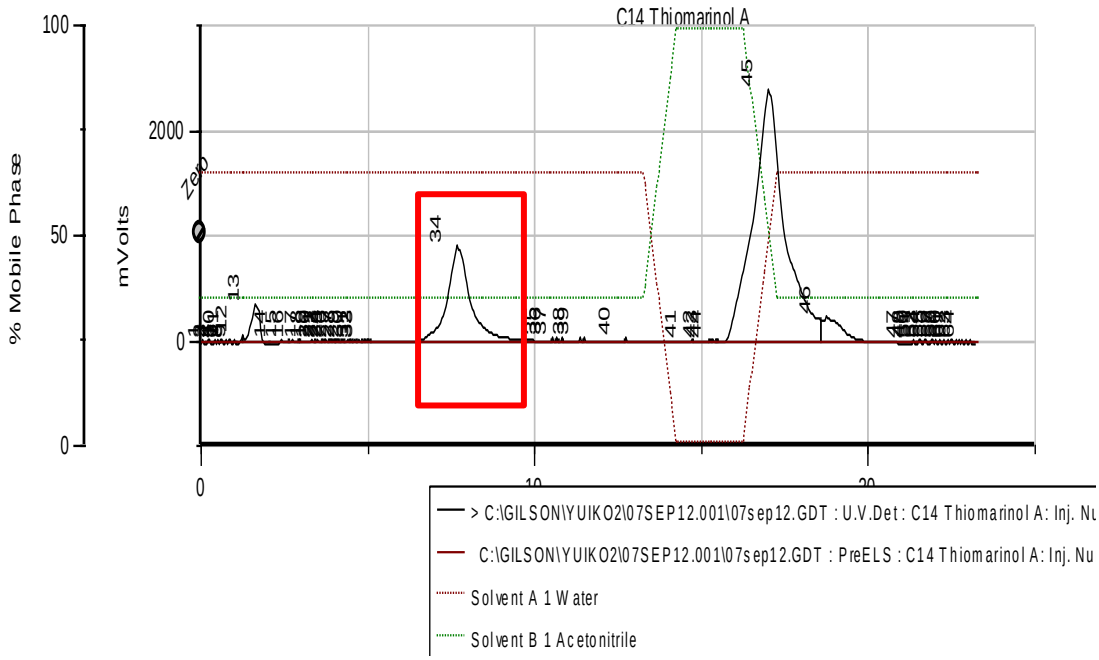

Figure 6.10. HPLC chromatogram quantifying the final [^{14}C] thiomarinol A stock highlighted in red (Peak 34). The retention area of Peak 34 is 8.19 x 10^7.

6.3.5 Optimisation of fraction collection and further processing of [^{14}C] pseudomonic acid A

Similar to the optimisation process for thiomarinol A isolation, non-radioactively labelled mupirocin was also used to determine the best method for isolating pseudomonic acid A. However, the 100 µl sample coil attached to the HPLC column was first exchanged with a 1 ml coil to accommodate larger sample sizes. The mupirocin programme is 60 minutes in duration compared to that of thiomarinol (24 minutes). It was hoped that by changing the coil to handle larger volumes, 2 x 500 µl of the [^{14}C] mupirocin stock could be fractionated within 2 hours instead of 10 x 100 µl as performed with [^{14}C] thiomarinol (which would take 10 hours).

The UniPoint programme for detecting mupirocin was altered to collect pseudomonic acid A fractions from 17 to 23 minutes. A 500 µl injection of 10 mg/ml mupirocin stock was

first tested using the new coil. The resulting chromatogram indicated that the window was too short, as the highly concentrated and larger injection volume of mupirocin took longer to pass through the column and into the collection tubes (Figure 6.11). The fraction collection window was increased to 10 to 30 minutes for isolation of [^{14}C] pseudomonic acid A.

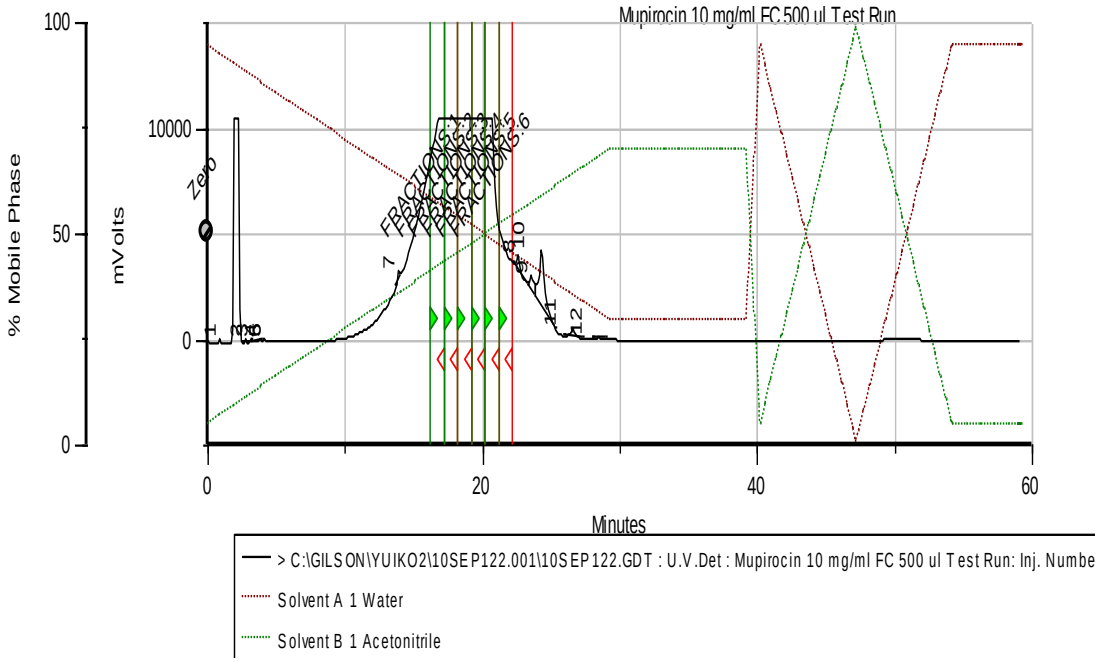

Figure 6.11. HPLC chromatogram of 500 µl mupirocin injection for fraction collection of pseudomonic acid A from 17 to 23 minutes.

6.3.6 Fraction collection of [^{14}C] pseudomonic acid A

2 x 500 µl of previously obtained [^{14}C] mupirocin was fractionated (Figure 6.12) as described above.

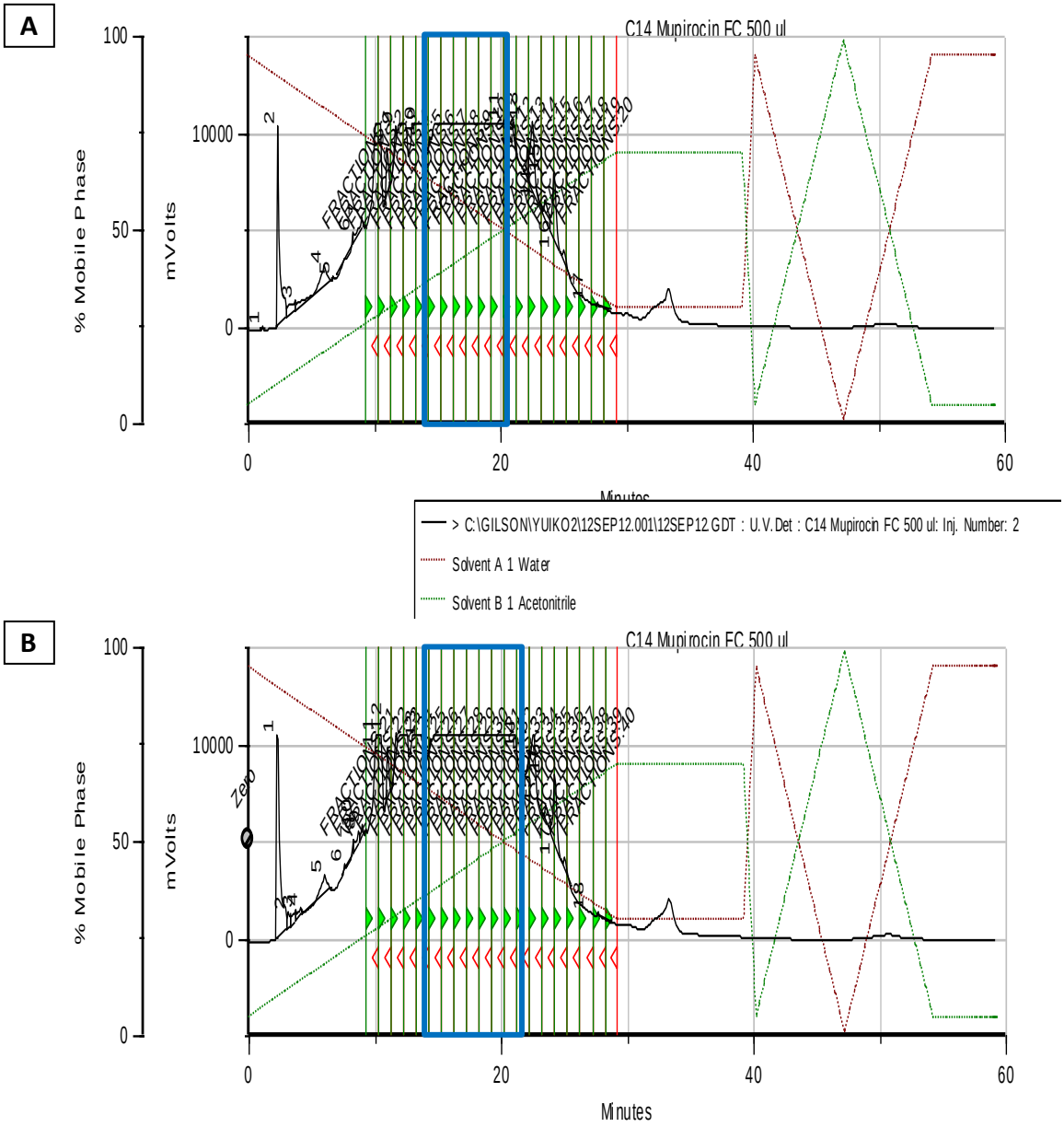

Figure 6.12. Chromatograms of (A and B) 2 x 500 µl injections of [^{14}C] mupirocin for fraction collecting [^{14}C] pseudomonic acid A. The peaks containing [^{14}C] pseudomonic acid A are not numbered due to the excess concentration and are located between (A) Peaks 10 and 11 and (B) 13 and 14, highlighted in blue.

The fractions were dried on the speedvac for approximately 16 hours and re-dissolved in a total of 1 ml methanol. 100 µl of the final [^{14}C] pseudomonic acid A stock was diluted 10-fold and quantified on the HPLC (Figure 6.13). A concentration of approximately 5 mg/ml of [^{14}C] pseudomonic acid A was obtained.

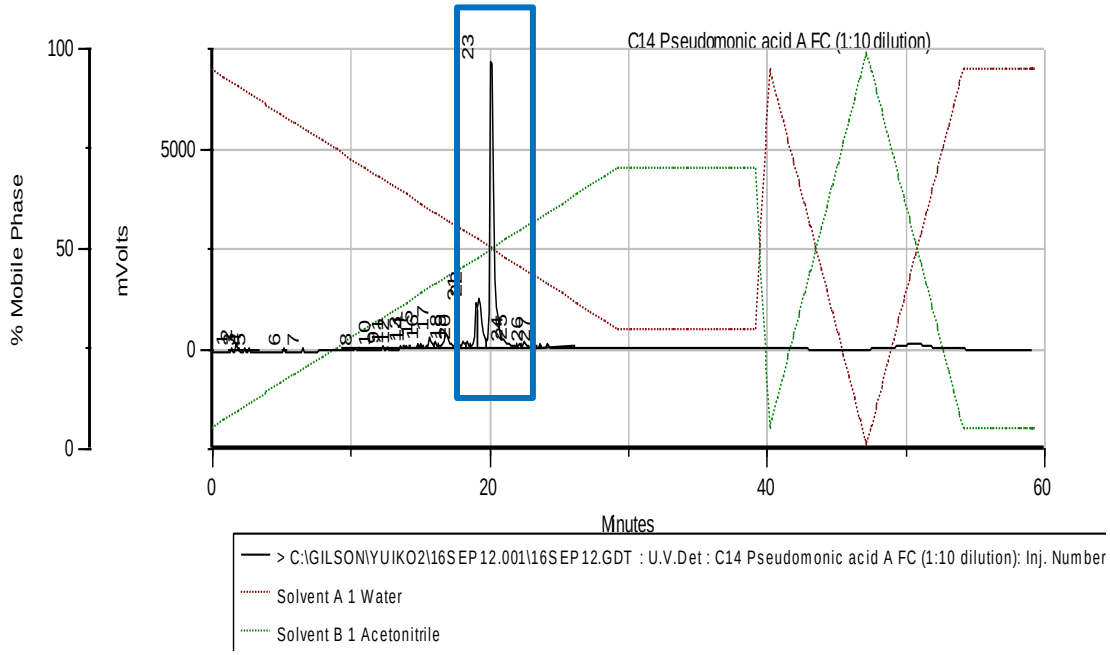

Figure 6.13 HPLC chromatogram of 100 µl injection of [^{14}C] pseudomonic acid A (Peak 23 in blue). The retention area of Peak 23 is 2.34 x 10^8.

6.3.7 Quantification of [^{14}C] incorporation on fractionated thiomarinol A and pseudomonic acid A

The scintillation counter used for generating the data in Table 6.3 (Packard 1600 TR) was replaced with a new machine (Perkin Elmer Tri-Carb 2810 TR) at this stage of the study. Hence, 10 µl of the original [^{14}C] thiomarinol and mupirocin stocks were re-counted on the new machine along with the newly isolated [^{14}C] thiomarinol A and pseudomonic acid A stocks in total volume aliquots of 1 ml Instagel. The samples were counted at 1 minute and again at 10 minutes (Table 6.6).

Table 6.6. 1 and 10 minute counts in CPM and DPM of original [^{14}C] thiomarinol and mupirocin stocks and after fractionation (AF) [^{14}C] thiomarinol A and pseudomonic acid A (PA-A) stocks (10 µl volumes)*

	CPM			DPM		
	1 min	10 min	Average	1 min	10 min	Average
Scintillant (Control)	26	28	**27**	27	30	**29**
Thiomarinol (Control)	34	46	**40**	36	49	**43**
Mupirocin (Control)	34	33	**34**	36	35	**36**
[^{14}C] Thiomarinol	374	410	**392**	396	438	**417**
[^{14}C] Thiomarinol A AF	74	79	**77**	78	84	**81**
[^{14}C] Mupirocin	919	1006	**963**	970	1068	**1019**
[^{14}C] PA-A AF	434	390	**412**	458	414	**436**

*The CPM and DPM counts of [^{14}C] thiomarinol stock are negligible due to stock evaporation during storage.

The original counts for [^{14}C] thiomarinol and mupirocin were 1177.64 and 617.61 CPM respectively (Table 6.3). The discrepancy between the original and new counts was unexpected; therefore a third counter was used to count the CPM value of the [^{14}C] thiomarinol stock. The value yielded was 388, indicating the new value of 392 to be reliable. The high initial count was disregarded.

An approximately 2-fold decrease in radioactivity was seen between the original [^{14}C] mupirocin and the fractionated pseudomonic acid A. The final level of ^{14}C incorporation in thiomarinol A was low, with an average CPM of 77 in 10 µl sample (from a 358 µg/ml stock). This is only double that of the background counts, with non-labelled thiomarinol yielding an average CPM of 40. Further attempts were made to obtain thiomarinol A and pseudomonic acid A stocks with higher specific activity. For the new machine, 10 minutes counting time was selected for accurate scintillation counting. In parallel, the stocks obtained already were used in preliminary uptake studies to determine whether their low incorporation was

enough to allow any differences in uptake between thiomarinol and mupirocin to be detected.

6.3.8 Determining the optimal feeding window for ^{14}C incorporation

Preliminary time course experiments performed by colleague Ahmed Omer-Bali observed thiomarinol production to take place at the onset of stationary phase, between 18 to 24 hours and peaking at around 21 hours of culture incubation (Omer-Bali, 2013). Observations of antibiotic production occurring at stationary phase have also been made in the literature, such as with actinomycete antibiotic genes being expressed at the onset of stationary phase in liquid cultures (Bibb, 2005). It was thus hypothesised that for efficient incorporation of [^{14}C] acetate into thiomarinol and mupirocin during biosynthesis, feeding should be done just before stationary phase instead of spaced across three feeds during lag, exponential and stationary phase as previously performed. To test this, the growth curves and levels of antibiotic production were monitored at 1 hour intervals using absorbance and HPLC, to determine the optimal window for feeding radioactive precursors.

First, thiomarinol and mupirocin production was monitored based on Omer-Bali's observation of the 18 to 24 hour stationary phase window for *P. rava*. 1 ml samples were collected from 17 hours up to 25 hours of incubation and processed as described in the Materials and Methods for HPLC quantification. Chromatograms revealed both thiomarinol and mupirocin to already be in production at the tested window (a selection of data shown in Figure 6.14 and Figure 6.15). The thiomarinol samples all had approximately 11 µg/ml of thiomarinol A. Likewise, the mupirocin samples all had approximately 25 µg/ml of pseudomonic acid A – although the concentration of the last sample taken at 25 hours

incubation was 45 µg/ml. This suggested the stationary phase windows to be earlier for both *P. rava* and *P. fluorescens* (pJH2) than previously determined by Omer-Bali.

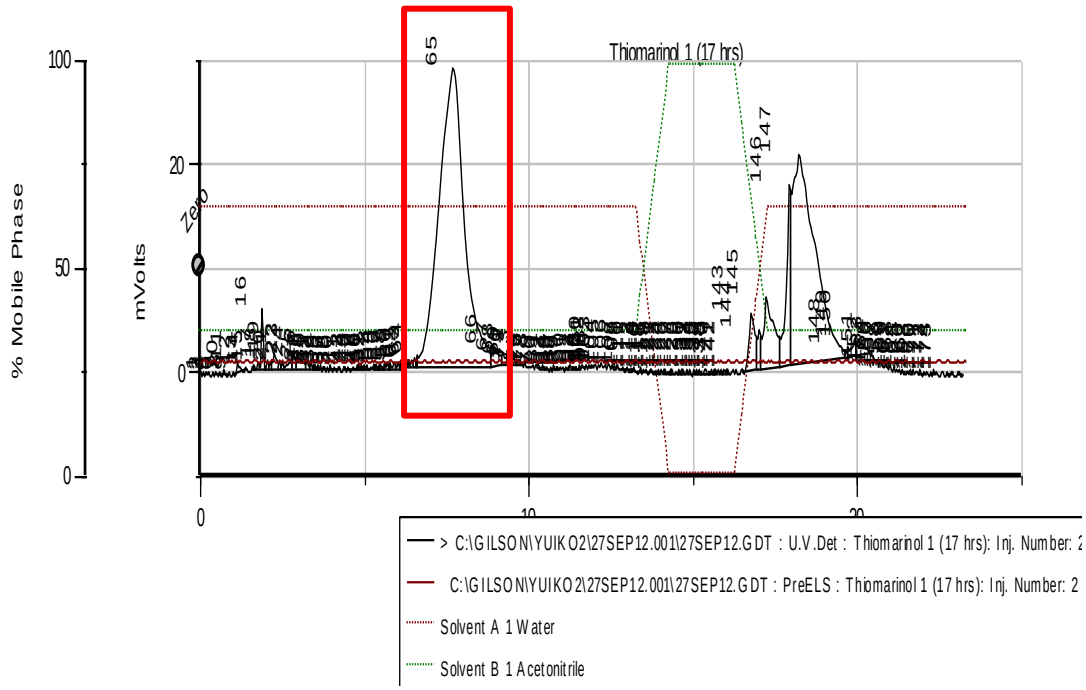

Figure 6.14. HPLC chromatogram of thiomarinol A peak detected at 17 hours incubation. The peak is highlighted in red and its retention area is 2.62 x 10^6.

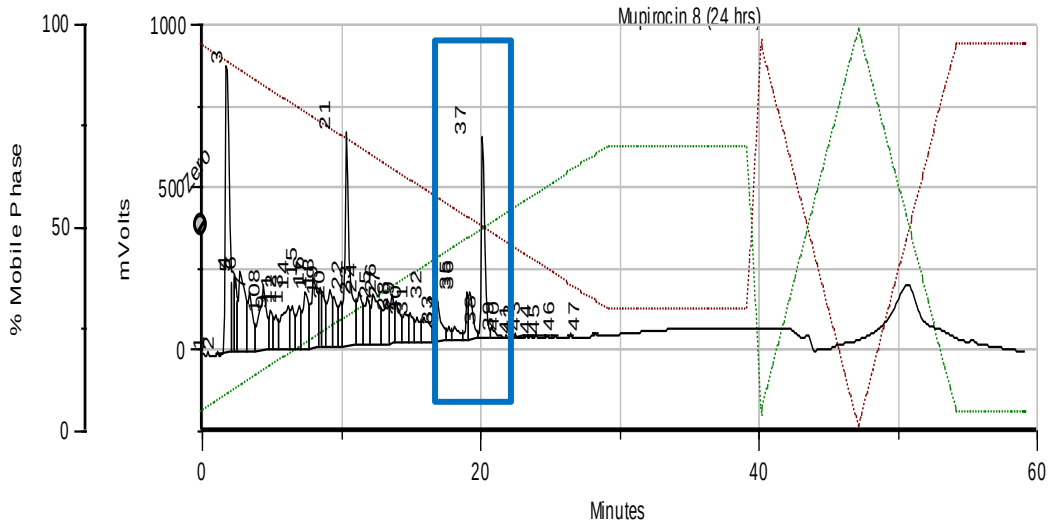

Figure 6.15. HPLC chromatograms of pseudomonic acid A peaks detected at 24 hours incubation. The peak is highlighted in blue and its retention area is 1.75 x 10^7.

Growth curve experiments were set up to monitor the changes in cell density of *P. rava* and *P. fluorescens* (pJH2) for the first 9 hours and at 24 hours after incubation (Figure 6.16).

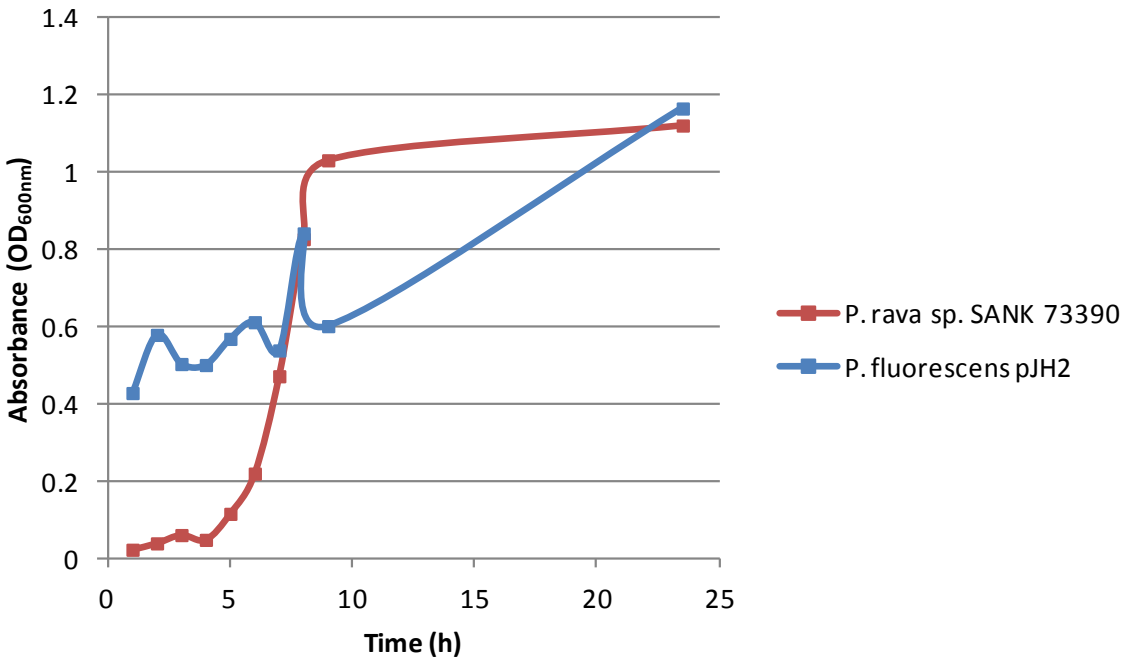

Figure 6.16. Growth curves of thiomarinol producer *P. rava* (in red) and mupirocin producer *P. fluorescens* pJH2 (in blue).

The samples were diluted 10-fold before absorbance determination, mainly to offset the high absorbance background of the *P. fluorescens* samples in SMM media. Nevertheless, the onset of stationary phase in *P. fluorescens* growth was not as clear as on the growth curve of *P. rava*. Stationary phase occurred anywhere between 7 and 24 hours for *P. fluorescens*. For *P. rava*, this phase was clearly between 8 and 9 hours in the first trial and between 7 and 8 hours in the repeated growth curve (data not shown). Overall, it was concluded that the onset of stationary phase for *P. rava* was somewhere between 7 to 9 hours. Subsequent time course experiments performed by Ahmed Omer-Bali found thiomarinol production to

also begin at around 9 hours, which increased exponentially until 18 hours before reaching a plateau of production, with a peak at around 36 hours (Omer-Bali, 2013).

6.3.9 Further optimisation of ^{14}C incorporation in thiomarinol A and pseudomonic acid A

Based on the above findings, feeding experiments were repeated but with one bulk feed of [^{14}C] acetate at 8 hours incubation for both thiomarinol and mupirocin production (Trial 2). When incorporation of radioactivity into antibiotics was determined in 10 µl of the ethyl acetate extract, the counts and overall yield had improved for thiomarinol A but surprisingly not for pseudomonic acid A (Table 6.7).

Table 6.7. Summary of [^{14}C] thiomarinol and mupirocin concentrations and counts before and after fractionation from Trial 1, 2 and 3*.

		Concentration (µg/ml)	CPM	DPM	Specific Activity[1] (mCi/mol)
1	[^{14}C] Thiomarinol	542	392	417	22
	[^{14}C] Thiomarinol A AF	358	77	81	7
	[^{14}C] Mupirocin	6358	963	1019	4
	[^{14}C] PA-A AF	4952	412	436	2
2	[^{14}C] Thiomarinol	1048	1871	2027	56
	[^{14}C] Thiomarinol A AF	650	222	235	10
	[^{14}C] Mupirocin	11017	704	744	2
	[^{14}C] PA-A AF	-	-	-	-
3	[^{14}C] Thiomarinol	698	2001	2181	90
	[^{14}C] Thiomarinol A AF	-	-	-	-
	[^{14}C] Mupirocin	11453	2207	2331	5
	[^{14}C] PA-A AF	-	-	-	-

*Abbreviation: AF after fractionation; PA-A pseudomonic acid A.

[1]Specific Activity calculated using molar mass of thiomarinol A = 640.81 g/mol and PA-A = 500.63 g/mol. 1 Ci = 2.22 x 10^{12} DPM.

[^{14}C] thiomarinol was collected after fractionation and quantified for use in the fourth uptake study described later in this section. [^{14}C] mupirocin was discarded due to its low incorporation and a third feeding experiment set up with the mupirocin-producing culture being fed after 21 hours of incubation instead of 8 hours. The feeding time was delayed to be closer to the production peak of 36 hours identified by Omer-Bali, in an attempt to encourage better incorporation.

The counts were a vast improvement from Trial 2 (Table 6.7) but the uptake studies had determined at this stage that much higher incorporation was necessary for the radioactive antibiotics to be useful in downstream uptake experiments. Hence, fractionation and collection of the antibiotics from Trial 3 was not pursued and the carbon source was changed from [^{14}C] acetate to methionine.

Methionine was the carbon source recommended by Dr. Zhongshu Song, University of Bristol due to its specific incorporation into the antibiotics in comparison to acetate that is readily used by metabolic pathways such as fatty acid synthesis. However, because labelled methionine is significantly more expensive than acetate, the latter was initially used in attempt to produce [^{14}C]-labelled antibiotics. Following the failed attempts to produce high specific activity radiolabelled antibiotics, [^{14}C] methionine was purchased and 4 µCi fed to each of the mupirocin and thiomarinol production cultures following the same procedure as in Trial 3. The collected [^{14}C] thiomarinol A fractions gave an apparent level of incorporation (Table 6.8) that was approximately 4 times more counts than the stock obtained from acetate feeding in Trial 2.

Table 6.8. [^{14}C] thiomarinol yielded from [^{14}C] methionine fed production cultures.

	Concentration (µg/ml)	CPM	DPM	Specific Activity (mCi/mol)
[^{14}C] Thiomarinol	-	9548	10384	-
[^{14}C] Thiomarinol A AF	485	873	930	55

Unfortunately, the ethyl acetate extracted [^{14}C] mupirocin could not be quantified and fractionated due to unforeseen problems with the HPLC machine. The extracted stock was stored at -20°C for future work.

6.3.10 Preliminary uptake study

In parallel to the optimisation of procedures to yield higher [^{14}C] thiomarinol A and pseudomonic acid A stocks, attempts were made to identify any differences in uptake of the two antibiotics by sensitive and/or resistant bacteria using the [^{14}C] antibiotic stocks already produced. The ability of antibiotics to enter the cells is of great importance, as the drugs are ineffective if unable to pass through the primary protective barrier of their target microorganisms. As such, it was hypothesised that thiomarinol may be more effective against a wider range of Gram-positive and negative organisms due to its superior ability (compared to mupirocin) to accumulate faster and better, and perhaps also avoid efflux to maintain a potent concentration in the cells.

The following uptake study was based on the method used by Capobianco *et al.* (1988) but altered to allow for the lower specific activity of the ^{14}C incorporated into thiomarinol A and pseudomonic acid A stocks used. It was aimed to address the possible role of uptake in thiomarinol efficacy. *E. coli* and *B. subtilis* were chosen as the test organisms to

represent mupirocin resistance and sensitivity respectively. It was expected that mupirocin would accumulate to a greater extent in *B. subtilis* cells than *E. coli*, as the latter has been proposed to be resistant due to its impermeable outer cell membrane (Capobianco *et al*., 1989). Various preliminary experiments were undertaken to determine the optimal bacterial density, sampling intervals and scintillation counting times for this study.

First, the optimal bacterial cell density for recovering the original amount of radioactivity put into the assay was determined. Due to the low specific activity of ^{14}C in the antibiotics, it was possible that too many cells in the assay might quench or obscure the counts and thus require increased volumes of antibiotics in the assay which were not available due to limitations described in the previous section.

[^{14}C] pseudomonic acid A was used for this exploratory experiment, as a more concentrated stock with higher specific activity was available compared to thiomarinol A. 2 ml L-broth volumes were chosen for the assay and amounts of bacteria to give the equivalent 2 ml intracellular cell volumes added to give an equal ratio of L-broth to intracellular volume. The appropriate intracellular volume was calculated based on the *E. coli* aqueous volume at 6.7×10^{-15} L per cell (Neidhardt *et al*., 1996) and *B. subtilis* at 1.0×10^{-14} L per cell (Bergey *et al*., 1974). A total of 3×10^{11} *E. coli* cells and 2×10^{11} *B. subtilis* cells were estimated to equate to 2 ml intracellular volumes.

Based on the estimation that 1 ml of bacterial overnight from one single colony inoculation yields approximately 10^9 bacteria, *E. coli* overnight cultures of 60, 150, 300 ml were set up to produce total intracellular volumes 0.5, 1, 2 ml (or 10, 25, 50% of the total 2

ml extra and intracellular volumes). Likewise, *B. subtilis* overnight cultures of 40, 100, 200 ml were prepared.

The overnight cultures were centrifuged as described in Methods and the pellet re-suspended in 2 ml L-broth before being separated into two 1 ml samples. 100 µl of each sample was taken for viable cell determination to confirm the number of cells added to the L-broth. 28 µl of [^{14}C] pseudomonic acid A was added to one of the 1 ml sample (equivalent to 140 µg/ml and 1220 DPM) and incubated at 30°C at 200 rpm for up to 30 minutes. This amount of [^{14}C] pseudomonic acid A was chosen to yield approximately double the DPM of blanks in the 100 µl samples to be taken (with Instagel blank samples counting approximately 30 DPM) and thus detectable over the background. The other 1 ml sample was not treated with [^{14}C] pseudomonic acid A but incubated under the same conditions as with the radioactive sample to identify any background noise. 100 µl samples were taken in triplicates at 5 and 30 minute intervals for *B. subtilis* and 30 and 60 minute intervals for *E. coli* from both 1 ml samples and processed as outlined in Methods to determine the extracellular and intracellular radioactive counts. The *E. coli* cultures were incubated longer before sampling than *B. subtilis*, as the latter was tested first in this initial experiment and indicated the need for longer incubation to check whether the samples had reached extra and intracellular equilibrium of [^{14}C] pseudomonic acid A concentrations.

Viable cell counts were obtained the day after the initial uptake study. The intracellular volumes of *B. subtilis* were approximately 13, 24 and 43% of the total 2 ml extra and intracellular volume, which is close to the proposed 10, 25 and 50% volumes. However, the intracellular volumes of *E. coli* were 25, 50 and 69% of the total 2 ml volume and far too dense. Nevertheless, results showed that the original amount of [^{14}C] pseudomonic acid

counts (122 DPM per 100 µl sample) could still be detected in the total counts of the cell pellet and supernatant samples (Figure 6.17; Figure 6.18).

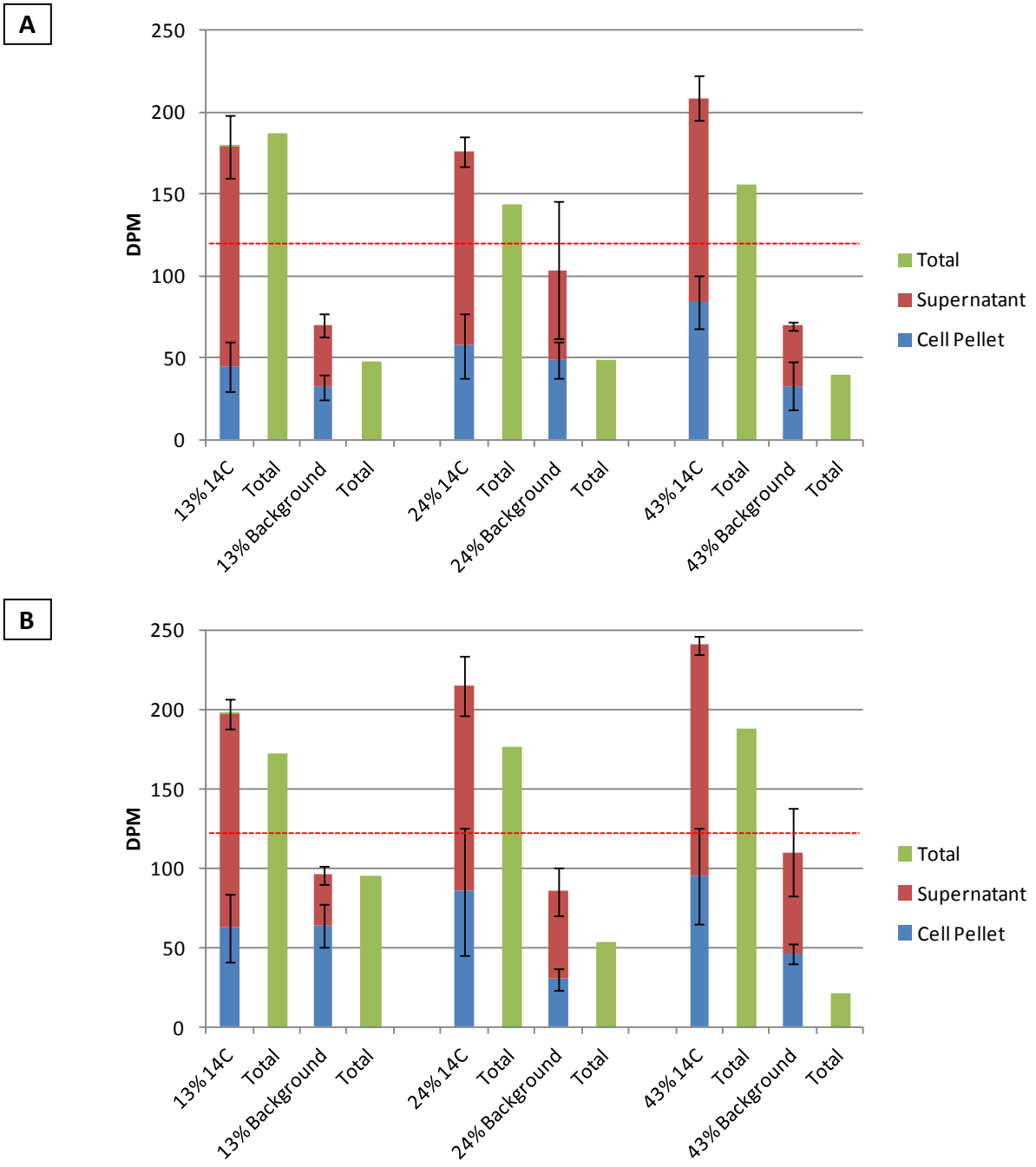

Figure 6.17. DPM counts of [^{14}C] pseudomonic acid A accumulation in cell pellet, supernatant and total *B. subtilis* samples at (A) 5 min and (B) 30 min incubation intervals. 13, 24 and 43% refer to the intracellular volumes of *B. subtilis*. The red dotted line indicates the 122 DPM per 100 µl of [^{14}C] pseudomonic acid A originally added to the experiment. The cell pellet and supernatant stacked bars (in red and blue) represent the intracellular and extracellular radioactive counts respectively that were detected from sample preparation described in the Methods. The total bars (in green) represent the total radioactive counts detected from 100 µl of non-processed samples. The "Background" samples represent the background DPM detected from the control non-radioactive samples. The cell pellet and supernatant samples were prepared in triplicates (and SD error bars determined) but the total samples were prepared singly.

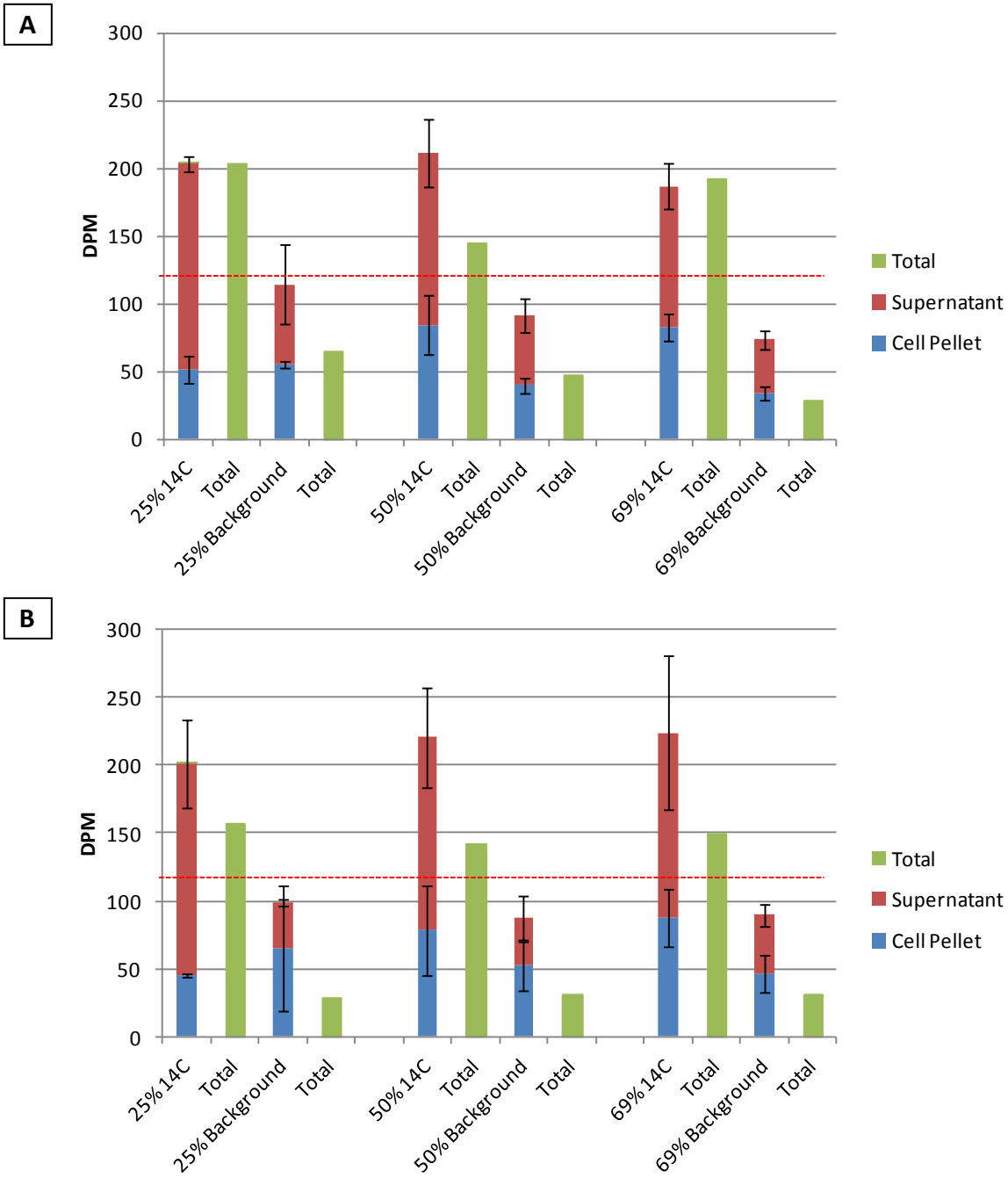

Figure 6.18. DPM counts of [^{14}C] pseudomonic acid A accumulation in cell pellet, supernatant and total *E. coli* samples at (A) 30 min and (B) 60 min incubation intervals. 25, 50 and 69% refer to the intracellular volumes of *E. coli*. The red dotted line indicates the 122 DPM per 100 µl of [^{14}C] pseudomonic acid A originally added to the experiment. The cell pellet and supernatant stacked bars (in red and blue) represent the intracellular and extracellular radioactive counts respectively that were detected from sample preparation described in the Methods. The total bars (in green) represent the total radioactive counts detected from 100 µl of non-processed samples. The "Background" samples represent the background DPM detected from the control non-radioactive samples. The cell pellet and supernatant samples were prepared in triplicates (and SD error bars determined) but the total samples were prepared singly.

In general, the total counts of cell pellet and supernatant when measured individually or combined were much higher than the original 122 DPM of [^{14}C] pseudomonic acid A added per 100 µl sample. This may be due to several reasons. First, there may be a limit to the cell density used in this experiment. While setting up samples for scintillation counting, cell densities of over 50 % appeared to settle in the sample when left static for scintillation counting. When vortexed, the samples remained cloudy, indicating that the cell densities had exceeded the Instagel's holding capacity. Counting efficiency decreases drastically when the sample is not in completely clear suspension with the Instagel because cloudiness causes interference with the counter detecting the photons emitted by the scintillant after collision with emissions from radioactive substrates. Hence, cell densities above 50% of the total volume were deemed inappropriate for future experiments.

Second, background counts may need to be taken into account to detect radioactive accumulation in the cell pellets. The total samples (in green, Figure 6.17 and Figure 6.18) had counts closer to the original 122 DPM and when the background total counts were deducted from the former counts (to take into account the issue mentioned above of sample viscosity), the total radioactivity was similar to what was originally added. Likewise with the individually measured samples (in red and blue, Figure 6.17 and Figure 6.18), once background was deducted, the remaining counts were also closer to 122 DPM (although more varied than the total (green) counts).

When background is taken into account, there is no evidence of uptake, i.e. no detection of radioactive accumulation in the cell pellet, at 13 and 25% bacterial density of *B. subtilis* and *E. coli* respectively (except *B. subtilis* at 5 minutes interval, Figure 6.17A).

However at around 50% cell density for both organisms, there is some radioactive detection after background deduction; therefore, a 50% bacterial suspension was chosen for further investigations. This preliminary experiment also identified the need to increase sampling intervals to determine whether the reactions reached equilibrium within the 60 minute time frame. It was hard at this stage to speculate on any differences in accumulation of [^{14}C] pseudomonic acid in *B. subtilis* and *E. coli* cells due to count variability across the triplicate samples and the high background noise.

The uptake experiment was repeated with 50% cell density for both organisms but with larger sampling intervals of 0, 1, 2, 4, 8, 10, 20, 30, 60, 90 and 120 minutes (in triplicates) to determine the time point in which the reactions reach equilibrium. The samples were counted for 1 minute on the scintillation counter. The total sample volumes were set up to be 4 ml total as initially intended, and therefore the overnight cultures were set up to yield 2 ml total intracellular volume.

The results obtained from this second uptake study were inconclusive, with high variability between the triplicate counts (as shown by the standard deviation error bars) (Figure 6.19; Figure 6.20).

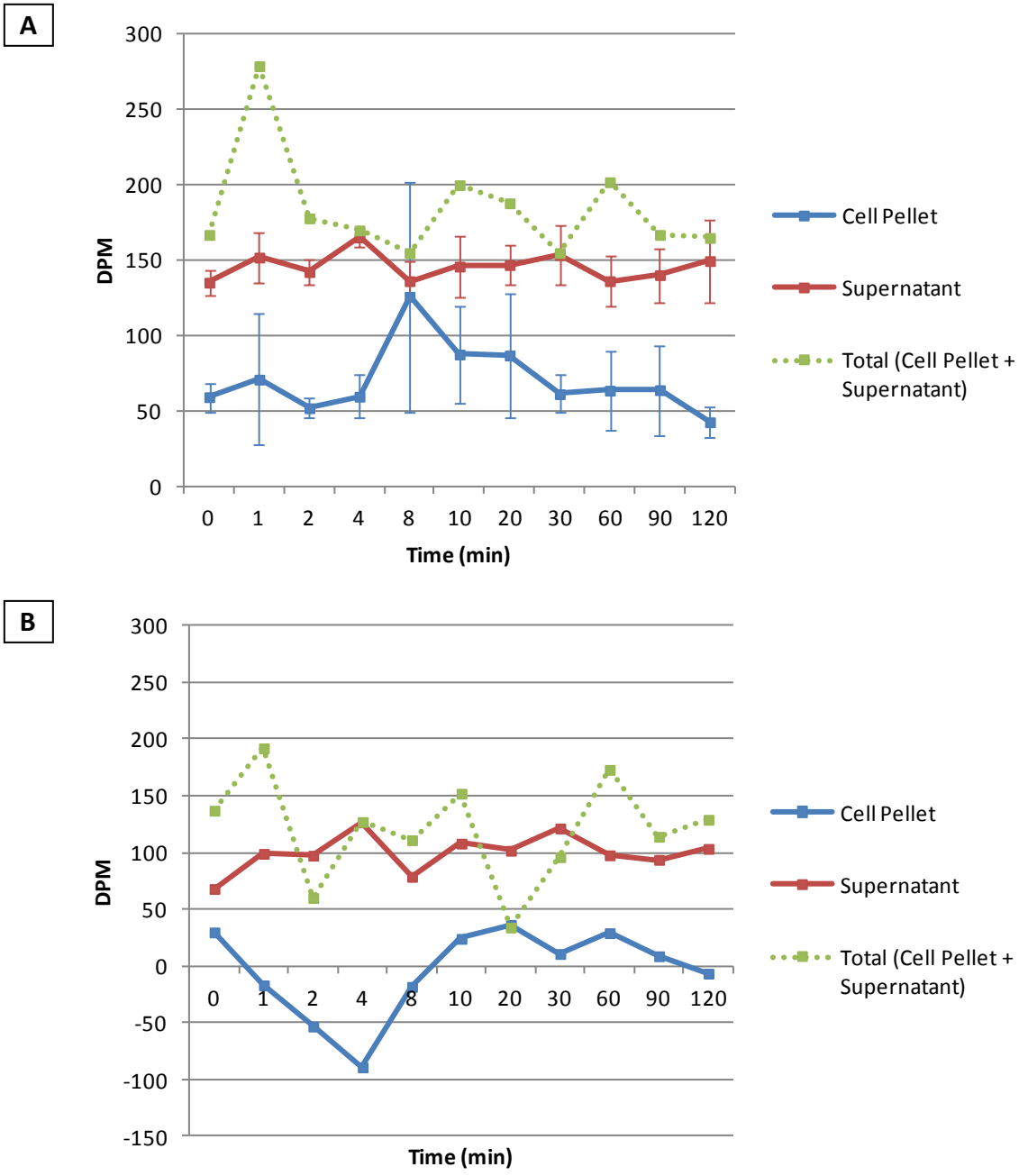

Figure 6.19. DPM counts of [^{14}C] pseudomonic acid A accumulation in cell pellet, supernatant and total *E. coli* samples at various time points. (A) The DPM counts are raw data and do not take into account the high background noise. **(B)** Background counts deducted from the above data points. The total samples (in green) represent the total radioactive counts detected from 100 µl of non-processed samples (which should theoretically equate to the sum of the cell pellet and supernatant counts but this is not always the case in this study.) The cell pellet and supernatant samples were taken and counted in triplicate (and SD error bars determined) but the total samples were prepared singly. The 0 min time point represents the sample taken as soon as the [^{14}C] pseudomonic acid A is added to initiate the assay.

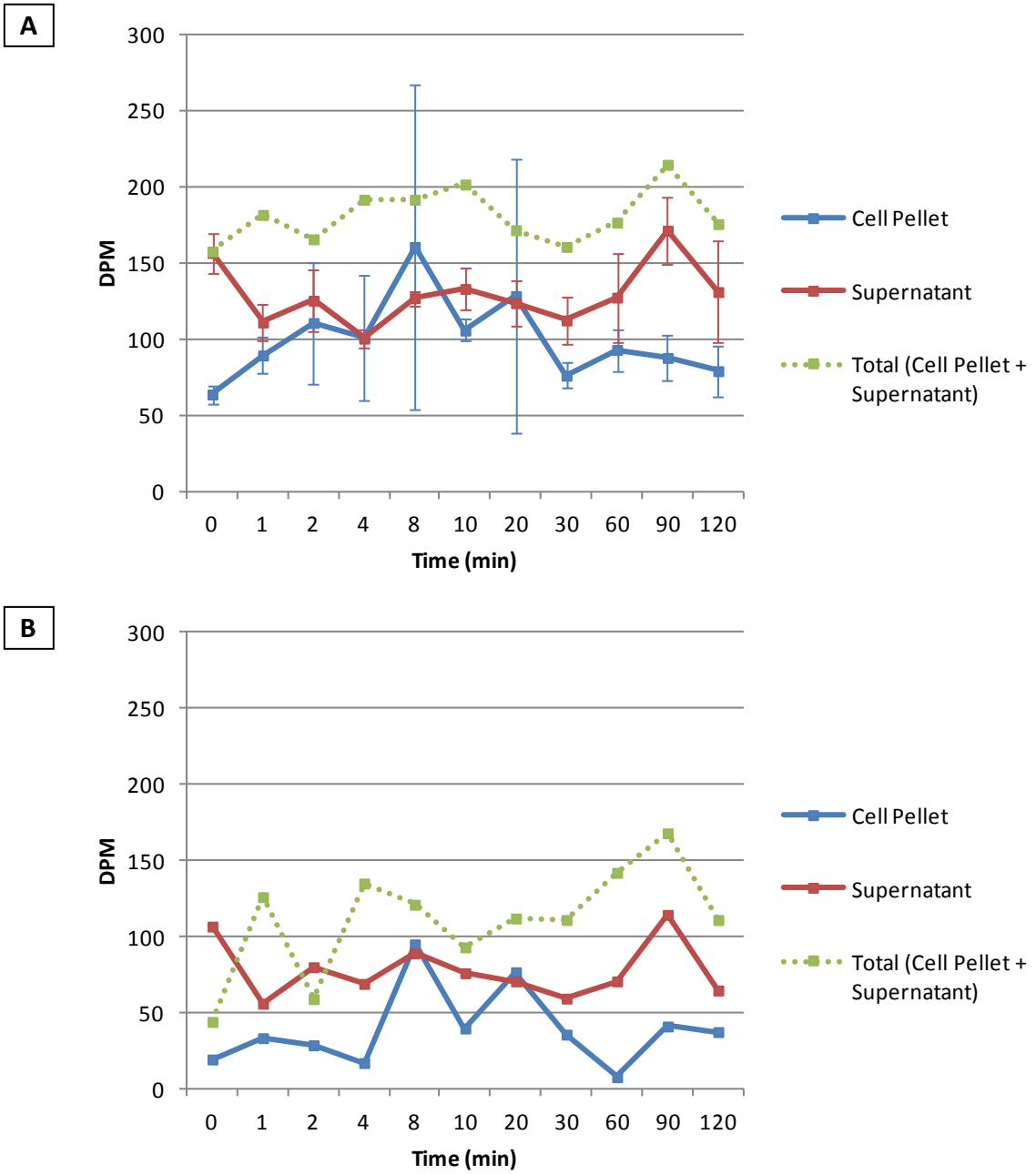

Figure 6.20. DPM counts of [^{14}C] pseudomonic acid A accumulation in cell pellet, supernatant and total *B. subtilis* samples at various time points. (A) The DPM counts are raw data and do not take into account the high background noise. **(B)** Background counts deducted from the above data points. The total samples (in green) represent the total radioactive counts detected from 100 µl of non-processed samples (which should theoretically equate to the sum of the cell pellet and supernatant counts but this is not always the case in this study.) The cell pellet and supernatant samples were taken and counted in triplicate (and SD error bars determined) but the total samples were prepared singly. The 0 min time point represents the sample taken as soon as the [^{14}C] pseudomonic acid A is added to initiate the assay.

The most concerning observation from the above data was the inconsistency in total counts (in green). While this should be more or less 122 DPM across all [^{14}C] samples, overall the counts were high. When the background DPM was deducted, the counts were still widely variable – with some samples having greater or less counts than what was initially added. This suggested the unreliability and unreproducibility of the results and also did not indicate at what time point the samples reach equilibrium.

In the third experiment, the scintillation counting time was increased from 1 to 10 minutes and the cell densities were lowered to 20% in an attempt to get more consistent counts across the triplicate samples. The total assay volume was increased to 5 ml to provide enough samples for the transport study, described below. 100 µl samples were taken at 0, 2, 5, 10, 20, 30 and 90 minutes intervals in triplicates and further processed as outlined above.

In addition to deducing the optimal incubation period, this experiment also ensured that the pH of the samples was optimal and consistent, by spotting each sample onto pH paper at all time points. This was done to settle any concerns of changing pH in high density cultures, which may affect the rate in which [^{14}C] pseudomonic acid A is influxed and/or effluxed out of cells. Additionally, pseudomonic acid A is known to lose activity outside the pH range of 4-9 (Clayton *et al*., 1979) and hence, a low pH would introduce unwanted experimental error. The pH of all samples was at the optimal 8.0. This eliminated pH from being a possible contributor to the inconsistent results.

Viable cell counts showed the intracellular volumes of *E. coli* to be 21% and *B. subtilis* to be 19% and within the 20% aim. A vast improvement was seen in the counts at this cell density, with majority of triplicates producing consistent results (Figure 6.21).

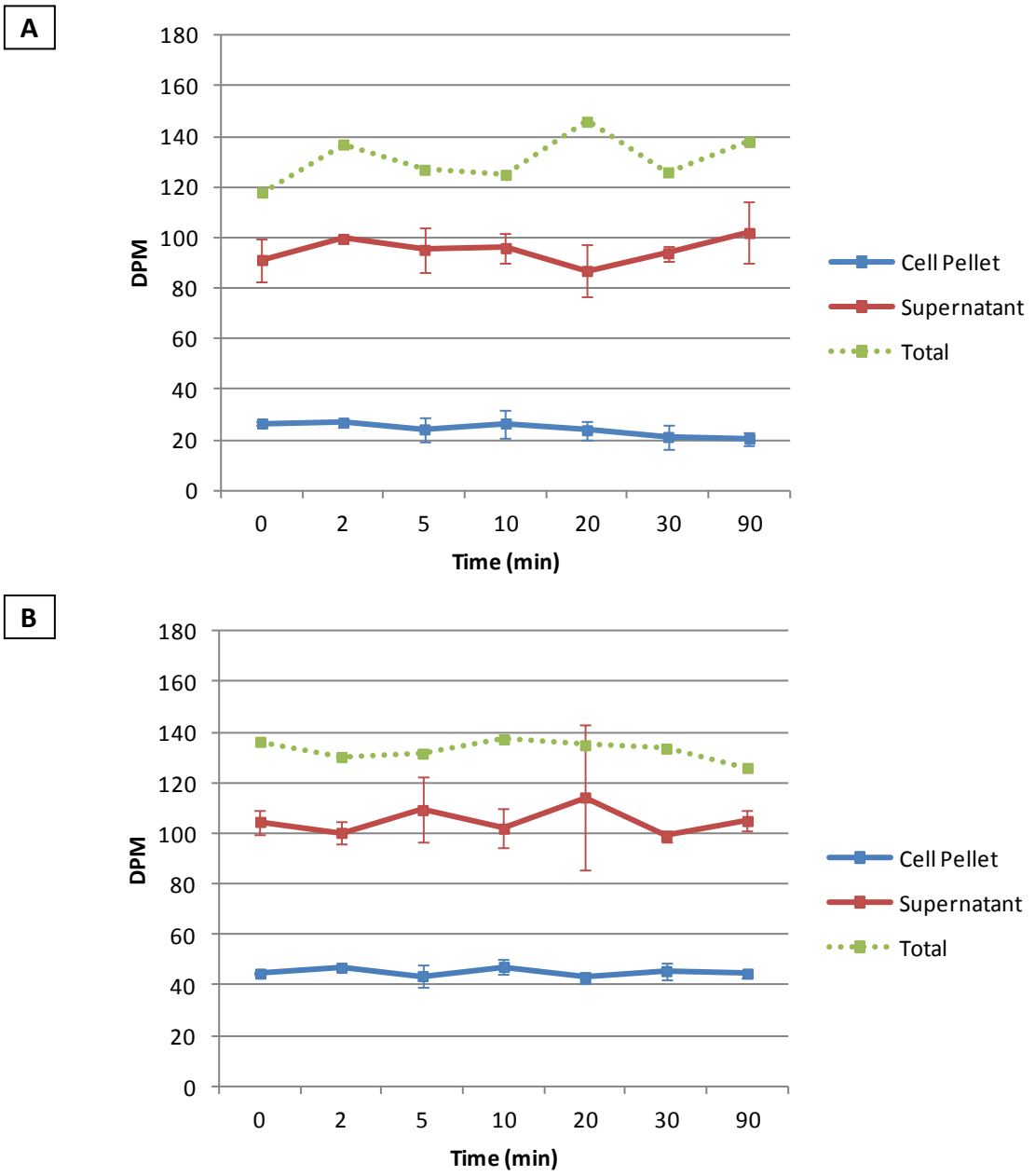

Figure 6.21. DPM counts of [^{14}C] pseudomonic acid A accumulation in cell pellet, supernatant and total samples of (A) *E. coli* and (B) *B. subtilis* at various time points. Background counts (on average 25 DPM) were deducted from (A) but not from (B) due to experimental error. The cell pellet and supernatant samples were taken and counted in triplicates (and SD error bars determined) but the total samples were prepared singly.

Although the issue of counting inconsistencies appear to have been solved by decreasing cell density to 20% and by increasing scintillation counting time to 10 minutes, no change in intracellular counts (in the cell pellet samples) suggested that at lower cell density, uptake cannot be detected using low specific activity antibiotics. Unfortunately at higher cell density of 50%, uptake can be detected but the results are too variable.

6.3.11 Uptake study using increased radioactivity of [^{14}C] thiomarinol A

[^{14}C] thiomarinol A yielded from bulk feeding acetate was used for the later uptake studies. This antibiotic stock had an increased count of 235 DPM per 10 µl sample compared to the 81 DPM yielded in the initial stages (and 436 DPM [^{14}C] pseudomonic acid A used in the above uptake studies). *E. coli* was prepared to an intracellular volume of 25% of the total 4 ml L-broth assay culture. The assay temperature was lowered to 22°C in an attempt to slow the rate of uptake to capturing this phenomenon, as previous experiments set at 30°C all appeared to have reached equilibrium at 0 minutes. Scintillation counting time was maintained at 10 minutes.

The results were promising, with a visible increase in intracellular radioactive count, before the counts plateau from 30 minutes to 60 minutes incubation intervals (blue line, Figure 6.22).

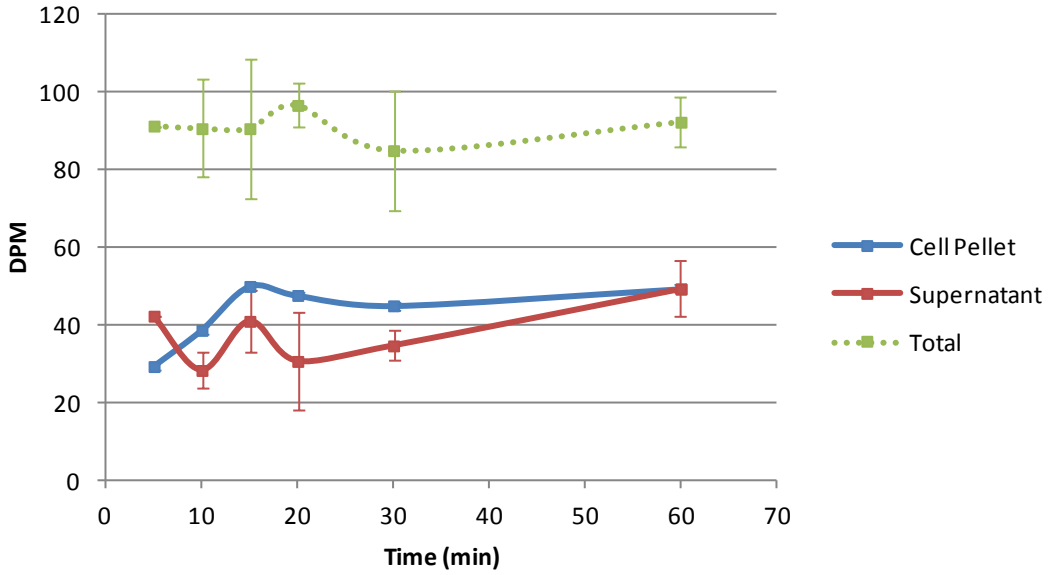

Figure 6.22. Average DPM (in triplicates) of [^{14}C] thiomarinol A accumulation in *E. coli* cell pellet, supernatant and total samples. Background counts were deducted from all sample counts.

The experiment was repeated at the lower temperature with *E. coli* and *B. subtilis* and using the remaining [^{14}C] pseudomonic acid A from previous uptake studies and [^{14}C] thiomarinol A. Unfortunately, the counts were inconsistent, with high DPM reads for background samples with no added radioactivity (data not shown). The samples were re-vortexed and recounted on the scintillation counter but were still inconsistent. At this stage, the last of the quantified [^{14}C] antibiotics had been used and therefore the experiments could no longer be continued.

6.3.12 Preliminary transport study

Contrary to uptake, inefficient efflux of thiomarinol from susceptible cells was considered as a possible contributing factor to the antibiotic's efficacy. To address this hypothesis, a transport study was devised in parallel to the uptake experiments to investigate the rate of [^{14}C] pseudomonic acid efflux from *E. coli* cells compared to *B. subtilis*.

Additional 100 µl samples were taken at the 60 minutes incubation interval from the third uptake experiment and processed as outlined in the methods. By re-suspending the cells with intracellular [^{14}C] pseudomonic acid A in fresh 2 ml L-broth and taking scintillation counts at various time points, it was hoped that the rate in which the antibiotic either passively diffused or effluxed out of the organisms could be observed. Further application of this study with thiomarinol A would determine whether slower rate of passive diffusion and /or efflux of the antibiotic out of the cells were contributing factors to its potency.

The uptake experiment was performed using *B. subtilis* cells before proceeding with *E. coli*. 100 µl samples were taken in triplicates and the cell pellets re-suspended in L-broth. 100 µl samples were taken in quadruplicates from each of the three uptake assays at 0, 2, 5, 10 and 20 minutes intervals and three from each assay processed to obtain counts in the cell pellet and in the supernatant. The last sample of each assay was counted for total radioactive counts. Due to the large sampling size of 9 samples per assay, timing issues were introduced, with cell pellets not being separated from the supernatants immediately after centrifugation. This created the concern of [^{14}C] pseudomonic acid A diffusing out of the cells while left static in the supernatant.

For assaying the transport of [^{14}C] pseudomonic acid A in *E. coli* cells, the starting L-broth volume was prepared at 3 ml and the sampling size was decreased to three assays with one sampling to avoid time delays in processing the samples. The sampling times were also delayed to start from 2 minutes instead of 0. The results obtained in both transport studies suggest basal to no radioactivity in the samples; background counts were approximately 25 DPM (Figure 6.23).

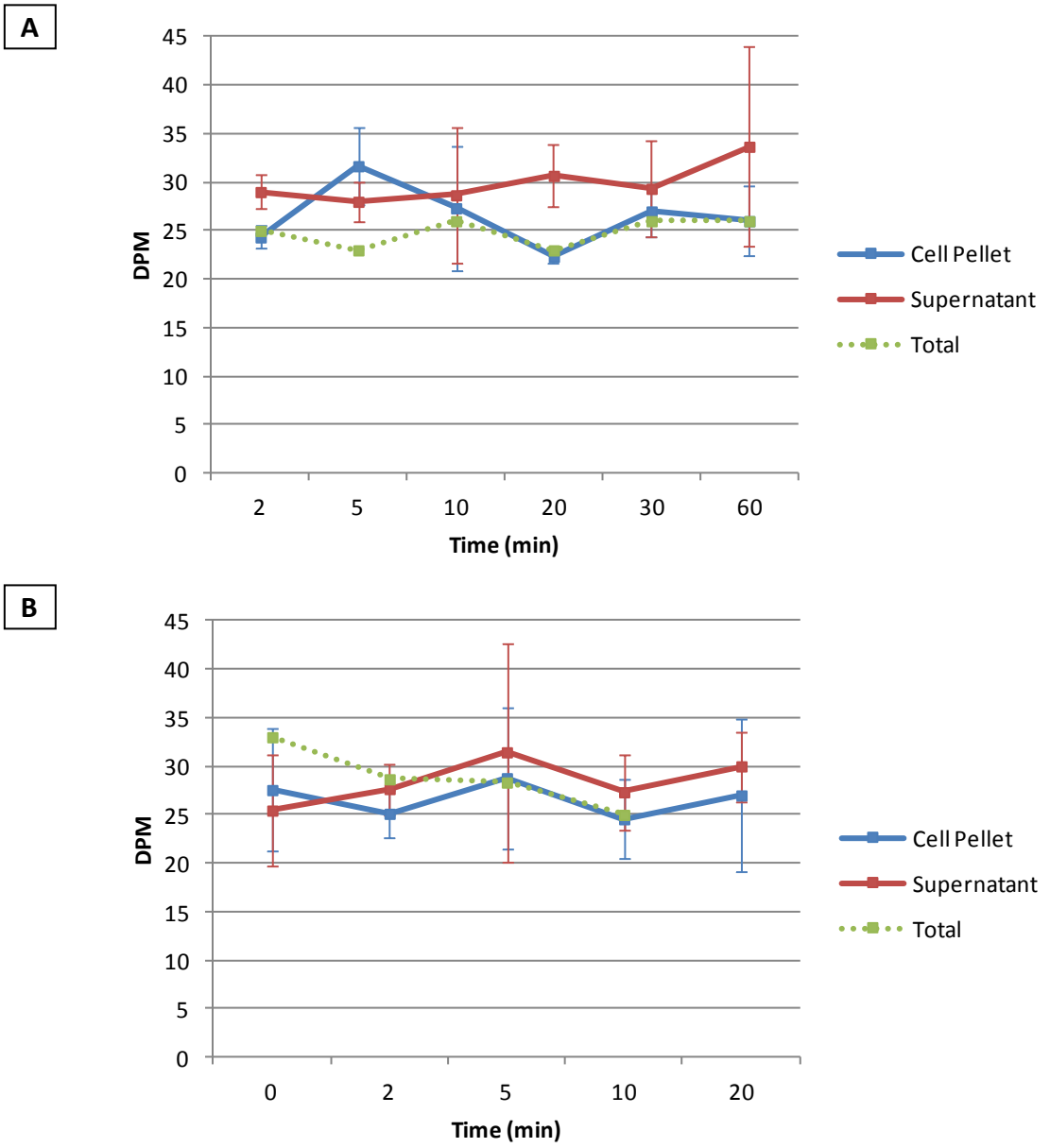

Figure 6.23. DPM counts of [^{14}C] pseudomonic acid A efflux from cell pellet to supernatant and total samples of (A) *E. coli* and (B) *B. subtilis* at various time points. Background counts have not been deducted. The cell pellet and supernatant samples were taken and counted in triplicates (and SD error bars determined) for *E. coli* and replicated nine times for *B. subtilis*. The total samples for *E. coli* were prepared in singles and in triplicates for *B. subtilis*.

This experiment required further optimisation and due to limitations in time and [^{14}C] antibiotics, efforts were placed solely on the uptake study. This preliminary transport study was put on hold for future work.

6.3.13 Thiomarinol appears not to be transported out of cells as efficiently as mupirocin

Although the above transport study was inconclusive in identifying any differences between the efflux of mupirocin and thiomarinol from bacterial cells, a different approach was taken in an attempt to address the hypothesis that thiomarinol's efficacy is due to its ability to avoid/delay efflux from sensitive cells. Ten efflux transporter deletion mutants of *S. typhimurium* were subjected to mupirocin and thiomarinol MIC testing as outlined in Chapter 2. These mutants carried single knockouts in various efflux transporter components ranging from TolC to MacAB. They were a kind donation from Dr. Jessica Blair and Prof. Laura JV Piddock from the University of Birmingham.

The MIC values obtained for each mutant was compared to that of the wild type *S. typhimurium* and the differences (in fold decrease) plotted on the following graph (Figure 6.24).

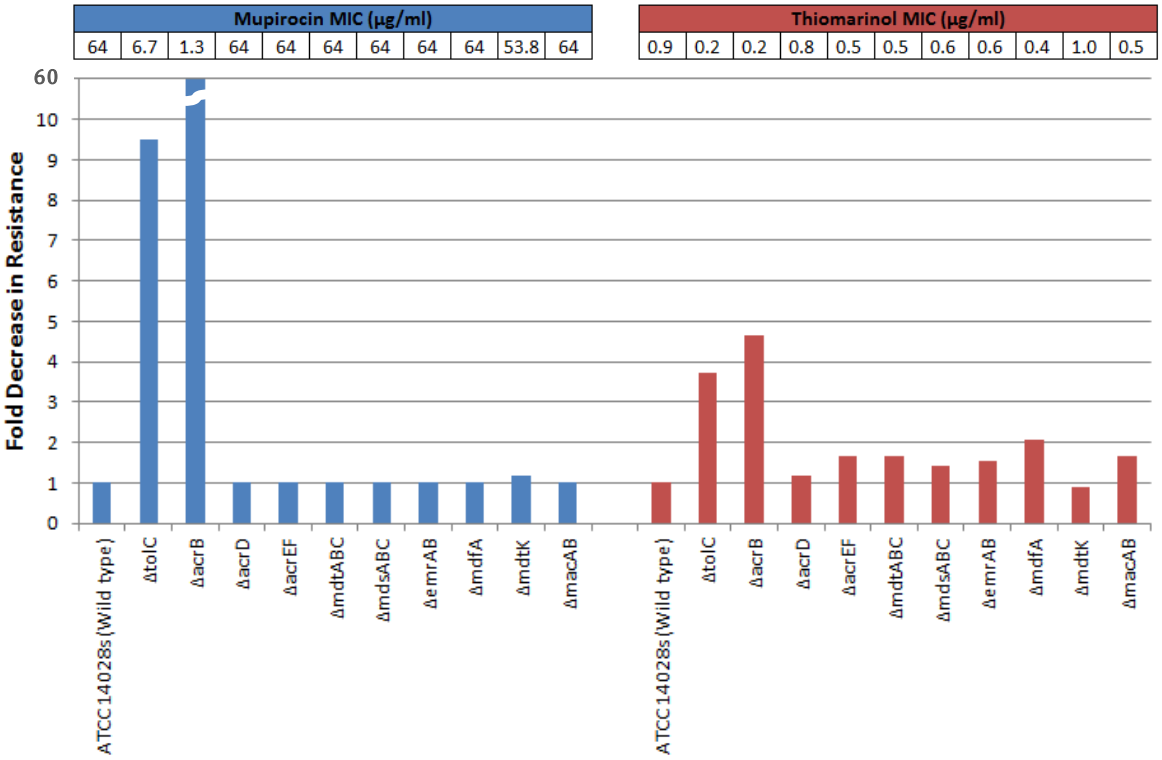

Figure 6.24. *S. typhimurium* ATCC14028s wild type and efflux transporter mutants tested against mupirocin (left in blue) and thiomarinol (right in red). The geometric MIC average of each strain is presented in the above tables, while the fold decrease in MIC (relative to wild type) is shown by the bar graph. The MIC tests were performed in triplicates. The MIC tests of wild-type, *ΔtolC, ΔacrB, ΔacrD* and *ΔmdtK* were repeated four times for mupirocin and six times for thiomarinol to confirm the reproducibility of the results. All other mutants showed no difference in MIC value compared to wild type and hence the MIC test repeated once for mupirocin and 3 times for thiomarinol.

The MIC tests identified two mutants, *ΔtolC* and *ΔacrB* to cause a much greater factor decrease in resistance against mupirocin compared to all other mutants tested. Furthermore, the effect on the mutants was greater with mupirocin than with thiomarinol, although there is still a significant 3-4 fold decrease in MIC of the latter. TolC and AcrB are part of a multi-drug resistance efflux transporter called the TolC-AcrAB complex. This complex is part of the Resistance Nodulation Division (RND) superfamily of efflux transporters and is commonly associated with intrinsic and acquired antibiotic resistance in Gram-negative microorganisms (Blair and Piddock, 2009). The MIC results suggest that one of the reasons why thiomarinol

may be a more effective antibiotic than mupirocin to Gram-negative pathogens is that it is able to avoid efficient efflux by the TolC-AcrAB complex.

6.4 Discussion

6.4.1 Limitations on producing enough [^{14}C] thiomarinol A and pseudomonic acid A

The above experiments attempted to optimise the parameters to yield highly radioactive [^{14}C] thiomarinol A and pseudomonic acid A. The preliminary counts obtained from the methionine feeding experiment showed promise and further optimisation may yield enough radiolabelled antibiotics to use in the uptake and transport studies. However, there were several issues that arose during this study that need to be rectified for future work.

First and foremost, the sample coil was changed half way through the study from the 100 µl volume to 1 ml volume to allow larger 500 µl injections of mupirocin to be taken up for fractionation. Although this minimised the number of times required to repeat the fraction collecting programme, the limiting factor still laid in the analytical HPLC column. When fraction collection was repeated with the larger injection, the peak area of pseudomonic acid A began to decrease and at times disappeared all together (data not shown). It was hypothesised that the analytical HPLC column was reaching saturation due to the higher volume of mupirocin being injected repetitively and the column washing incorporated at the end of each mupirocin HPLC programme was not enough to remove residual samples from the column before the next run.

An additional washing programme was run between each sample and absolute methanol periodically run on the HPLC mupirocin programme to check for residual samples coming off the column. This prevented the column from being saturated but was not the most time efficient solution. A preparative HPLC column (Discovery C18, Sigma-Aldrich, UK) was purchased for future fraction collection of larger antibiotic volumes.

Although a higher radioactive count was detected from the [^{14}C] thiomarinol A fed with [^{14}C] methionine, uptake studies need to be repeated using this antibiotic stock to determine whether there is enough ^{14}C incorporation. If incorporation is insufficient, a possible solution to yield more radiolabelled antibiotics would be to produce methionine auxotrophs of *P. fluorescens* and *P. rava*. Possible candidates for gene knockouts were *metH* or *metE*, responsible for the downstream and final steps of methionine biosynthesis from homocysteine (Augustus and Spicer, 2011). The methionine auxotrophs would be supplemented with non-radioactive methionine during its growth stage and only fed [^{14}C] methionine at onset of the stationary phase and antibiotic production as identified by Omer-Bali (2013). This should ensure all antibiotics produced to be ^{14}C labelled.

6.4.2 The possible role of efflux in the potency of thiomarinol

The MIC results obtained from testing *S. typhimurium* efflux transporter mutants suggest that the TolC-AcrAB multidrug-resistant efflux transporter is crucial for removing mupirocin from the cells. The complex also appears to remove thiomarinol but the decrease in MIC of *ΔtolC* and *ΔacrB* mutants is not as drastic. Mutants that were tested represented a range of efflux transporter families. These families included the resistance-nodulation division RND (*acrB, acrD, acrEF*, *mdtABC* and *mdsABC*), major facilitator MFS (*emrAB* and

mdfA), multidrug and toxic compound extrusion MATE (*mdtK*) and ATP-binding cassette ABC (*macAB*) transporter families. (*tolC*, *mdtA*, *mdsA* and *mdsC* genes encode outer membrane and membrane fusion proteins) (Nishino *et al*., 2006). The MIC results suggest that perhaps the TolC-AcrAB complex does not remove thiomarinol from *S. typhimurium* as efficiently as it does with mupirocin and this allows the former to have increased activity against this bacterium and other Gram-negative microorganisms compared to mupirocin. Interestingly in Gram-positive *S. aureus*, overexpression of the major facilitator *mdeA* was reported to increase its mupirocin MIC by 16-folds (0.03 to 0.5 µg/ml), although the increase and contribution of the transporter were deemed insignificant as it was still susceptible to the drug (Huang *et al*., 2004). The multifunctional efflux transporter identified by Whatling *et al.* (1995) showed 88% homology to the MATE family; however ΔmdtK in the MIC tests appeared not to be involved in the efflux of mupirocin nor thiomarinol.

Similarly to the work carried out by Huang *et al.* (2004), it would be of interest to challenge *S. typhimurium* overexpressing *tolC-acrAB* with mupirocin and thiomarinol, and to see whether there is an increase in resistance against either antibiotic. If thiomarinol is not as efficiently transported out of the cell by this tripartite complex as mupirocin, it should be evident from the lack of MIC increase.

Nikaido argues in his published review that MIC results are not at all indicative of the ligand's affinity to the transporters and that kinetic parameters must be determined to measure the efficiency of drug efflux (Nikaido and Pagès, 2012). As an example, he observed the MIC values of isoxazolylpenicillins to decrease by 256-fold or more when AcrB was deleted in wild-type *E. coli* K12. In traditional MIC methods, this would indicate AcrB to have strong affinity to these antibiotics. On the contrary, compounds such as ampicillin were

considered to be poor substrates due to the smaller decrease in MIC by 2-fold. However, efflux kinetics showed that both antibiotics had identical $K_{0.5}$ values and only a 2-fold difference in V_{max}, indicating they are both good substrates of AcrAB (Lim and Nikaido, 2010). It would thus be sensible to determine the kinetic parameters of TolC-AcrAB and mupirocin/thiomarinol to ensure the difference in efflux efficiency is true.

It would be of interest to replicate the work done by Jo Hothersall and determine whether *tmlM* is expressed from the onset of the log phase and whether high thiomarinol resistance is detectable at the exponential phase of the thiomarinol producer or only during antibiotic production. If resistance is conferred throughout the producer's growth cycle, it would also suggest additional resistance mechanisms involved in the thiomarinol resistance phenotype. This may shed further light on the role the pyrrothine moiety plays in thiomarinol potency and any other contributors to the antibiotic's increase efficacy compared to mupirocin.

Finally, it would also be useful to search for homologues of the MATE-type transporter found in *P. fluorescens* in *P. rava*. A possible transport transporter gene *tmlY* (Thomas, unpublished data) was found on the pTML1 plasmid (Fukuda *et al.*, 2011). When a BLAST search was performed on this gene, the search results indicated it to share approximately 50% identity with membrane proteins from various bacteria. Interestingly, one of these microorganisms was *Yersinia ruckeri*, a fish pathogen and holomycin-producer, recently observed to carry an RNA methyltransferase called Hom12 (Qin *et al*., 2013b). Hom12 methylates RNA and is thought to protect the host from autotoxity, by somehow interfering with the interaction of holomycin and its target RNA polymerase. The expression of *hom12* in *E. coli* has also been shown to confer tolerance to holomycin (Qin *et al*., 2013b).

Although only a hypothetical membrane protein from *Y. ruckeri*, it would be interesting to determine the kinetic parameters of this transporter and of *tmlY*, in order to elucidate whether specific efflux transporters are important in thiomarinol and/or pyrrothine export, resistance and prevention of autotoxicity.

6.4.3 Concluding Remarks

In summary, this study heavily focused on optimising the methodology for producing highly ^{14}C labelled thiomarinol A and pseudomonic acid A. Although high enough specific activity was not achieved in this study for subsequent use and collection of data in the uptake and transport studies, the MIC results from the *S. typhimurium* efflux transporter mutants suggest efflux of thiomarinol to differ from mupirocin in at least Gram-negative organisms. This leads to further questions of whether the pyrrothine moiety has any role in hindering the efflux efficiency of thiomarinol from susceptible cells and whether a holomycin-specific membrane transporter (such as *tmlY*) is required for thiomarinol resistance. This study has merely scraped the surface of understanding the transport mechanisms of thiomarinol and much more work is required to truly understand the contributing factors to its potency.

CHAPTER 7

7 GENERAL DISCUSSION

With the ever increasing prevalence of multidrug resistant bacteria and the urgent need for newer or improved antibiotics, there is great relevance in understanding the mode of action of the hybrid antibiotic thiomarinol. This thesis has attempted to understand what mediates the potency of thiomarinol compared to its structural companion, mupirocin by computational and experimental means. It was hoped that from the data obtained, informed changes could be made to mupirocin and/or thiomarinol to produce analogues with increased specificity and binding to target enzymes of clinically significant microorganisms such as mupirocin-resistant MRSA.

Chapters 2 to 5 explored the possibility that increased binding of thiomarinol to its target IleS enzyme is a contributing factor to the antibiotic's potency. Chapter 2 showed that it is possible for *Escherichia coli*, carrying pJH10mupM and subjected to high concentrations of thiomarinol, to acquire thiomarinol resistance mutations; however, this resistance phenotype appeared to be caused by overexpression of the target. Chapter 3 highlighted an important hydrophobic patch near the KMSKS loop and multiple amino acids in the IleS active site that may increase or decrease the binding affinity of thiomarinol. However, Chapter 4 showed that changing these active site residues on MupM to mimic the active site of TmlM does not increase the thiomarinol resistance phenotype. This was in agreement with the findings of Chapter 2, that perhaps it is difficult for single or even multiple amino acid changes in MupM to confer the thiomarinol resistance phenotype. Finally in Chapter 5, preliminary results of the aminoacylation assay indicated that thiomarinol may have a greater binding affinity to IleS than mupirocin.

Chapter 6 on the other hand explored the role of transport in thiomarinol potency and found that thiomarinol may be able to avoid efficient efflux from a wide range of efflux transporter families in Gram-negative organisms, allowing it to accumulate and effectively reach its intracellular target at a lower external concentration. The results obtained in all chapters suggest the potency of thiomarinol to be a combination of increased binding and inefficient efflux out of susceptible cells. The current proposed model (Figure 7.1) of thiomarinol potency is as follows: 1) thiomarinol is able to accumulate rapidly in susceptible cells due to its ability to avoid efflux, maintain its potent intracellular concentration and reach its IleS target and 2) thiomarinol binds strongly to its target which may consequently quicken the rate of protein synthesis inhibition and eventual cell death.

Furthermore, findings from Chapter 2 suggest that overexpression of the target IleS may be a mechanism for thiomarinol tolerance/resistance – a phenomenon that has not yet been reported for thiomarinol. As to date, no resistance mechanism against thiomarinol has been observed except TmlM in the producer. There is great importance in understanding the possible resistance mechanisms of antibiotics, as this knowledge can be utilised to develop analogues that will not easily induce resistance in bacteria.

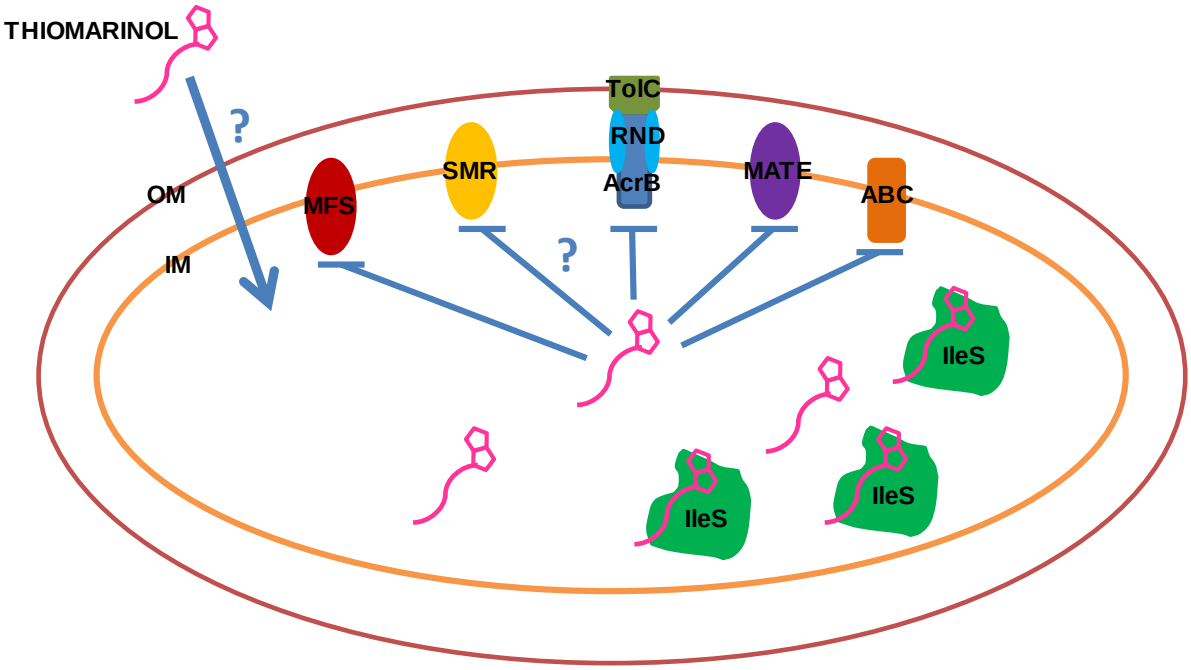

Figure 7.1. Proposed model of thiomarinol mode of potency. The mechanism of thiomarinol uptake is yet to be elucidated. Thiomarinol accumulates in the cell and binds strongly to its target IleS enzyme. Intracellular thiomarinol is unable to be removed from the cell by the major efflux transporter families (except SMR – no representative transporters were tested in this thesis). For Gram-negative organisms with an outer membrane, TolC is a common outer membrane protein that forms a complex with the transporters situated in the inner membrane (Piddock, 2006). Abbreviations: OM, outer membrane; IM, inner membrane; MFS, major facilitator superfamily; SMR, small multidrug resistance; RND, resistance-nodulation division; MATE, multidrug and toxic compounds efflux; ABC, ATP-binding cassette.

7.1 The proposed mechanisms of increased thiomarinol binding to susceptible IleS

There were some key findings from the computational work in Chapter 3 that proposed how the pyrrothine moiety on thiomarinol may be increasing its binding to the IleS enzyme in comparison to mupirocin. These were the hydrophobic patch identified by Pocket v.2 near the KMSKS motif, the specific length of the 8-hydroxyoctanoic acid and the additional amide groups on the pyrrothine moiety with their hydrogen bonding capacity. The pharmacophore model of MupM complexed with mupirocin (Chapter 3, Figure 3.2A)

suggests that the 9 carbon chain length of the antibiotic's carboxylate tail is optimal for binding by forming a salt bridge with the amine of the second lysine of the KMSKS loop. However for thiomarinol, the pharmacophore model suggests a shorter eight carbon chain to be more appropriate – a longer fatty acid chain could push the additional pyrrothine moiety out of the hydrophobic patch and into solution, causing an overall decrease in the binding strength of thiomarinol to IleS. Although the model for thiomarinol A structure has not yet been optimised as discussed in Chapter 3, the pharmacophore suggests that the two amide groups on the pyrrothine moiety could interact by hydrogen bonding with the residues on the KMSKS loop in the hydrophobic patch. The multiple hydrogen bonds formed by the pyrrothine would also be more stable in the hydrophobic patch compared to the single salt bridge formed with mupirocin. An even shorter fatty acid chain, on the other hand, would also be disadvantageous, as the pyrrothine would fall short from the hydrophobic patch for KMSKS interaction, suggesting that the eight carbon chain has been selected to optimise binding to this target.

These computational observations are partially supported by results from our collaborators, who isolated new compounds from *P. rava* sp. Nov. SANK73390 that only consisted of the fatty acid chain (in varied lengths) and the holomycin moiety (Figure 7.2) (Murphy *et al*., 2011). They observed all analogues to be less effective against *B. subtilis* and MRSA than thiomarinol A but their ineffectiveness appeared to increase with the longer carbon chains (n>8). It would be useful to create analogues that are identical to thiomarinol A, except for the altered length in the fatty acid chain, to determine whether the length of 8-hydroxyoctanoic acid plays a role in thiomarinol efficacy.

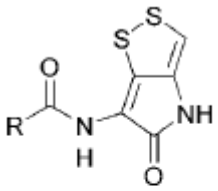

R = octanyl
R = decanoyl
R = dodecanoyl
R = *E*-dec-3-enoyl
R = *Z*-dec-**4**-enoyl
R = *E*-tetradecenoyl
R = *Z*-hexadecenoyl

Figure 7.2. Pyrrothine metabolites isolated by Murphy *et al*., 2011. The isolate with R = octanyl has been identified NMR as the metabolite xenorhabdin 3, commonly produced by *Xenorhabdus* spp.

The overall decrease in effectiveness of these analogues compared to thiomarinol A can perhaps be explained by the absence of the marinolic acid component and suggests that this component is as important in thiomarinol potency as the additional pyrrothine moiety. During detailed analysis of the IleS active sites of 1QU2, MupM and TmlM in Chapter 3, most residues that appeared to be involved in thiomarinol sensitivity or resistance were found in the catalytic groove where the marinolic acid was hypothesised to bind. Although their importance is yet to be confirmed by testing the functionality of some of the mutants created in Chapter 4, it would be hard to believe that the marinolic acid has no importance in the binding affinity of thiomarinol to IleS. The observations from this thesis suggest that thiomarinol has increased binding affinity due to a combination of the marinolic acid and pyrrothine moiety interacting with the IleS active site.

Detailed kinetic and computational analyses of mupirocin and analogues by Brown and colleagues revealed that the closer the analogue is to isoleucyl-adenylate (Ile-AMP), the stronger the binding to the active site (Brown *et al*., 2000). This is because mupirocin binds

where Ile-AMP normally sits in an aminoacylation reaction (Brown *et al*., 2000; Pope *et al*., 1998a). However, the C14 terminus of mupirocin does not mimic isoleucine very well and analysis of the X-ray structure of IleS complexed with mupirocin showed that the terminus arm is too short to bind to the isoleucine binding site. Brown and colleagues found that if this terminus was changed to better mimic isoleucine and be within similar distance to the pyran ring as the amino acid is to the ribose ring in Ile-AMP, the K_i values are significantly reduced (by up to <0.001). It would be of great interest to continue the work carried out in Chapter 5 and to deduce the K_i value of thiomarinol. This could then lead to the generation of thiomarinol analogues with perfect isoleucine side chains and deduction of their K_i values to see whether they render greater potency than the original antibiotic and also than the analogues created by Brown *et al*.

In addition to the proposed future work on thiomarinol analogues, further computational work can also be undertaken to improve the quality of the structures used and the consequent data obtained in Chapter 3. As discussed previously, quantum mechanics calculations were undertaken to determine the rotation of the pyrrothine moiety using MolPro. Once this pyrrothine is attached to the marinolic acid and the overall thiomarinol A structure optimised, molecular dynamics simulations can be run to determine the flexibility of the 8-hydroxyoctanoic acid of the marinolic acid, which will allow visualisation of where the pyrrothine moiety can bind to in the IleS. The same simulations can be run on thiomarinol analogues with shorter or longer fatty acid chains. This will allow better structural observation of the pyrrothine moiety binding to the identified hydrophobic zone.

7.2 The proposed role of inefficient efflux in thiomarinol potency

The MIC tests of *Salmonella typhimurium* efflux transporter mutants in Chapter 6 suggest that the efficacy of thiomarinol is not only due to its increased binding to the target enzyme but also from its ability to avoid efflux from susceptible cells. If efflux can be avoided, drugs in theory can accumulate quicker in cells and consequently be effective at lower concentrations. The MIC of thiomarinol is significantly lower than mupirocin against a wide range of microorganisms (Chapter 1, Table 1.5). Furthermore, thiomarinol appears not to be a substrate for a range of efflux transporter families. It appears to be transported by the wide substrate specific TolC-AcrAB tripartite RND transporter; however the MIC results suggest its efflux efficiency to be lower than when transporting mupirocin. Efflux transporters can be substrate-specific or accept a wide range of substrates. The broad range of substrates exported by some transporters has led to the theory that antimicrobial resistance via efflux transporters is a coincidental phenomenon (Piddock, 2006). If thiomarinol is able to slow down efflux by these broad substrate transporters, and no organism other than the producer carries the hypothetical thiomarinol-specific transporter (TmlY), it bodes well as an effective antibiotic.

In essence, thiomarinol may be an antibiotic that encompasses what the combinatory therapy of antibiotic and efflux pump inhibitors (EPI) is trying to achieve. The hope is that EPIs are a class of drugs that, if used in combination with existing antibiotics that have been made redundant by acquired resistance, will restore their efficacy (Schindler *et al*., 2013; Zechini and Versace, 2009). By understanding the mechanism by which thiomarinol avoids or slows efflux, a new method for reviving redundant drugs may be a possibility. Perhaps

simple alterations to existing antibiotics to hinder or prevent their efflux would allow many drugs to be effective once more.

In terms of investigating the role the pyrrothine moiety plays in the proposed inefficient efflux of thiomarinol out of susceptible cells, it would be interesting to test analogues of marinolic acid hybridised with other bulky and non-bulky moieties other than holomycin, against the *S. typhimurium* efflux transporter mutants (either overproducing or deleted) and to also determine their kinetic affinity to different efflux transporters as outlined by Nikaido in Chapter 6 (Nikaido and Pagès, 2012).

On the other hand, the uptake of thiomarinol into cells is yet to be understood. Whether accumulation plays a role also needs further experimentation with better labelled [^{14}C] antibiotics or perhaps even the exploration of other tracking methods such as visualising transport with fluorescently tagged antibiotics and confocal laser scanning microscopy (CLSM), as demonstrated with *S. aureus* and BODIPY-vancomycin (Oubekka *et al*., 2012). By using fluorescently tagged antibiotics, efflux in theory can also be tracked in the same experiment. Alternatively, the use of LC-MS requires no labelling of the antibiotics and can rapidly identify the presence of intracellular and extracellular thiomarinol. It would be interesting to visualise the difference in uptake, accumulation and efflux of mupirocin, thiomarinol A and marinolic acid, to see whether holomycin is crucial for improved transport in susceptible cells and/or in a wider range of microorganisms.

REFERENCES

REFERENCES

Aarestrup, F.M. (2004). Monitoring of antimicrobial resistance among food animals: principles and limitations. J. Vet. Med. B Infect. Dis. Vet. Public Health *51*, 380–388.

Alekshun, M.N., and Levy, S.B. (2007). Molecular mechanisms of antibacterial multidrug resistance. Cell *128*, 1037–1050.

Antonellis, A., and Green, E.D. (2008). The Role of Aminoacyl-tRNA Synthetases in Genetic Diseases*. Annu. Rev. Genomics Hum. Genet. *9*, 87–107.

Antonio, M., McFerran, N., and Pallen, M. (2002). Mutations affecting the Rossman fold of isoleucyl-tRNA synthetase are correlated with low-level mupirocin resistance in *Staphylococcus aureus*. Antimicrob. Agents Chemother. 438–442.

Augustus, A.M., and Spicer, L.D. (2011). The MetJ regulon in gammaproteobacteria determined by comparative genomics methods. BMC Genomics *12*, 558.

Austin, J., and First, E.A. (2002a). Potassium functionally replaces the second lysine of the KMSKS signature sequence in human tyrosyl-tRNA synthetase. J. Biol. Chem. *277*, 20243–20248.

Austin, J., and First, E.A. (2002b). Comparison of the catalytic roles played by the KMSKS motif in the human and *Bacillus stearothermophilus* trosyl-tRNA synthetases. J. Biol. Chem. *277*, 28394–28399.

Baouz, S., Schmitter, J.-M., Chenoune, L., Beauvallet, C., Blanquet, S., Woisard, A., and Hountondji, C. (2009). Primary Structure Revision and Active Site Mapping of *E. coli* Isoleucyl-tRNA Synthetase by Means of Maldi Mass Spectrometry. Open Biochem. J. *3*, 26–38.

Baquero, F. (2001). Low-level antibacterial resistance: a gateway to clinical resistance. Drug Resist. Updat. *4*, 93–105.

Berg, J.M., Tymoczko, J.L., and Stryer, L. (2002). Biochemistry. 5th edition. (New York: W.H. Freeman).

Bergey, D.H., Buchanan, R.E., Gibbons, N.E., and American Society for Microbiology (1974). Bergey's manual of determinative bacteriology (Baltimore: Williams & Wilkins Co.).

Bibb, M.J. (2005). Regulation of secondary metabolism in streptomycetes. Curr. Opin. Microbiol. *8*, 208–215.

Blair, J.M.A., and Piddock, L.J.V. (2009). Structure, function and inhibition of RND efflux pumps in Gram-negative bacteria: an update. Curr. Opin. Microbiol. *12*, 512–519.

Brazas, M.D., and Hancock, R.E.W. (2005). Using microarray gene signatures to elucidate mechanisms of antibiotic action and resistance. Drug Discov. Today *10*, 1245–1252.

Brown, J.R., Gentry, D., Becker, J.A., Ingraham, K., Holmes, D.J., and Stanhope, M.J. (2003). Horizontal transfer of drug-resistant aminoacyl-transfer-RNA synthetases of anthrax and Gram-positive pathogens. EMBO Rep. *4*, 692–698.

Brown, M.J., Mensah, L.M., Doyle, M.L., Broom, N.J., Osbourne, N., Forrest, A.K., Richardson, C.M., O'Hanlon, P.J., and Pope, A.J. (2000). Rational design of femtomolar inhibitors of isoleucyl tRNA synthetase from a binding model for pseudomonic acid-A. Biochemistry (Mosc.) *39*, 6003–6011.

Cadwell, R.C., and Joyce, G.F. (1994). Mutagenic PCR. PCR Methods Appl. *3*, S136–140.

Capobianco, J.O., Doran, C.C., and Goldman, R.C. (1989). Mechanism of mupirocin transport into sensitive and resistant bacteria. Antimicrob. Agents Chemother. *33*, 156–163.

Chen, J., and Lai, L. (2006). Pocket v.2: further developments on receptor-based pharmacophore modeling. J. Chem. Inf. Model. *46*, 2684–2691.

Clayton, J.P., Oliver, R.S., Rogers, N.H., and King, T.J. (1979). The chemistry of pseudomonic acid. Part 3. The rearrangement of pseudomonic acid A in acid and basic solution. J. Chem. Soc., Perkin Trans. 1. 838–846.

Cooper, S.M., Laosripaiboon, W., Rahman, A.S., Hothersall, J., El-Sayed, A.K., Winfield, C., Crosby, J., Cox, R.J., Simpson, T.J., and Thomas, C.M. (2005). Shift to Pseudomonic acid B production in *P. fluorescens* NCIMB10586 by mutation of mupirocin tailoring genes mupO, mupU, mupV, and macpE. Chem. Biol. *12*, 825–833.

Cox, G., and Wright, G.D. (2013). Intrinsic antibiotic resistance: Mechanisms, origins, challenges and solutions. Int. J. Med. Microbiol. *303*, 287–292.

Cusack, S., Yaremchuk, A., and Tukalo, M. (2000). The 2 A crystal structure of leucyl-tRNA synthetase and its complex with a leucyl-adenylate analogue. EMBO J. *19*, 2351–2361.

D'Costa, V.M., McGrann, K.M., Hughes, D.W., and Wright, G.D. (2006). Sampling the antibiotic resistome. Science *311*, 374–377.

Dacre, J.E., Emmerson, A.M., and Jenner, E.A. (1983). Nasal carriage of gentamicin and methicillin resistant *Staphylococcus aureus* treated with topical pseudomonic acid. Lancet *2*, 1036.

Davies, S.C. (2013). Chief Medical Officer Annual Report: Volume 2. https://www.gov.uk/government/publications/chief-medical-officer-annual-report-volume-2.

Delcour, A.H. (2009). Outer Membrane Permeability and Antibiotic Resistance. Biochim. Biophys. Acta *1794*, 808–816.

Demple, B., and Harrison, L. (1994). Repair of oxidative damage to DNA: enzymology and biology. Annu. Rev. Biochem. *63*, 915–948.

Drlica, K., and Zhao, X. (2007). Mutant Selection Window Hypothesis Updated. Clin. Infect. Dis. *44*, 681–688.

Dureković, A., Flossdorf, J., and Kula, M.R. (1973). Isolation and properties of isoleucyl-tRNA synthetase from *Escherichia coli* MRE 600. Eur. J. Biochem. FEBS *36*, 528–533.

El-Sayed, A., Hothersall, J., and Thomas, C. (2001). Quorum-sensing-dependent regulation of biosynthesis of the polyketide antibiotic mupirocin in *Pseudomonas fluorescens* NCIMB 10586. Microbiol.-Sgm 2127–2139.

El-Sayed, A., Hothersall, J., Cooper, S., Stephens, E., Simpson, T., and Thomas, C. (2003). Characterization of the mupirocin biosynthesis gene cluster from *Pseudomonas fluorescens* NCIMB 10586. Chem. Biol. 419–430.

Eriani, G., Delarue, M., Poch, O., Gangloff, J., and Moras, D. (1990). Partition of tRNA synthetases into two classes based on mutually exclusive sets of sequence motifs. Nature *347*, 203–206.

Eswar, N., Webb, B., Marti-Renom, M.A., Madhusudhan, M.S., Eramian, D., Shen, M.-Y., Pieper, U., and Sali, A. (2006). Comparative protein structure modeling using Modeller. Curr. Protoc. Bioinforma. Ed. Board Andreas Baxevanis Al *Chapter 5*, Unit 5.6.

Ferreira, R.B.R., Nunes, A.P.F., Kokis, V.M., Krepsky, N., Fonseca, L. de S., Bastos, M. do C. de F., Giambiagi-deMarval, M., and Santos, K.R.N. dos (2002). Simultaneous detection of the mecA and ileS-2 genes in coagulase-negative *Staphylococci* isolated from Brazilian hospitals by multiplex PCR. Diagn. Microbiol. Infect. Dis. *42*, 205–212.

Francklyn, C.S., First, E.A., Perona, J.J., and Hou, Y.-M. (2008). Methods for kinetic and thermodynamic analysis of aminoacyl-tRNA synthetases. Methods San Diego Calif *44*, 100–118.

Freiberg, C., Brötz-Oesterhelt, H., and Labischinski, H. (2004). The impact of transcriptome and proteome analyses on antibiotic drug discovery. Curr. Opin. Microbiol. *7*, 451–459.

Fukuda, D., Haines, A.S., Song, Z., Murphy, A.C., Hothersall, J., Stephens, E.R., Gurney, R., Cox, R.J., Crosby, J., Willis, C.L., *et al*. (2011). A natural plasmid uniquely encodes two biosynthetic pathways creating a potent anti-MRSA antibiotic. PLoS One *6*, e18031.

Fukunaga, R., and Yokoyama, S. (2006). Structural Basis for Substrate Recognition by the Editing Domain of Isoleucyl-tRNA Synthetase. J. Mol. Biol. *359*, 901–912.

Garcia-Migura, L., Hendriksen, R.S., Fraile, L., and Aarestrup, F.M. (2014). Antimicrobial resistance of zoonotic and commensal bacteria in Europe: the missing link between consumption and resistance in veterinary medicine. Vet. Microbiol. *170*, 1–9.

Gilpin, D.F., Small, S., Bakkshi, S., Kearney, M.P., Cardwell, C., and Tunney, M.M. (2010). Efficacy of a standard methicillin-resistant *Staphylococcus aureus* decolonisation protocol in routine clinical practice. J. Hosp. Infect. *75*, 93–98.

Girgis, H.S., Hottes, A.K., and Tavazoie, S. (2009). Genetic architecture of intrinsic antibiotic susceptibility. PloS One *4*, e5629.

Gouy, M., Guindon, S., and Gascuel, O. (2010). SeaView version 4: A multiplatform graphical user interface for sequence alignment and phylogenetic tree building. Mol. Biol. Evol. *27*, 221–224.

Guo, M., and Schimmel, P. (2012). Structural analyses clarify the complex control of mistranslation by tRNA synthetases. Curr. Opin. Struct. Biol. *22*, 119–126.

Hawkey, P.M., and Jones, A.M. (2009). The changing epidemiology of resistance. J. Antimicrob. Chemother. *64 Suppl 1*, i3–10.

Hodgson, J.E., Curnock, S.P., Dyke, K.G., Morris, R., Sylvester, D.R., and Gross, M.S. (1994). Molecular characterization of the gene encoding high-level mupirocin resistance in *Staphylococcus aureus* J2870. Antimicrob. Agents Chemother. *38*, 1205.

Hothersall, J., Wu, J., Rahman, A.S., Shields, J.A., Haddock, J., Johnson, N., Cooper, S.M., Stephens, E.R., Cox, R.J., Crosby, J., *et al*. (2007). Mutational analysis reveals that all tailoring region genes are required for production of polyketide antibiotic mupirocin by *Pseudomonas fluorescens*: pseudomonic acid B biosynthesis precedes pseudomonic acid A. J. Biol. Chem. *282*, 15451–15461.

Hothersall, J., Murphy, A.C., Iqbal, Z., Campbell, G., Stephens, E.R., Wu, J., Cooper, H., Atkinson, S., Williams, P., Crosby, J., *et al*. (2011). Manipulation of quorum sensing regulation in *Pseudomonas fluorescens* NCIMB 10586 to increase mupirocin production. Appl. Microbiol. Biotechnol. *90*, 1017–1026.

Huang, J., O'Toole, P.W., Shen, W., Amrine-Madsen, H., Jiang, X., Lobo, N., Palmer, L.M., Voelker, L., Fan, F., Gwynn, M.N., *et al*. (2004). Novel Chromosomally Encoded Multidrug Efflux Transporter MdeA in *Staphylococcus aureus*. Antimicrob. Agents Chemother. *48*, 909–917.

Hughes, J., and Mellows, G. (1980). Interaction of pseudomonic acid A with *Escherichia coli* B isoleucyl-tRNA synthetase. Biochem. J. *191*, 209–219.

Hurdle, J.G., O'Neill, A.J., Ingham, E., Fishwick, C., and Chopra, I. (2004). Analysis of mupirocin resistance and fitness in *Staphylococcus aureus* by molecular genetic and structural modeling techniques. Antimicrob. Agents Chemother. *48*, 4366-4376.

Ilyin, V.A., Temple, B., Hu, M., Li, G., Yin, Y., Vachette, P., and Carter, C.W., Jr (2000). 2.9 A crystal structure of ligand-free tryptophanyl-tRNA synthetase: domain movements fragment the adenine nucleotide binding site. Protein Sci. Publ. Protein Soc. *9*, 218–231.

Imlay, J.A., and Linn, S. (1988). DNA damage and oxygen radical toxicity. Science *240*, 1302–1309.

James, C.E., Mahendran, K.R., Molitor, A., Bolla, J.-M., Bessonov, A.N., Winterhalter, M., and Pagès, J.-M. (2009). How β-Lactam Antibiotics Enter Bacteria: A Dialogue with the Porins. PLoS ONE *4*, e5453.

John, B., and Sali, A. (2003). Comparative protein structure modeling by iterative alignment, model building and model assessment. Nucleic Acids Res. *31*, 3982–3992.

Kabsch, W., and Sander, C. (1983). Dictionary of protein secondary structure: pattern recognition of hydrogen-bonded and geometrical features. Biopolymers *22*, 2577–2637.

Keren, I., Kaldalu, N., Spoering, A., Wang, Y., and Lewis, K. (2004). Persister cells and tolerance to antimicrobials. FEMS Microbiol. Lett. *230*, 13–18.

Kester, J.C., and Fortune, S.M. (2014). Persisters and beyond: mechanisms of phenotypic drug resistance and drug tolerance in bacteria. Crit. Rev. Biochem. Mol. Biol. *49*, 91–101.

Khachatourians, G.G., and Tipper, D.J. (1974). Inhibition of messenger ribonucleic acid synthesis in *Escherichia coli* by thiolutin. J. Bacteriol. *119*, 795–804.

Kobayashi, T., Takimura, T., Sekine, R., Kelly, V.P., Vincent, K., Kamata, K., Sakamoto, K., Nishimura, S., and Yokoyama, S. (2005). Structural snapshots of the KMSKS loop rearrangement for amino acid activation by bacterial tyrosyl-tRNA synthetase. J. Mol. Biol. *346*, 105–117.

Kohanski, M.A., DePristo, M.A., and Collins, J.J. (2010). Sublethal antibiotic treatment leads to multidrug resistance via radical-induced mutagenesis. Mol. Cell *37*, 311–320.

Krásný, L., and Gourse, R.L. (2004). An alternative strategy for bacterial ribosome synthesis: *Bacillus subtilis* rRNA transcription regulation. EMBO J. *23*, 4473–4483.

Landès, C., Perona, J.J., Brunie, S., Rould, M.A., Zelwer, C., Steitz, T.A., and Risler, J.L. (1995). A structure-based multiple sequence alignment of all class I aminoacyl-tRNA synthetases. Biochimie *77*, 194–203.

Larkin, M.A., Blackshields, G., Brown, N.P., Chenna, R., McGettigan, P.A., McWilliam, H., Valentin, F., Wallace, I.M., Wilm, A., Lopez, R., *et al*. (2007). Clustal W and Clustal X version 2.0. Bioinforma. Oxf. Engl. *23*, 2947–2948.

Lichtarge, O., Bourne, H.R., and Cohen, F.E. (1996). An evolutionary trace method defines binding surfaces common to protein families. J. Mol. Biol. *257*, 342–358.

Lim, S.P., and Nikaido, H. (2010). Kinetic parameters of efflux of penicillins by the multidrug efflux transporter AcrAB-TolC of *Escherichia coli*. Antimicrob. Agents Chemother. *54*, 1800–1806.

Maddipati, S.V.V.S. (2007). Advanced Computational and Machine Learning Tools in Pharmaceutical Informatics. Ph.D. Thesis. Purdue University: U.S.

Marion, O., Gao, X., Marcus, S., and Hall, D.G. (2009). Synthesis and preliminary antibacterial evaluation of simplified thiomarinol analogs. Bioorg. Med. Chem. *17*, 1006–1017.

Martinis, S.A., and Boniecki, M.T. (2010). The balance between pre- and post-transfer editing in tRNA synthetases. FEBS Lett. *584*, 455–459.

Melo, F., Sánchez, R., and Sali, A. (2002). Statistical potentials for fold assessment. Protein Sci. Publ. Protein Soc. *11*, 430–448.

Mihalek, I., Res, I., and Lichtarge, O. (2004). A family of evolution-entropy hybrid methods for ranking protein residues by importance. J. Mol. Biol. *336*, 1265–1282.

Miroux, B., and Walker, J.E. (1996). Over-production of proteins in *Escherichia coli*: mutant hosts that allow synthesis of some membrane proteins and globular proteins at high levels. J. Mol. Biol. *260*, 289–298.

Moran, L.A., Horton, R.A., Scrimgeour, G., Perry, M., and Rawn, D. (2011). Principles of Biochemistry (Pearson).

Morell, E.A., and Balkin, D.M. (2010). Methicillin-resistant *Staphylococcus aureus*: a pervasive pathogen highlights the need for new antimicrobial development. Yale J. Biol. Med. *83*, 223–233.

Murphy, A.C., Fukuda, D., Song, Z., Hothersall, J., Cox, R.J., Willis, C.L., Thomas, C.M., and Simpson, T.J. (2011). Engineered thiomarinol antibiotics active against MRSA are generated by mutagenesis and mutasynthesis of *Pseudoalteromonas* SANK73390. Angew. Chem. Int. Ed Engl. *50*, 3271–3274.

Nakama, T., Nureki, O., and Yokoyama, S. (2001). Structural Basis for the Recognition of Isoleucyl-Adenylate and an Antibiotic, Mupirocin, by Isoleucyl-tRNA Synthetase. J. Biol. Chem. *276*, 47387–47393.

Neidhardt, F.C., Curtiss, R., Ingraham, J. l, Lin, E.C.C., Low, K.B., Magasanik, B., Reznikoff, W., Riley, M., Schaechter, M., and Umbarger, H.E. (1996). *Escherichia coli* and *Salmonella*: Cellular and Molecular Biology (Washington, D.C: American Society for Microbiology).

Nicolaou, K.C., Chen, J.S., Edmonds, D.J., and Estrada, A.A. (2009). Recent advances in the chemistry and biology of naturally occurring antibiotics. Angew. Chem. Int. Ed Engl. *48*, 660–719.

Nikaido, H., and Pagès, J.-M. (2012). Broad-specificity efflux pumps and their role in multidrug resistance of Gram-negative bacteria. FEMS Microbiol. Rev. *36*, 340–363.

Nishino, K., Latifi, T., and Groisman, E.A. (2006). Virulence and drug resistance roles of multidrug efflux systems of *Salmonella enterica* serovar Typhimurium. Mol. Microbiol. *59*, 126–141.

Ochsner, U.A., Sun, X., Jarvis, T., Critchley, I., and Janjic, N. (2007). Aminoacyl-tRNA synthetases: essential and still promising targets for new anti-infective agents. Expert Opin. Investig. Drugs *16*, 573–593.

Oliva, B., O'Neill, A., Wilson, J.M., O'Hanlon, P.J., and Chopra, I. (2001). Antimicrobial properties and mode of action of the pyrrothine holomycin. Antimicrob. Agents Chemother. *45*, 532–539.

Omer-Bali, A.M. (2013). Studies on key steps controlling biosynthesis of antibiotics thiomarinol and mupirocin. Ph.D. Thesis. University of Birmingham: U.K.

Oubekka, S.D., Briandet, R., Fontaine-Aupart, M.-P., and Steenkeste, K. (2012). Correlative Time-Resolved Fluorescence Microscopy To Assess Antibiotic Diffusion-Reaction in Biofilms. Antimicrob. Agents Chemother. *56*, 3349–3358.

Patel, J., Gorwitz, R., and Jernigan, J. (2009). Mupirocin resistance. Clin. Infect. Dis. 935–941.

Perona, J.J., Rould, M.A., and Steitz, T.A. (1993). Structural basis for transfer RNA aminoacylation by *Escherichia coli* glutaminyl-tRNA synthetase. Biochemistry (Mosc.) *32*, 8758–8771.

Pettersen, E.F., Goddard, T.D., Huang, C.C., Couch, G.S., Greenblatt, D.M., Meng, E.C., and Ferrin, T.E. (2004). UCSF Chimera--a visualization system for exploratory research and analysis. J. Comput. Chem. *25*, 1605–1612.

Piddock, L.J.V. (2006). Multidrug-resistance efflux pumps — not just for resistance. Nat. Rev. Microbiol. *4*, 629–636.

Pope, A.J., Moore, K.J., McVey, M., Mensah, L., Benson, N., Osbourne, N., Broom, N., Brown, M.J., and O'Hanlon, P. (1998a). Characterization of isoleucyl-tRNA synthetase from *Staphylococcus aureus*. II. Mechanism of inhibition by reaction intermediate and pseudomonic acid analogues studied using transient and steady-state kinetics. J. Biol. Chem. *273*, 31691–31701.

Pope, A.J., Lapointe, J., Mensah, L., Benson, N., Brown, M.J., and Moore, K.J. (1998b). Characterization of isoleucyl-tRNA synthetase from *Staphylococcus aureus*. I: Kinetic mechanism of the substrate activation reaction studied by transient and steady-state techniques. J. Biol. Chem. *273*, 31680–31690.

Qin, Z., Huang, S., Yu, Y., and Deng, H. (2013a). Dithiolopyrrolone natural products: isolation, synthesis and biosynthesis. Mar. Drugs *11*, 3970–3997.

Qin, Z., Baker, A.T., Raab, A., Huang, S., Wang, T., Yu, Y., Jaspars, M., Secombes, C.J., and Deng, H. (2013b). The fish pathogen *Yersinia ruckeri* produces holomycin and uses an RNA methyltransferase for self-resistance. J. Biol. Chem. *288*, 14688–14697.

Ranade, R.M., Gillespie, J.R., Shibata, S., Verlinde, C.L.M.J., Fan, E., Hol, W.G.J., and Buckner, F.S. (2013). Induced Resistance to Methionyl-tRNA Synthetase Inhibitors in *Trypanosoma brucei* Is Due to Overexpression of the Target. Antimicrob. Agents Chemother. *57*, 3021–3028.

Reiss, S., Pané-Farré, J., Fuchs, S., François, P., Liebeke, M., Schrenzel, J., Lindequist, U., Lalk, M., Wolz, C., Hecker, M., *et al*. (2012). Global analysis of the *Staphylococcus aureus* response to mupirocin. Antimicrob. Agents Chemother. *56*, 787–804.

Sassanfar, M., Kranz, J.E., Gallant, P., Schimmel, P., and Shiba, K. (1996). A eubacterial *Mycobacterium tuberculosis* tRNA synthetase is eukaryote-like and resistant to a eubacterial-specific antisynthetase drug. Biochemistry (Mosc.) *35*, 9995–10003.

Schindler, B.D., Jacinto, P., and Kaatz, G.W. (2013). Inhibition of drug efflux pumps in *Staphylococcus aureus*: current status of potentiating existing antibiotics. Future Microbiol. *8*, 491–507.

Seah, C., Alexander, D.C., Louie, L., Simor, A., Low, D.E., Longtin, J., and Melano, R.G. (2012). MupB, a new high-level mupirocin resistance mechanism in *Staphylococcus aureus*. Antimicrob. Agents Chemother. *56*, 1916–1920.

Serafini, F., Bottacini, F., Viappiani, A., Baruffini, E., Turroni, F., Foroni, E., Lodi, T., van Sinderen, D., and Ventura, M. (2011). Insights into Physiological and Genetic Mupirocin Susceptibility in *Bifidobacteria*. Appl. Environ. Microbiol. *77*, 3141–3146.

Shen, M., and Sali, A. (2006). Statistical potential for assessment and prediction of protein structures. Protein Sci. *15*, 2507–2524.

Shiozawa, H., and Takahashi, S. (1994). Configurational studies on thiomarinol. J. Antibiot. (Tokyo) *47*, 851–853.

Shiozawa, H., Kagasaki, T., Kinoshita, T., Haruyama, H., Domon, H., Utsui, Y., Kodama, K., and Takahashi, S. (1993). Thiomarinol, a new hybrid antimicrobial antibiotic produced by a marine bacterium fermentation, isolation, structure, and antimicrobial activity. J. Antibiot. (Tokyo) 1834–1842.

Shiozawa, H., Kagasaki, T., Torikata, A., Tanaka, N., Fujimoto, K., Hata, T., Furukawa, Y., and Takahashi, S. (1995). Thiomarinol B and thiomarinol C, new antimicrobial antibiotics produced by a marine bacterium. J. Antibiot. (Tokyo) 907–909.

Shiozawa, H., Shimada, A., and Takahashi, S. (1997). Thiomarinols D, E, F and G, new hybrid antimicrobial antibiotics produced by a marine bacterium; Isolation, structure, and antimicrobial activity. J. Antibiot. (Tokyo) 449–452.

Silvian, L.F., Wang, J., and Steitz, T.A. (1999). Insights into Editing from an Ile-tRNA Synthetase Structure with tRNAIle and Mupirocin. Science *285*, 1074–1077.

Soll, D., RajBhandary, U.L., and Rajbhandary, T.L. (1995). Trna: Structure, Biosynthesis, and Function (Washington, D.C: ASM Press).

Spellberg, B., Guidos, R., Gilbert, D., Bradley, J., Boucher, H.W., Scheld, W.M., Bartlett, J.G., and Edwards, J., Jr (2008). The epidemic of antibiotic-resistant infections: a call to action for the medical community from the Infectious Diseases Society of America. Clin. Infect. Dis. Off. Publ. Infect. Dis. Soc. Am. *46*, 155–164.

Stapleton, P.D., and Taylor, P.W. (2002). Methicillin resistance in *Staphylococcus aureus*: mechanisms and modulation. Sci. Prog. *85*, 57–72.

Stierle, D.B., and Stierle, A.A. (1992). Pseudomonic acid derivatives from a marine bacterium. Cell. Mol. Life Sci. *48*, 1165–1169.

Sutherland, R., Boon, R.J., Griffin, K.E., Masters, P.J., Slocombe, B., and White, A.R. (1985). Antibacterial activity of mupirocin (pseudomonic acid), a new antibiotic for topical use. Antimicrob. Agents Chemother. *27*, 495–498.

Tenover, F.C. (2006). Mechanisms of Antimicrobial Resistance in Bacteria. Am. J. Med. *119*, S3–S10.

Thomas, C.M., Hothersall, J., Willis, C.L., and Simpson, T.J. (2010). Resistance to and synthesis of the antibiotic mupirocin. Nat. Rev. Microbiol. *8*, 281–289.

Vondenhoff, G.H.M., and Van Aerschot, A. (2011). Aminoacyl-tRNA synthetase inhibitors as potential antibiotics. Eur. J. Med. Chem. *46*, 5227–5236.

Wallace, A.C., Laskowski, R.A., and Thornton, J.M. (1995). LIGPLOT: a program to generate schematic diagrams of protein-ligand interactions. Protein Eng. *8*, 127–134.

Walsh, C. (2003). Antibiotics: Actions, Origins, Resistance (Washington, D.C.: ASM Press).

Webber, M.A., and Piddock, L.J.V. (2003). The importance of efflux pumps in bacterial antibiotic resistance. J. Antimicrob. Chemother. *51*, 9–11.

Werner, H.J., Knowles, P.J., Knizia, G., Manby, F.R., and Schütz, M. (2012). Molpro: a general‐purpose quantum chemistry program package. WIREs Comput. Mol. Sci. *2*, 242–253.

Whatling, C., Hodgson, J., Burnham, M., Clarke, N., Franklin, F., and Thomas, C. (1995). Identification of a 60-Kb region of the chromosome of *Pseudomonas fluorescens* NCIB 10586 required for the biosynthesis of pseudomonic acid (mupirocin). Microbiol.-UK 973–982.

Wietz, M., Mansson, M., Gotfredsen, C.H., Larsen, T.O., and Gram, L. (2010). Antibacterial compounds from marine *Vibrionaceae* isolated on a global expedition. Mar. Drugs *8*, 2946–2960.

Wu, J., Cooper, S.M., Cox, R.J., Crosby, J., Crump, M.P., Hothersall, J., Simpson, T.J., Thomas, C.M., and Willis, C.L. (2007). Mupirocin H, a novel metabolite resulting from mutation of the HMG-CoA synthase analogue, mupH in *Pseudomonas fluorescens*. Chem. Commun. Camb. Engl. 2040–2042.

Wuite, J., Davies, B.I., Go, M., Lambers, J., Jackson, D., and Mellows, G. (1983). Pseudomonic acid: a new topical antimicrobial agent. Lancet *2*, 394.

Yanagisawa, T., and Kawakami, M. (2003). How does *Pseudomonas fluorescens* avoid suicide from its antibiotic pseudomonic acid? Evidence for two evolutionarily distinct isoleucyl-tRNA synthetases conferring self-defense. J. Biol. Chem. 25887–25894.

Yanagisawa, T., Lee, J., Wu, H., and Kawakami, M. (1994). Relationship of protein structure of isoleucyl-transfer-RNA synthetase with pseudomonic acid resistance of *Escherichia coli* proposed mode of action of pseudomonic acid as an inhibitor of isoleucyl-transfer-RNA synthetase. J. Biol. Chem. 24304–24309.

Yaremchuk, A., Kriklivyi, I., Tukalo, M., and Cusack, S. (2002). Class I tyrosyl-tRNA synthetase has a class II mode of cognate tRNA recognition. EMBO J. *21*, 3829–3840.

Yu, E.W., Aires, J.R., and Nikaido, H. (2003). AcrB multidrug efflux pump of *Escherichia coli*: composite substrate-binding cavity of exceptional flexibility generates its extremely wide substrate specificity. J. Bacteriol. *185*, 5657–5664.

Zechini, B., and Versace, I. (2009). Inhibitors of multidrug resistant efflux systems in bacteria. Recent Patents Anti-Infect. Drug Disc. *4*, 37–50.

Zhang, T., Muraih, J.K., Tishbi, N., Herskowitz, J., Victor, R.L., Silverman, J., Uwumarenogie, S., Taylor, S.D., Palmer, M., and Mintzer, E. (2014). Cardiolipin prevents membrane translocation and permeabilization by daptomycin. J. Biol. Chem. *289*, 11584–11591.